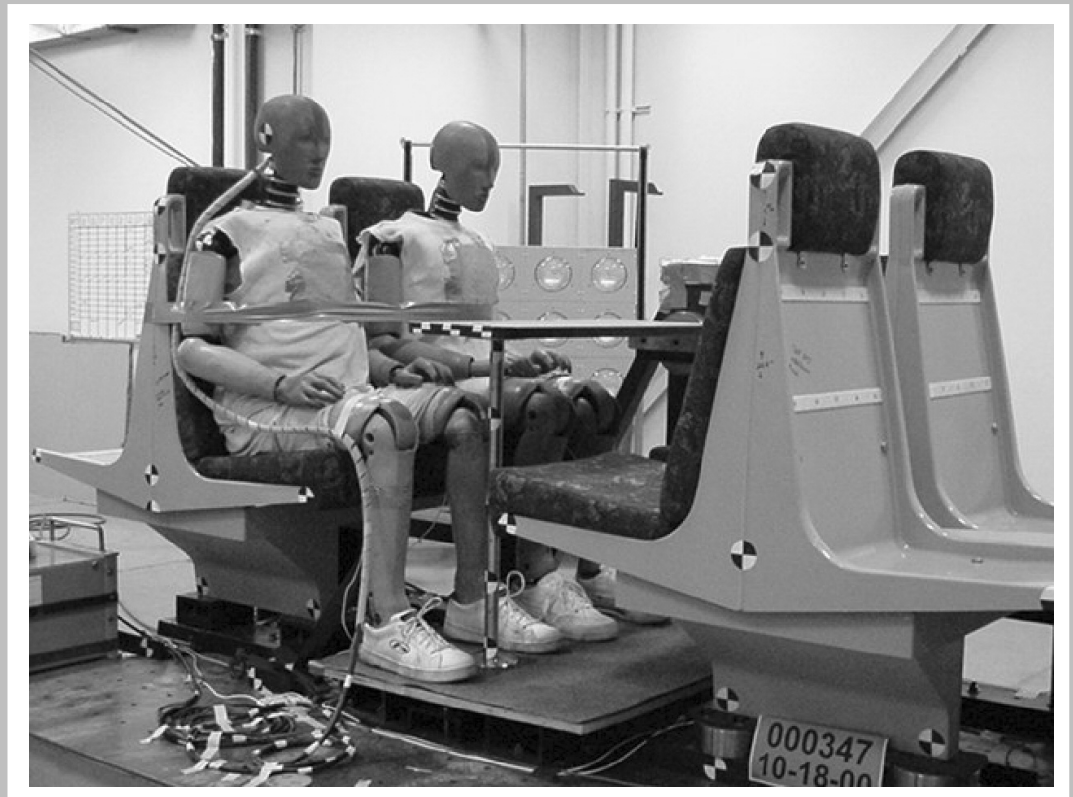U.S. Department
of Transportation

**Federal Railroad
Administration**

# Commuter Rail Seat
# Testing and Analysis
# of Facing Seats

000347
10-18-00

| 1. AGENCY USE ONLY (Leave blank) | 2. REPORT DATE<br>December 2003 | 3. REPORT TYPE AND DATES COVERED<br>Final Report |
|---|---|---|

| 4. TITLE AND SUBTITLE<br><br>Commuter Rail Seat Testing and Analysis of Facing Seats | 5. FUNDING NUMBERS<br><br>R2067/RR228 |
|---|---|
| 6. AUTHOR(S)<br>Caroline VanIngen-Dunn* | |

| 7. PERFORMING ORGANIZATION NAME(S) AND ADDRESS(ES)<br>U.S. Department of Transportation<br>Research and Special Programs Administration<br>John A. Volpe National Transportation Systems Center<br>Cambridge, MA  02142 | 8. PERFORMING ORGANIZATION REPORT NUMBER<br><br>DOT-VNTSC-FRA-03-10 |
|---|---|

| 9. SPONSORING/MONITORING AGENCY NAME(S) AND ADDRESS(ES)<br>U.S. Department of Transportation<br>Federal Railroad Administration<br>1120 Vermont Ave., NW<br>Washington, DC  20590 | 10. SPONSORING/MONITORING AGENCY REPORT NUMBER<br><br>DOT/FRA/ORD-03/06 |
|---|---|

11. SUPPLEMENTARY NOTES

*Simula Technologies, Inc.
2700 N. Central Ave., Suite 1000
Phoenix, AZ  85004

| 12a. DISTRIBUTION/AVAILABILITY STATEMENT<br>This document is available to the public through the National Technical Information Service, Springfield, Virginia 22161. | 12b. DISTRIBUTION CODE |
|---|---|

13. ABSTRACT (Maximum 200 words)

Tests have been conducted on the Bombardier back-to-back commuter rail seat in a facing-seat configuration to evaluate its performance under static and dynamic loading conditions. Quasi-static tests have been conducted to establish the load-deflection characteristics and failure mechanisms of the seat. Dynamic tests have also been conducted with 50th and 95th percentile male, and 5th percentile female instrumented Hybrid III anthropometric test devices (ATDs) to evaluate the collision performance of the seat and a table, and to verify analytical simulation models of the seat/occupant. Reasonable agreement between analytical predictions and dynamic test results was found, given the variability in the stiffness of the seats under different loading conditions.

The quasi-static test results show that the seats are sufficiently strong to withstand the loads predicted from computer simulations, but the dynamic tests resulted in partial or complete failure of the seat back across the base of the headrest. The injury criteria measured from the dynamic tests for the head, chest, and femur were within the acceptable human tolerance levels as specified in standards by the National Highway Traffic Safety Administration (NHTSA), however, the measured neck loads exceeded NHTSA neck injury criteria in all but the test with a table between seat pairs.

| 14. SUBJECT TERMS<br>anthropometric test devices, crashworthiness, facing seats, neck injury criteria, railroad, passenger seat, passenger rail vehicles | 15. NUMBER OF PAGES<br>192 |
|---|---|
| | 16. PRICE CODE |

| 17. SECURITY CLASSIFICATION OF REPORT<br>Unclassified | 18. SECURITY CLASSIFICATION OF THIS PAGE<br>Unclassified | 19. SECURITY CLASSIFICATION OF ABSTRACT<br>Unclassified | 20. LIMITATION OF ABSTRACT |
|---|---|---|---|

# PREFACE

Simula Technologies, Inc., conducted static and dynamic crashworthiness testing of commuter rail seats in a series of back-to-back facing-seat configurations.  These tests were a continuation of a similar series of tests conducted in 1998 at Simula Technologies on commuter rail seats in forward-facing row-to-row seat configurations.  This program supports the American Public Transportation Association (APTA), as well as the Federal Railroad Administration, and the results of the testing will be used as a basis for making recommendations and regulations for passenger rail equipment safety.  The tests were conducted under a Task Order contract between the Volpe National Transportation Systems Center and the Arthur D. Little/Simula Technologies research team.  The testing was conducted at Simula Technologies' dynamic sled and seat certification test facility, located in Phoenix, Arizona.  The testing was conducted in cooperation with APTA, which purchased the seats from Bombardier.  This report describes the approach used to construct a computer model of the seat/occupant system for test prediction purposes, and the methods used to conduct four dynamic sled tests.  The tests were conducted in accordance with the APTA Standard for Seating in Commuter Rail Cars (APTA SS-C&S-016-99).  The test results and post-test recommendations are provided.
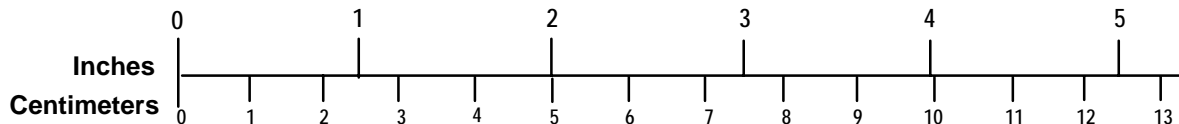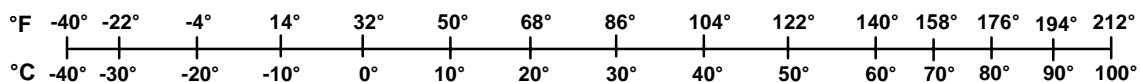
# METRIC/ENGLISH CONVERSION FACTORS

## ENGLISH TO METRIC | METRIC TO ENGLISH

### LENGTH (APPROXIMATE)

| ENGLISH TO METRIC | METRIC TO ENGLISH |
|---|---|
| 1 inch (in) = 2.5 centimeters (cm) | 1 millimeter (mm) = 0.04 inch (in) |
| 1 foot (ft) = 30 centimeters (cm) | 1 centimeter (cm) = 0.4 inch (in) |
| 1 yard (yd) = 0.9 meter (m) | 1 meter (m) = 3.3 feet (ft) |
| 1 mile (mi) = 1.6 kilometers (km) | 1 meter (m) = 1.1 yards (yd) |
| | 1 kilometer (km) = 0.6 mile (mi) |

### AREA (APPROXIMATE)

| ENGLISH TO METRIC | METRIC TO ENGLISH |
|---|---|
| 1 square inch (sq in, $in^2$) = 6.5 square centimeters ($cm^2$) | 1 square centimeter ($cm^2$) = 0.16 square inch (sq in, $in^2$) |
| 1 square foot (sq ft, $ft^2$) = 0.09 square meter ($m^2$) | 1 square meter ($m^2$) = 1.2 square yards (sq yd, $yd^2$) |
| 1 square yard (sq yd, $yd^2$) = 0.8 square meter ($m^2$) | 1 square kilometer ($km^2$) = 0.4 square mile (sq mi, $mi^2$) |
| 1 square mile (sq mi, $mi^2$) = 2.6 square kilometers ($km^2$) | 10,000 square meters ($m^2$) = 1 hectare (ha) = 2.5 acres |
| 1 acre = 0.4 hectare (he) = 4,000 square meters ($m^2$) | |

### MASS - WEIGHT (APPROXIMATE)

| ENGLISH TO METRIC | METRIC TO ENGLISH |
|---|---|
| 1 ounce (oz) = 28 grams (gm) | 1 gram (gm) = 0.036 ounce (oz) |
| 1 pound (lb) = 0.45 kilogram (kg) | 1 kilogram (kg) = 2.2 pounds (lb) |
| 1 short ton = 2,000 pounds (lb) = 0.9 tonne (t) | 1 tonne (t) = 1,000 kilograms (kg) |
| | = 1.1 short tons |

### VOLUME (APPROXIMATE)

| ENGLISH TO METRIC | METRIC TO ENGLISH |
|---|---|
| 1 teaspoon (tsp) = 5 milliliters (ml) | 1 milliliter (ml) = 0.03 fluid ounce (fl oz) |
| 1 tablespoon (tbsp) = 15 milliliters (ml) | 1 liter (l) = 2.1 pints (pt) |
| 1 fluid ounce (fl oz) = 30 milliliters (ml) | 1 liter (l) = 1.06 quarts (qt) |
| 1 cup (c) = 0.24 liter (l) | 1 liter (l) = 0.26 gallon (gal) |
| 1 pint (pt) = 0.47 liter (l) | |
| 1 quart (qt) = 0.96 liter (l) | |
| 1 gallon (gal) = 3.8 liters (l) | |
| 1 cubic foot (cu ft, $ft^3$) = 0.03 cubic meter ($m^3$) | 1 cubic meter ($m^3$) = 36 cubic feet (cu ft, $ft^3$) |
| 1 cubic yard (cu yd, $yd^3$) = 0.76 cubic meter ($m^3$) | 1 cubic meter ($m^3$) = 1.3 cubic yards (cu yd, $yd^3$) |

### TEMPERATURE (EXACT)

| ENGLISH TO METRIC | METRIC TO ENGLISH |
|---|---|
| $[(x-32)(5/9)]$ °F = y °C | $[(9/5) y + 32]$ °C = x °F |

## QUICK INCH - CENTIMETER LENGTH CONVERSION

Inches: 0 1 2 3 4 5

Centimeters: 0 1 2 3 4 5 6 7 8 9 10 11 12 13

## QUICK FAHRENHEIT - CELSIUS TEMPERATURE CONVERSION

| °F | -40° | -22° | -4° | 14° | 32° | 50° | 68° | 86° | 104° | 122° | 140° | 158° | 176° | 194° | 212° |
|---|---|---|---|---|---|---|---|---|---|---|---|---|---|---|---|
| °C | -40° | -30° | -20° | -10° | 0° | 10° | 20° | 30° | 40° | 50° | 60° | 70° | 80° | 90° | 100° |

For more exact and or other conversion factors, see NIST Miscellaneous Publication 286, Units of Weights and Measures. Price $2.50 SD Catalog No. C13 10286

**Updated 6/17/98**

**TABLE OF CONTENTS**

**TABLE OF CONTENTS (cont.)**

# LIST OF FIGURES

# LIST OF TABLES

# EXECUTIVE SUMMARY

With the current emphasis on occupant safety and passenger equipment crashworthiness, there is a heightened interest in knowing the level of crashworthiness of existing rail car seats. The results of this program effort established the level of existing seat crashworthiness in facing seats, in particular the Bombardier facing-seat system, and provided information needed to update the American Public Transportation Association (APTA) Seat Safety Standards (SS-C&S-016-99), specifically the human injury and dynamic seat strength testing protocol, which were designed primarily towards row-to-row seat configurations.

The crashworthiness of the Bombardier-designed two-passenger back-to-back commuter rail seat in a facing-seat configuration with two average-size Anthropomorphic Test Devices (ATDs) was tested against parts of the APTA Seat Safety Standard for seat dynamic testing, which defines a 250-msec-duration dynamic triangular crash pulse with an 8 G peak. A total of four occupant variants of this baseline test configuration were tested. They were:

1. Baseline test: Two facing seats, with the launch (forward-facing) seat occupied by two 50th-percentile ATDs, and a triangular crash pulse duration of 250 msec with an 8 G peak
2. Baseline test, with the addition of a table between the two facing seats
3. Baseline test, with a 9 G crash pulse peak
4. Baseline test, with the launch seat occupied by 5th-percentile and 95th-percentile ATDs

As a part of the program, a seat/occupant rigid-body computer model was developed using the Mathematical Dynamic Model modeling analysis program and was subsequently used to predict the occupant responses to the dynamic tests. Using the seat stiffness data gathered during static testing, a preliminary assessment of seat strength and occupant safety was determined by the model through an analysis of various seat/occupant configurations. After comparing the dynamic test data with results from the simulations, refinements to the model were made, resulting in a validated simulation that can be used for additional studies.

There are three key guidelines for seats demonstrating an acceptable level of dynamic structural integrity and passenger safety. These guidelines are defined in a portion of the APTA Standard and were used to evaluate the safety of the Bombardier facing-seat system. The guidelines are:

- All seat components should remain attached (or should not become free-flying objects).
- Passengers should remain compartmentalized between the two seat rows.
- Occupant injury criteria values should be within acceptable limits.

The results of this program show that the Bombardier facing-seat configuration does not meet the APTA Safety Standard for dynamic testing. Specifically:

- In two out of three dynamic tests that were conducted without a table, the headrest failed, detaching from the seat.
- In all four tests, at least one of the two ATDs was not compartmentalized.

- In three out of four tests, the injury criteria values exceeded the limits (only the test with the table resulted in injury criteria values below the limits).

# 1. INTRODUCTION

With the current emphasis on occupant safety and passenger equipment crashworthiness, there is a heightened interest in knowing the level of crashworthiness of existing rail car seats. The results of this program effort established the level of existing seat crashworthiness in facing seats, and provided information needed to update the American Public Transportation Association (APTA) Standard for Seating in Commuter Rail Cars (SS-C&S-016-99) which was designed primarily toward row-to-row seat configurations.[1] A series of tests had previously been conducted on three different row-to-row commuter seat types in an earlier contract with the Volpe National Transportation Systems Center (Volpe Center).[2]

The principal goal of this program was to provide information about seat and occupant response in a collision where occupants are sitting in seats that face one another. To achieve this goal, the Bombardier two-passenger back-to-back commuter rail seat in a facing-seat configuration was tested against the new dynamic test standards (a 250-msec-duration dynamic triangular crash pulse with an 8 G peak) and against a similar crash pulse with a peak acceleration of 9 G. Two seat units, positioned so that the seat occupants could be facing each other, were analyzed and dynamically tested both with and without a table between them. Static tests were first conducted to produce the load/deflection information about the seat for the seat/occupant computer modeling development. A seat/occupant rigid-body model was then developed with the Mathematical Dynamic Model (MADYMO) modeling analysis program and used to predict the occupant responses during dynamic testing. A preliminary assessment of seat strength and occupant safety was determined with the model through an analysis of various seat/occupant configurations. After comparing the dynamic test data with the results from the simulations, refinements to the model were made, resulting in a validated simulation that can be used for additional rail seat studies.

There are three key guidelines for seats demonstrating an acceptable level of dynamic structural integrity and passenger safety. These guidelines are defined in the APTA Seat Safety Standard and were used to measure the safety of the Bombardier facing-seat system.[2] The three guidelines are:

- All seat components should remain attached (or should not become free-flying objects).
- Passengers should remain compartmentalized between the two seat rows.
- Occupant injury loads should be within acceptable injury criteria.

There are several other related issues in rail passenger seat design that need to be addressed, not only for row-to-row seat configurations, but also for facing-seat configurations, such as the seats that were tested in this program. For example:

- *Seat Strength* - Is the seat back strong enough to prevent the occupants from bending or breaking the seat back and impacting other interior features of the rail car (tertiary impact)?

- *Seat Attachment Strength* - Is the seat and its means of attachment to the car strong enough to prevent the seat from detaching and becoming a missile during a collision? The same considerations need to be made in regard to the table's attachment to the car.

- *Secondary Impact Features of the Seat* - Is the seat back padded? Have all of the seat's sharp corners and edges been removed? Is the seat back structure compliant enough to absorb the energy of impacting passengers, and yet not fold over completely, thus allowing a tertiary impact? Are grab handles or seat-mounted stanchion posts padded or compliantly mounted? Should the seat be designed to mitigate injuries?

The results of this testing and analysis program are compared to these guidelines, and are provided in this final report. This final report includes a description of the seat (Section 2), the static test implementation and results (Section 3), the dynamic test implementation (Section 4), the dynamic test results (Section 5), the seat/occupant modeling and results (Section 6), and a comparison between the dynamic test results and the seat/occupant modeling output (Section 7). The program's conclusions and recommendations are provided in Section 8 and Section 9, respectively. Section 10 lists the references used in this report. Data plots and tables can be found in the appendices; seat stiffness curves from the static test are in Appendix A, and sled crash pulses are in Appendix B. Appendix C tabulates all the dynamic test data, and Appendix D follows with the occupant Neck Injury Criteria (Nij) table and compares it with the Nij calculations from the modeling data. Appendix E has the schematics of the seat attachment loads. Appendix F provides the time-history plots for the seat attachment loads, and Appendix G provides the time-history plots for the occupant injury data. Finally, Appendix H provides "snapshot" comparisons between the dynamic test results and their corresponding computer simulation output.

## 2.  SEAT DESCRIPTION

The Bombardier facing seat is a four-place, back-to-back seating system.  Two adjoining seats share a common seat back interface with two adjoining seats in the opposite direction.  One four-place seating system consists of a welded aluminum base frame (see Figure 1) and pre-assembled fiber-reinforced thermoplastic seat pan/back structures (see Figure 2).  Each single seat pan/back structure is bolted to its adjoining seat pan/back structure through a u-shaped aluminum bracket.  The tops of the seat backs are directly bolted together near the grab handles at the top of the seats.  The resulting two-place, back-to-back seat is bolted to the aluminum base frame next to another two-place seat pan/back structure.  A thermoplastic armrest is bolted between the two seats.  The aluminum base frame consists of square tubing and angle tubing, which is bolted together to form the seat pan base frame and the pedestal.  One end of the frame is bolted through two aluminum brackets to the sidewall, and, near the other end, the pedestal is bolted to the floor.  Threaded bolts are used to attach the thermoplastic parts together and also attach those parts to the aluminum frame.  Thermoplastic shrouds cover the base frame and pedestal for aesthetic purposes.  Figure 3 shows the assembled seats mounted on Simula's dynamic test sled with ATDs seated in the forward-facing seat.
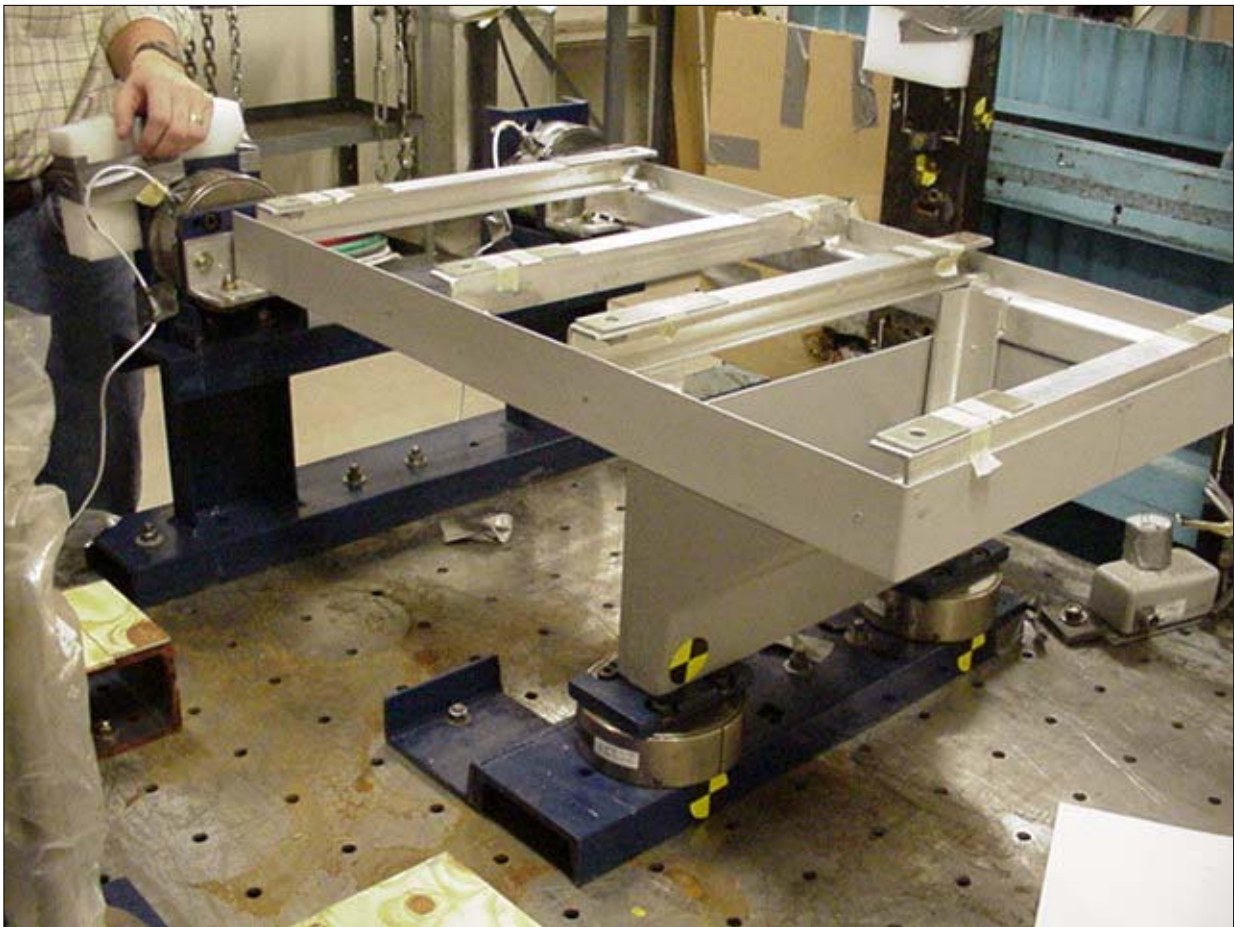


**Figure 1.  Aluminum Seat Base Frame and Pedestal**

**Figure 2. Thermoplastic Seat Pan/Back Structure**



**Figure 3. Bombardier Back-to-Back Opposing-Facing Seats Mounted on Simula's Dynamic Test Sled**

# 3.  STATIC TESTING AND RESULTS

Simula first conducted a static test to measure seat force/deflection characteristics for incorporation into the seat/occupant computer simulation model.

## 3.1  STATIC TEST EQUIPMENT

The static test facility is a 10-feet-wide, 9-feet-high and 2-feet-deep rigid static loading frame system for conducting upward, downward, forward, backward, lateral, combined, and headrest testing.  This static loading frame is capable of conducting single and simultaneous multi-axis loading up to 25,000 pounds.  It is constructed of 10-inch structural steel I-beams to provide sufficient rigidity of the mounting structure so that test component deflection measurements can be taken without the need to correct for loading frame deformation (see Figure 4).  The mounting points for the test article, the load cylinders, and the string potentiometers (displacement transducers) can be positioned in a manner that most closely represents installation in the field.

Two double-acting hydraulic cylinders (each was a 3-inch cylinder with a 24-inch stroke) were used to apply a load to the seat.  The hydraulic cylinders were controlled from a remote console, and a load was applied at a rate of 2 in/min until seat failure occurred.  The remote console, fed by a single, electrically driven hydraulic pump, provides directional control, pressure regulation, and flow rate control.  The electronic load transducers were located between the cylinders and the test components to provide the primary loading indicators.

### 3.1.1  Static Test Instrumentation

Two 10,000-pound-range strain gage load transducers (load cells) were used to measure the applied load to each seat back.  The readings were electronically recorded and visually monitored.  Various potentiometric displacement transducers (string pots), ranging in length from 5 inches to 30 inches, were used between the test frame and the test article, and to measure the displacement of the hydraulic cylinders.  Four 10,000-pound tri-axial floor load cells were installed on the floor in the load path between the seat assembly and test fixture to measure the interface loads.

String potentiometers were used to measure vertical and horizontal seat-bottom and seat-back deflections, and a load cell was used to measure the force on the load application bar.  Load cells also measured the force that the seat transmitted to the floor through its four attachment points.  Specifically, the seat reaction loads were measured at the seat/floor and seat/wall attachment points.  A video camera was positioned to record from the left-front angle view of the seat.  Figure 5 is a pre-test photograph of the static test on the seat system.
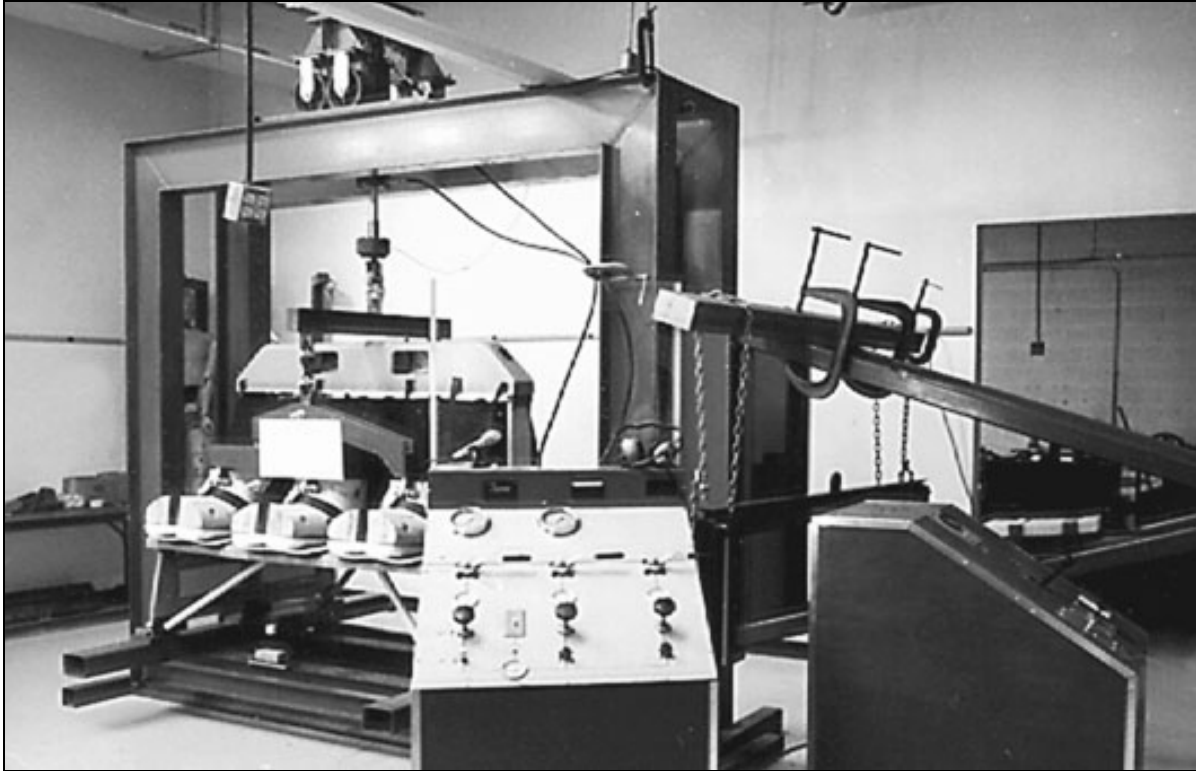
**Figure 4.  Static Test Frame**

### 3.1.2  Static Testing Data Acquisition System

The static test facility used a fully programmable signal conditioning and recording data acquisition system that can accommodate up to 28 transducer channels.  The signal conditioning equipment accepts a variety of transducers, including full- and partial-bridge-type transducers. The transducer signals are amplified, filtered, digitized, and recorded in an on-board solid-state memory.

### 3.1.3  Photographic Documentation

Two rolls of 35-mm film were used to photograph the pre-test set-up and post-test residue.  One real-time video camera was used to capture the behavior of the test article during testing.

**Figure 5. Seat Static Test - Pre-test Photo of Seat System and Test Equipment**

## 3.2 STATIC TEST RESULTS

One static test was conducted on August 23, 2000. The load was applied independently at the top of each seat back at a rate of 2 inches/minute. The seat proved to be stiffer than anticipated. The seat stiffness was greater than that measured for the Long Island Railroad commuter seat (tested in October 1998), which is a cantilevered two-place passenger seat system comprised of a thermoplastic casing surrounding an extremely rugged tubular frame[2]. Failure of the thermoplastic casing of the seat occurred at the seat/pan junction. The primary failure on the aisle side of the seat was initiated at the point where the seat pan turns upward to the seat back. The failure propagated at a 45-degree angle toward the outer corner of the seat pan/seat back intersection. The window side of the seat also experienced a fracture at the same location, but the primary failure occurred across the top of the seat back. The load-deflection curve (Figure 6) shows that while the aisle- and window-side seats had different modes of failure, the stiffness characteristics were identical up to failure. Figures 7 and 8 show the window- and aisle-side seats and their failure modes.

The results of this static loading test on the seat helped define the approach for developing the seat/occupant computer simulation model. Initially, a finite-element model (FEM) was thought to be the more appropriate method of simulating the seat, because the seat was not expected to perform in a manner that could best be represented by a rigid-body model. The Bombardier commuter facing seats are built up using a welded aluminum frame consisting of square tubes and angle braces, and a fiber-reinforced thermoplastic seat pan/seat back assembly is then bolted over the frame. Simula's expectation was that the seat/pan structure above the base frame would

likely bend, then fracture, but not necessarily at the point where the seat pan transitions to the seat back. They did not expect that a rigid-body model would be adequate to predict the complex failure mode that was expected; consequently, the development of an FEM was initially proposed. However, the results of the static test revealed that, while the seat did react differently from the previously tested seats, its primary interaction with the occupants still occurred in a manner that could be sufficiently modeled using rigid bodies. Quantitatively, the loads required to cause structural failure were relatively high, so a rigid-body model was used to simulate the seat.
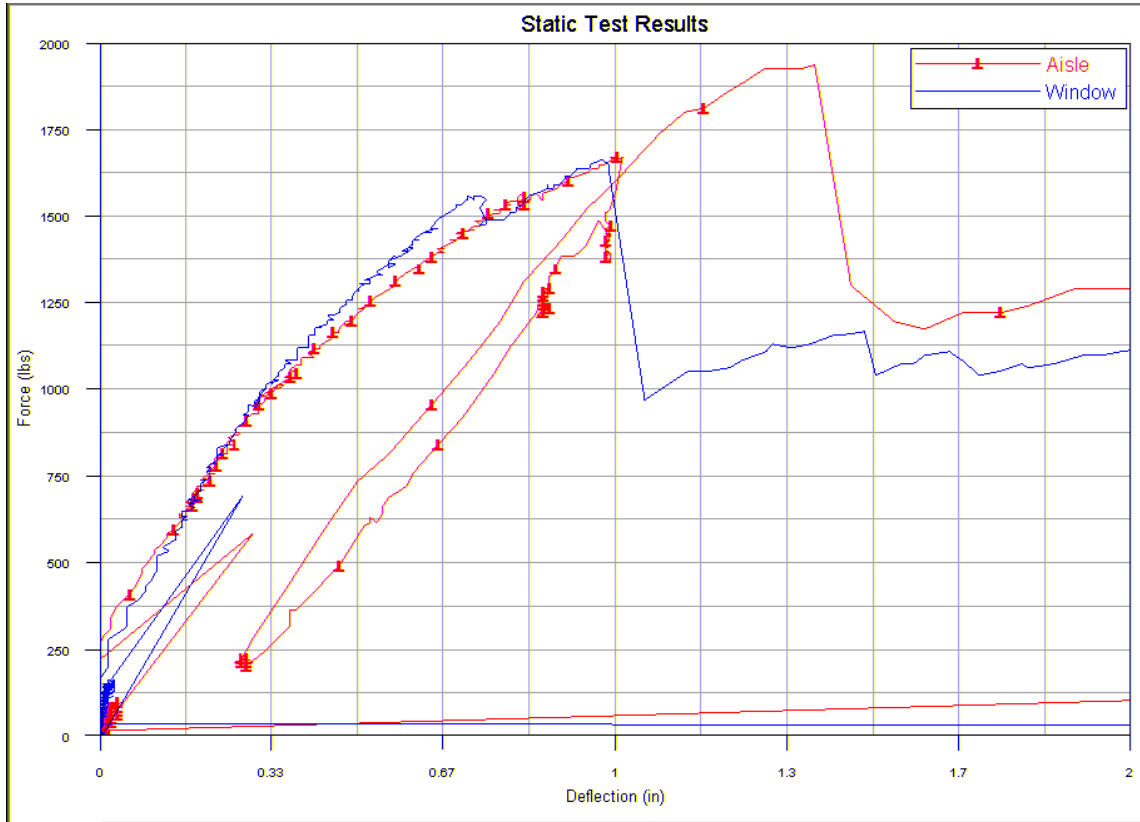


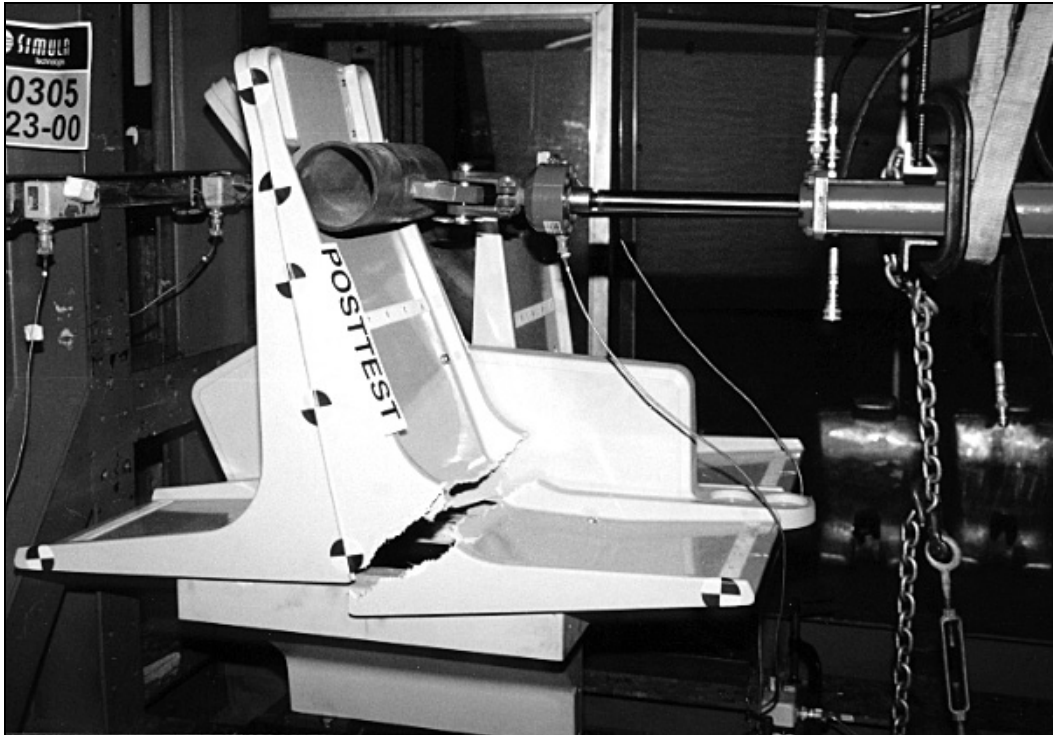**Figure 6. Static Test - Load-Deflection Curve**

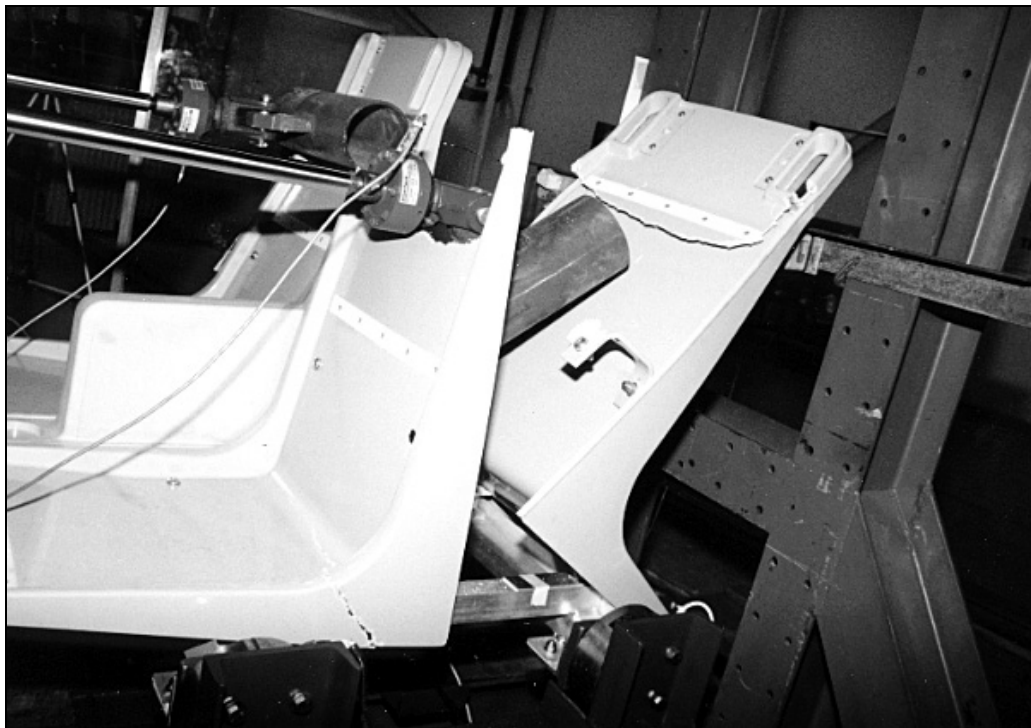**Figure 7.  Static Post-test Photo of the Failure of the Aisle-Side Seat Test**



**Figure 8.  Static Test - Post-test Photo of the Failure of the Window-Side Seat**

# 4. DYNAMIC TESTING

The purpose for conducting dynamic tests was to observe and record the responses of the seat and occupant to a given dynamic impact environment. Four dynamic tests were conducted, requiring five seat assemblies (each assembly includes a two-place passenger back-to-back seat configuration, for a total of four passenger placements) and one table. Each dynamic sled test was performed with two seat assemblies, and in one test, a table was positioned between the seats (see Figures 9 and 10). The APTA procured the seats and table(s) used in the program from Bombardier. The seat assemblies and the table were mounted on a test buck that accommodated the proper attachment points for the test articles. The seat pitch for the traditional back-to-back facing seat system provided by Bombardier was 65 inches. In all the tests, the four seats (two forward- and two rear-facing seats) of the front seat assembly were empty, and the forward-facing seats of the back assembly (the launch seat) were occupied by the specified sizes and numbers of ATDs. The launch seat was re-used in each subsequent test because it was not damaged during the testing. The focus of each dynamic test was on the manner in which the forward-facing seat occupants impacted the table or the seat assembly in the front row. The reaction of the impacted seat and/or table, as well as the launch seat, was observed.



**Figure 9. Dynamic Sled Test Configuration of Two Back-to-Back Facing Seats
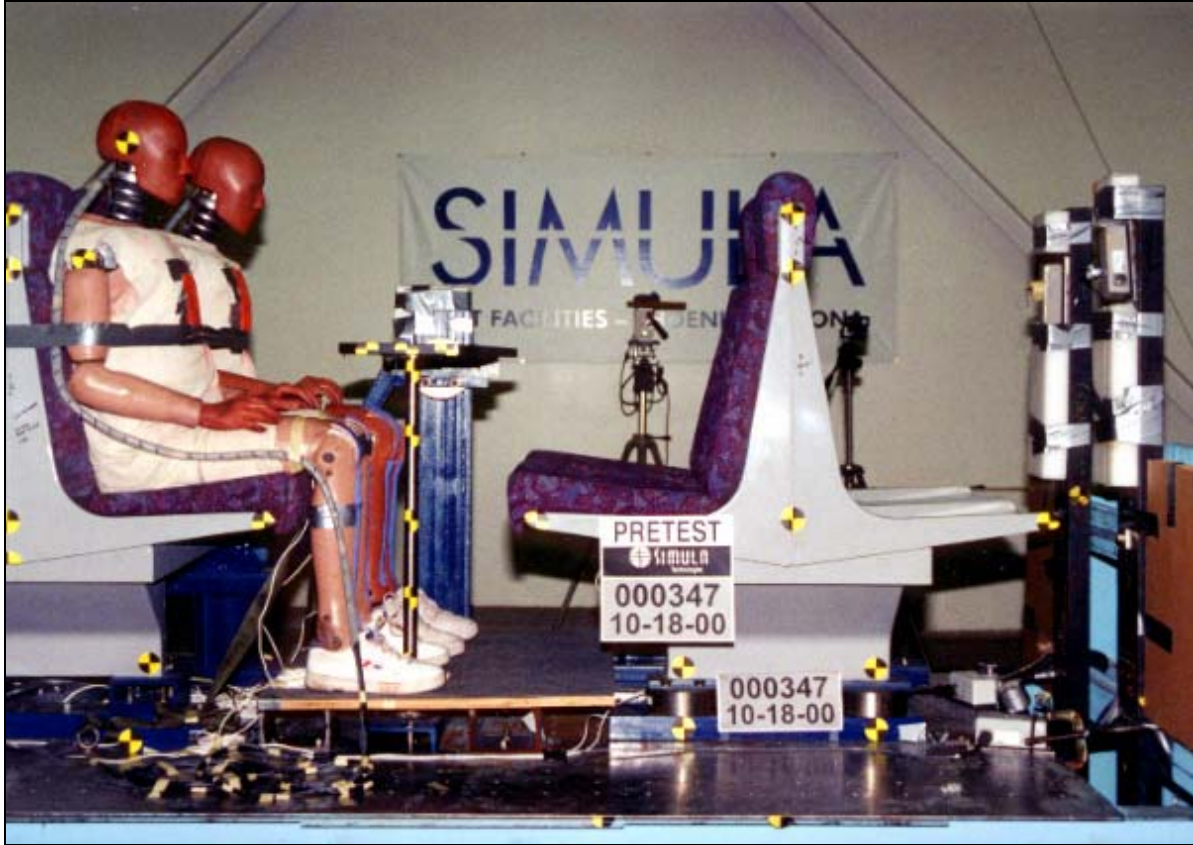with 65-inch Seat Pitch, No Table**

**Figure 10. Dynamic Sled Test Configuration of Two Back-to-Back Facing Seats with 65-inch Seat Pitch, with a Table Between the Two Seats**

Table 1 lists the four seating configurations that were dynamically tested.

**Table 1. Description of Dynamic Testing Conducted**

| Test | Test Date | Test Description | Forward-Facing Seat Occupants (ATDs) on Installed Back Seat Assembly | | Install Front Seat Assembly? | Install Table? | Crash Pulse Peak G |
| --- | --- | --- | --- | --- | --- | --- | --- |
| | | | Window | Aisle | | | |
| 1 | Oct. 18 | Baseline test, no table | 50th-percentile | 50th-percentile | Yes | No | 8 |
| 2 | Oct. 19 | Baseline test, with table | 50th-percentile | 50th-percentile | Yes | Yes | 8 |
| 3 | Oct. 19 | Baseline test, with 9 G peak acceleration | 50th-percentile | 50th-percentile | Yes | No | 9 |
| 4 | Oct. 20 | Passenger injury tolerance and seat strength test, no table | 95th-percentile | 5th-percentile | Yes | No | 8 |

## 4.1 DYNAMIC TEST EQUIPMENT

### 4.1.1 Dynamic Test Facility

The dynamic test facility is located in the same building that houses the static test facility. It contains both a 120-foot horizontal track and sled system for performing longitudinal dynamic testing, and a 30-foot guided vertical drop tower system for performing vertical dynamic testing. The Bombardier facing-seat tests were conducted in the indoor testing facility, which is environmentally conditioned to maintain temperatures of 66 to 78 °F and 10- to 70-percent relative humidity. There are provisions for high-speed filming, and state-of-the-art signal conditioning and data recording equipment for all tests.

The 120-foot horizontal track and deceleration sled system used for performing the dynamic tests consists of a 5 X 10 foot sled with a capacity to hold a 2,500-pound payload, multi-row seats, and bulkheads (Figure 11). The dynamic sled's maximum velocity with a 2,500-pound payload is 60-70 ft/sec, or approximately 45 mph. The sled is composed of a steel composite plate that was specially designed to optimize weight and strength.
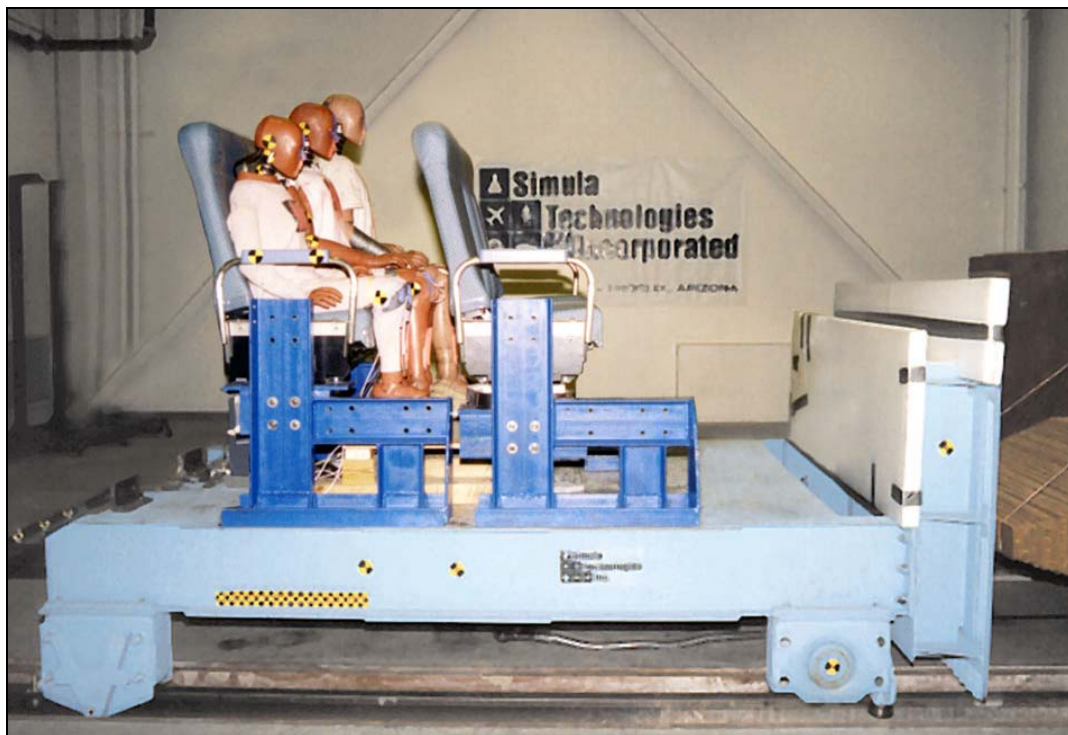


**Figure 11.  Indoor Deceleration Sled Configured with Two Row-to-Row Walkover Seats**

The longitudinal sled system is operated by connecting the front of the sled to a drop weight through a pulley and cable system (Figure 12). The aft end of the sled is connected to a haul-back winch via a cable system. By pulling the sled back a calculated distance and locking it to a release mechanism, the drop weight is raised, storing the potential energy required to accelerate the sled down the track towards a cardboard honeycomb stack placed directly in front of the impact barrier. The drop weights used to accelerate the sled are in segments of 2,500 pounds up

to 20,000 pounds.  The desired input deceleration pulse is achieved as the specially configured paper honeycomb stack crushes in a controlled manner.  The velocity change required for the test pulse is a function of 80 percent input velocity and 20 percent returned to the sled from rebound energy stored in the honeycomb stack.  Due to the method of construction used for Simula's impact-rebound decelerator sled and drop towers, a speed trap cannot be used to directly measure the impact velocity.  The system is designed to integrate the 80-percent impact energy with the 20-percent rebound to calculate the total velocity change, or the area under the deceleration curve.  This integration is performed by an internally developed computer software program.
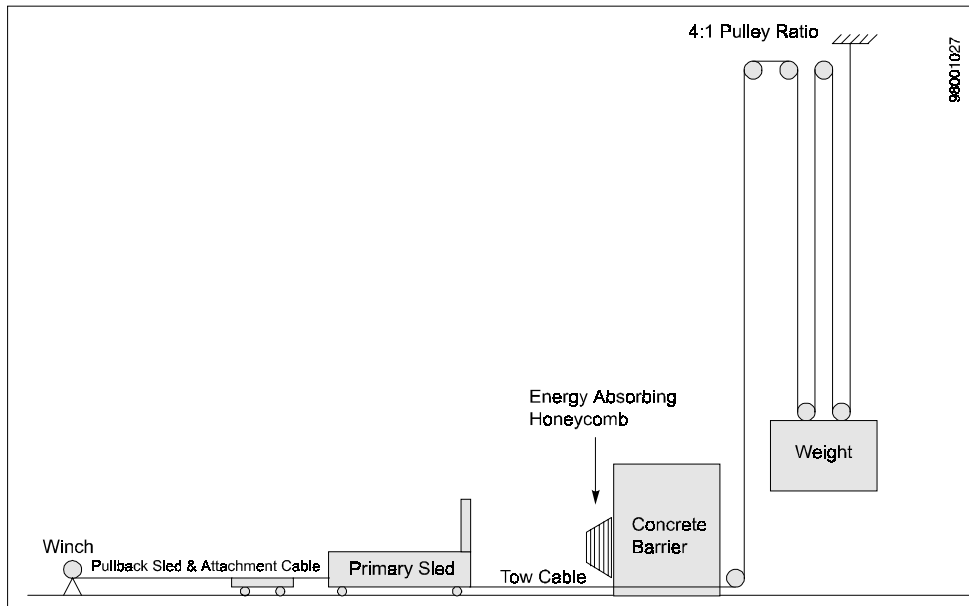


**Figure 12.  Schematic of the Longitudinal Sled System**

## 4.1.2  Anthropometric Test Devices (ATDs)

The three ATD sizes used in the dynamic testing were:  5th-, 50th-, and 95th-percentile.  All ATDs were provided by Simula, with the exception of one Hybrid III 50th-percentile dummy, on loan to Simula from the U.S. Army.  Government approval was obtained in order to borrow this Government-Furnished Equipment (GFE) ATD for the purpose of this test series.

The weights of the ATDs used for testing are listed in Table 2.

**Table 2.  Instrumented ATD Weights**

| ATDs (Number required) | Weight With Instrumentation (lb) | Weight Without Instrumentation (lb) |
|---|---|---|
| Hybrid III 5th-percentile (1) | 110.2 | 105 |
| Hybrid III 50th-percentile (2) | 177 | 172 |
| Hybrid III 95th-percentile (1) | 226 | 221 |

All ATDs used met the standards and requirements needed to comply with 48 CFR Part 572, *Anthropomorphic Test Devices*, Subpart E, *Hybrid III Test Dummy*.  The calibration, adjustment, positioning, and care of all ATDs used in the testing process was in accordance to the standards

and requirements of SAE AS8049, *Performance Standard for Seats in Civil Rotorcraft and Transport Aircraft, and General Aviation Aircraft*. Each ATD was clothed in a form-fitting, cotton stretch garment with short sleeves, and mid-thigh-length bottoms. The ATDs were also fitted with shoes that weighed approximately 2.5 pounds. The types of soles of these shoes and their relative friction coefficient became an issue, and this was addressed during testing and during the development of the computer model simulation. The friction in each limb joint was adjusted to support a 1 G weight when extended horizontally prior to each test.

Each ATD was placed in the center of the seat, in as nearly a symmetrical position as possible, and in a uniform manner so as to obtain reproducible test results. The ATD's back was placed against the seat back, thus minimizing the clearance between the ATD and the seat back. The ATD's knees were separated by approximately 4 inches, and its hands were placed on the top of its upper legs, just behind the knees. The ATD's feet were placed flat on the floor so that the centerlines of the lower legs were approximately parallel. The vertical angle of the tibia (lower leg) was measured and kept as close to perpendicular to the floor as possible.

All ATDs were tethered to the sled to prevent excessive motion and damage to the ATD. Head accelerometers, neck load cells, chest accelerometers, and femur load cells were installed in the ATD in accordance with the ATD's specification and the instructions of the transducer manufacturer. Figure 13 shows the basic instrumentation locations in a Hybrid III ATD.
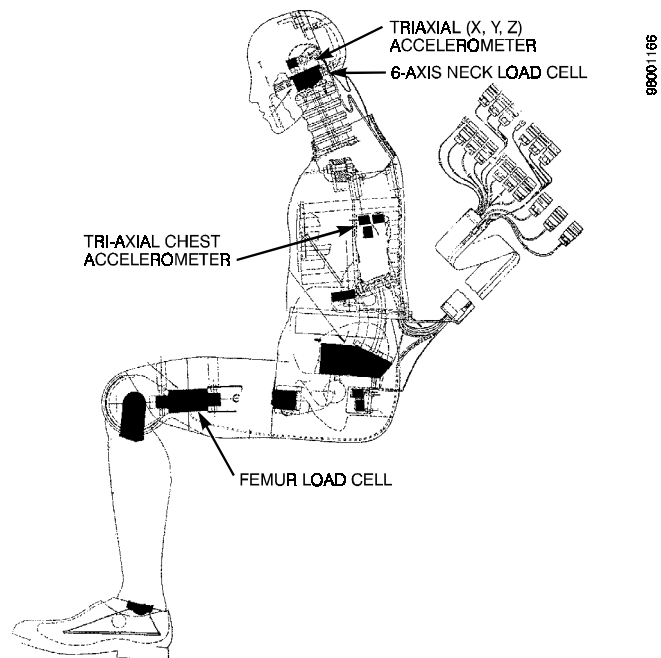


**Figure 13. Cross-Section of a Fully Instrumented Hybrid III ATD**

A light coat of chalk was applied to specific parts of each ATD to determine where it contacted the impacted seat assembly. Three colors were used to represent the different body locations: blue for the face, orange for the chest, and red on the knees and upper shins. A 1- to 2-inch-wide stripe of chalk was applied from the top surface of the head to the chin, and from the top surface

of the knee to the middle of the shin.  A patch of duct tape, approximately 6-inch square, was placed on the middle of the ATD's chest and was covered with orange chalk.

### 4.1.3  Instrumentation

Simula uses the required sampling rate for digitizing data and channel class filters specified in SAE AS 8049 and SAE J211/1.  All instrumentation is calibrated at least once a year and maintained in accordance with company Standard Policies and Procedures.  Load cells measured the longitudinal, lateral, and vertical loads imparted by the seats to the floor panel.  High-speed cameras recorded the motions of the seats and ATDs used during each of the test runs.  The test sled was instrumented with accelerometers to measure sled acceleration.  The sled's velocity and displacement results were calculated by integrating the output from the accelerometers.  Fully instrumented ATDs were used to measure applied loads in the head, chest, femurs, and neck.  Raw acceleration, force, and displacement data sensed by accelerometers, load cells, and displacement transducers were amplified through signal conditioners and recorded on a computer.  Table 3 lists the capabilities of the instrumentation used to conduct the dynamic tests.

**Table 3.  Instrumentation and Photographic Documentation Capabilities**

| Instrumentation | Manufacturer | Model | Range | Response |
|---|---|---|---|---|
| Tri-axial floor load cell | Denton | 2177A | 10,000 lb | DC-1,250 Hz |
| Uni-axial load cell | Interface | 1210 | 10,000 lb | DC-1,250 Hz |
| Horizontal string potentiometers | Celesco | PT-101-xxC | 5 to 30 in. | 100 G |
| Uni-axial sled accelerometer | CEC | 4-202 | 50 G | DC-1,250 Hz |
| Tri-axial head accelerometer | Endevco | 7232C-750 | 100 G | DC-2,000 Hz |
| Six-axis neck transducer | Denton | 1716 | 3,000 lb 2,500 lb/in. | DC-1250 Hz |
| Chest tri-axial accelerometer | Endevco | 7232C-750 | 100 G | DC-2,000 Hz |
| Uni-axial femur load cells | Denton | 2121 | 3,000 lb | DC-1,250 |
| High-speed 16-mm cameras, 500 frames/sec (max) | Redlake | Locam/51 | N/A | N/A |
| High-speed video camera, 1,000 frames/sec (max) | Kodak | Ektapro HG | N/A | N/A |
| 35-mm still camera | Nikon | - | - | N/A |

Instrumentation for the tests with two seat assemblies included the following:

- Four (4) tri-axial load cells at the seat/floor attachments for the front-row seat assembly,
- Four (4) tri-axial load cells at the seat/floor attachments for the aft-row seat assembly,
- Eight (8) horizontal and vertical string potentiometers to measure front seat deflection,
- Two sled accelerometers,
- Head x, y, and z accelerometers,
- Chest x, y, and z accelerometers,
- Two neck transducers, and
- Left- and right-femur load cells in both ATDs.

Test articles (seats, tables, and ATDs) were tethered to the sled, limiting any possibility of causing severe damage to the equipment.

Three off-board 16-mm, 500-frames/sec motion-picture cameras were positioned to capture left- and right-side views and a rear-angle view, thus providing high-speed film coverage of the dynamic tests. One high-speed motion analysis system (1,000-frames/sec video camera) was used to record the motion of the test article. Pre-test and post-test still photographs of the test setup were taken using a 35-mm camera.

The raw acceleration, force, and displacement data recorded by the accelerometers, load cells, and displacement transducers were recorded. This data was plotted for permanent records.

### 4.1.4  Dynamic Testing Data Acquisition System

Simula has two high-speed, self-contained data acquisition systems available for dynamic sled testing that together can support up to 76 data channels. They maintain all electronic instrumentation, including transducers, signal conditioners, and data recorders, and collects, filters, and processes data through instrumentation in accordance with SAE J211 and SAE AS 8049. The Data Brick Data Acquisition System was used to collect data from the ATDs, and the Pacific Instruments Data Acquisition System collected data from the sled and floor load cells.

**GMH Engineering, Data Brick Data Acquisition System**
This system consists of 6 brick modules of 8 data channels, totaling 48 channels of data acquisition. Each eight-data-channel module is battery operated, and provides transducer power, signal conditioning, filtering, triggering, and offset compensation via a host computer software program. Each data channel can sample at a rate of up to 12,800 samples/sec and a total of 524,218 data points can be collected during a test.

**Pacific Instruments, Model 5600A Data Acquisition System**
This system is a fully programmable signal conditioning and recording system for transducers and events. It will accommodate up to 28 transducer channels and 32 events. The signal-conditioning equipment accepts a variety of transducers, including full- and partial-bridge-type transducers. The transducer signals are amplified, filtered, digitized, and recorded in an on-board solid-state memory. Real-time data is provided for calibration and to verify installation. The system is controlled and data is off-loaded via an IEEE-488.1 interface using a developed General Purpose Interface Bus (GPIB) instruction language.

The typical instrumentation and filter classes for rail seat testing are listed in Table 4.

When digitizing data, the sample rate is at least 5 times the -3-dB cut-off frequency of the highest channel class used. The minimum sampling rate, therefore, is 1,650 Hz x 5, which equals 8,250 samples/sec. For the dynamic testing, Simula sampled data at a rate of 10,000 samples/sec.

**Table 4. Dynamic Testing Instrumentation and Filter Class**

| Instrumentation | SAE Channel Frequency Class (CFC) |
|---|---|
| Sled/Carriage Accelerations | 60 or 180 |
| ATD Head Acceleration (x, y, and z) | 1,000 |
| Neck Transducer | 600 (moments) and 1,000 (forces) |
| Chest Acceleration (x, y, and z) [spine only] | 180 [at the spine] |
| ATD Femur Loads (z) | 600 |
| Floor Reaction Loads (x, y, and z) | 60 |

### 4.1.5 Photographic Documentation

All tests were photographically documented with a focus on the occupants impacting the seat or table in front of the launch seat system and observing the reaction of the front-row seat or table, as well as observing the occupant kinematics. All photographic instrumentation is maintained in accordance with SAE J211 Part 2, "Photographic Instrumentation for Impact Tests." Prior to and after each test, a number of 35-mm still photographs were taken of the test setup and post-test conditions. To document the response of the ATDs and the test articles during the dynamic test, high-speed film and video cameras were used.

The nominal operating rate used at Simula for these cameras is 500 frames/sec. Cameras were positioned to capture the view of the experiments from above and from both the window and aisle sides. Figure 14 shows the positions of the cameras used.
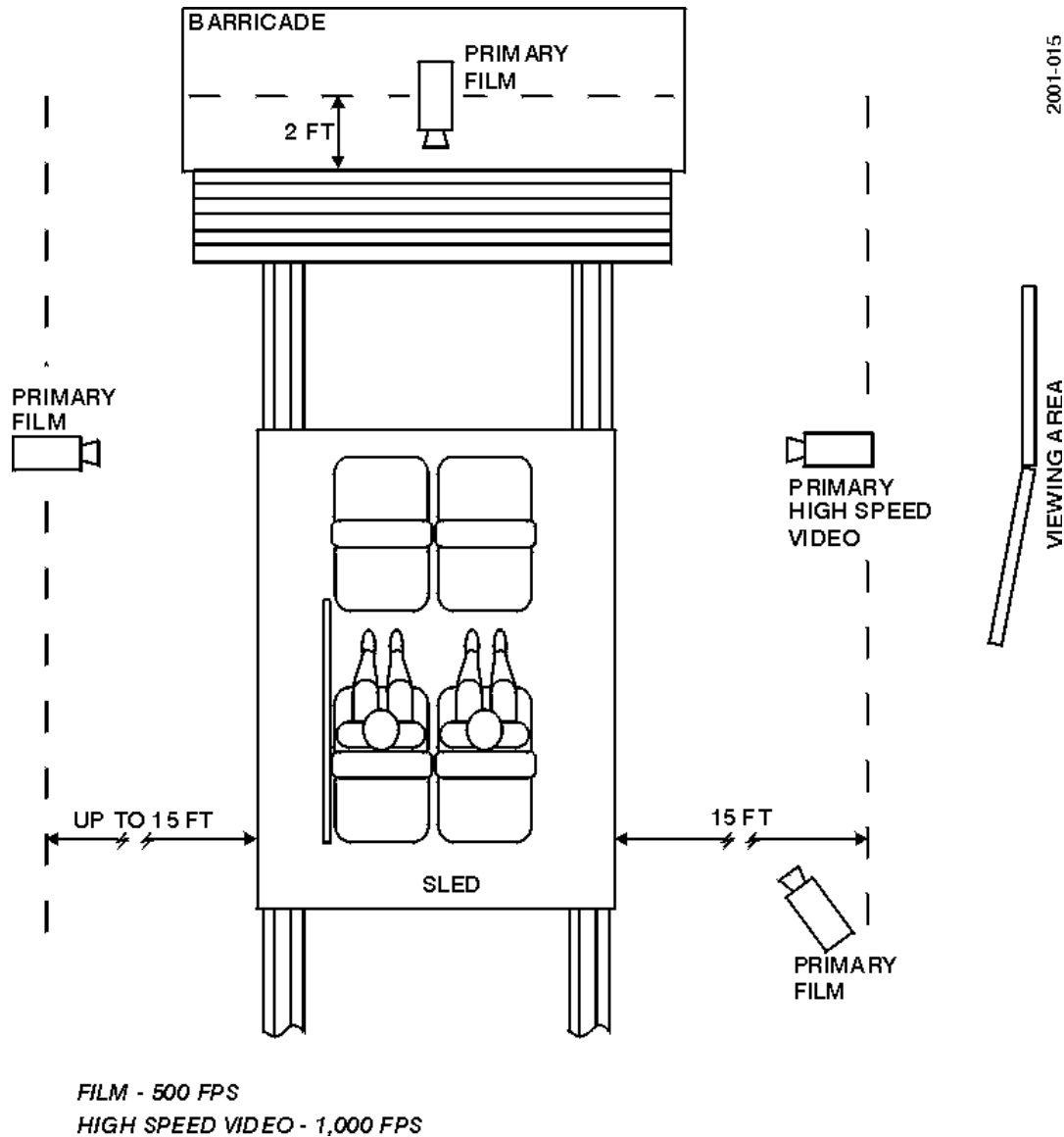
**Figure 14. Camera Positions for the Dynamic Sled Tests**

## 4.2 DYNAMIC TEST MEASUREMENT REQUIREMENTS

Load cells were used to measure the longitudinal, lateral, and vertical loads imparted by the seats to the floor. High-speed cameras recorded the motions of the seats and ATDs during each test. The ATD instrumentation included accelerometers to measure accelerations experienced by the head and the chest, load cells to measure loads and moments experienced by the neck, and load cells to measure loads experienced by the femurs. The test sled was instrumented to measure sled deceleration.

## 4.3 CRASH PULSE TIME-HISTORIES

All dynamic tests represented a triangular crash pulse with a duration of 250 msec and, except for third test, an 8 G peak acceleration that occurs at approximately 125 msec. Test No. 3 was conducted with a 9 G peak acceleration. Figure 15 shows the "ideal" triangular crash pulse and a corresponding pulse that was produced during an actual sled test (Test No. 4).
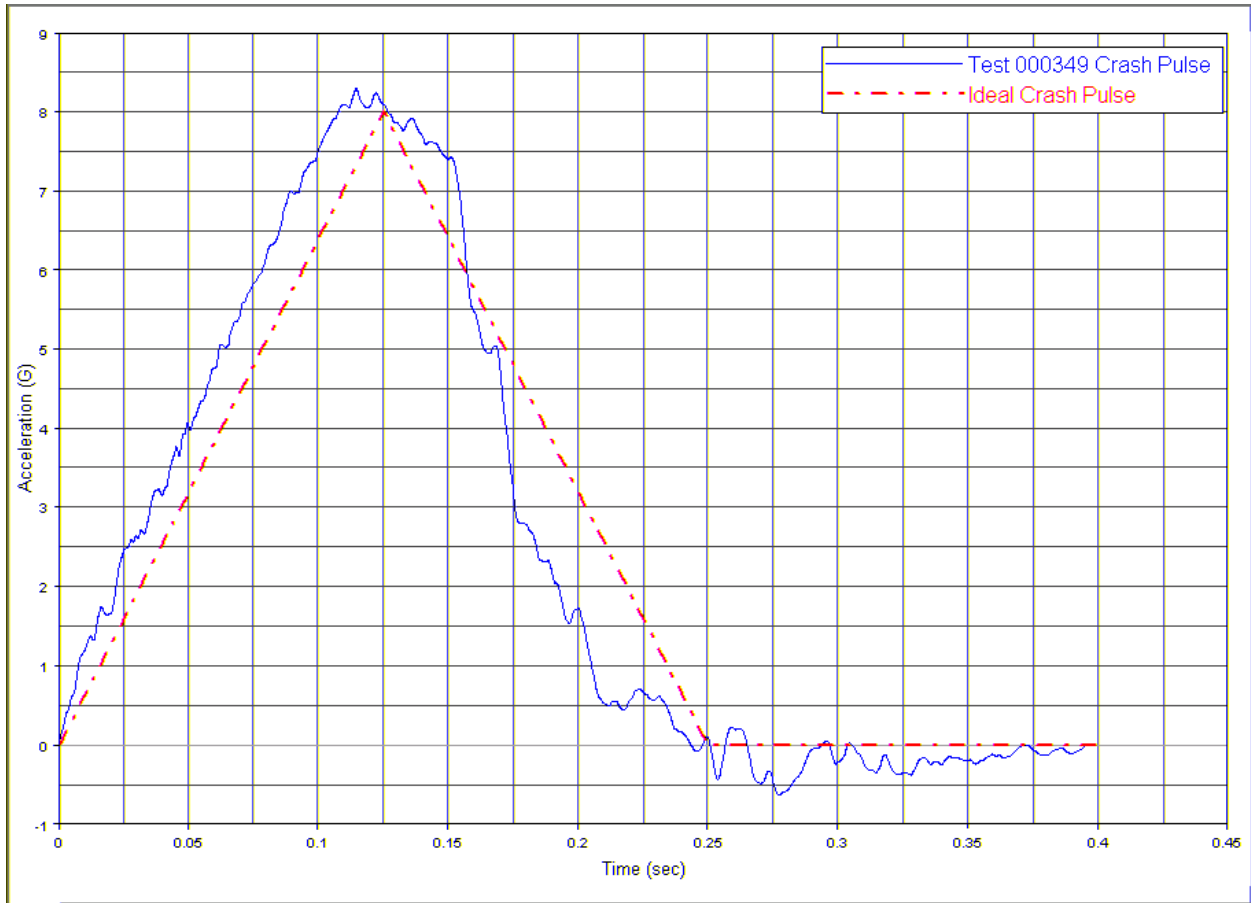


**Figure 15. Sled Crash Pulse (Actual and Ideal)**

A calibration test was conducted to ensure that the desired crash pulse could be achieved. This calibration test was conducted for the heaviest seat/ATD configuration. The combined weight of the ATDs and the seats for the heaviest seat/ATD configuration was used to calibrate the crash pulse.

# 5. DYNAMIC TEST RESULTS

Four dynamic tests were conducted during the week of October 16, 2000. The test set-up occurred on Monday and Tuesday, October 16 and 17, and the testing was conducted on October 18–20. Testing was observed by Caroline VanIngen-Dunn and Joe Manning (Simula), John Zolock (TTI at Volpe Center, Cambridge, Massachusetts), Ed Janssens (Bombardier, Thunder Bay, Canada) and Art Mallette (Metrolink, Los Angeles, California). The four tests that were conducted are shown again in Table 5 with the results (A "Yes" is the desired result). All but Test No. 3 were conducted with an 8 G peak triangular crash pulse (Test No. 3 was conducted with a more severe 9 G peak triangular crash pulse).

**Table 5. Dynamic Testing Configuration and Results Summary**

| Test | Scheduled Test Date | Test Description | Forward-Facing Seat Occupants (ATDs) on Installed Back Seat Assembly | | Did Seat Components Stay Attached? | Were Both Occupants Compart-mentalized? [1] | Were Occupant Loads All Below Injury Criteria? |
|---|---|---|---|---|---|---|---|
| | | | **Window** | **Aisle** | | | |
| 1 | Oct. 18 | Baseline test | 50th-percentile | 50th-percentile | Yes | No | No |
| 2 | Oct. 19 | Baseline test, with table | 50th-percentile | 50th-percentile | No | No | Yes |
| 3 | Oct. 19 | Baseline test, with 9 G peak acceleration | 50th-percentile | 50th-percentile | No | No | No |
| 4 | Oct. 20 | Baseline test with different size ATDs | 95th-percentile | 5th-percentile | No | No | No |

[1] Occupant compartmentalization was defined for these tests as the ability to limit the occupant from traveling outside the confines created by the two seat rows. Occupants (lower torso and below) traveling beyond the top of the seat back and/or their entire bodies falling into the aisle were considered to not be compartmentalized.

The results summarized in Table 5 show that the seat system, as currently designed and in the configurations tested, does not meet all the requirements of the portion of the APTA Standard for Seating in Commuter Rail Cars (SS-C&S-016-99) that details dynamic strength and human injury testing. Details of the test results are provided in this section, including a description of each experiment, the seat outcome, and the ATD outcome.

## 5.1 DYNAMIC TEST EVALUATION CRITERIA

In anticipation of dynamic testing, the following three guidelines were defined as the desirable indicators for seats demonstrating an acceptable level of structural integrity and passenger safety:

- All seat components should remain attached (or should not become free-flying objects).
- Passengers should remain compartmentalized between the two seat rows.
- Occupant injury loads should be within acceptable injury criteria.

Seat component attachment was measured by observing which, if any, seat components detached from the seat's main frame. Seat-to-car attachment, however, could not be determined, because the seats were rigidly mounted to the test fixture. However, load cells placed between the seat

and test fixture and the table and the wall mount measured the forces that were developed at the attachment points.  Information about the rail car structure(s), to which the seats and tables would be installed, may subsequently be used to help determine whether the seat/floor, seat/wall, or table/wall attachments are strong enough to support the loads in a collision environment.  The peak attachment loads measured during dynamic testing are provided in tables in Appendix C, are schematically presented in Appendix E, and are presented as data plots that are compared to the corresponding modeling output curves in Appendix F.

Occupant results are determined from the occupant kinematics recorded on film by the high-speed cameras and from the loads recorded by the instrumented ATDs.  To interpret and evaluate ATD response measurements from the tests, occupant injury criteria are specified.  These injury criteria values refer to a human response level below which a specified significant injury is considered unlikely to occur for a given individual.

Table 6 lists the injury criteria to which the test data was compared.  The head, chest, and femur injury criteria values used in this report are from the National Highway Transportation Safety Administration (NHTSA) Interim Final Rule that modifies the Federal Motor Vehicle Safety Standard (FMVSS) No. 208 (Occupant Crash Protection).[3] Neck injury was evaluated using two different sets of injury criteria:  (1) the injury values defined in Reference 4, and (2) the Nij prescribed in Reference 3.

The Nij defined in Reference 4 were originally the "gold standard" for evaluating neck injury.[5] However, these criteria do not account for the complex combined loading scenarios that can occur during an accident.  Instead, the individual loads and moments are assumed to be independently linked to the resulting neck injury.  For example, the injury criteria values defined for tensile injuries were set assuming that no flexion or extension moments contributed to the injury.

The new Nij accounts for these types of complex combined loading scenarios by defining four combined neck loading modes:  tension-extension, tension-flexion, compression-extension, and compression-flexion.[5] The load and moment values that define the threshold for the four neck loading modes are normalized with respect to four critical intercept values that are defined for tension, compression, flexion, and extension.  The values that are used to calculate the Nij are uniquely defined for each Hybrid III ATD ranging from the CRABI 12-month-old ATD up to the 95th-percentile male ATD.  Since the NHTSA Interim Final Rule prescribes the Nij as a new optional comparison for injury probability, it was calculated in addition to using the standard neck injury values from Reference 4.

## Table 6.  Injury Criteria

| | 5th-Percentile (F) | 50th-Percentile (M) | 95th-Percentile (M) |
|---|---|---|---|
| HIC | 1,000[1] | 1,000[1] | 1,000[2] |
| Neck Fx (lb) | +/- 438[1] | +/- 697[1] | +/-856[2] |
| Neck Fz (lb) | +468 / -567[1] | +742 / -900[1] | +910/-1,104[2] |
| Neck My (ft-lb) | +70 / -21[1] | +140/-42[1] | +190/-58[2] |
| Chest (G) | 60[2] | 60[1] | 60[2] |
| Femur (lb) | -1,530[1] | -2,250[1] | -2,594[2] |

[1]FMVSS 208 Requirement[3]
[2]Melvin, J. W., Nahum, A. M., Eds., *Accidental Injury, Biomechanics & Prevention*, Springer[4]

## 5.2  DYNAMIC SLED TEST RESULTS

The results of the four dynamic sled tests are presented in the following sections.

### 5.2.1  Test 1 – Baseline Test Results

**5.2.1.1  Pre-test Description -** This baseline test consisted of two rows of seats facing each other, with the forward-facing seat occupied by two average-size occupants (two 50th-percentile Hybrid III ATDs).  There was no table between the seats.  The sled was decelerated on impact over a 250-msec duration with an 8 G peak acceleration at 125 msec.  The actual sled deceleration parameters, compared to the specified parameters, are provided in Table 7.  Figure 16 is a pre-test photo of the test.

**Table 7.  Test No. 1 – Baseline Test, No Table, Two 50th-Percentile ATDs, 8 G Peak, Sled Acceleration**

| Sled | | | |
|---|---|---|---|
| | Peak G | Peak Time (msec) | Delta V (ft/sec) |
| Specification | 8 | 125 | 32.2 |
| Primary Sled Accelerometer | 7.5 | 132.5 | 32.3 |

**5.2.1.2  Post-test Description -** The seat components remained attached during this test.  While there was no damage to the aluminum base frame, the thermoplastic grab handles cracked.  The cracks did not propagate, however, so the entire headrest did not tear off of the seat back.  The seat cushions remained attached as well.  The window-side ATD remained compartmentalized, while the aisle-side ATD traveled over the seat back in front of it, landing on top of the headrest.

The head of the window-side ATD in this test impacted relatively low on the seat back in front of it, while the head of the aisle-side ATD hit higher up on the seat back, near the top of the headrest, causing it to crack almost to complete failure.  The reason for the difference in head impact location is due in part to the translational differences of the ATD's feet.  While both ATDs wore shoes that complied with the standard (J211), the shoes' soles were not made of the same material, and they reacted differently across the floor; specifically, the shoes on the aisle-side ATD had "bumpier" soles, which caused greater friction, and this caused the ATD to rotate forward nearly about the tip of its feet.  For the window-side ATD, the shoes allowed the ATD's feet to slide along the floor, carrying the entire body of the ATD across to the seat in front.  The

ATD's knees impacted the lip of the seat pan, causing the ATD to rotate at that time about the knees, with the head impacting the top of the seat back below the headrest. This ATD rebounded back toward the launch seat. The feet on the aisle-side ATD, however, stuck to the floor near their initial position, so the body of the ATD pivoted more about the feet than the knees, which then impacted the seat cushion (not the front lip of the seat pan) keeping the ATD more upright, allowing its head to impact the uppermost portion of the seat back, at the top of the headrest. This aisle-side ATD then traveled over the top of the seat back and did not remain compartmentalized. Figure 17 provides a three-frame sequence of the occupant kinematics for the Baseline Test No. 1, and Figure 18 provides the post-test view.
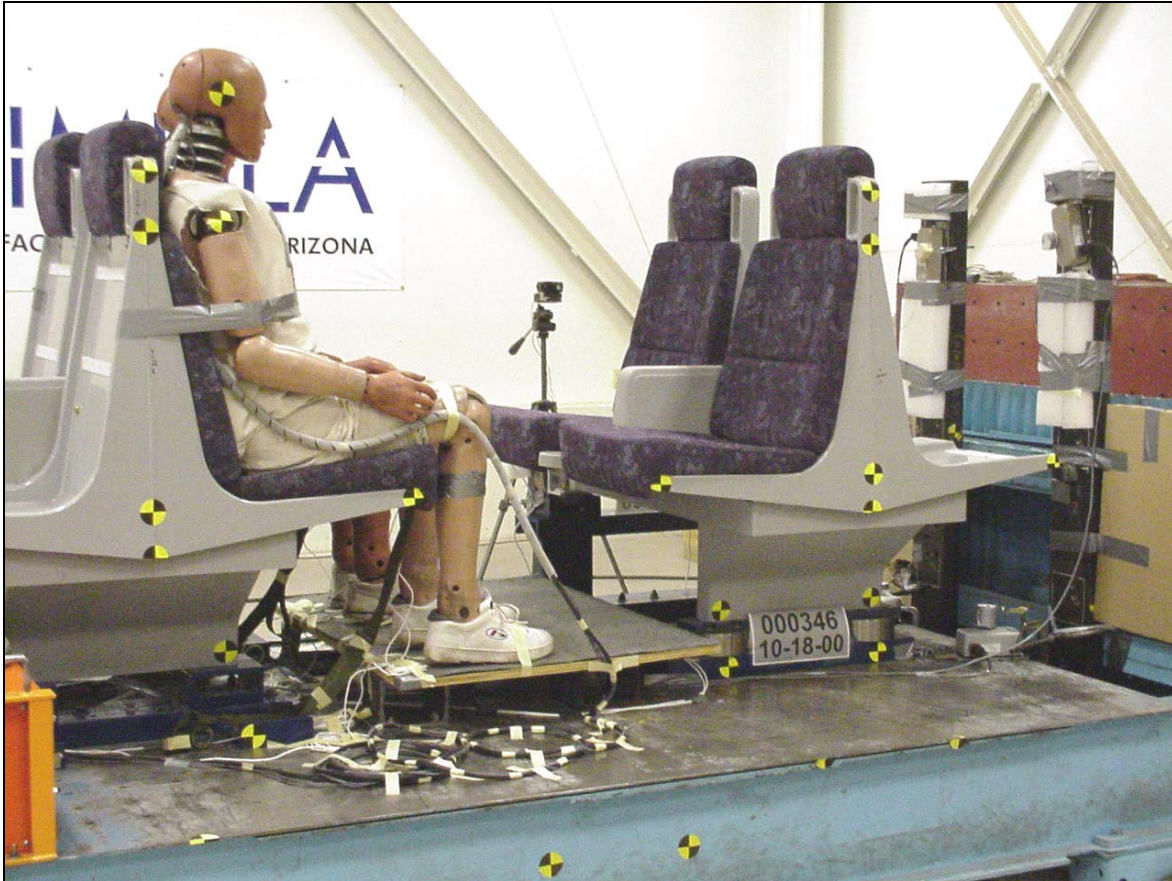


**Figure 16.  Pre-test Photo of Baseline Test No. 1**



**Figure 17.  Test No. 1, Occupant Kinematic Sequence for Two 50th-percentile ATDs, 8 G Peak, No Table**

The neck forces and moments exceeded the peak neck injury criteria in both the ATDs, and the Nij criterion was also exceeded.  Although the femur loads in both ATDs were below the injury criterion, the loads measured on the aisle-side ATD were quite a bit lower than those measured for the window-side ATD.  See Table 8 for the results of the test.

**Table 8.  Test No. 1 – Baseline Test, No Table, Two 50th-Percentile ATDs, 8 G Peak, Injury Criteria Values**

| ATD | Left Window Seat Hybrid III - ATD6 50th-Percentile | | Right Aisle Seat Hybrid III – ATD9 50th-Percentile | |
|---|---|---|---|---|
| | Spec. | Actual | Spec. | Actual |
| HIC (36-msec) | 1,000 | 265.7 | 1,000 | 104.1 |
| Neck Shear (FX)- Head aft (lb) | 697 | 694.6 | 697 | 458.4 |
| Neck Shear (FX) - Head fwd (lb) | -697 | -50 | -697 | -40 |
| Neck Flexion (My) - (ft-lb) | 140 | 64.5 | 140 | 162.9 |
| Neck Extension (My) - (ft-lb) | -42 | -37 | -42 | -25 |
| Neck Tension (FZ) - (lb) | 742 | 1,043.4 | 742 | 250 |
| Neck Compression (FZ) - (lb) | -900 | -850 | -900 | -339.0 |
| Maximum Nij | 1.0 | 1.007 | 1.0 | 0.961 |
| Chest G (max for continuous 3-msec) | 60 | 18.2 | 60 | 14.2 |
| Femur Left - (+Fx fwd) (lb) | -2,250 | -1,597.4 | -2,250 | -796.4 |
| Femur Right - (+Fx fwd) (lb) | -2,250 | -1,613.0 | -2,250 | -373.8 |

NOTE:  Shaded areas indicate where the injury criterion was exceeded.



**Figure 18.  Post-test Photo of Test No. 1, Baseline Test**

### 5.2.2  Test 2 – Baseline Test with Table

**5.2.2.1  Pre-test Description -** This test consisted of two rows of seats facing each other with a table placed between them.  The table was rigidly attached at one end to the wall using mounting hardware provided by Bombardier, and, near the other end, it was mounted to the floor with one pedestal.  The forward-facing seat was occupied by two 50th-percentile Hybrid III ATDs.  The sled was decelerated on impact over a 250-msec duration with an 8 G peak acceleration at 125 msec.  The actual sled deceleration parameters, compared to the specified parameters, are provided in Table 9.  Figures 19 and 20 are pre-test photos of the test showing an overall view of the test set-up and a closer view of the mounting fixture for the table.

**Table 9.  Test No. 2 – Baseline Test, with Table, Two 50th-Percentile ATDs, 8 G Peak, Sled Acceleration**

| | Sled | | |
|---|---|---|---|
| | **Peak G** | **Peak time (msec)** | **Delta V (ft/sec)** |
| Specification | 8 | 125 | 32.2 |
| Primary Sled Accelerometer | 8.0 | 114.8 | 33.1 |



**Figure 19.  Pre-test Photo of Test No. 2, Baseline with Table**

**Figure 20. Pre-test Photo of Test No. 2, Focusing on the Table Attachment**

**5.2.2.2 Post-test Description -** While there was no damage to the aluminum base frame, there was significant damage to the window-side grab handles on the headrest, and complete failure of the headrest on the aisle side. The table attachments sheared at the wall connection; specifically, the vertical attachment pulled the screws out of the table and failed the weld at the table's base. The table detached completely from the wall and landed on the seat in front of it.

The table restricted the window-side occupant's forward motion, preventing the head from ever hitting the seat back. The upper abdomen/lower torso of the occupant impacted the table first, causing the table to shear from its attachment points. As the occupant and table continued to travel forward, the table bounced back after impacting the front row seat, colliding again with the ATD's head. Despite these collisions with the table, this ATD remained compartmentalized.

The head of the aisle-side ATD hit the higher portion of the headrest, causing the headrest to completely fail across the seat back. This ATD again wore the shoes with the "bumpier" soles that prevented the feet from sliding across the floor, again introducing an occupant response repeatable from the last test. The higher-friction shoes caused the ATD to pivot more about the feet (instead of the knees), allowing the ATD's head to impact the top of the headrest, which completely failed. While the table prevented the aisle-side ATD from launching over the seat

back, it instead caused the ATD to pivot about the end of the table, to face toward the window, and then fall out into the aisle. Therefore, this aisle-side ATD did not remain compartmentalized. All seat cushions remained attached. Figure 21 provides a 3-frame sequence of the occupant kinematics, and Figure 22 is a post-test view of the test.



**Figure 21. Test No. 2, Occupant Kinematic Sequence for Two 50th-Percentile ATDs, 8 G Peak, with Table Installed**
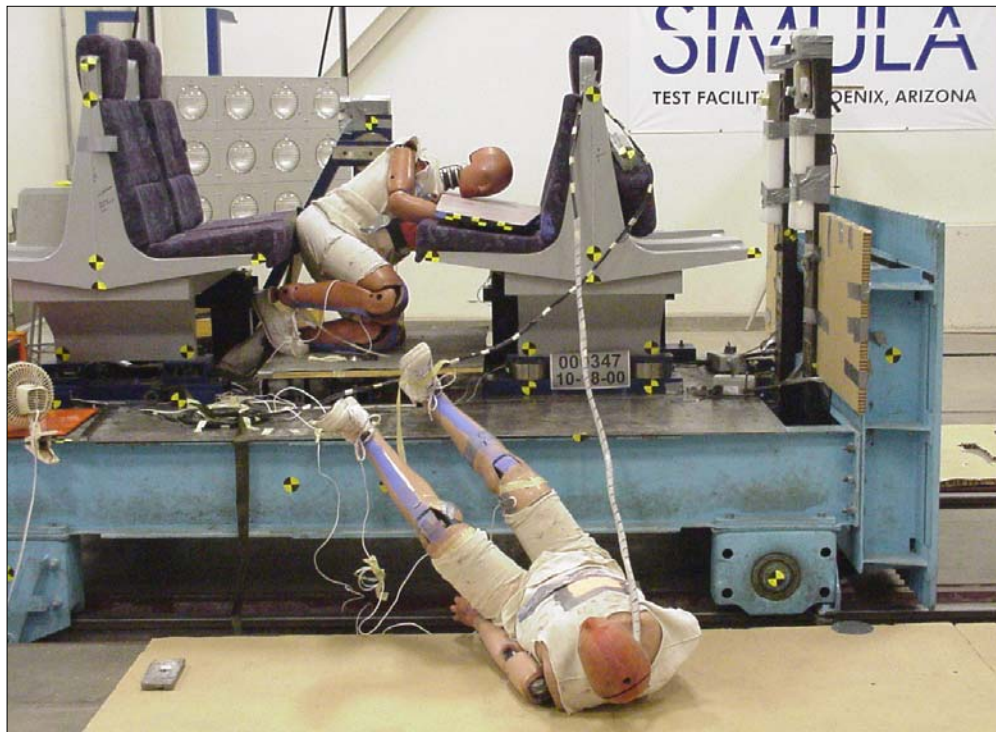


**Figure 22. Post-test Photo of Test No. 2, Baseline with Table**

The injury loads measured in this test were below the injury criteria, including the Nij criteria. While abdominal loads were not measurable, there is concern over the potential for abdominal injuries to occur when the occupant impacts the table, but these injuries are not typically life-threatening. This seat did not pass the structural strength standard, and while the injury measurements were below the criteria, it also did not pass the human injury components of the standard because the aisle-side ATD was not compartmentalized. See Table 10 for the results of the test.

**Table 10. Test No. 2 – Baseline Test, with Table, Two 50th-Percentile ATDs, 8 G Peak, Injury Criteria Values**

| ATD | Left Window Seat | | Right Aisle Seat | |
|---|---|---|---|---|
| | Hybrid III - ATD6 50th-Percentile | | Hybrid III - ATD9 50th-Percentile | |
| | Spec. | Actual | Spec. | Actual |
| HIC (36 msec) | **1,000** | 17.5 | **1,000** | 216.1 |
| Neck Shear (FX)- Head aft (lb) | **697** | 15 | **697** | 606 |
| Neck Shear (FX) - Head fwd (lb) | **-697** | -62 | **-697** | -25 |
| Neck Flexion (My) - (ft-lb) | **140** | 13 | **140** | 136.3 |
| Neck Extension (My) - (ft-lb) | **-42** | -11 | **-42** | -17 |
| Neck Tension (FZ) - (lb) | **742** | 177 | **742** | 180 |
| Neck Compression (FZ) - (lb) | **-900** | -155 | **-900** | -326.5 |
| Maximum Nij | **1.0** | 0.181 | **1.0** | 0.810 |
| Chest G ( max for continuous 3-msec) | **60** | 23.3 | **60** | 14.9 |
| Femur Left - (+Fx fwd) (lb) | **-2,250** | -1,291 | **-2,250** | -600 |
| Femur Right - (+Fx fwd) (lb) | **-2,250** | -1,282 | **-2,250** | -900 |

Note: All injury values were measured with an upper-neck load cell.

### 5.2.3  Test 3 – Baseline Test with 9 G Peak Acceleration

**5.2.3.1  Pre-test Description -** This test consisted of two rows of seats facing each other with the forward-facing seat occupied by two average size occupants (two 50th-percentile Hybrid III ATDs).  There was no table between the seats.  The sled was decelerated more severely on impact over a 250-msec duration with a 9 G peak acceleration at 125 msec. The actual sled deceleration parameters, compared to the specified parameters, are provided in Table 11.  Figure 23 is a pre-test photo of the test set up.

**Table 11.  Test No. 3 – Baseline Test, No Table, Two 50th-Percentile ATDs, 9 G Peak Sled Acceleration**

| Sled | | | |
|---|---|---|---|
| | Peak G | Peak Time (msec) | Delta V (ft/sec) |
| Specification | **9** | **125** | **36.2** |
| Primary Sled Accelerometer | 9.1 | 127.5 | 36.1 |

**5.2.3.2  Post-test Description -** The seat/occupant system in this test experienced a higher peak deceleration.  While there was no damage to the aluminum base frame, there was significant damage to the grab handles on the aisle side, causing complete failure of the headrest on that side.  The seat cushions detached from the aisle-side seat pan and seat back.

**Figure 23. Pre-test Photo of Test No. 3, Baseline Configuration with 9 G Peak Acceleration**

Due to the higher deceleration forces, the window-side ATD impacted the seat back in front of it (below the headrest) and rebounded into the back of the launch seat. The window-side ATD remained compartmentalized. The knees of the aisle-side ATD impacted the seat pan cushion rather than the lip of the seat pan, causing the ATD to translate forward more than in previous tests. The head impacted the seat back and then the torso followed. The aisle-side ATD then landed the top of its head on the seat pan of the forward-facing front-row seat. The aisle-side ATD fell outside of the compartmentalized area. Figure 24 provides a three-frame sequence of the occupant kinematics, and Figure 25 is a post-test view.



**Figure 24. Test No. 3, Occupant Kinematic Sequence for Two 50th-percentile ATDs, 9 G Peak Acceleration**
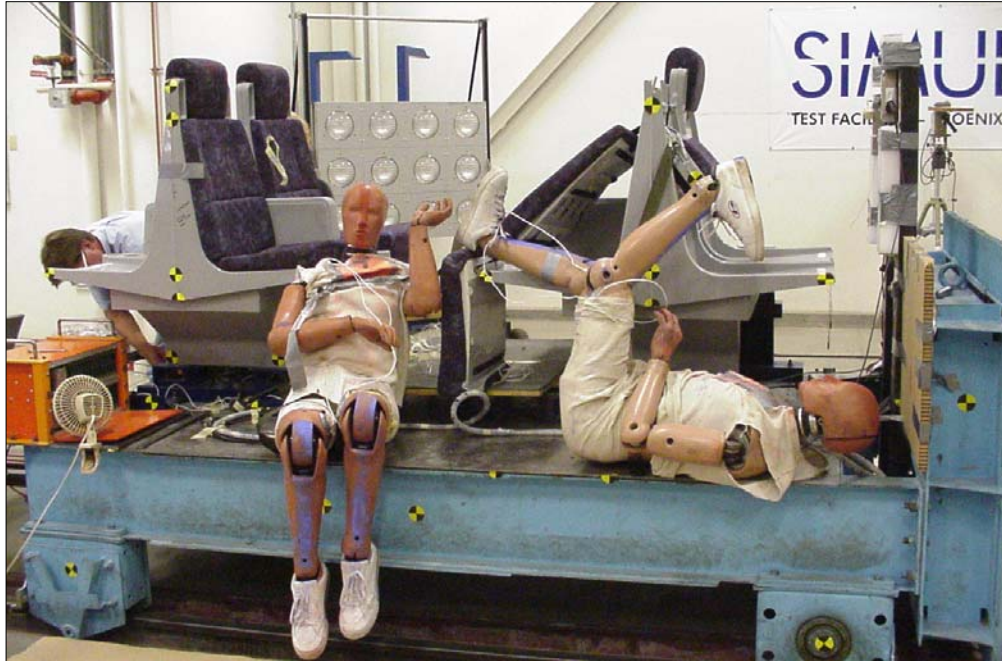
**Figure 25. Post-test Photo of Test No. 3, Baseline with 9 G Peak Acceleration (Note: The occupant shown seated on the sled was manually positioned there after the test to prevent it from falling from its precarious post-test position.)**

The window-side ATD neck forces and moments exceeded the injury criteria, and the neck-compression forces were exceeded in the aisle side ATD. This seat did not pass the structural portion of the APTA Standard, nor did it pass the human test components of the APTA Standard. See Table 12 for the results of the test.

**Table 12. Test No. 3 – Baseline Test, No Table, Two 50th-Percentile ATDs, 9 G Peak, Injury Criteria Values**

| ATD | Left Window Side Hybrid III - ATD6 50th-Percentile | | Right Aisle Side Hybrid III - ATD9 50th-Percentile | |
|---|---|---|---|---|
| | Spec. | Actual | Spec. | Actual |
| HIC (36 msec) | **1,000** | 274.6 | **1,000** | 127.8 |
| Neck Shear (FX)- Head aft (lb) | **697** | 1,183.1 | **697** | 501.2 |
| Neck Shear (FX) - Head fwd (lb) | **-697** | -75 | **-697** | -110 |
| Neck Flexion (My) - (ft-lb) | **140** | 183.7 | **140** | 126.4 |
| Neck Extension (My) - (ft-lb) | **-42** | -42 | **-42** | -33 |
| Neck Tension (FZ) - (lb) | **742** | 397.6 | **742** | 200 |
| Neck Compression (FZ) - (lb) | **-900** | -396 | **-900** | -937.8 |
| Maximum Nij | **1.0** | 1.019 | **1.0** | 0.715 |
| Chest G (max for continuous 3-msec) | **60** | 22.8 | **60** | 15.3 |
| Femur Left - (+Fx fwd) (lb) | **-2,250** | -1,689 | **-2,250** | -514.4 |
| Femur Right - (+Fx fwd) (lb) | **-2,250** | -1,375 | **-2,250** | -701.1 |

Note: Shaded regions indicate injury values above the specified injury criteria. All injury values were measured with an upper-neck load cell.

### 5.2.4  Test 4 – Baseline Test with Different Sizes of ATDs

**5.2.4.1  Pre-test Description -** This test consisted of two rows of seats facing each other with the forward-facing seat occupied by two different sizes of ATDs; one 5th-percentile female ATD in the aisle seat, and one 95th-percentile ATD in the window seat.  There was no table between the seats.  The sled was decelerated on impact over a 250-msec duration with an 8 G peak acceleration at 125 msec.  The actual sled deceleration parameters, compared to the specified parameters, are provided in Table 13.  Figure 26 is a pre-test photo of the test.

**Table 13.  Test No. 4 – Passenger Injury Seat Strength Test, No Table, Two ATDs - One 5th- and One 95th-Percentile, 8 G Peak, Sled Acceleration**

| | Sled | | |
|---|---|---|---|
| | **Peak G** | **Peak time (msec)** | **Delta V (ft/sec)** |
| Specification | **8** | **125** | **32.2** |
| Primary Sled Accelerometer | 8.3 | 115.0 | 32.6 |



**Figure 26.  Pre-test Photo of Test No. 4, Baseline with 5th- and 95th-Percentile Size ATDs**

**5.2.4.2  Post-test Description -** While there was no damage to the aluminum base frame, there was significant damage to the window-side grab handle, causing complete failure of the headrest on the window side.  In previous tests, the headrests on the aisle side failed, but in this test, the window-side seat was occupied by a 95th-percentile ATD that created a higher impact load on the headrest.  Additionally, the added height of the 95th-percentile ATD caused its head to

impact the upper part of the seat back (the headrest area), failing the headrest. There was very little head/neck bending during the transition of the ATD through the headrest. The ATD's chest hooked on top of the headrest, and then the body traveled forward until the abdomen landed on the headrest. The top of the head of the ATD landed severely on top of the seat pan of the forward-facing front-row seat. The window-side ATD did not stay compartmentalized.

The aisle-side was occupied by a 5th-percentile ATD that did not have the height or the weight to impact high on the seat back or induce forces high enough to cause seat failure. The 5th-percentile ATDs feet did not touch the floor, so its shoes or feet did not play any role in the ATD's motion. The top of the head of the 5th-percentile ATD impacted well below the base of the headrest, causing its head/neck to bend severely. Since the seat did not absorb as much energy through a structural failure, the 5th-percentile ATD absorbed the loads instead, thus creating neck forces and moments that exceeded the injury criteria. The seat cushions remained attached in this test (there was no translational motion of the seat pan cushion from the knees of the 5th-percentile ATD). The 5th-percentile ATD remained compartmentalized between the two seat rows.

This seat did not meet the structural requirements of the APTA Standard. While the 95th-percentile ATD did not remain compartmentalized, it is currently only a requirement for the 50th-percentile ATD to remain compartmentalized during testing. Figure 27 provides a three-frame sequence of the occupant kinematics, and Figure 28 is a post-test view of the test. See Table 14 for the results of the test.



**Figure 27. Test No. 4, Occupant Kinematic Sequence for the 5th- and 95th-Percentile ATDs, 8 G Peak Acceleration**

**Figure 28. Post-test Photo of Test No. 4, Baseline Test with 5th- and 95th-Percentile ATDs**

**Table 14. Test No. 4 – Passenger Injury Seat Strength Test, No Table, Two ATDs - One 5th- and One 95th-Percentile, 8 G Peak, Injury Criteria Values**

| ATD | Window (Left Side) Hybrid III - ATD8 95th-Percentile | | Aisle (Right Side) Hybrid III - ATD5 5th-Percentile | |
|---|---|---|---|---|
| | Spec. | Actual | Spec. | Actual |
| HIC (36 msec) | **957** | 139.3 | **1,113** | 205.5 |
| Neck Shear (FX)- Head aft (lb) | **856** | 556.4 | **438** | 382.7 |
| Neck Shear (FX) - Head fwd (lb) | **856** | -50 | **438** | -40 |
| Neck Flexion (My) - (ft-lb) | **190** | 145.2 | **70** | 31.7 |
| Neck Extension (My) - (ft-lb) | **58** | -33.3 | **-21** | -37.0 |
| Neck Tension (FZ) - (lb) | **910** | 170 | **468** | 180 |
| Neck Compression (FZ) - (lb) | **1,104** | -1,020.3 | **-567** | -783.3 |
| Maximum Nij | **1.0** | 0.513 | **1.0** | 1.704 |
| Chest G (max for continuous 3-msec) | **54** | 20.7 | **73** | 10.9 |
| Femur Left - (+Fx fwd) (lb) | **-2,594** | -1,517.0 | **-1,391** | -1,051.1 |
| Femur Right - (+Fx fwd) (lb) | **-2,594** | -1,629.8 | **-1,391** | -940.5 |

Note: Shaded regions indicate injury values above the specified injury criteria. All injury values were measured with an upper-neck load cell.

## 5.3 TYPICAL SEAT FAILURES

There were several seat failures that were repeated in all four tests. The headrest portion of the seat back sheared completely from the remaining part of the seat back, leaving a jagged, fiber-pronged edge (see Figure 29). The headrest failure occurred after the grab handles cracked (see Figure 30). Figure 31 shows the markings of a typical collision between the launched ATD and

the seat in front of it.  The knees impacted the cushion, causing it to translate forward.  The head of the ATD squarely impacted the center of the headrest, in many cases causing its failure.  The window-side headrest predominantly stayed intact.



**Figure 29.  Jagged Seat Back Edge Resulting from Failed Headrest**



**Figure 30.  Broken Grab Handles**
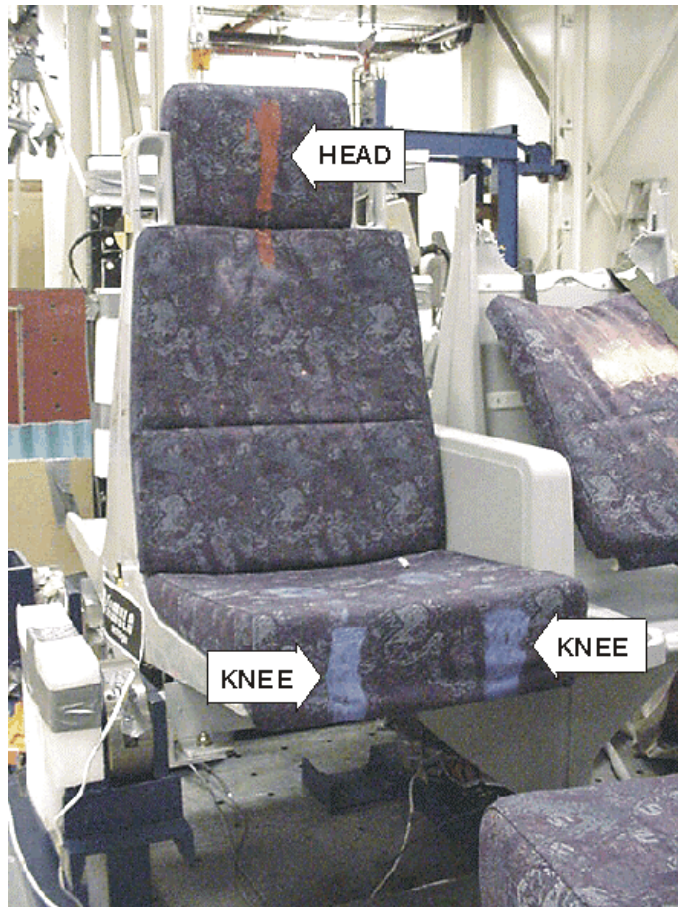
**Figure 31. Chalk Markings Left on Opposite Seat by Forward-Traveling ATD**

# 6. SEAT/OCCUPANT COMPUTER MODELING

The Bombardier seat/occupant computer model was designed to serve three major functions in this investigation: (1) to predict the dynamic response of the occupants and the seat during the dynamic tests, (2) to help researchers identify the most significant parameters to be investigated during the dynamic tests, and (3) to serve as a seat design tool for future use.

## 6.1 THE MADYMO COMPUTER SIMULATION TOOL

Computer model simulations of the seat/occupant crash dynamics were created using the MADYMO analysis program supplied by TNO, which is based in the Netherlands. The MADYMO software utilizes multi-body techniques to simulate the gross motion of systems of rigid and deformable bodies that are connected by complex kinematical joints. The components of the system that are to be modeled are represented as individual bodies using planes, ellipsoids, and/or cylinders. A unique set of characteristics is defined for each body, which includes appropriate dimensions, inertial properties, loading and unloading characteristics, damping, hysteresis, friction, and orientation. Kinematic joints are then used to connect the bodies to each other and to inertial space. The joints are also used to provide constraints for the motion of the bodies and their components in inertial space. Detailed contact interactions are defined between bodies that are expected to come into contact with each other during the simulated crash sequence. In addition, for the multi-body techniques, finite-element techniques can be used to simulate the behavior of structures. Finite-element meshes are created within systems or as separate systems to represent structural components that have very detailed or complex geometric and/or material properties. Contact interactions can be defined between meshes and/or between meshes and rigid bodies.

## 6.2 DESCRIPTION OF THE SEAT/OCCUPANT COMPUTER MODEL

### 6.2.1 Occupant Model

The software vendor, TNO, provides a complete library of validated child and adult ATD models for use in frontal, side, rear, and rollover impacts, as well as pedestrian-vehicle interactions. The most widely used ATD model for frontal impact applications is the Hybrid III ATD. Three different-sized Hybrid III ATDs were selected for use in this model: the 5th-percentile female, the 50th-percentile male, and the 95th-percentile male. These three Hybrid III ATDs represent a wide range of occupant sizes from a small female to a large male. As illustrated in Figure 32, each adult Hybrid III ATD is modeled in a seated position as a system of elliptically shaped masses, interconnected by joints.

### 6.2.2 Seat Model

Design of the Bombardier seat model required detailed knowledge of the seat's geometric, inertial, and material properties. To re-create the physical characteristics of the Bombardier seat, the model designer utilized several different references including: (1) engineering design drawings of the seat, (2) descriptions of the seat materials, (3) data collected from a quasi-static load/deformation test of the seat, and (4) the seat itself. Using this information, the components

of the seat were created using both the multi-body and finite-element features of the MADYMO program.



**(a)**                     **(b)**                     **(c)**
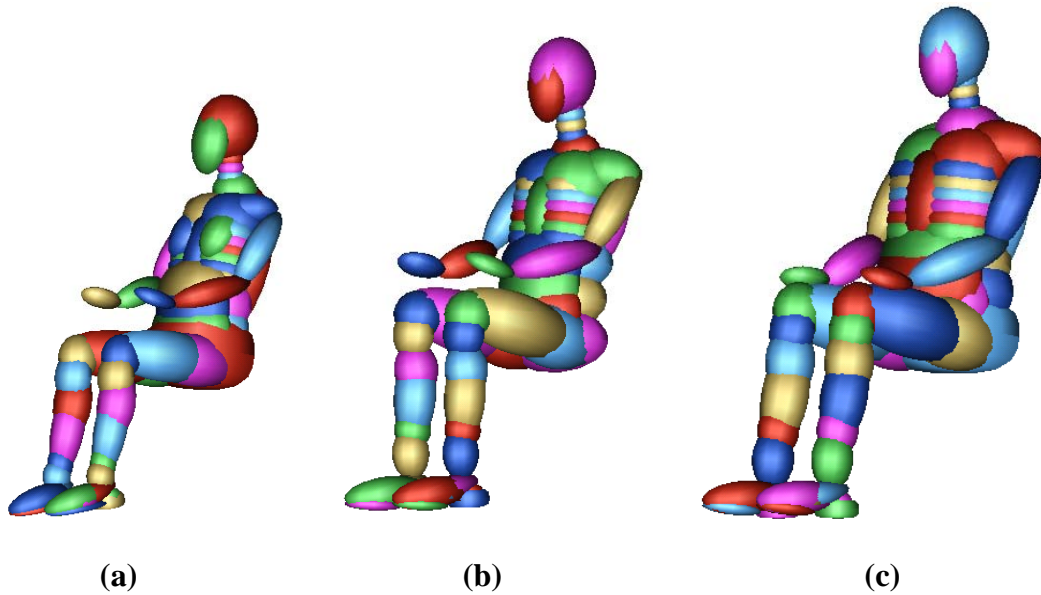
**Figure 32.  MADYMO Hybrid III Seated Adult ATD Models:**
**(a) 5th-Percentile Female, (b) 50th-Percentile Male, and (c) 95th-Percentile Male**

As illustrated in Figure 33, the seat model was organized into three separate systems:  the sled floor, the front seat assembly, and the back seat assembly.  A 65-inch seat pitch separated the front and back seat assemblies on the sled floor.  Ellipsoids were used to represent the bottom, back, and headrest seat cushions, while finite-element meshes represented the complex contour of the seat pan/back structure and the pedestal.  The original design of the model was created based on the results generated from the quasi-static load/deformation test.  This test revealed that the Bombardier seat structure is extremely rigid and, as a result, minimal deflection of the seat was observed.  Since the test was conducted by loading the cushions and seat pan/back structure together as a single unit, the model designer elected to lump the load/deformation characteristics of these two components into a single component.  This was accomplished by simulating the rigidity of the entire seat structure; i.e., the seat cushions and the seat pan/back structure that included the rigid aluminum base frame, using only the cushion ellipsoids.  Appropriate penetration parameters were defined to allow the ellipsoids to mimic the crush of the cushion foam during occupant loading.  Contact interactions were defined between the occupants and the ellipsoid seat cushions.  The finite-element meshes were only added for visual effect, and thus, no contacts were defined between the occupants and the meshes.

The Bombardier seat is secured to the interior of a passenger rail car via four attachment points: two attachment points between the seat frame and the wall of the car, and two attachment points between the pedestal and the floor of the car.  Load cells were added to the seat model to measure the loads exerted at each of the four attachment points on the seat during impact.
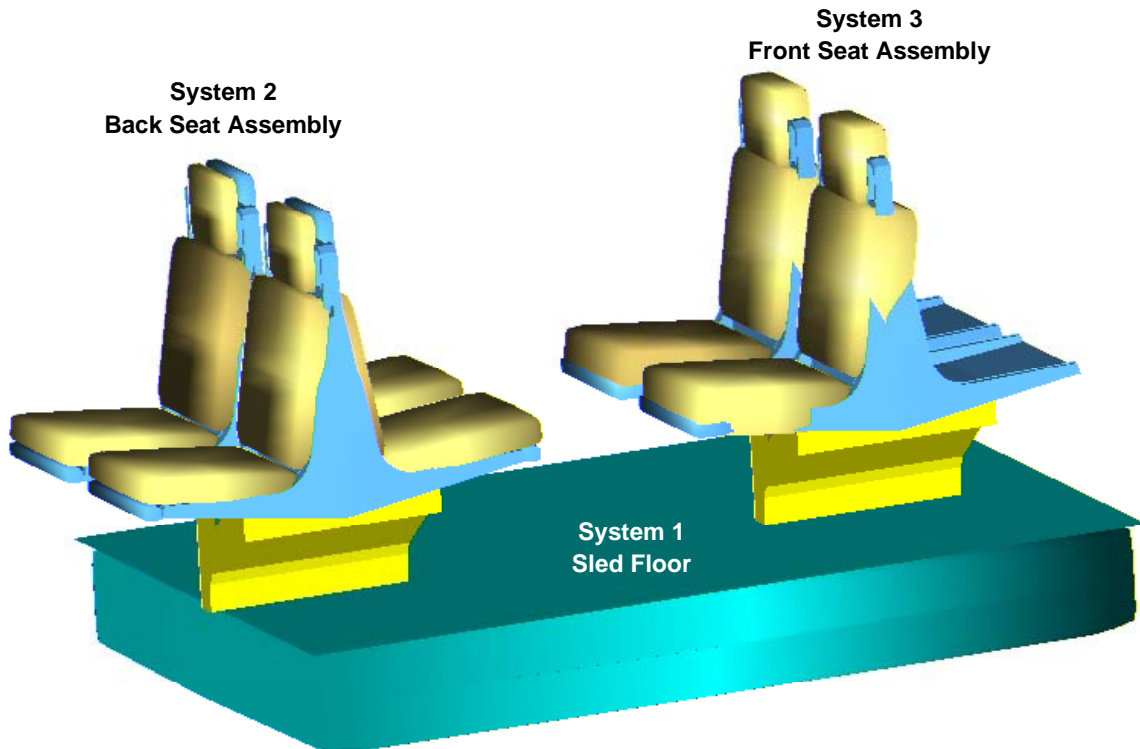
**Figure 33.  Bombardier Seat Computer Model**

## 6.3  MODELING ANALYSIS AND RESULTS

Once the initial seat/occupant models were developed, a series of simulations was conducted to help to understand the effects of altering specific parameters of the model on the gross motion, forces, and accelerations experienced by each occupant.  The purpose of the computer analysis was to determine which combinations should be considered and incorporated into the dynamic sled tests to ensure adequate occupant protection under probable seating combinations.  As shown in Table 15, five parameters were varied for the analysis:  (1) occupant size, (2) occupant position in the front-facing seats, (3) occupant position in the rear-facing seats, (4) set-up with or without a table, and (5) crash pulse.  Initially, the crash pulse for all configurations was to remain as the APTA Standard dynamic triangular pulse of 250-msec duration and an 8 G peak.  However, the last five simulations, which incorporated occupants in the rear-facing seats, were replaced with simulations that incorporated a range of crash pulses instead.  Seat pitch and seat type remained constant.

When preparing to run the last five simulations, No. 11 through 15, there was difficulty achieving the desired occupant configuration(s).  It was difficult to position the two aft-facing 95th-percentile male ATDs across from the front-facing ATDs, because an appropriate initial position of the occupants' feet and legs could not be achieved without drastically biasing the kinematics of the occupants during the impact.  For example, there is knee interaction when the two 95th-percentile ATDs are facing each other.  In this situation, the ATD in the direction of travel is biased to land in the aisle if its knees are positioned toward the aisle to avoid the opposing-facing ATD's knees.  Given this biased and potentially difficult validation scenario, the

last five configurations were replaced with the baseline configuration in a variety of crash pulses that could be compared with results found in actual full-scale passenger rail collision tests and sled tests.

Analysis of the data from the full-scale rail crash passenger vehicle passenger impact tests conducted in November 1999 (a single-car test) and April 2000 (a two-car test), revealed that the specified crash pulse (8 G at 125 msec) that was being used in the modeling work was not completely representative of the crash pulses that were measured during full-scale testing.[6, 7, 8] The measured crash pulses had slightly higher peaks than the prescribed pulse. As a result, the decision was made to conduct simulation runs with the crash pulses that were produced during the two full-scale crash tests for the single-car crash test[6] and the leading and trailing cars of the two-car crash test.[7, 8] Simulation runs were also conducted with the ideal, triangular pulse with 7 G and 9 G peaks. A sled test with the 9 G peak was conducted and compared with this simulation run.

**Table 15. Model Simulation Matrix**

| Configuration No.[2] | Occupant Size Front-Facing Seats Back Assembly | | Occupant Size Rear-Facing Seats | | Table | Crash Pulse[1] (G) |
| --- | --- | --- | --- | --- | --- | --- |
| | Aisle | Window | Front Assembly | Back Assembly | | |
| 1 (baseline) | 50 | 50 | | | | 8 |
| 2 | 0 | 5 | | | | 8 |
| 3 | 95 | 5 | | | | 8 |
| 4 | 5 | 95 | | | | 8 |
| 5 | 95 | 95 | | 2x 50 | | 8 |
| 6[3] | 50 | 50 | | | Table | 8 |
| 7 | 0 | 5 | | | Table | 8 |
| 8 | 95 | 5 | | | Table | 8 |
| 9 | 5 | 95 | | | Table | 8 |
| 10 | 95 | 95 | | 2x 50 | Table | 8 |
| 11 (void) | 50 | 50 | 2x 95 | | | 8 |
| 12 (void) | 0 | 5 | 2x 95 | | | 8 |
| 13 (void) | 95 | 5 | 2x 95 | | | 8 |
| 14 (void) | 5 | 95 | 2x 95 | | | 8 |
| 15 (void) | 95 | 95 | 2x 95 | 2x 50 | | 8 |
| 11 | 50 | 50 | | | | 7 |
| 12 | 50 | 50 | | | | 9 |
| 13 | 50 | 50 | | | | Single car[4] |
| 14 | 50 | 50 | | | | Lead car[5] |
| 15 | 50 | 50 | | | | Trailing car[5] |

(1) Standard Crash pulse is 250-msec triangular with 8 G peak[1]
(2) Shaded configurations were tested
(3) The baseline configuration with table was not correlated with the test results because the table attachment failed in the dynamic test
(4) Longitudinal acceleration pulse from the single-car crash test[6]
(5) Longitudinal acceleration pulse from the two-car crash test[7, 8]

The size and positioning of the occupants were selected to evaluate the most potentially vulnerable scenarios for the seat and the occupant. For instance, using two 95th-percentile Hybrid III ATDs will severely test the integrity of the seat during impact. However, they will

not likely sustain high injury values due, in part, to the probability of large amounts of seat deformation and energy absorption. On the other hand, one 5th-percentile Hybrid III ATD tested in the same seat may sustain high injury values, but will not test the structural integrity of the seat.

Observations were made of the output produced by the 15 simulation runs. These observations represent trends based on the initial model configurations, and are not of the models that were later validated against dynamic test data. The original seat model did not include the frangible headrest or the seat cushion that could compress and translate as was modified for the final model. Based on the rigid configuration of the original model, the forward motions of the occupants were not affected by their seat position (window versus aisle), nor were they affected when they were seated alone, or with a larger/smaller occupant, or with an occupant of the same size. The typical forward occupant motion began with the occupant sliding forward in its seat, its feet sliding forward on the floor, and its knees impacting the seat pan in front of it, with little penetration into the seat pan cushion. The occupant then pivoted about the knees, causing the head/neck to impact the lower portion of the headrest. The 5th-percentile occupant impacted the middle of the seat back and the 95th-percentile occupant impacted the upper part of the headrest.

The occupant responses to the variations in the crash pulse were most notable for those simulations using actual crash pulses from the single- and two-car collision tests. The occupants in these simulations were not contained between the seats, but instead broke the seat at the lower pivot point that had been determined from the static testing. The 7 G and 9 G crash pulses produced occupant responses that could be extrapolated from the occupant responses to the standard 8 G pulse.

Simulations that included rear-facing occupants seated in the back seat assembly did not have any noticeable affects on the kinematics of the front-facing occupants in the back seat assembly. As a result, the rear-facing occupants (50th-percentile male ATDs) seated in the back seat assembly were removed from the simulation matrix. Simulations that included the table consistently prevented the occupants from traveling beyond the table's edge and produced low injury values in the head, neck, chest, and femurs.

Four configuration models (Configurations No. 1, 4, 6, and 12) were dynamically tested and then compared with the results of these simulations. Data input files for three of these configurations were then refined and correlated with the test results. Configuration No. 4 was not validated, because it consisted of a rigidly attached table that could not be compared with test results that showed that the table attachment failed.

Table 16 displays the parameter values of the configuration models that were tested and later validated.

### Table 16. Final Model Simulation Matrix

| Model No. | Aisle Occupant (Percentile) | Window Occupant (Percentile) | Table? | Pulse (G) |
|-----------|------------------------------|-------------------------------|--------|-----------|
| 1 | 50th | 50th | No | 8 |
| 2 | 50th | 50th | No | 9 |
| 3 | 5th | 95th | No | 8 |

## 6.4 MODIFICATIONS TO THE MODEL

The purpose of correlating the model to the testing was to design a baseline Bombardier seat model that could be used to simulate the kinematics and kinetics of any adult Hybrid III occupant size in either the aisle or window seat, in both the front- and/or back-seat assembly. Following the dynamic-impact tests, the test video was compared to the animation generated from the model simulations. The comparison revealed that the gross motion of the occupants did not correlate well with the dynamic test video. To improve the correlation between the test video and the model animation, and to validate the model for future use, several modifications were made to both the occupants and the seats in the model. The selected modifications were performed in an effort to closely match the timing, shape, and magnitude of the head acceleration and femur loads recorded during the dynamic tests. Since three different sizes of occupants were being used in the model, several compromises had to be made among the three occupant sizes in order to generate the desired baseline model.

### 6.4.1 Occupant Positioning

The initial seating position and sitting height of the occupants in the model did not replicate the occupant positioning in the dynamic test video. The ATD's seating position was corrected by re-orienting the position of the ATD in the plane of the seat and by modifying the ATD's elbow, hip, knee, and ankle joint angles until they mirrored the ATD's joint angles in the test video. The sitting height was adjusted by altering the position of the occupant perpendicular to the plane of the seat and by adjusting the material characteristics of the seat cushion.

### 6.4.2 Crash Pulse

Initially, the ideal crash pulse (8 G at 125 msec) was used to run the model simulations. Following the impact testing, the recorded crash pulses from each test were input into the model. The crash pulse time-history from Test No. 4 was input directly into Model Configuration 3. The crash pulses recorded for Test No. 1 and 3 were re-created from hard-copy plots of the recorded time histories and were input into Model Configurations 1 and 2, respectively.

### 6.4.3 Coefficients of Friction

The shoes worn by the aisle-side 50th-percentile ATDs in Tests No. 1 and 3 had knobbier soles than the shoes worn by their counterparts in the window seats. These knobby shoes apparently "stuck" to the floor, preventing the ATD's feet from sliding. The shoes worn by the aisle-side ATD in the model had a lower coefficient of friction than its counterpart in the dynamic test did, which allowed the aisle-side ATD in the model to translate forward at a faster rate than the aisle-

side ATD in the dynamic test.  To correct for the differences between the test video and the model's animation, the coefficient of friction between the model's aisle-side occupant's shoes and the sled floor was increased until the motion and timing of the occupant's translation matched the test video.

### 6.4.4  Seat Cushion Parameters

Each seat cushion for the window and the aisle seats was modeled as two separate components. However, the seat characteristics remained constant between the two cushions to allow the occupants to be placed in any seat for future modeling work.  Two different seat cushion parameters were altered in the model:  seat cushion stiffness and translation.

Seat cushion stiffness was adjusted to match the penetration of the occupant into the seat bottom, back, and headrest.  An average stiffness was used in order to accommodate all three occupants.

Forward translation of the seat cushion was added to simulate the crushing of the cushion under shear loading from the occupant's femur. The 5th-percentile female ATD was the occupant that was most affected by the absence of this feature in the model and, as a result, the translational joint characteristics were matched to the test video based primarily on the motion of the 5th-percentile female ATD.  The amount of cushion translation that was needed was determined by evaluating the impact timing, cushion travel distance, and the occupant femur loads.

### 6.4.5  Break-Away Headrest

In the dynamic tests, the impact that occurred between the heads of the 50th-percentile and 95th-percentile male ATDs and the headrest of the front seat assembly forced the headrest to rotate forward and break away from the seat assembly.  To simulate this headrest motion in the model, the designer had to determine the torque versus time and torque versus angle of the headrest, as well as the location of the center of rotation of the headrest.  The location of the breakpoint of the headrest was determined by examining the tested seats.  The fracture sites were located on the actual test articles and were used to define the center of rotation of the headrest.  A revolute joint was added at the center of rotation and a joint torque was defined to simulate when the break-away would occur.  The joint torque values were adjusted until the timing of the break-away matched the test video and the head accelerations of the 50th-percentile and 95th-percentile male ATD occupants in the model matched the head accelerations recorded during the test.  Since the headrest motion affected the kinematics and kinetics of both the 50th-percentile and 95th-percentile male ATDs, a compromise was made between the ATDs when defining the characteristics of the joint.

### 6.4.6  ATD Knee Joint

The femur load data from the original model contained numerous spikes that were not observed in the femur load data recorded during the dynamic test.  These spikes originated due to a difference in the construction of the Hybrid III's knee joint.  The knee joint of the Hybrid III ATDs used in the dynamic tests was a pure rotational joint, allowing only one degree of freedom. The knee joint of the Hybrid III ATD used in the MADYMO model was a revolute and

translational joint, which allowed two degrees of freedom. A two-degree of freedom joint is available as an option in the Hybrid III ATD, but it was not used in these tests. The spikes in the femur load data were caused by the translational motion occurring at the occupant's knee joint in the model. The spikes were eliminated by removing the translational degree of freedom from the ATD's knee joint.

# 7.  COMPARISON OF TEST AND MODELING RESULTS

This section compares the results from three of the dynamic sled tests and their three corresponding seat/occupant computer model simulations.  The comparative models for Tests 1 (Model 1), 3 (Model 2), and 4 (Model 3) were refined and validated.  Test No. 2 (the baseline test with the table) was not refined; the table attachment in the dynamic test failed, while the table in the model was rigid.  Due to the failure modes of the table attachment points, some of which included metal shearing, Volpe decided not to include the table configuration with failure in the validation and comparison task.

Injury threshold comparisons for each test are provided in Tables 17, 18, and 19.  These tables contain the Head Injury Criterion (HIC) (36 msec), the maximum Nij, and the percent of neck injury risk.  Details about the Nij and the percent injury risk values are provided in Appendix D.  The percent injury risk values are based on the maximum Nij value, where an Nij of 1 is equivalent to a 15-percent risk of an AIS-3 neck injury.[5]  The tables for each test also contain the maximum chest acceleration during a continuous 3-msec period and the maximum left and right femur loads.  Appendices B, D, G, and H provide comparisons between the test results and the validated modeling outputs.  A comparison of the sled pulse is in Appendix B.  Appendix D compares the Nij in a data table, and Appendix G compares the occupant injury data plots.  A visual comparison between the dynamic test's results and the model's outputs is provided in Appendix H.  It is important to note that the original parametric analysis was conducted with the specified idealistic crash pulse; i.e., a triangular, 250-msec, 8 G peak pulse.  After the dynamic tests were conducted, the actual sled deceleration pulse for each test was input into the corresponding model and re-run.

## 7.1  DYNAMIC TEST NO. 1, MODEL CONFIG. 1 – BASELINE TEST

*Comparison to Injury Threshold*:  Table 17 compares the injury parameters calculated for Test No. 1 and Model 1.  In the dynamic test, all of the injury parameters for both occupants were below their respective injury thresholds, with the exception of the Nij for the window occupant.  The maximum Nij for the window occupant slightly exceeded the maximum allowable Nij value of 1.0, indicating that the risk for neck injury was greater than 15 percent.  Similar to the dynamic test, the model predicted that the maximum Nij for the window occupant would also exceed the injury tolerance criteria.  However, the model predicted that the injury risk to the occupant would be significantly greater (94.2 percent).  The model also predicted that the Nij for the aisle occupant would exceed the injury criteria.  This differed from the test results, which indicated that the Nij for the aisle occupant remained below the injury criteria.  In addition to exceeding the Nij criteria, the window occupant also significantly exceeded the HIC value in the model.  The model predicted all other injury criteria to remain below their respective threshold values.  Good correlation between the test and the model is observed for the Nij, chest, and left femur load for the aisle occupant and the right femur load for the window occupant.

**Table 17. Comparison of Maximum Injury Parameters for Test No. 1 and Model 1**

| | Aisle | | | Window | | |
|---|---|---|---|---|---|---|
| | Injury Criteria | Test No. 1 | Model 1 | Injury Criteria | Test No. 1 | Model 1 |
| Occupant | **50th male** | **50th male** | **50th male** | **50th male** | **50th male** | **50th male** |
| HIC (36 msec) | **1,000** | 104.1 | 566.7 | **1,000** | 265.7 | 4,218.8 |
| Max Nij | **1.0** | 0.961 | 1.857 | **1.0** | 1.007 | 3.063 |
| Percent neck injury risk (%) | **15** | 14.11 | 53.92 | **15** | 15.39 | 94.20 |
| 3-msec chest acceleration (G) | **60** | 14.2 | 21.48 | **60** | 18.2 | 29.26 |
| Left femur load (lb) | **-2,250** | -796.4 | -708.3 | **-2,250** | -1,597.4 | -1,811.2 |
| Right femur load (lb) | **-2,250** | -373.8 | -709.0 | **-2,250** | -1,613.0 | -1,762.3 |

Note: Shaded regions indicate injury values above the specified injury criteria.

*Comparison of Occupant Injury Data Time-History Curves*: Overall, the time-history curves indicate a good correlation in the timing and shape of the curves. Minor delays in the onset of head acceleration and of neck loads and moments in the model resulted from the slight difference in the kinematics of the torso following knee impact. In the model, the occupant's knees do not translate along the seat cushion as far as they do in the dynamic test; therefore, the model occupant's lower body is stopped sooner by its knees impacting the seat pan during the crash sequence. The result is that the model occupants travel a longer distance before impacting the front seat assembly. The occupant's head ends up impacting the seat later in time and at a lower location along the height of the seat back. The difference in head impact locations on the seat contributes to the differences noted in the head accelerations (HIC). Time delays for the various curves averaged 11 msec.

In terms of the correlation between the magnitudes of the injury data from the model and the dynamic test, the aisle occupant maintained values that are both higher and lower than the peak magnitudes of the corresponding dynamic test data. For example, the neck moments and left femur loads were all lower in magnitude than the dynamic test values. The head acceleration, shear neck force, axial neck force, and right femur loads were slightly higher that the dynamic test values. The window occupant maintained values that were generally higher in magnitude (head acceleration, chest acceleration in the x and z directions, neck loads, neck bending moments, and femur loads) than the dynamic test values. This may have resulted from differences in the stiffness characteristics and cushion properties of the model's seat and the dynamic test's seat, and is based on the difference in the way that the occupants impacted the seat structure.

*Seat Attachment Load Comparisons*: The predicted and actual loads at the seat attachments are compared in Appendix F. A comparison of the model and dynamic test data revealed that the model seat attachment load curves were very close in magnitude, timing, and shape to the dynamic test seat attachment load curves. The onset of the loads consistently occurred around 150 to 160 msec.

## 7.2  DYNAMIC TEST NO. 3, MODEL CONFIG. 2 – BASELINE WITH 9 G PEAK

*Comparison to Injury Threshold*: Table 18 compares the injury parameters calculated for Test No. 3 and Model 2. In the dynamic test, the maximum Nij for the window occupant slightly exceeded the maximum allowable Nij value of 1.0, indicating that the risk for neck injury was

greater than 15 percent. Similar to the dynamic test, the model predicted that the maximum Nij for the window occupant would also exceed the injury tolerance criteria. However, the model predicted that the injury risk to the occupant would be significantly greater (72.47 percent). The aisle occupant also exceeded the Nij criteria in the model at an injury risk value of 21.52 percent. In addition to exceeding the Nij criteria, the window occupant also exceeded the femur loads for both the right and left femur. The model predicted all other injury criteria to remain below their respective threshold values. Good correlation between the test and the model is observed for the chest and right femur load for the aisle occupant, as well as the chest load for the window occupant. The HIC values recorded in the model were greater for both occupants.

*Comparison of Occupant Injury Data Time-History Curves*: Overall, the occupant injury time-history curves indicate a good correlation in the timing and shape between the dynamic test results and the modeling data. In the model, the head and chest accelerations are delayed in time and the magnitudes are slightly higher than recorded in the dynamic test. Minor delays in the onset of head acceleration resulted from the slight difference in the kinematics of the torso following knee impact. In the model, the occupants' knees do not translate along the seat cushion as far as they do in the dynamic test. Since the lower body of the model is stopped sooner during the crash sequence, the model's occupants have a longer distance to travel before their upper body impacts the front seat assembly. The head ends up impacting the seat later in time and at a lower location along the height of the seatback.

**Table 18. Comparison of Maximum Injury Parameters for Test No. 3 and Model 2**

|  | Aisle | | | Window | | |
|---|---|---|---|---|---|---|
|  | **Injury Criteria** | **Test No. 3** | **Model 2** | **Injury Criteria** | **Test No. 3** | **Model 2** |
| Occupant | **50th Male** | **50th Male** | **50th Male** | **50th Male** | **50th Male** | **50th Male** |
| HIC (36 msec) | **1,000** | 127.8 | 685.2 | **1,000** | 274.6 | 734.8 |
| Max Nij | **1.0** | 0.715 | 1.195 | **1.0** | 1.019 | 2.230 |
| Percent neck injury risk (%) | **15** | 8.76 | 21.52 | **15** | 15.73 | 72.47 |
| 3-msec chest acceleration (G) | **60** | 15.3 | 10.33 | **60** | 22.8 | 27.69 |
| Left femur load (lb) | **-2,250** | -514.4 | -901.0 | **-2,250** | -1,689 | -2,323.5 |
| Right femur load (lb) | **-2,250** | -701.1 | -898.4 | **-2,250** | -1,375 | -2,542.3 |

Note: Shaded regions indicate injury values above the specified injury criteria.

Good shape and timing correlation were observed among the shear neck load and the femur loads. The magnitude of these curves is slightly higher in the model than in the test.

*Seat Attachment Load Comparisons*: The predicted and actual loads at the seat attachments are compared in Appendix F. A comparison of the model and dynamic test data revealed that the model's seat attachment load curves were very close in magnitude, timing, and shape to the dynamic test's seat attachment load curves. The onset of the loads consistently occurred around 150 to 160 msec.

## 7.3 DYNAMIC TEST NO. 4, MODEL CONFIG. 3 – BASELINE WITH 5TH- AND 95TH-PERCENTILE ATDS

*Comparison to Injury Threshold*: Table 19 compares the injury parameters calculated for Test No. 4 and Model 3. In the dynamic test, the neck injury loads in the 5th-percentile female aisle

occupant exceeded the injury criteria, whereas in the model, the neck injury loads exceeded the injury parameters for both the aisle and window occupant. All other injury loads for both occupants were below their respective injury thresholds. The 5th-percentile aisle-side occupant significantly exceeded the maximum allowable Nij value in the model, yielding a 99.96-percent risk of neck injury in the model and a 45.48-percent risk of neck injury in the dynamic test. The window occupant also exceeded the Nij criteria in the model, although these values were not exceeded by the 95th-percentile occupant in the dynamic test. The model predicted all other injury criteria to remain below their respective threshold values. Good correlation between the dynamic test and the model is observed for the left femur load for the aisle occupant and the chest and left and right femur loads for the window occupant.

**Table 19. Comparison of Maximum Injury Parameters for Test No. 4 and Model 3**

|  | Aisle | | | Window | | |
|---|---|---|---|---|---|---|
|  | **Injury Criteria** | **Test No. 4** | **Model 3** | **Injury Criteria** | **Test No. 4** | **Model 3** |
| Occupant | **5th female** | **5th female** | **5th female** | **95th male** | **95th male** | **95th male** |
| HIC (36 msec) | 1,000 | 205.5 | 671.6 | 1,000 | 139.3 | 473.9 |
| Max Nij | 1.0 | 1.704 | 5.483 | 1.0 | 0.513 | 1.916 |
| Percent neck injury risk (%) | 15 | 45.48 | 99.96 | 15 | 5.81 | 57.00 |
| 3-msec chest acceleration (G) | 73 | 10.9 | 32.5 | 54 | 20.7 | 19.15 |
| Left femur load (lb) | -1,530 | -1051.1 | -1,309.4 | -2,594 | -1,517.0 | -1,686.2 |
| Right femur load (lb) | -1,530 | -940.5 | -1,250.5 | -2,594 | -1,629.8 | -1,692.7 |

Note: Shaded regions indicate injury values above the specified injury criteria.

*Comparison of Occupant Injury Data Time-History Curves*: The correlation between the test and model data varied greatly between the two occupants. The majority of the data curves for the 5th-percentile female in the model were late and high in magnitude. The best correlation was achieved with both the right and left femur loads, which were slightly late in time and lower in magnitude than the dynamic test data. The poor correlation of the 5th-percentile female data may be tied to rate-dependent characteristics of the seat cushion and seat back foams. The 50th-percentile and 95th-percentile males are closer in size, thus making it easier to achieve reasonable correlation with all of the data. In order to achieve a better correlation for the 5th-percentile female, additional improvements to the seat cushions, focusing on rate-dependent foams, should be considered.

The majority of the data curves for the 95th-percentile male in the model correlated well with the dynamic test data. The shear neck force and femur loads from the model were slightly higher in magnitude than the dynamic test data. However, the timing and shape of these curves matched very well. The model's shear neck force, chest acceleration, and fore/aft bending moment were slightly lower in magnitude than the dynamic test data, but maintained good curve shape and timing.

*Seat Attachment Load Comparisons*: The predicted and actual loads at the seat attachments are compared in Appendix F. A comparison of the model and dynamic test data revealed that the model's seat attachment load curves were very close in magnitude, timing, and shape to the dynamic test's seat attachment load curves. The onset of the loads consistently occurred around 150 to 160 msec.

# 8. CONCLUSIONS

The purpose for conducting these tests was to evaluate the performance of facing-seat configurations, in particular with and without a table between them, with different occupant sizes, and at a higher crash pulse. The Bombardier facing-seat configuration was used to perform the tests. Using MADYMO (an analysis software program), a seat/occupant model was developed to represent the seating configuration(s), and then the model was validated using the results of the dynamic sled tests. Seat stiffness characteristics were measured using uniform quasi-static loading of the seat back. One test was conducted with a load applied uniformly across the upper portion of the seat backs. All seats were uniformly tested against a triangular crash pulse of 250 msec duration and 8 G peak acceleration (one test was conducted against a 9 G peak acceleration for comparison purposes). This crash pulse has been defined as the test pulse in the APTA Standard for Seating in Commuter Rail Cars (SS-C&S-016-99).

Each test in this program was composed of two seat rows spaced 65 inches apart, with unrestrained ATDs in the forward-facing seats of the aft seat assembly. Commuter seats in the facing-seat configuration are typically attached with this spacing between them. The seat/occupant computer models that were used in the parametric analysis were later validated with the actual crash test pulse that was produced by the tests (rather than the idealized crash pulse) and also with improved pre-positioning of the ATDs and other modifications.

## 8.1 GENERAL

The measured static seat stiffness was greater than that measured for the Long Island Railroad (LIRR) commuter seat (tested in October 1998). The LIRR seat is a stiff, cantilevered two-place passenger seat system comprised of a thermoplastic casing around a tubular frame. The Bombardier seat was equally stiff on both the window and aisle sides, as was expected, due to the symmetric design.

Failure of the thermoplastic casing occurred at the seat back/pan junction, and this led to the development of a rigid-body computer model rather than a finite-element model.

The validated model, in general, produced time-history curves for the upper body that were delayed compared to those of the dynamic test results, while timing of the femur load matched well. The peak values were higher in the model for the neck injury data and, in some cases, for the head acceleration and the femur loads. The primary reason for the upper body timing and load differences was the difference in seat pan cushion behavior upon femur loading. In the model, the occupant's lower body (legs) was stopped from translating as far forward as was determined in dynamic testing, causing the upper body to travel further about the knees before impacting the seat back. The upper body timing of impact could be improved with corresponding improvements to the seat cushion that consider rate-dependent loading as well as sheet metal bending.

The dynamic sled test results demonstrated that these tests were repeatable and provided consistent information. Since the seats were rigidly mounted to the test fixture, however, the effect of the rail car structure on the outcome of the tests was not directly taken into account.

## 8.2  SEAT STRUCTURE

The seat does not meet the dynamic seat structural strength standard (APTA Standard for Seating in Commuter Rail Cars SS-C&S-016-99), not only with the 95th-percentile ATD, but also with the 50th-percentile ATD.  Specifically:

- The headrest failed;
- The seat cushions detached; and
- The table sheared at the wall attachment and failed at the floor/table attachment.

The headrest attachment was not strong enough to withstand the impact load of a 50th-percentile ATD.  In two of the three tests conducted without a table between the seats, the aisle-side seat failed completely across the base of the headrest.  In the test with the 5th- and 95th-percentile ATDs, the side with the heavier ATD (window side) failed at the same location (the base of the headrest).

The jagged edges of the failed portion of the headrest created a hazardous situation for flailing ATD's, which, in two cases, landed with their abdomens on top of the broken edge.

Both the launch seat and the impacted seat remained attached to the floor mounts in all tests. Little deformation was observed on the aluminum seat base structure.

The table did not remain attached to its wall mount during the test.  The attachments sheared at the wall connection; the vertical attachment pulled the screws out of the table, and then the weld failed at the base of the table/floor connection on the aisle side.

The cushions were tethered and attached with Velcro to the seats.  They remained attached in all but one test, and that was the test with the higher crash pulse.

The likelihood of abdominal injuries caused by the table or the jagged edge of the broken seat back could not be determined (no abdominal sensor is certified for the ATD).  However, there was concern expressed over the potential for abdominal injuries, which typically may not be life threatening.

## 8.3  OCCUPANT INJURY

The measured head, chest, and femur loads in all of the tests were below the human injury criteria denoted in the APTA Standards.

However, measured neck loads exceeded standard injury criteria in all but the test with the table. The neck injury criteria are currently *not* included in the APTA Standards requirements.

While the injury loads specified in the APTA standard were all below the criteria, the results of this test program show that the human injury requirement was not met because the occupants were not compartmentalized.  Specifically:

- At least one ATD was not compartmentalized in each test;
- The aisle-side ATD was not compartmentalized in any test, except for the test that had the 5th-percentile ATD in the aisle seat; and
- The 95th-percentile ATD was not compartmentalized even when it was seated on the window side.

In all four tests, at least one ATD was not compartmentalized. Typically, the ATDs traveled over the seat back in front of them with little resistance from the seat backs and headrests after seat failure occurred.

In three out of four tests, the injury loads exceeded the injury criteria (only the test with the table resulted in injury loads below the criteria). All injury loads that exceeded the injury criteria were in the neck area.

The table appears to reduce the occupant injury values, which were measured in the testing, but because it failed structurally, the table does not meet dynamic test standards.

The higher crash pulse in the third test resulted in higher recorded neck loads for both ATDs, and could therefore result in a more probable injury.

The 5th-percentile ATD experienced higher neck injury values and is more susceptible to injury in this higher-seat-stiffness environment.

Occupants on the window side (closer to the wall attachment) recorded higher injury loads than occupants in the aisle side did. Typically, the headrest failed upon impact on the aisle side, resulting in lower recorded injury loads.

# 9.  RECOMMENDATIONS

This program performed controlled dynamic tests on, and analyzed, the Bombardier commuter rail facing-seat configuration, with and without a table between the seats.

Results of these tests suggest that the headrest should be strengthened to:

- Prevent loose objects from flying about and impacting passengers;
- Improve occupant compartmentalization;
- Minimize the potential for human injury on jagged broken edges of the seats; and
- Mitigate the likelihood of neck injuries (as indicated by neck injury loads that exceed the injury criteria).

The neck injury criteria should be incorporated into the APTA Seat Safety Standard because:

- Even though prescribed injury values were below the injury criteria, neck loads exceeded criteria values in every test except the test with the table; and
- Neck injury values were higher for the window-side ATD than for the aisle-side ATD.

The results of this testing emphasized the importance of creating a seat design that balances the stiffness requirements needed to provide occupant compartmentalization without increasing the risk of inducing higher injury loads.

Finally, the seat/occupant model developed in this test program can be used to study seat design strategies and occupant injury mitigation strategies.

# 10. REFERENCES

1.  APTA Standard SS-C&S-016-99, "Standard for Seating in Commuter Rail Cars," *Manual of Standards and Recommended Practices for Rail Passenger Equipment*, American Public Transportation Association, Washington, DC, July 1, 1999.

2.  VanIngen-Dunn, C., and Manning, J., "Commuter Rail Seat Testing and Analysis," Draft Final Report, U.S. Department of Transportation, Cambridge, MA, 2000.

3.  Federal Motor Vehicle Safety Standards 49 CFR Parts 571, 585, 587, and 595, Docket No. NHTSA 98-4405; Notice 1, RIN 2127-AG70, *Occupant Crash Protection*, National Highway Traffic Safety Administration, Department of Transportation, Washington, DC, September 18, 1998.

4.  J.W. Melvin and A.M. Nahum, eds., *Accidental Injury, Biomechanics and Prevention*, Springer-Verlag, NY, 1993.

5.  Eppinger, R., Sun, E., Kuppa, S., and Saul, R., *Supplement: Development of Improved Injury Criteria for the Assessment of Advanced Automatic Restraint Systems - II*, National Highway Traffic Safety Administration, Department of Transportation, Washington, DC, March 2000.

6.  VanIngen-Dunn, C., *Single Passenger Rail Car Impact Test Volume II: Summary of Occupant Protection Program*, DOT/FRA/ORD-00/02.2, U.S. Department of Transportation, Washington, DC, March 2000.

7.  Tyrell, D., Brickle, B., Severson, K., Perlman, A. B., and VanIngen-Dunn, C., "Rail Passenger Equipment Crashworthiness Testing: Requirements and Implementation," paper presented at the 2000 ASME IMEC, RTD Volume 19.

8.  Tyrell, D., Zolock, J., VanIngen-Dunn, C., "Rail Passenger Collision Tests: Analysis of Occupant Protection Measurements," paper presented at the 2000 ASME IMEC.

# APPENDIX A

## STATIC TEST RESULTS

## SEAT STIFFNESS CURVES
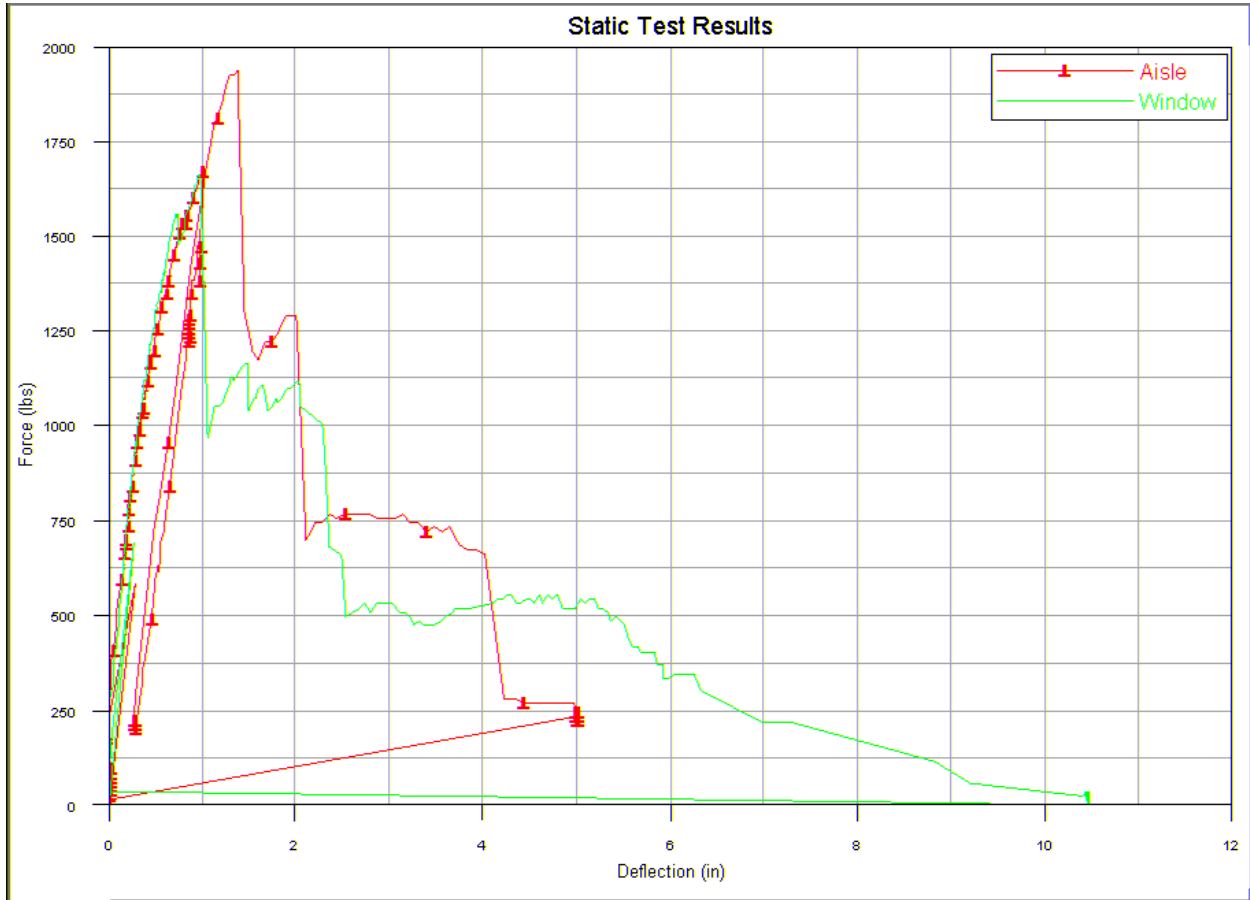


**Figure A1. Static Test - Load-Deflection Curve on a 12-in. Scale**
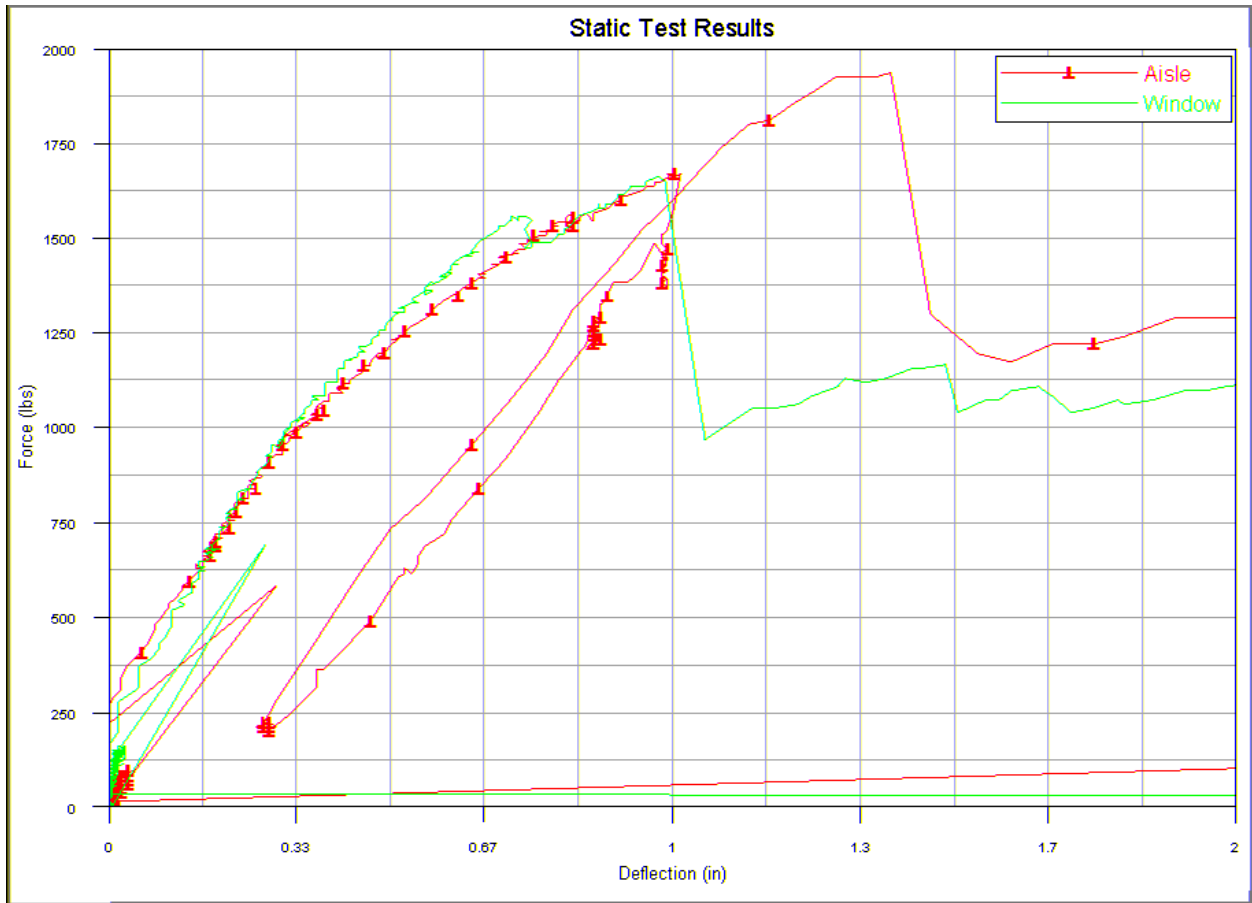
**Figure A2.  Static Test - Load-Deflection Curve on a 2-in. Scale**

# APPENDIX B

## DYNAMIC TEST RESULTS

## CRASH PULSE FOR EACH TEST AND CORRESPONDING CRASH PULSE USED IN SIMULATION MODELS
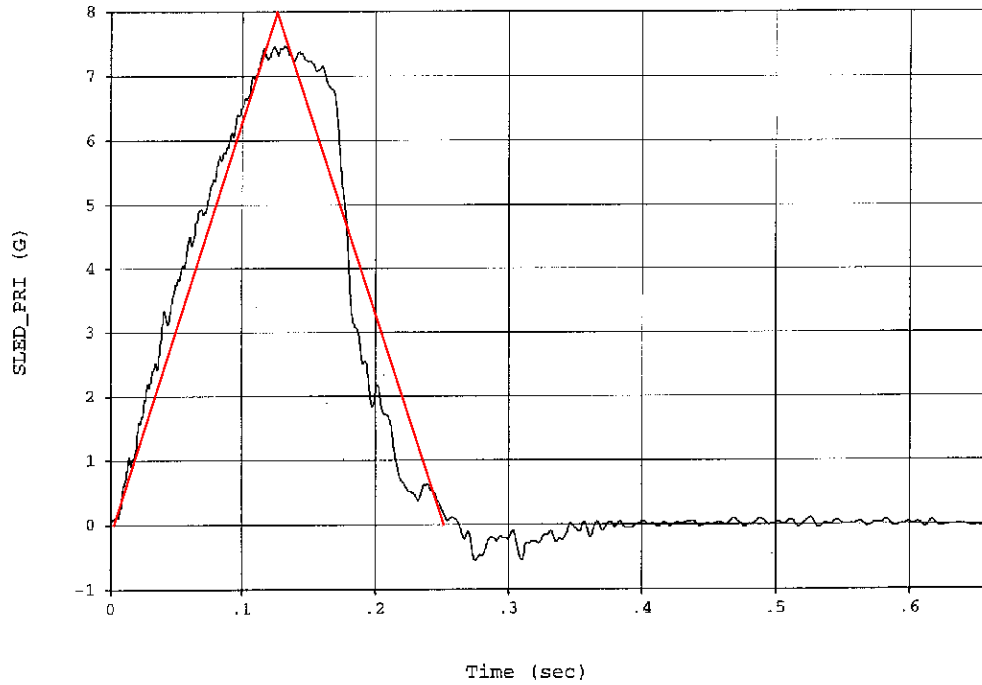


**Figure B1.  Comparison of Test No. 1 Crash Pulse vs. Ideal Crash Pulse**
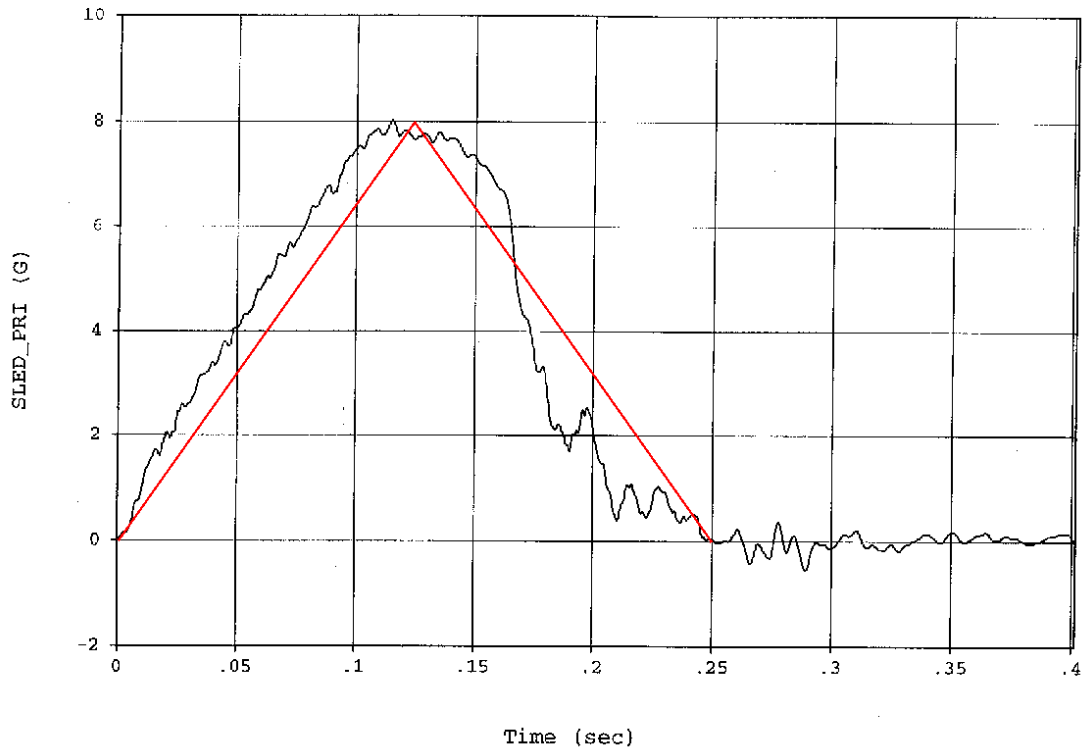
**Figure B2. Comparison of Test No. 2 Crash Pulse vs. Ideal Crash Pulse**
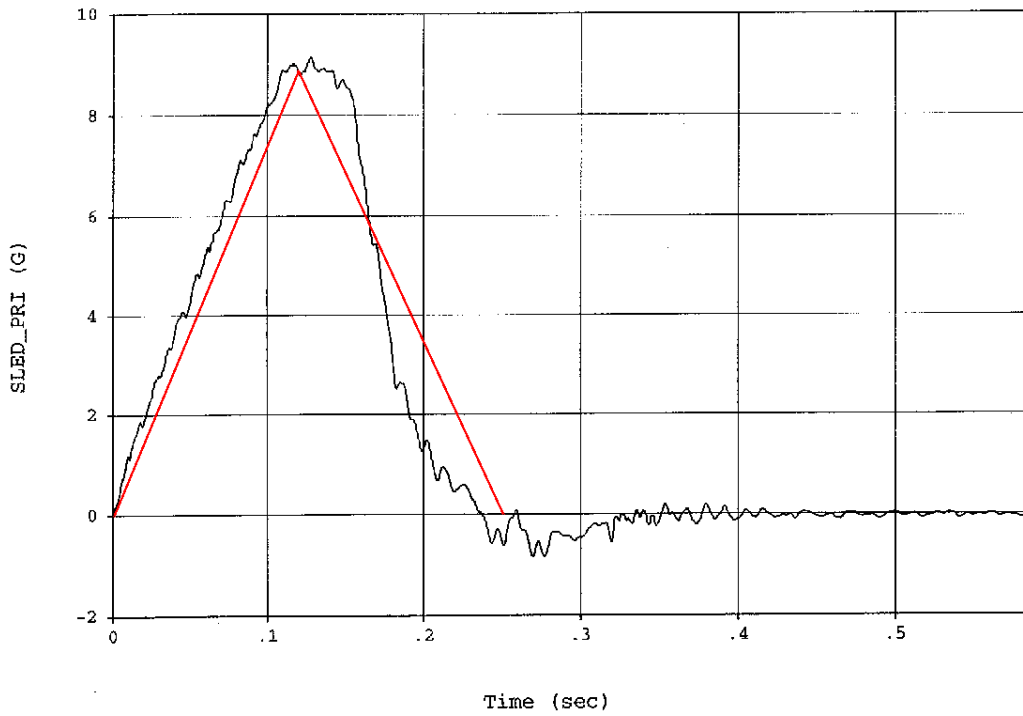


**Figure B3. Comparison of Test No. 3 Crash Pulse vs. Ideal Crash Pulse**
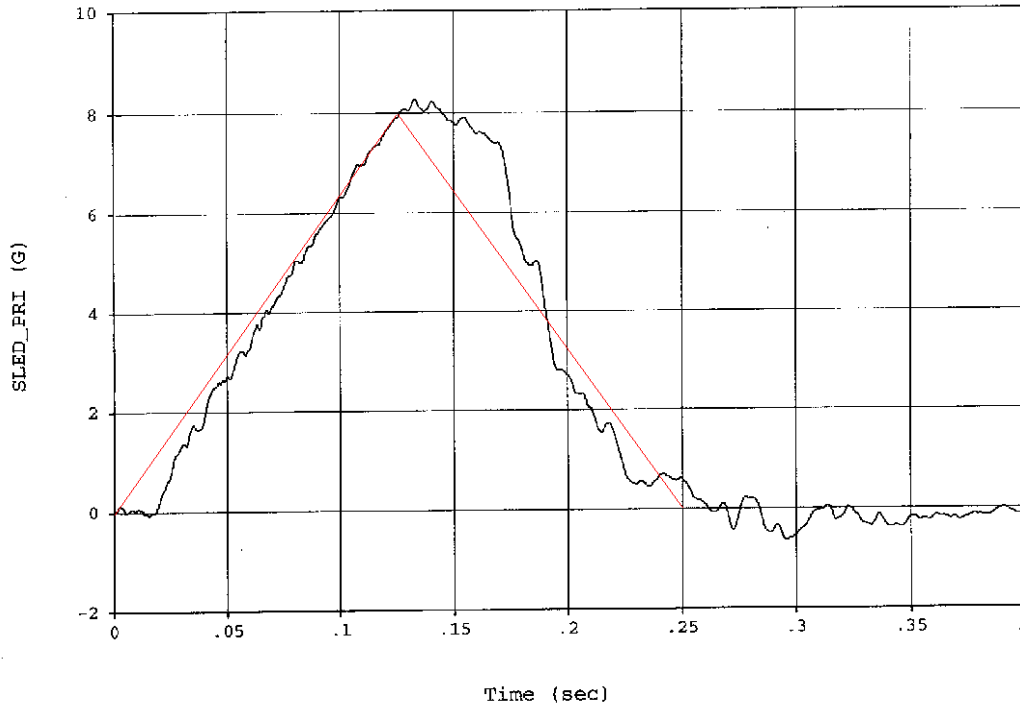
**Figure B4. Comparison of Test No. 4 Crash Pulse vs. Ideal Crash Pulse**

# APPENDIX C

## DYNAMIC TEST RESULTS

## DATA TABLES

**NOTE:  Shaded regions indicate data exceeds injury criteria values**

**Table C1.  Test No. 1 – Baseline Test, No Table, Two 50th-Percentile ATDs, 8 G Peak
Test No.: 1,  Test Date:  October 18, 2000**

| Sled | | | | |
|---|---|---|---|---|
| | **Peak G** | **Peak time (msec)** | **Delta V (ft/sec)** | **Total Pulse (msec)** |
| Specification | **8** | **125** | **32.2** | **250** |
| Primary Sled Accelerometer | 7.5 | 132.5 | 32.3 | |

| Floor Load Cells, +X Fwd, +Y Up, +Z Right (lb) | | | | |
|---|---|---|---|---|
| | **Location** | **X** | **Y** | **Z** |
| Load Cell 129 | #129 Aft wall mount attachment | 1,540.4 | 1,216.2 | 832.1 |
| Load Cell 130 | #130 fore wall mount attachment | 2,489.5 | -1,056.1 | -707.2 |
| Load Cell 131 | #131 fore floor attachment | 2,382.7 | 399.4 | -2,452.6 |
| Load Cell 132 | #132 Aft floor attachment | 889.3 | 528.2 | 2,016.2 |

| Test No. 1 – Baseline Test, No Table, Two 50th-Percentile ATDs, 8 G Peak Test No.: 1 Test Date: October 18, 2000 | | | | |
|---|---|---|---|---|
| | **Left window seat** | | **Right aisle seat)** | |
| **ATD** | **Hybrid III - ATD6 50th-Percentile** | | **Hybrid III - ATD9 50th-Percentile** | |
| | **Spec.** | **Actual** | **Spec.** | **Actual** |
| Head X (+Gx Aft) - Peak G | | -100.3 | | -54.0 |
| Head Y (+Gy right) - Peak G | | 15.1 | | -6.9 |
| Head Z (+Gz up) - Peak G | | 23.2 | | 19.9 |
| HIC (36 msec) | **1,000** | 265.7 | **1,000** | 104.1 |
| Neck (FX)- Head Aft (lb) | **697** | 694.6 | **697** | 458.4 |
| Neck (FX) - Head fwd (lb) | **-697** | -50 | **-697** | -40 |
| Neck Flexion (My) - (ft-lb) | **140** | 64.5 | **140** | 162.9 |
| Neck Extension (My) - (ft-lb) | **-42** | -37 | **-42** | -25 |
| Neck T (FZ) - (lb) | **742** | 1,043.4 | **742** | 250 |

**Table C1.  Test No. 1 – Baseline Test, No Table, Two 50th-Percentile ATDs, 8 G Peak**
**Test No.:  1,  Test Date:  October 18, 2000 (cont.)**

| ATD | Left window seat | | Right aisle seat) | |
|---|---|---|---|---|
| | Hybrid III - ATD6 50th-Percentile | | Hybrid III - ATD9 50th-Percentile | |
| | Spec. | Actual | Spec. | Actual |
| Neck C (FZ) - (lb) | **-900** | -850 | **-900** | -339.0 |
| Neck side bending (Mx) | | 65.4 | | -31.0 |
| Neck shear force (Fy) | | 76.2 | | 52.1 |
| Neck twist (Mz) | | 9.4 | | 10.3 |
| Chest X (+Gx Aft) - Peak G | | -9.5 | | -11.4 |
| Chest Y (+Gy right) - Peak G | | 3.8 | | -3.4 |
| Chest Z (+Gz up) - Peak G | | 17.6 | | 10.9 |
| Chest G (3 msec) | **60** | 18.2 | **60** | 14.2 |
| Femur L - (+Fx fwd) (lb) | **-2,250** | -1,597.4 | **-2,250** | -796.4 |
| Femur R - (+Fx fwd) (lb) | **-2,250** | -1,613.0 | **-2,250** | -373.8 |

The table title row above reads: *Test No. 1 – Baseline Test, No Table, Two 50th-Percentile ATDs, 8 G Peak / Test No.:  1 / Test Date:  October 18, 2000*

NOTE:  Shaded areas indicate where injury criterion was exceeded.  Neck injury loads were measured from an upper neck load cell.

**Table C2.  Test No. 2 – Baseline Test, With Table, Two 50th-Percentile ATDs, 8 G Peak**
**Test No.:  2, Test Date:  October 19, 2000**

| Sled | | | | |
|---|---|---|---|---|
| | Peak G | Peak time (msec) | Delta V (ft/sec) | Total Pulse (msec) |
| Specification | **8** | **125** | **32.2** | **250** |
| Primary Sled Accelerometer | 8.0 | 114.8 | 33.1 | |

| Floor Load Cells, +X Fwd, +Y Left, +Z Up (lb) | | | | |
|---|---|---|---|---|
| | Location | X | Y | Z |
| Load Cell 1 | #129 Aft wall mount attachment | 1,547.3 | 634.0 | 675.1 |
| Load Cell 2 | #130 fore wall mount attachment | 2,117.4 | -877.8 | -503.7 |
| Load Cell 3 | #131 fore floor attachment | 1,851.8 | 551.3 | -2194.5 |
| Load Cell 4 | #132 Aft floor attachment | 951.0 | -333.3 | 1,636.8 |
| Load Cell 5 | #95 table-to-wall attachment | -442.3 | -89.2 | -442.5 |
| Load Cell 6 | #96 table-to-floor attachment | -2,421.7 | 471.3 | -1,355.8 |

**Table C2. Test No. 2 – Baseline Test, With Table, Two 50th-Percentile ATDs, 8 G Peak**
**Test No.: 2, Test Date: October 19, 2000 (cont.)**

| ATD | Left window seat | | Right aisle seat | |
|---|---|---|---|---|
| | Hybrid III - ATD6 50th-Percentile | | Hybrid III - ATD9 50th-Percentile | |
| | **Spec.** | **Actual** | **Spec.** | **Actual** |
| Head X (+Gx Aft) - Peak G | | -14.1 | | -100.7 |
| Head Y (+Gy right) - Peak G | | -7.8 | | -7.5 |
| Head Z (+Gz up) - Peak G | | 20.5 | | -35.3 |
| HIC (36 msec) | **1,000** | 17.5 | **1,000** | 216.1 |
| Neck (FX)- Head Aft (lb) | **697** | 15 | **697** | 606 |
| Neck (FX) - Head fwd (lb) | **-697** | -62 | **-697** | -25 |
| Neck Flexion (My) - (ft-lb) | **140** | 13 | **140** | 136.3 |
| Neck Extension (My) - (ft-lb) | **-42** | -11 | **-42** | -17 |
| Neck T (FZ) - (lb) | **742** | 177 | **742** | 180 |
| Neck C (FZ) - (lb) | **-900** | -155 | **-900** | -326.5 |
| Neck side bending (Mx) | | -16.7 | | 20.2 |
| Neck shear force (Fy) | | -52 | | -92.9 |
| Neck twist (Mz) | | -5.8 | | 15.9 |
| Chest X (+Gx Aft) - Peak G | | -28.5 | | -19.4 |
| Chest Y (+Gy right) - Peak G | | 10.3 | | 13.2 |
| Chest Z (+Gz up) - Peak G | | 10.5 | | -33.7 |
| Chest G (3 msec) | **60** | 23.3 | **60** | 14.9 |
| Femur L - (+Fx fwd) (lb) | **-2,250** | -1,291 | **-2,250** | -600 |
| Femur R - (+Fx fwd) (lb) | **-2,250** | -1,282 | **-2,250** | -900 |

NOTE: Shaded areas indicate where injury criterion was exceeded. Neck injury loads were measured from an upper neck load cell.


**Table C3. Test No. 3 – Baseline Test, No Table, Two 50th-Percentile ATDs, 9 G Peak**
**Test No.: 3, Test Date: October 19, 2000**

| Sled | | | | |
|---|---|---|---|---|
| | **Peak G** | **Peak time (msec)** | **Delta V (ft/sec)** | **Total Pulse (msec)** |
| Specification | **8** | **125** | **32.2** | **250** |
| Primary Sled Accelerometer | 9.1 | 127.5 | 36.1 | |

| Floor Load Cells, +X Fwd, +Y Left, +Z Up (lb) | | | | |
|---|---|---|---|---|
| | **Location** | **X** | **Y** | **Z** |
| Load Cell 1 | #129 Aft wall mount attachment | 2,025.0 | 1,166.3 | 865.3 |
| Load Cell 2 | #130 fore wall mount attachment | 2,621.8 | -1,766.9 | -825.3 |
| Load Cell 3 | #131 fore floor attachment | 2,168.8 | 461.5 | -3,095.0 |
| Load Cell 4 | #132 Aft floor attachment | 1,452.0 | -437.8 | 2,978.7 |

**Table C3. Test No. 3 – Baseline Test, No Table, Two 50th-Percentile ATDs, 9 G Peak Test No.: 3 Test Date: October 19, 2000 (cont.)**

| ATD | Left window side Hybrid III - ATD6 50th-Percentile | | Right aisle side Hybrid III - ATD9 50th-Percentile | |
|---|---|---|---|---|
| | Spec. | Actual | Spec. | Actual |
| Head X (+Gx Aft) - Peak G | | -79.7 | | 86.1 |
| Head Y (+Gy right) - Peak G | | -16.0 | | -19.4 |
| Head Z (+Gz up) - Peak G | | 32.1 | | -26.1 |
| HIC (36 msec) | **1,000** | 274.6 | **1,000** | 127.8 |
| Neck (FX)- Head Aft (lb) | **697** | 1,183.1 | **697** | 501.2 |
| Neck (FX) - Head fwd (lb) | **-697** | -75 | **-697** | -110 |
| Neck Flexion (My) - (ft-lb) | **140** | 183.7 | **140** | 126.4 |
| Neck Extension (My) - (ft-lb) | **-42** | -42 | **-42** | -33 |
| Neck T (FZ) - (lb) | **742** | 397.6 | **742** | 200 |
| Neck C (FZ) - (lb) | **-900** | -396 | **-900** | -937.8 |
| Neck side bending (Mx) | | -15.8 | | -33.7 |
| Neck shear force (Fy) | | -131.0 | | 70.1 |
| Neck twist (Mz) | | -21.5 | | -6.1 |
| Chest X (+Gx Aft) - Peak G | | -10.1 | | -13.0 |
| Chest Y (+Gy right) - Peak G | | 4.9 | | -3.3 |
| Chest Z (+Gz up) - Peak G | | 22.5 | | 15.5 |
| Chest G (3 msec) | **60** | 22.8 | **60** | 15.3 |
| Femur L - (+Fx fwd) (lb) | **-2,250** | -1,689 | **-2,250** | -514.4 |
| Femur R - (+Fx fwd) (lb) | **-2,250** | -1,375 | **-2,250** | -701.1 |

NOTE: Shaded areas indicate where injury criterion was exceeded. Neck injury loads were measured from an upper neck load cell.

**Table C4. Test No. 4 – Passenger Injury Seat Strength Test, No Table Two ATDs - One 5th- and One 95th-Percentile, 8 G Peak Test No.: 4, Test Date: October 20, 2000**

| Sled | | | | |
|---|---|---|---|---|
| | Peak G | Peak time (msec) | Delta V (ft/sec) | Total Pulse (msec) |
| Specification | **8** | **125** | **32.2** | **250** |
| Primary Sled Accelerometer | 8.3 | 115.0 | 32.6 | |

| Floor Load Cells, +X Fwd, +Y Left, +Z Up (lb) | | | | |
|---|---|---|---|---|
| | Location | X | Y | Z |
| Load Cell 1 | #129 Aft wall mount attachment | 2,076.6 | 763.7 | 1,466.2 |
| Load Cell 2 | #130 fore wall mount attachment | 2,883.5 | -1,139.8 | -1,447.1 |
| Load Cell 3 | #131 fore floor attachment | 2,698.9 | 1,016.4 | -2,911.4 |
| Load Cell 4 | #132 Aft floor attachment | 1,607.7 | 507.6 | 2,624.0 |

**Table C4. Test No. 4 – Passenger Injury Seat Strength Test, No Table Two ATDs - One 5th- and One 95th-Percentile, 8 G Peak Test No.: 4, Test Date: October 20, 2000 (cont.)**

| ATD | Window (Left Side) Hybrid III - TD8 95th-Percentile | | Aisle (Right Side) Hybrid III - ATD5 5th-Percentile | |
|---|---|---|---|---|
| | Spec. | Actual | Spec. | Actual |
| Head X (+Gx Aft) - Peak G | | -85.4 | | -68.8 |
| Head Y (+Gy right) - Peak G | | -7.5 | | 5.4 |
| Head Z (+Gz up) - Peak G | | 19.2 | | 46.8 |
| HIC (36 msec) | **957** | 139.3 | **1,113** | 205.5 |
| Neck (FX)- Head Aft (lb) | **856** | 556.4 | **438** | 382.7 |
| Neck (FX) - Head fwd (lb) | **856** | -50 | **438** | -40 |
| Neck Flexion (My) - (ft-lb) | **190** | 145.2 | **70** | 31.7 |
| Neck Extension (My) - (ft-lb) | **58** | -33.3 | **-21** | -37.0 |
| Neck T (FZ) - (lb) | **910** | 170 | **468** | 180 |
| Neck C (FZ) - (lb) | **1,104** | -1,020.3 | **-567** | -783.3 |
| Neck side bending (Mx) | | 12.5 | | -6.9 |
| Neck shear force (Fy) | | 71.5 | | 30.7 |
| Neck twist (Mz) | | 5.2 | | 6.9 |
| Chest X (+Gx Aft) - Peak G | | -7.9 | | -10.4 |
| Chest Y (+Gy right) - Peak G | | 1.8 | | 5.6 |
| Chest Z (+Gz up) - Peak G | | 11.1 | | 23.3 |
| Chest G (3 msec) | **54** | 20.7 | **73** | 10.9 |
| Femur L - (+Fx fwd) (lb) | **-2,594** | -1,517.0 | **-1,391** | -1,051.1 |
| Femur R - (+Fx fwd) (lb) | **-2,594** | -1,629.8 | **-1,391** | -940.5 |

NOTE: Shaded areas indicate where injury criterion was exceeded. Neck injury loads were measured from an upper neck load cell.

# APPENDIX D

## DYNAMIC TEST RESULTS

## OCCUPANT INJURY Nij CRITERIA RESULTS AND CORRESPONDING OUTPUT FOR SIMULATION MODELS

### Table D1.  Nij Values Calculated for Test Nos. 1, 2, 3, and 4

| Test No. | ATD | Position | Nij Values | | | | | |
|---|---|---|---|---|---|---|---|---|
| | | | Ten-Flex | Ten-Ext | Comp-Flex | Comp-Ext | Max | % Injury Risk* |
| 1 | 50th | Window | 0.678 | **1.007** | 0.758 | 0.625 | 1.007 | 15.39 |
| | 50th | Aisle | 0.713 | 0.304 | **0.961** | 0.249 | 0.961 | 14.11 |
| 2 | 50th | Window | 0.130 | **0.181** | 0.114 | 0.161 | 0.181 | 2.90 |
| | 50th | Aisle | 0.595 | 0.238 | **0.810** | 0.219 | 0.810 | 10.58 |
| 3 | 50th | Window | 0.802 | 0.411 | **1.019** | 0.459 | 1.019 | 15.73 |
| | 50th | Aisle | 0.549 | 0.262 | **0.715** | 0.211 | 0.715 | 8.76 |
| 4 | 95th | Window | 0.103 | 0.367 | **0.513** | 0.470 | 0.513 | 5.81 |
| | 5th | Aisle | 1.269 | 0.778 | **1.704** | 0.630 | 1.704 | 45.48 |

### Table D2.  Nij Values Calculated for Models 1, 2, and 3

| Model No. | ATD | Position | Nij Values | | | | | |
|---|---|---|---|---|---|---|---|---|
| | | | Ten-Flex | Ten-Ext | Comp-Flex | Comp-Ext | Max | % Injury Risk* |
| 1 | 50th | Window | 0.542 | 0.777 | **3.063** | 2.578 | 3.063 | 94.21 |
| | 50th | Aisle | 1.774 | **1.859** | 1.092 | 1.280 | 1.859 | 53.92 |
| 2 | 50th | Window | 0.242 | 0.905 | 2.213 | **2.231** | 2.231 | 72.47 |
| | 50th | Aisle | 0.198 | 0.369 | 1.022 | **1.195** | 1.195 | 21.52 |
| 3 | 95th | Window | 0.398 | 0.516 | 1.745 | **1.916** | 1.916 | 57.00 |
| | 5th | Aisle | 2.103 | **5.483** | 2.139 | 5.104 | 5.483 | 99.97 |

# NOTES FOR TABLES D1 AND D2

\* The % Injury Risk values are based on the **maximum** Nij value recorded for each dummy.

1.  An Nij value of 1.0 is equivalent to a 15-pct risk of neck injury.

    Percent Injury Risk for Max Nij is $PercentRisk = p(AIS \geq 3) * 100$

    where the probability that the neck injury will be an AIS 3 injury is

    $$p(AIS \geq 3) = \left[ \frac{1}{1 + e^{3.906 - 2.185(MaxNij)}} \right]$$    (Kleinberger, et al, see below)

2.  The 15-pct injury risk value is equivalent to a serious neck injury (AIS >= 3), based on the Abbreviated Injury Scale (AIS).

3.  Shaded regions indicate **maximum** Nij values that exceed an injury risk of 15 pct.

4.  Model No. 1 corresponds to Test No. 346;  Model No. 2 corresponds to Test No. 348;  Model No. 3 corresponds to Test No. 349

## Reference

Kleinberger, M., Sun, E., Eppinger, R., Kuppa, S., and Saul, R., *Development of Improved Injury Criteria for the Assessment of Advanced Automotive Restraint Systems*, National Highway Transportation Safety Administration, September 1998.

# APPENDIX E

## DYNAMIC TEST RESULTS

## PEAK SEAT ATTACHMENT LOADS - SCHEMATICS

**NOTE:  Wall attachment loads are on window side of seat
Floor attachment loads are on aisle side of seat**
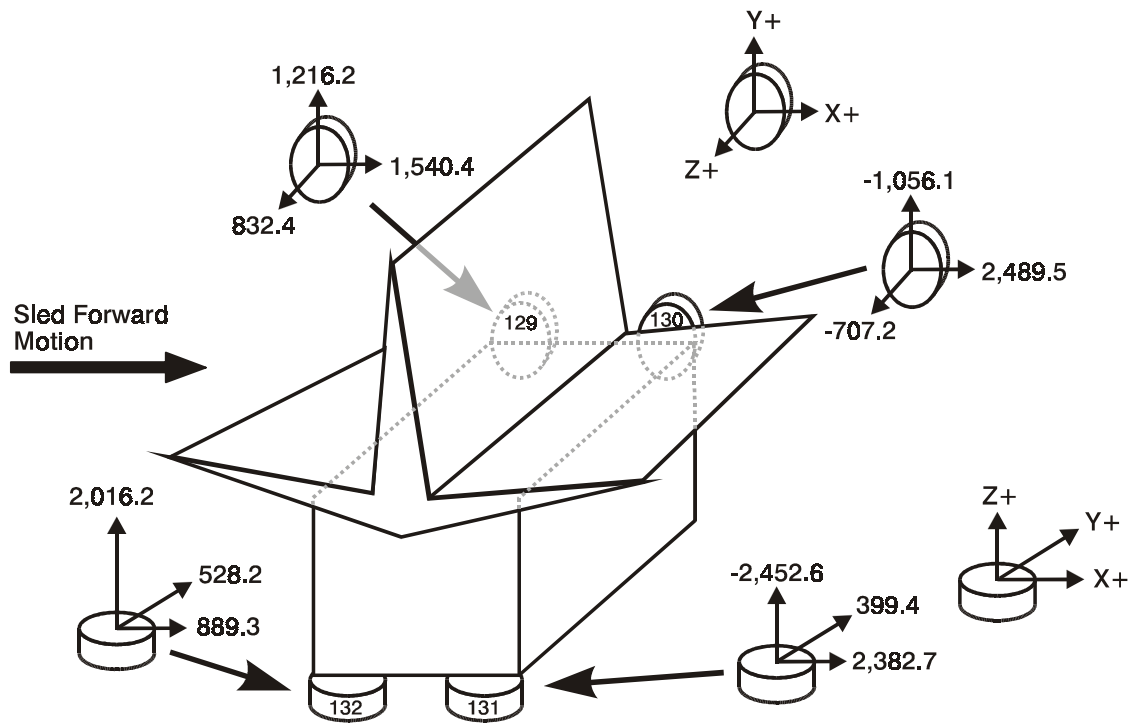


**Figure E1.  Peak Measured Seat Attachment Loads (lb) for Test No. 1 - Baseline Test**
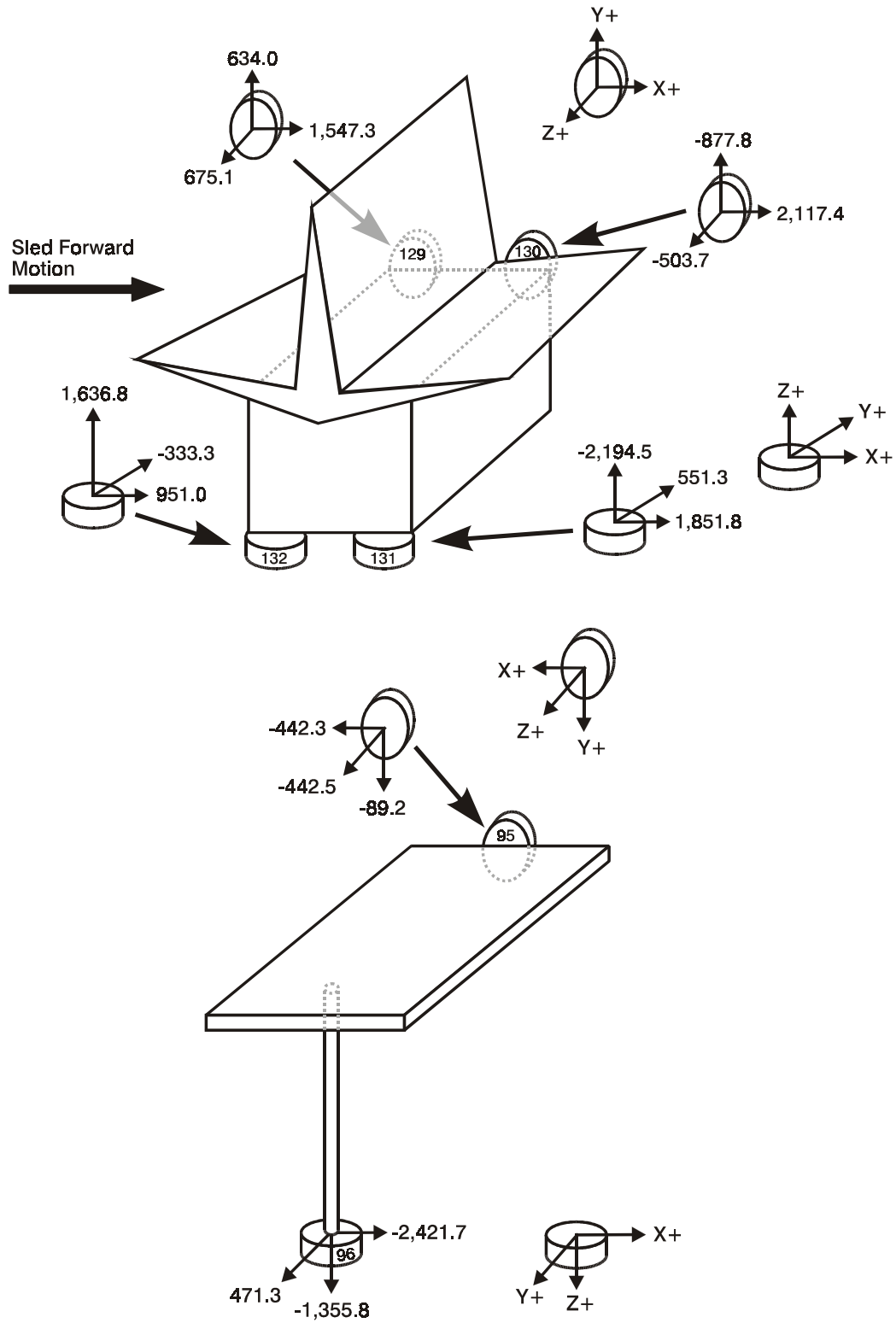
**Figure E2. Peak Measured Seat and Table Attachment Loads (lb) for Test No. 2 - Baseline Test with Table**
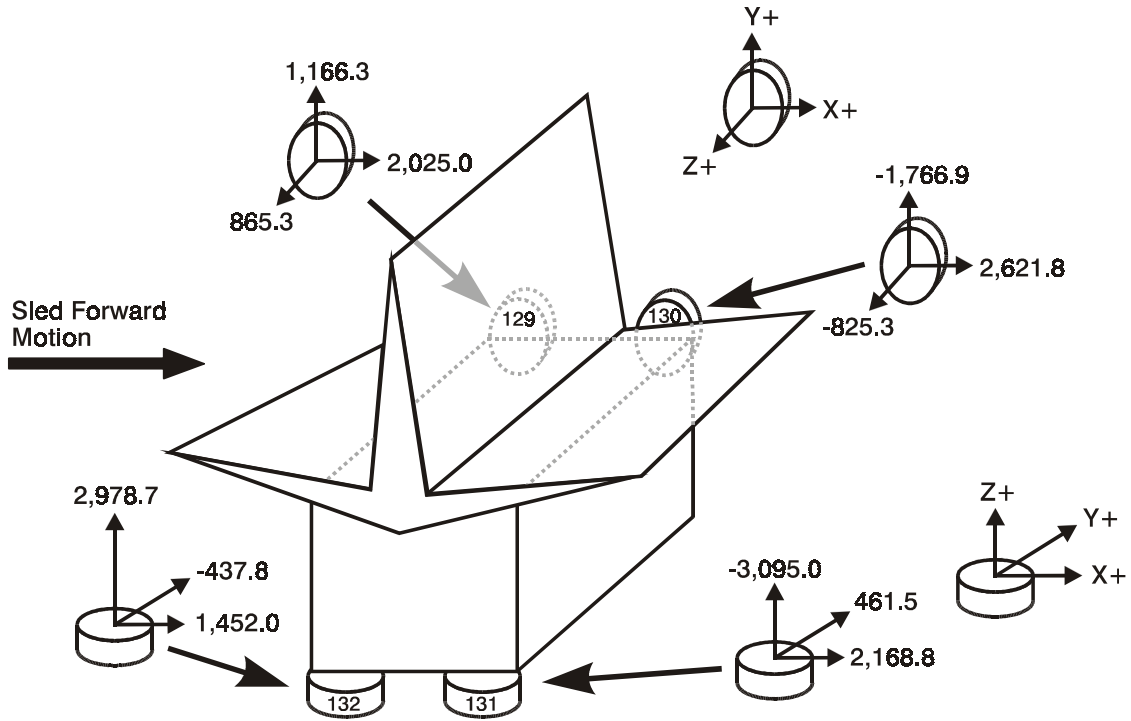
**Figure E3.  Peak Measured Seat Attachment Loads (lb) for Test No. 3 - Baseline Test with 9 G Peak Acceleration**
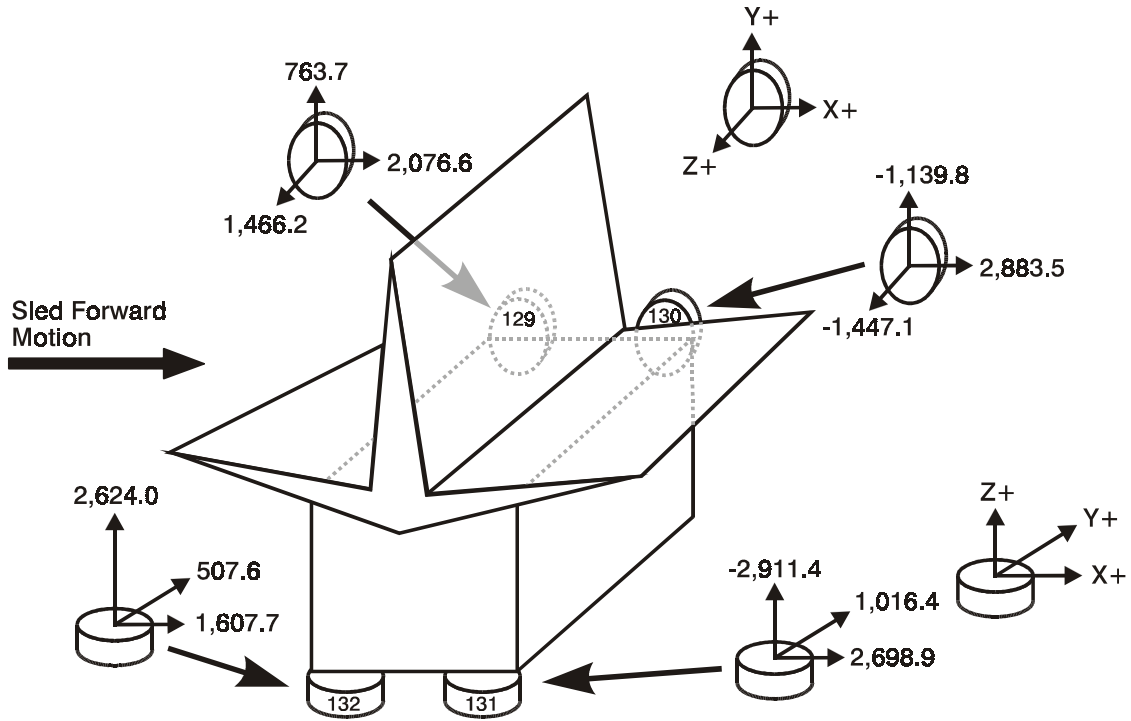
**Figure E4. Peak Measured Seat Attachment Loads (lb) for Test No. 4 -
Baseline Test with 5th-(aisle-side) and 95th-(window-side) Percentile Occupants**

# APPENDIX F

## SEAT ATTACHMENT LOAD-TIME DATA PLOTS
## FROM TESTING AND MODELING RESULTS

### NOTE FOR TEST DATA PLOTS

**Load Cell 129 = Aft wall seat attachment**
**Load Cell 130 = Fore wall seat attachment**
**Load Cell 131 = Fore floor seat attachment**
**Load Cell 132 = Aft floor seat attachment**


**TEST NO. 1 AND MODEL 1 SEAT ATTACHMENT LOADS**
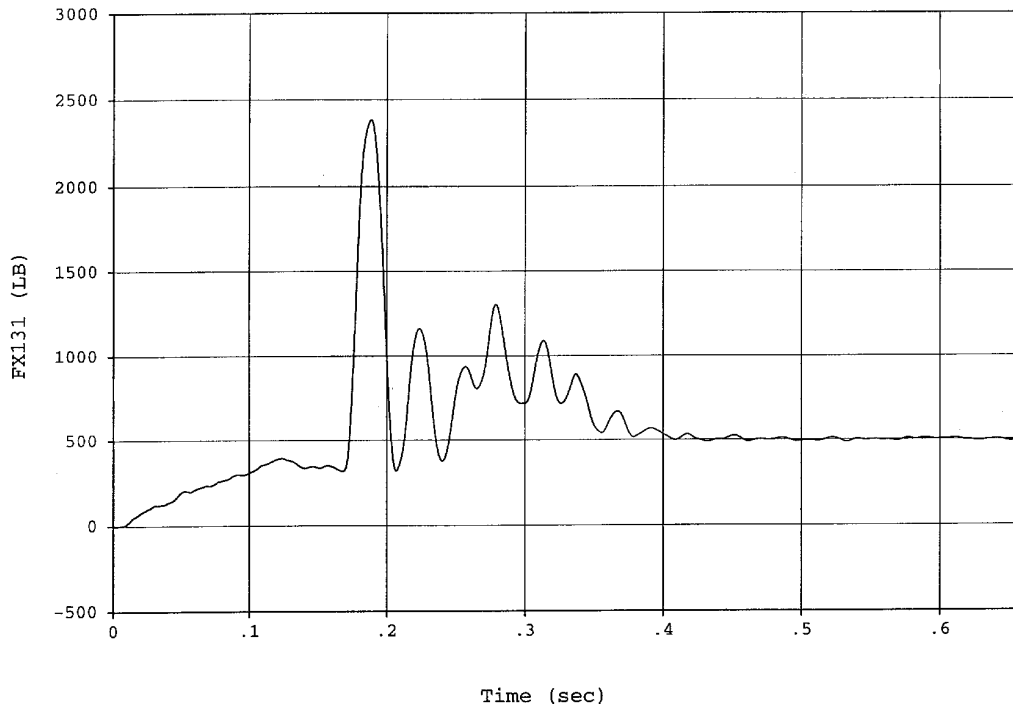


**Figure F1.  Test No. 1 Fore Floor Seat Attachment, x-Direction**

**Figure F2.  Model 1 Fore Floor Seat Attachment, x-Direction**
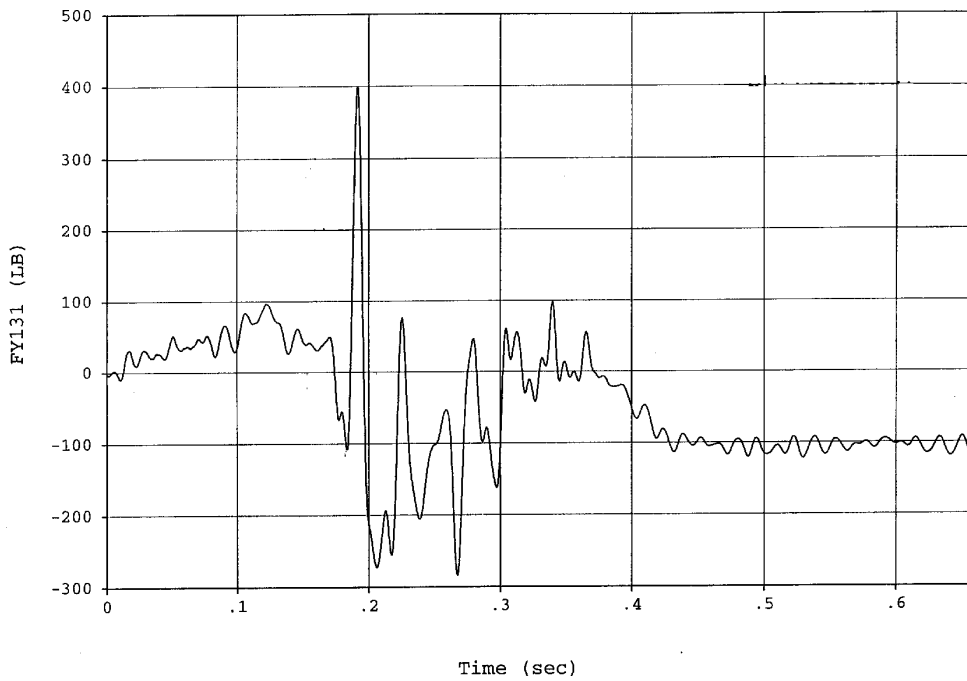


**Figure F3.  Test No. 1 Fore Floor Seat Attachment, y-Direction**

**Figure F4.  Model 1 Fore Floor Seat Attachment, y-Direction**
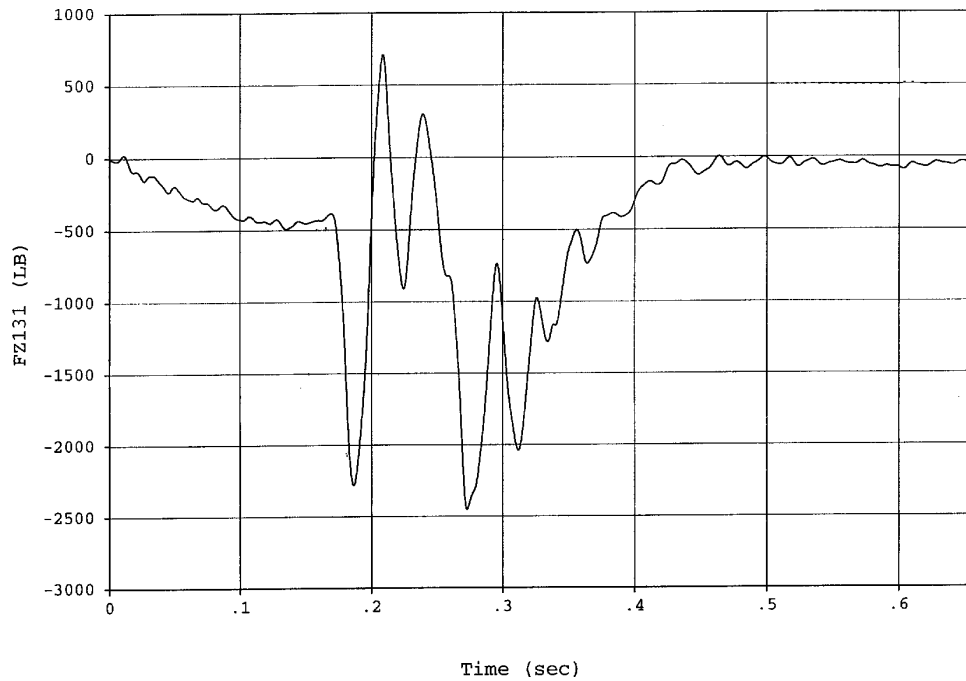


**Figure F5.  Test No. 1 Fore Floor Seat Attachment, z-Direction**

**Figure F6.  Model 1 Fore Floor Seat Attachment, z-Direction**
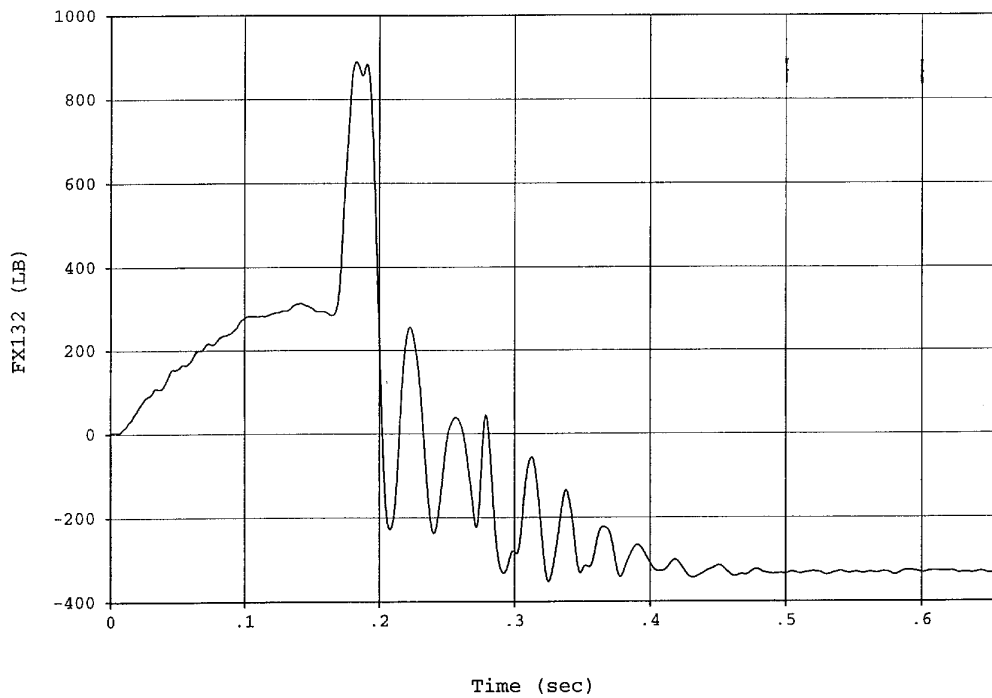


**Figure F7.  Test No. 1 Aft Floor Seat Attachment, x-Direction**

**Figure F8.  Model 1 Aft Floor Seat Attachment, x-Direction**
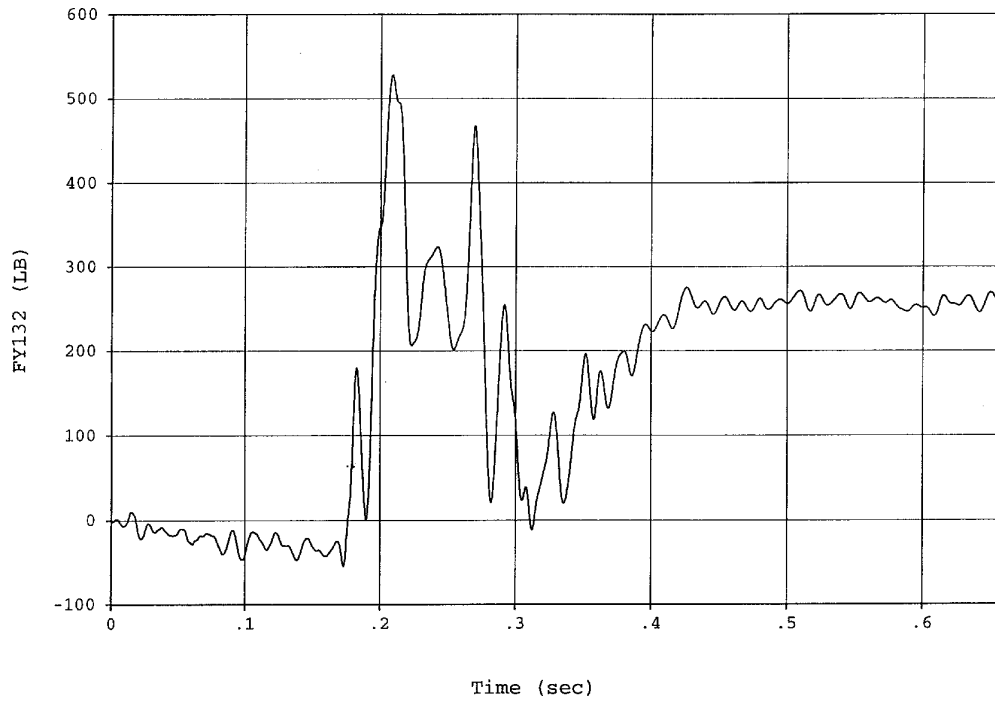


**Figure F9.  Test No. 1 Aft Floor Seat Attachment, y-Direction**

**Figure F10.  Model 1 Aft Floor Seat Attachment, y-Direction**
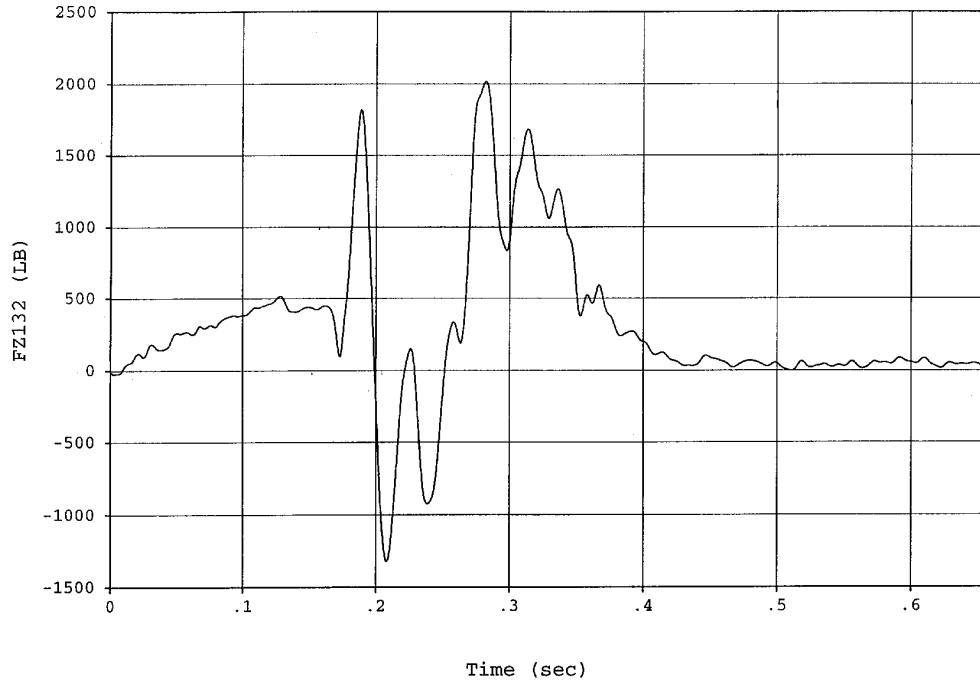


**Figure F11.  Test No. 1 Aft Floor Seat Attachment, z-Direction**

**Figure F12.  Model 1 Aft Floor Seat Attachment, z-Direction**
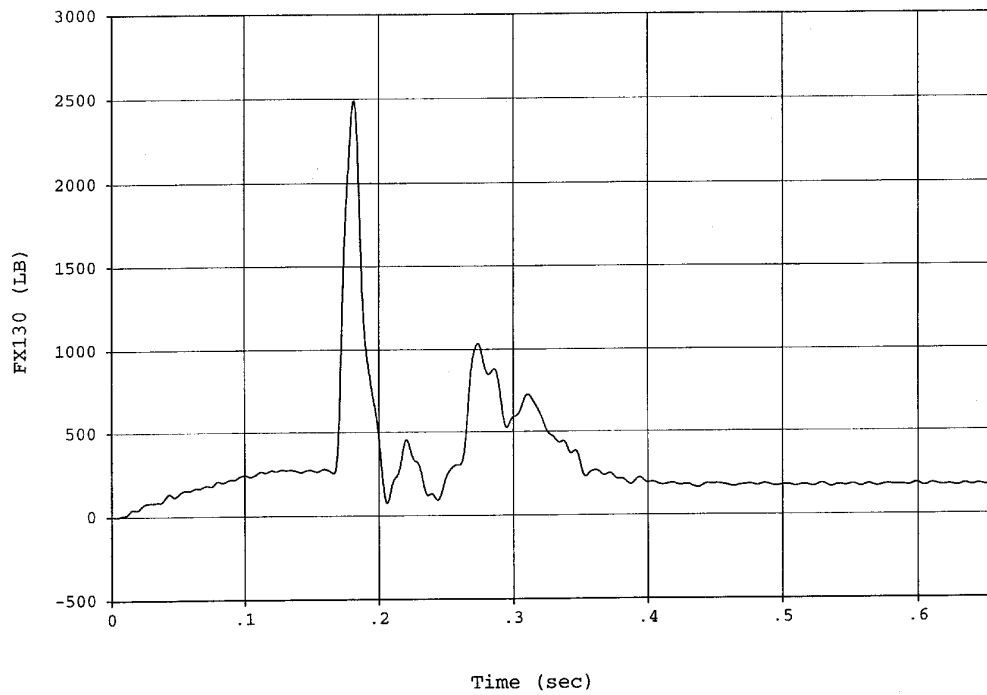


**Figure F13.  Test No. 1 Fore Wall Seat Attachment, x-Direction**

**Figure F14.  Model 1 Fore Wall Seat Attachment, x-Direction**
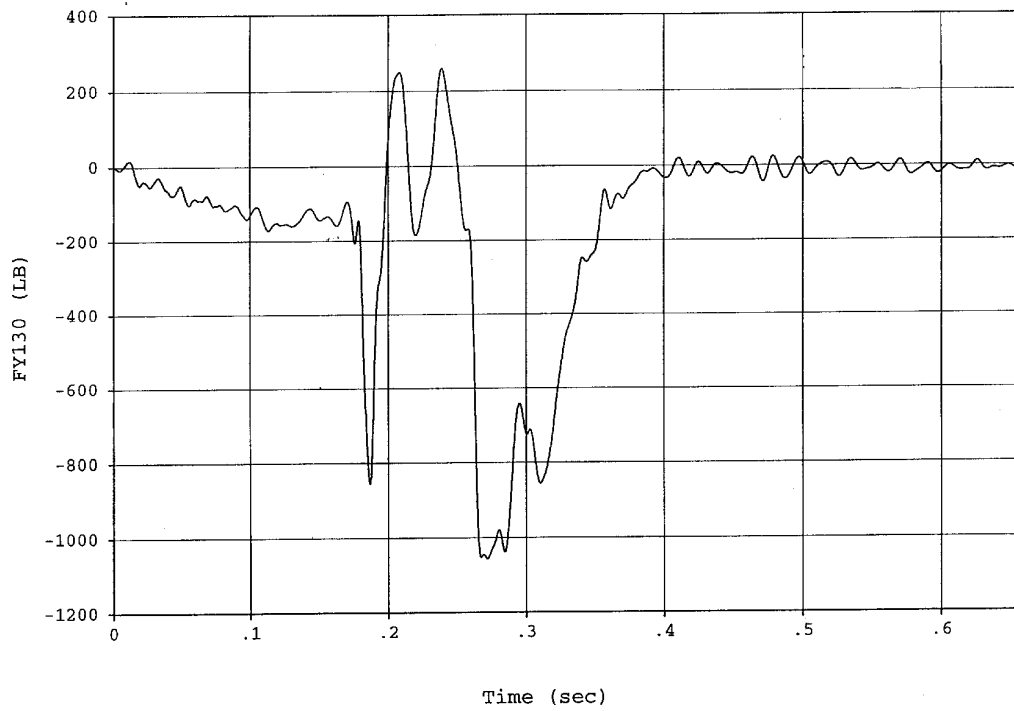


**Figure F15.  Test No. 1 Fore Wall Seat Attachment, y-Direction**

**Figure F16.  Model 1 Fore Wall Seat Attachment, y-Direction**
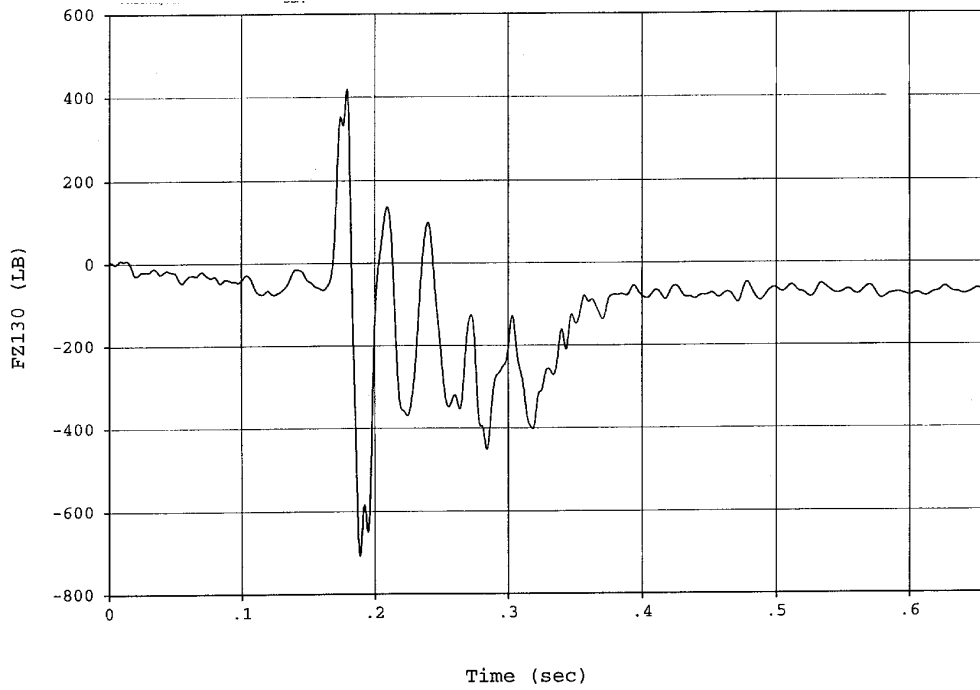


**Figure F17.  Test No. 1 Fore Wall Seat Attachment, z-Direction**

**Figure F18.  Model 1 Fore Wall Seat Attachment, z-Direction**
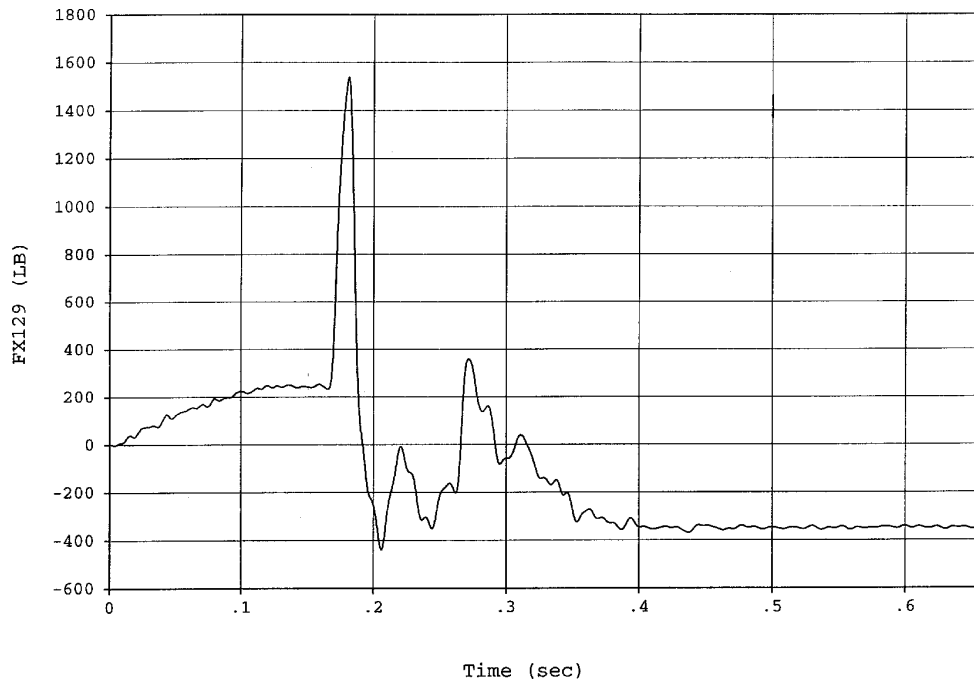


**Figure F19.  Test No. 1 Aft Wall Seat Attachment, x-Direction**

**TEST NO. 1 AND MODEL 1 SEAT ATTACHMENT LOADS (cont.)**
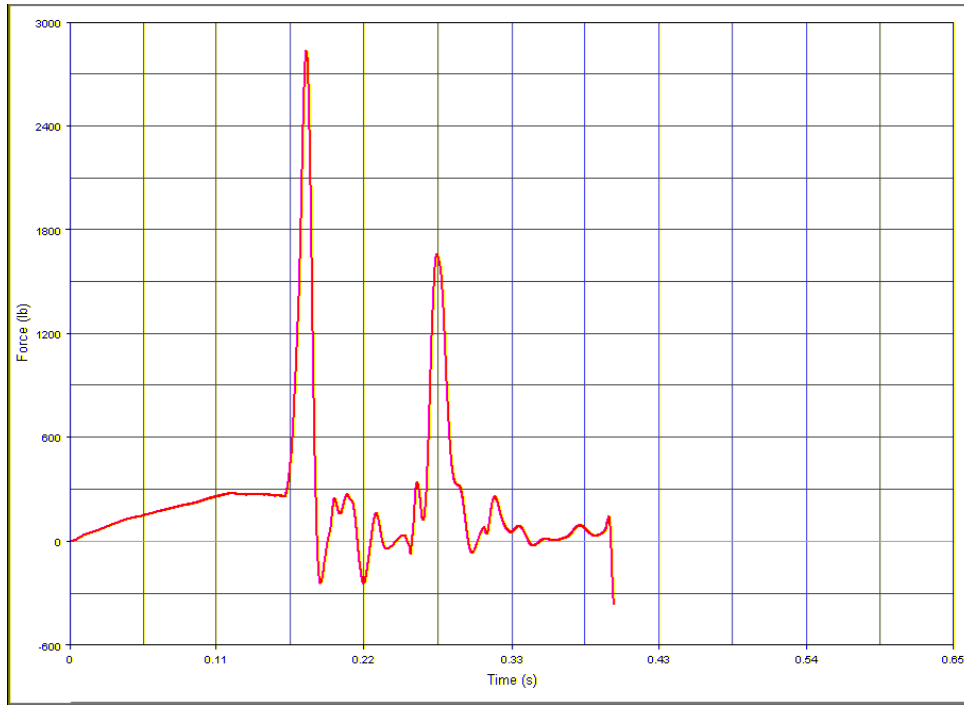


**Figure F20.  Model 1 Aft Wall Seat Attachment, x-Direction**
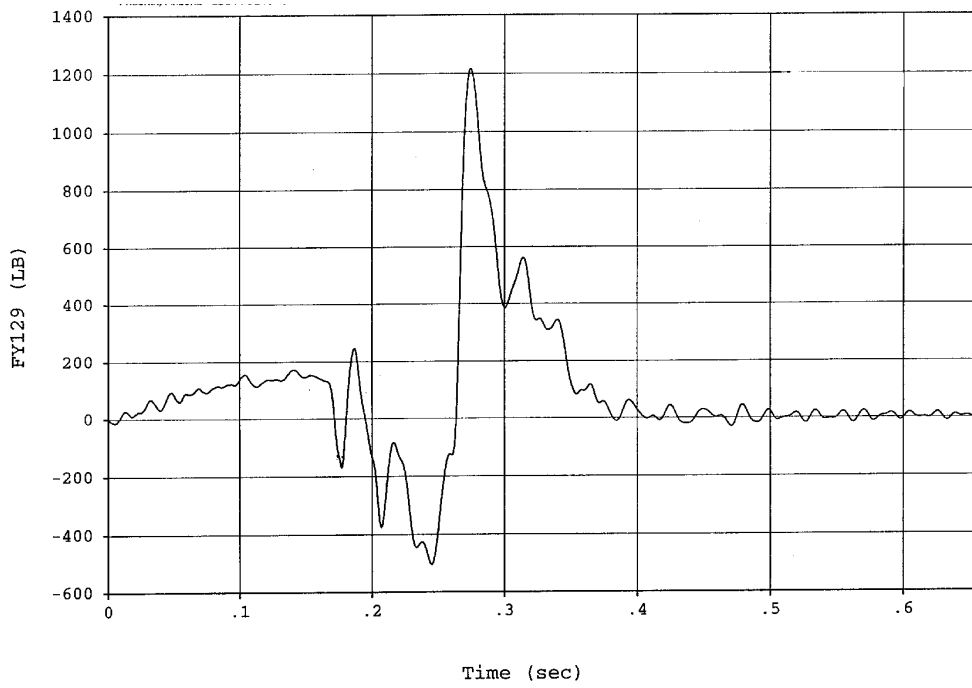


**Figure F21.  Test No. 1 Aft Wall Seat Attachment, y-Direction**
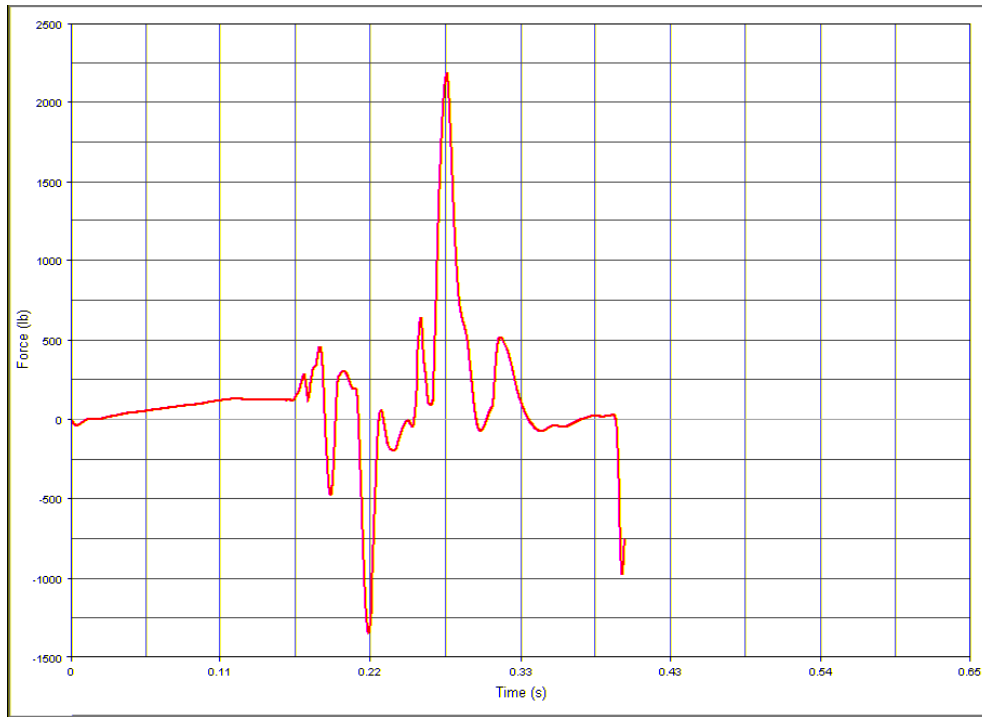
**Figure F22.  Model 1 Aft Wall Seat Attachment, y-Direction**
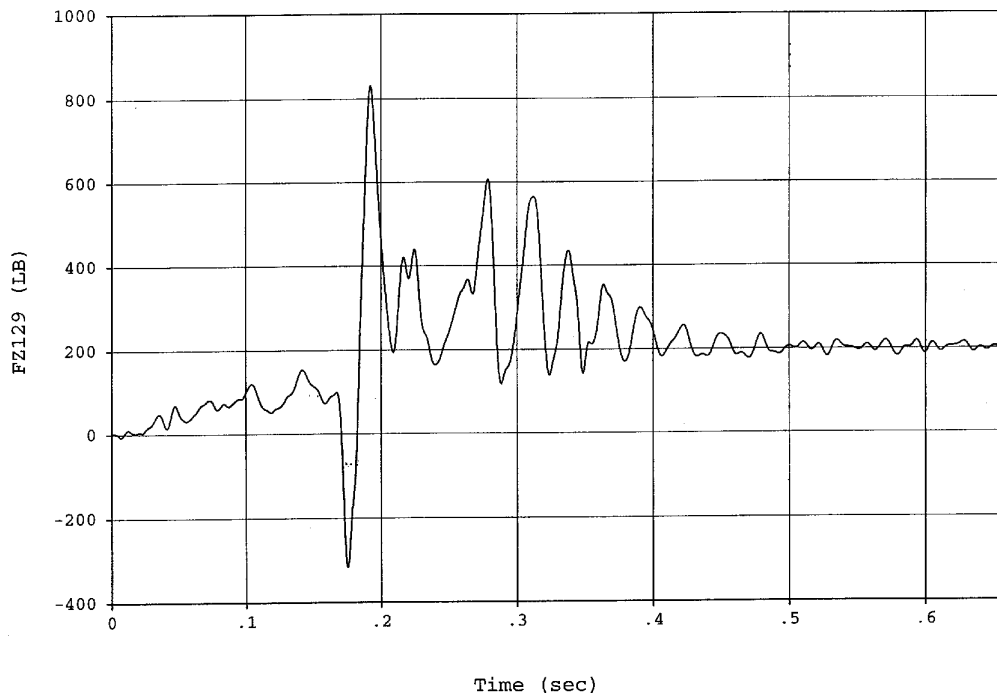


**Figure F23.  Test No. 1 Aft Wall Seat Attachment, z-Direction**

**TEST NO. 2 SEAT ATTACHMENT LOADS**
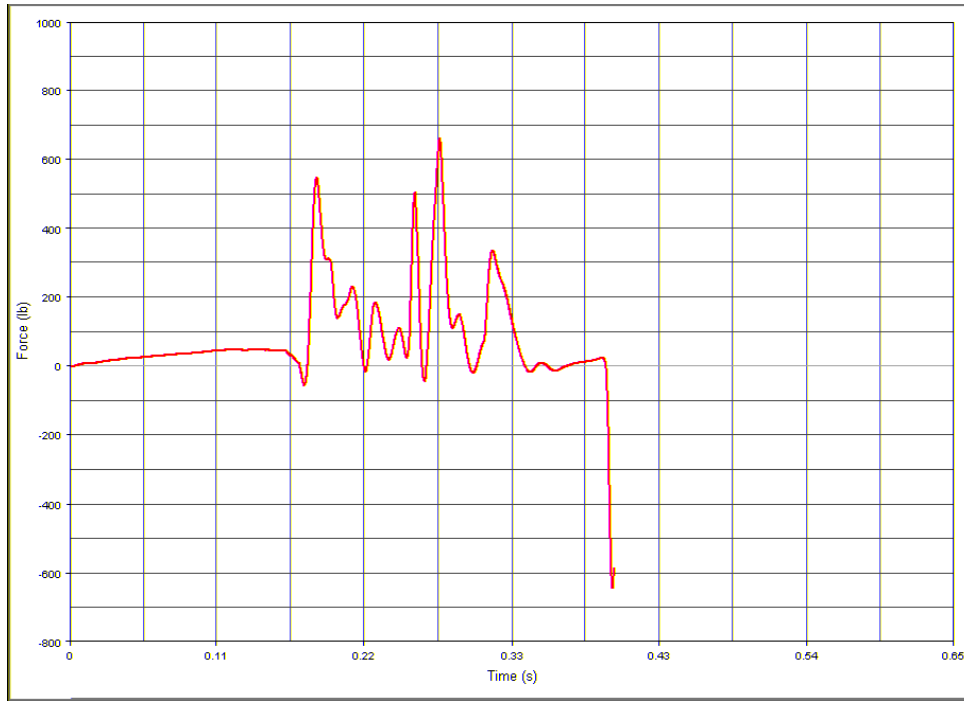


**Figure F24.  Model 1 Aft Wall Seat Attachment, z-Direction**
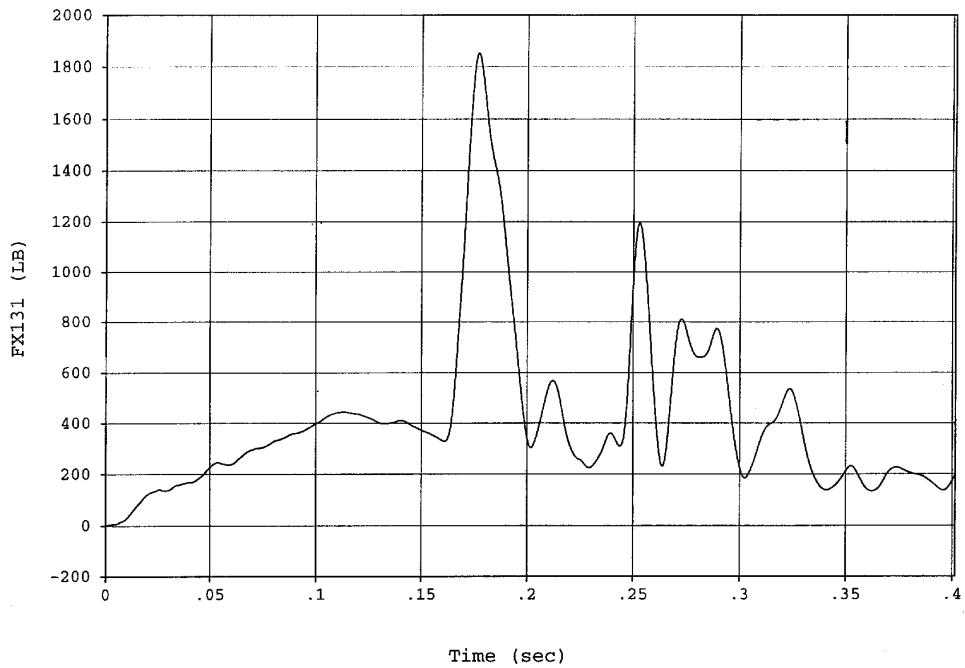


**Figure F25.  Test No. 2 Fore Floor Seat Attachment, x-Direction**

**TEST NO. 2 SEAT ATTACHMENT LOADS (cont.)**
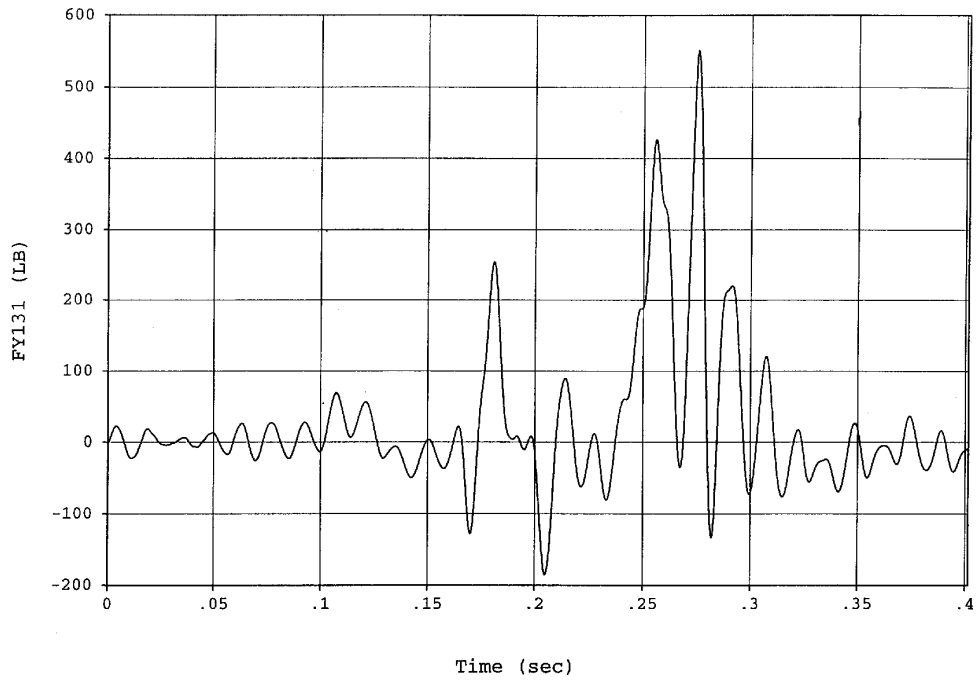


**Figure F26.  Test No. 2 Fore Floor Seat Attachment, y-Direction**
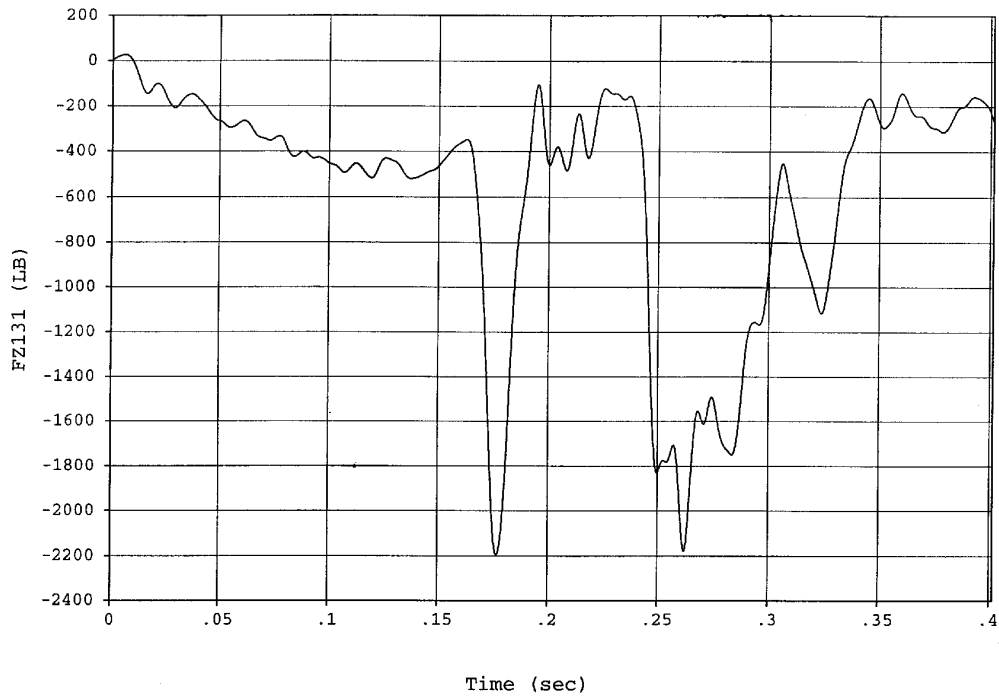


**Figure F27.  Test No. 2 Fore Floor Seat Attachment, z-Direction**

**TEST NO. 2 SEAT ATTACHMENT LOADS (cont.)**
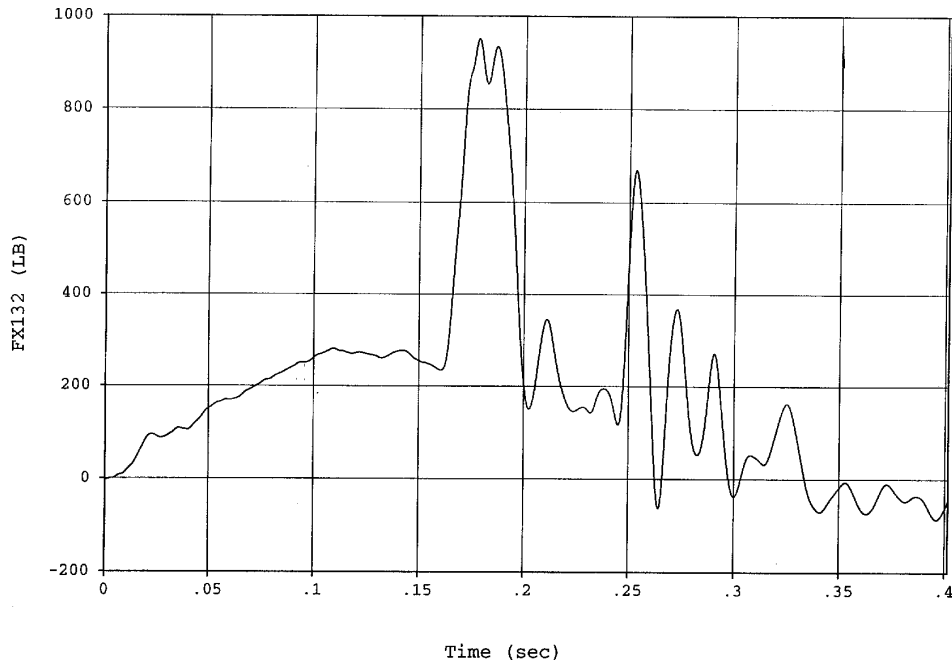


**Figure F28. Test No. 2 Aft Floor Seat Attachment, x-Direction**
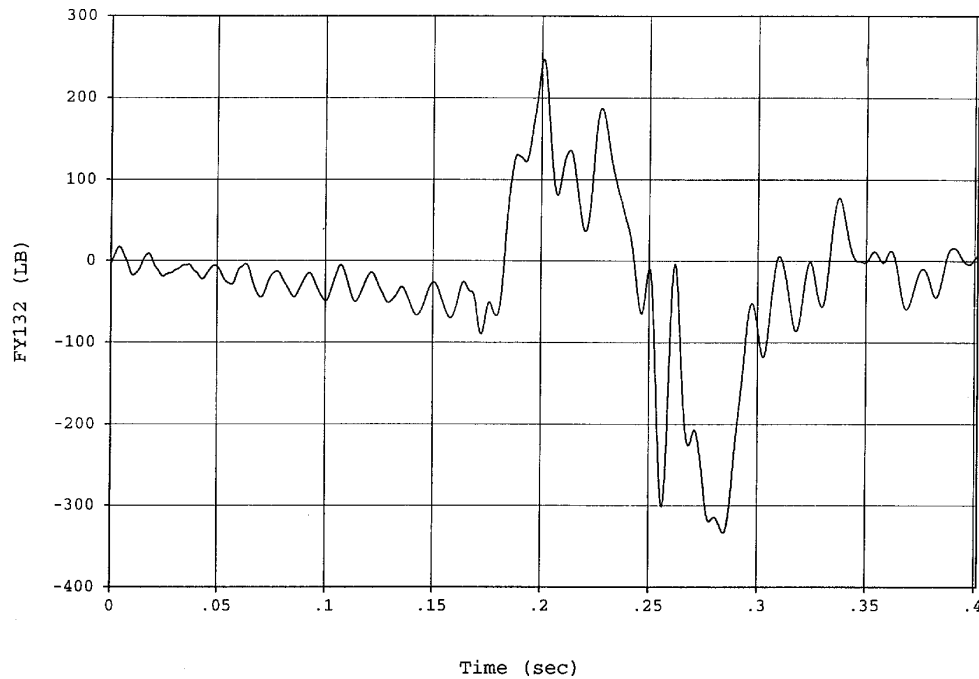


**Figure F29. Test No. 2 Aft Floor Seat Attachment, y-Direction**

**TEST NO. 2 SEAT ATTACHMENT LOADS (cont.)**
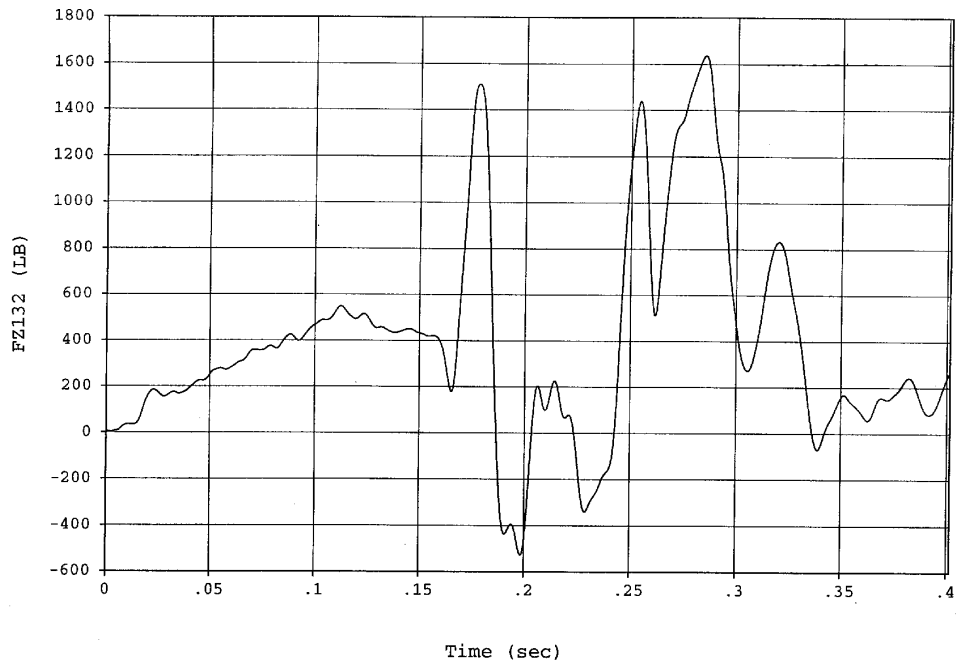


**Figure F30.  Test No. 2 Aft Floor Seat Attachment, z-Direction**
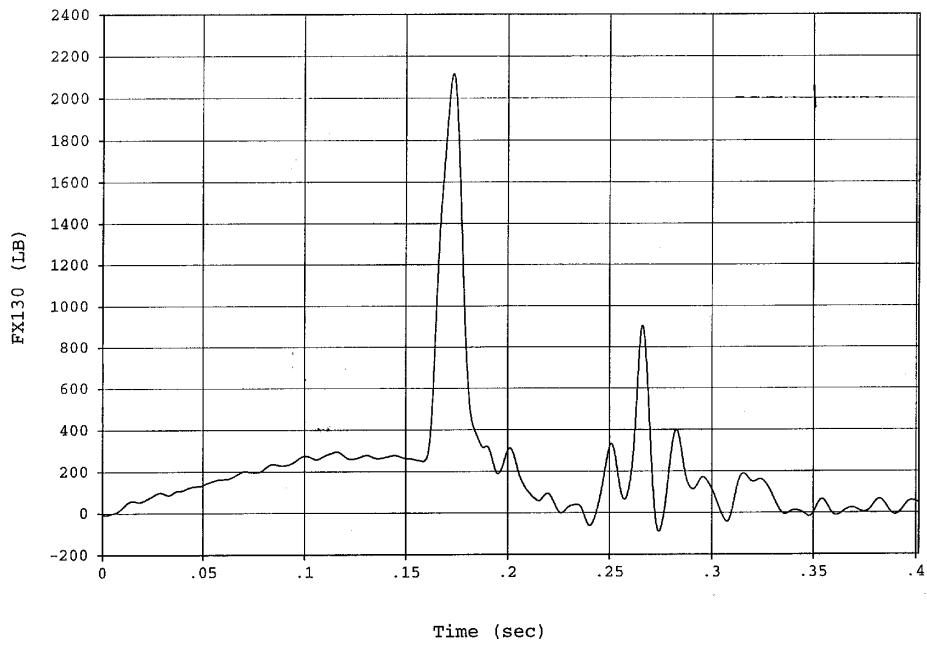


**Figure F31.  Test No. 2 Fore Wall Seat Attachment, x-Direction**

**TEST NO. 2 SEAT ATTACHMENT LOADS (cont.)**
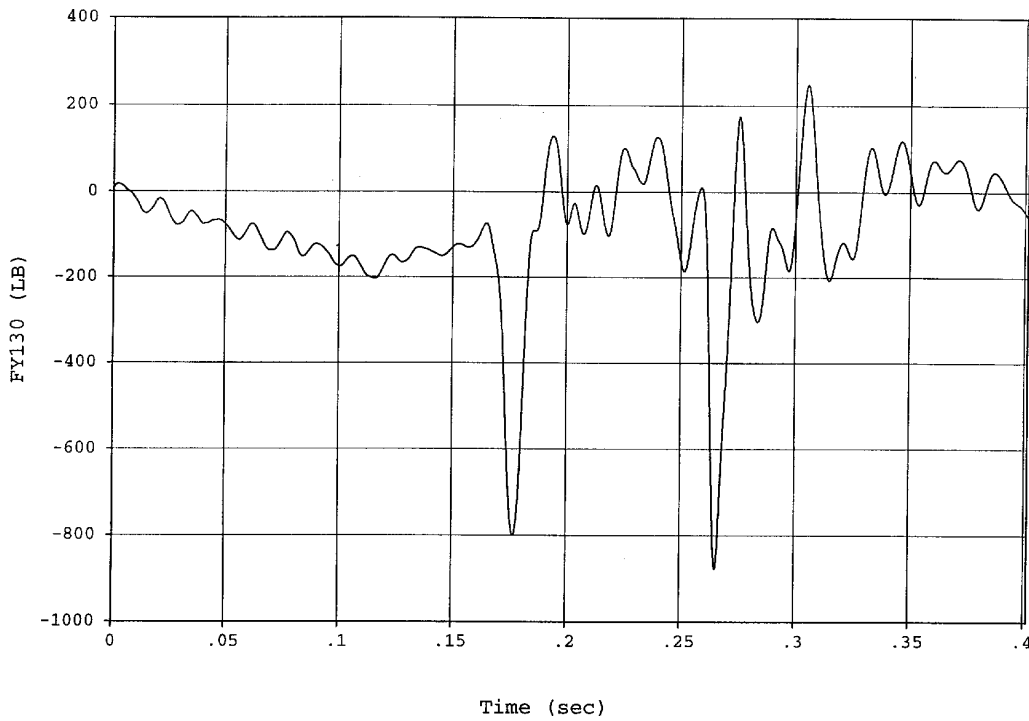


**Figure F32. Test No. 2 Fore Wall Seat Attachment, y-Direction**
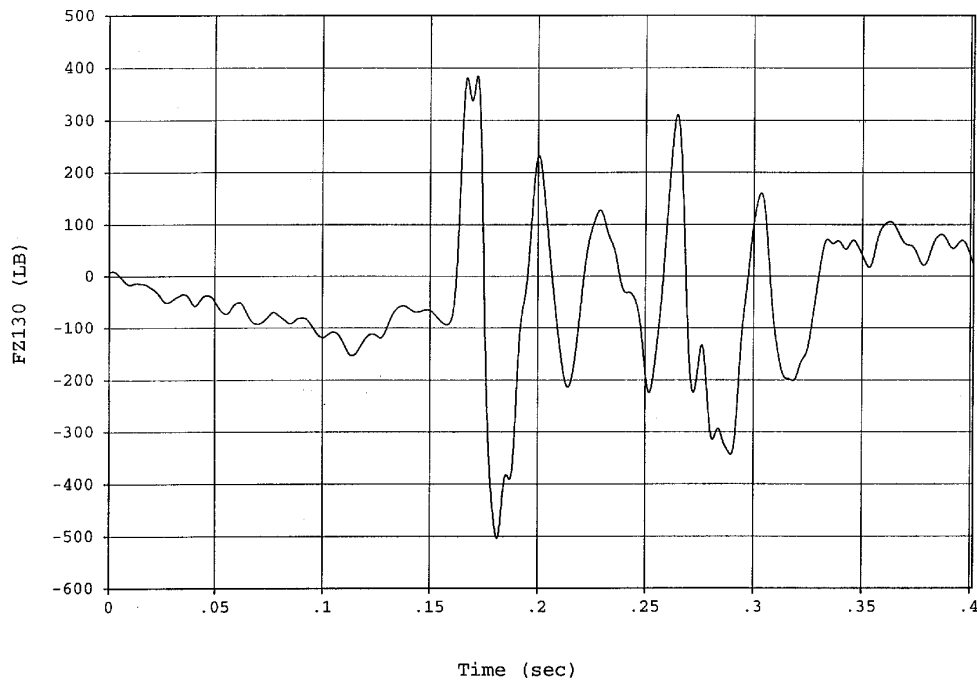


**Figure F33. Test No. 2 Fore Wall Seat Attachment, z-Direction**

**TEST NO. 2 SEAT ATTACHMENT LOADS (cont.)**
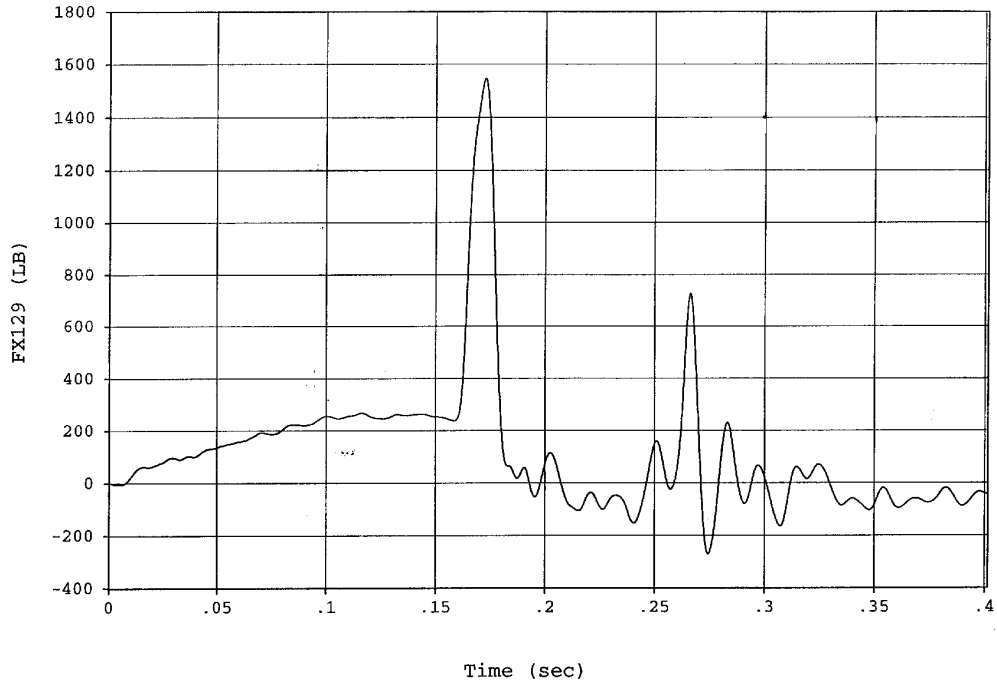


**Figure F34. Test No. 2 Aft Wall Seat Attachment, x-Direction**
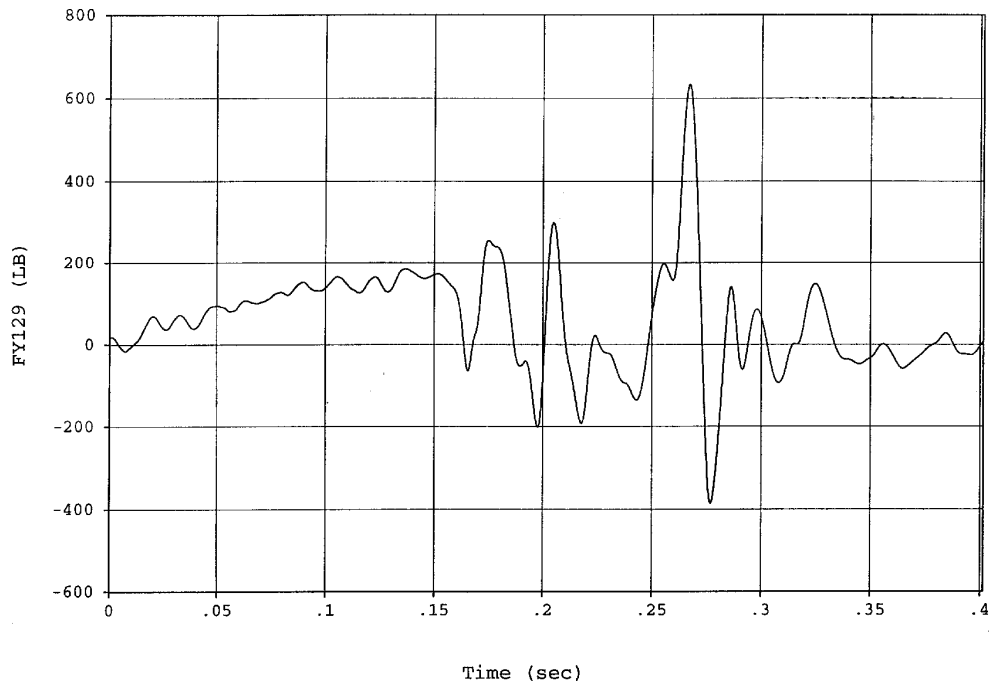


**Figure F35. Test No. 2 Aft Wall Seat Attachment, y-Direction**

**TEST NO. 2 SEAT ATTACHMENT LOADS (cont.)**
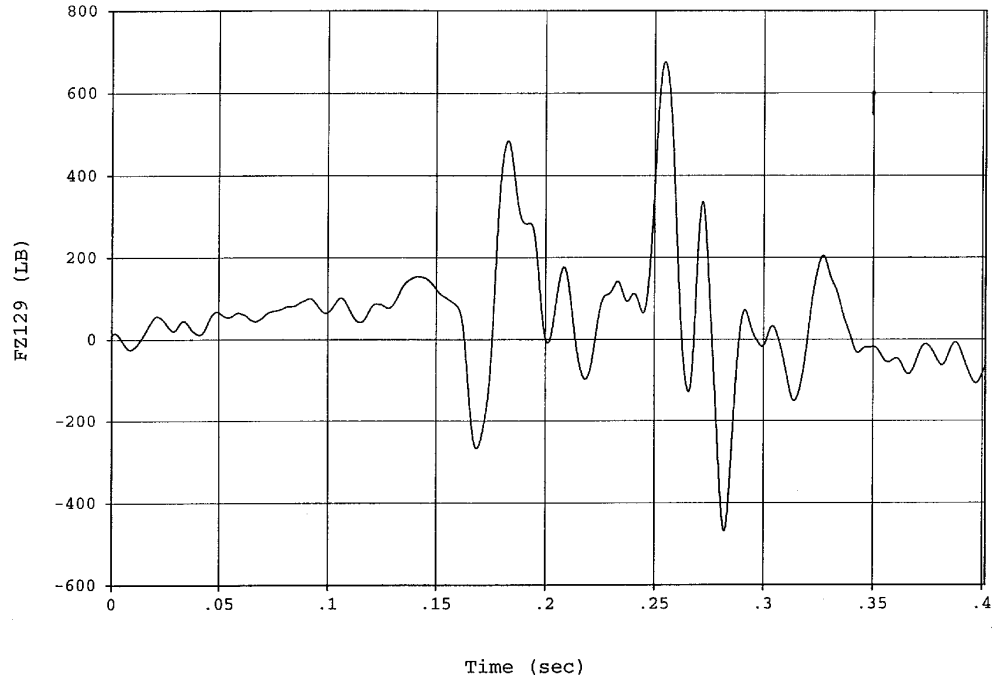


**Figure F36.  Test No. 2 Aft Wall Seat Attachment, z-Direction**

**TEST NO. 3 AND MODEL 2 SEAT ATTACHMENT LOADS**
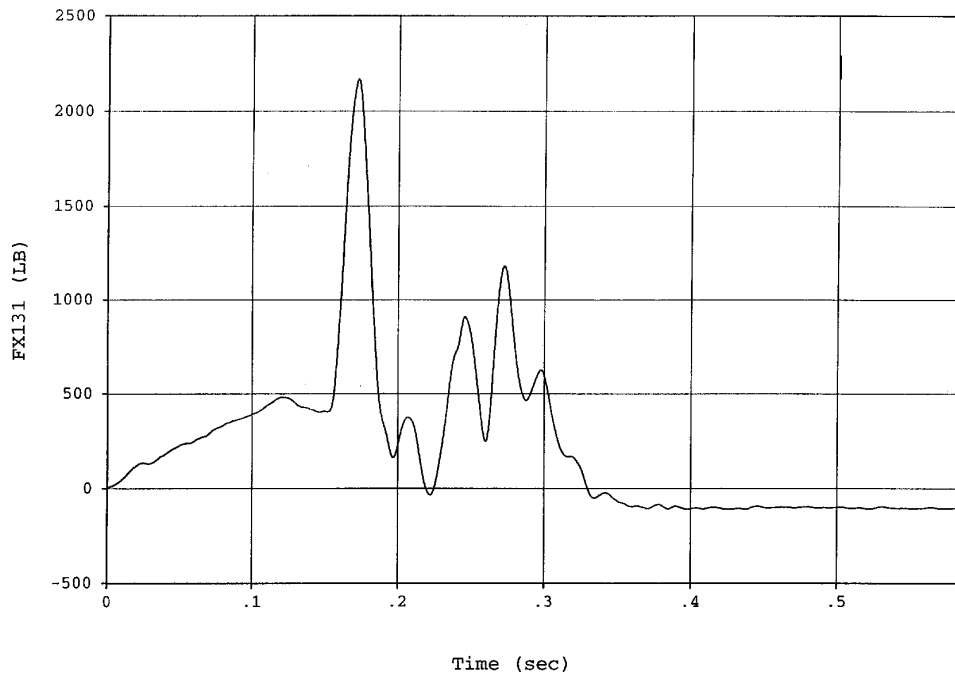


**Figure F37.  Test No. 3 Fore Floor Seat Attachment, x-Direction**
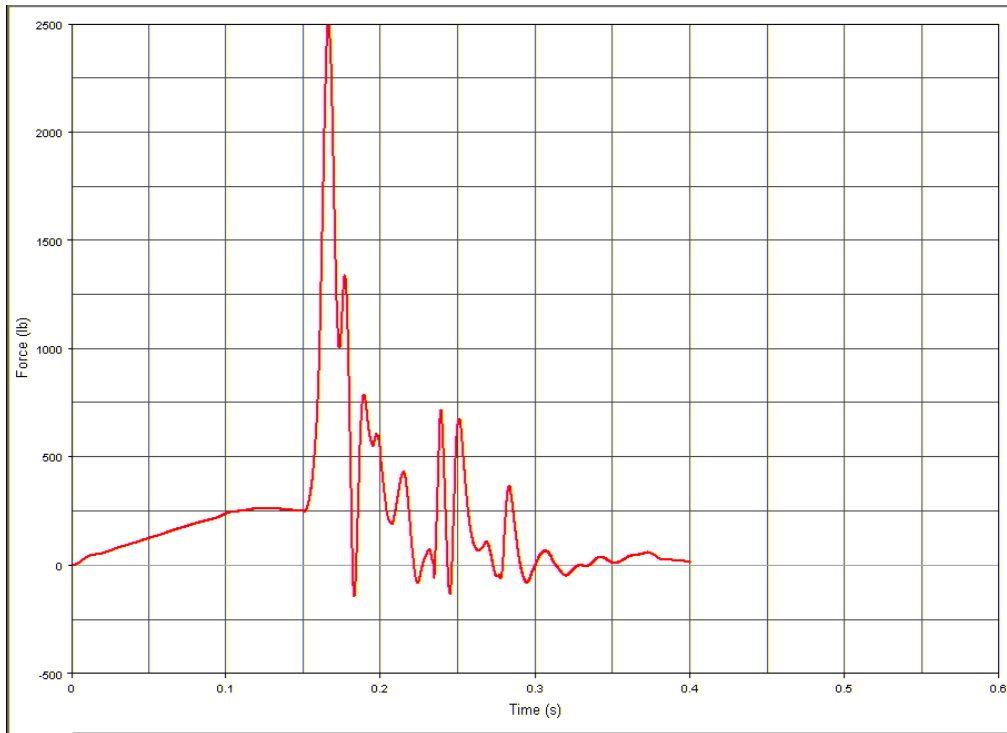
**Figure F38.  Model 2 Fore Floor Seat Attachment, x-Direction**
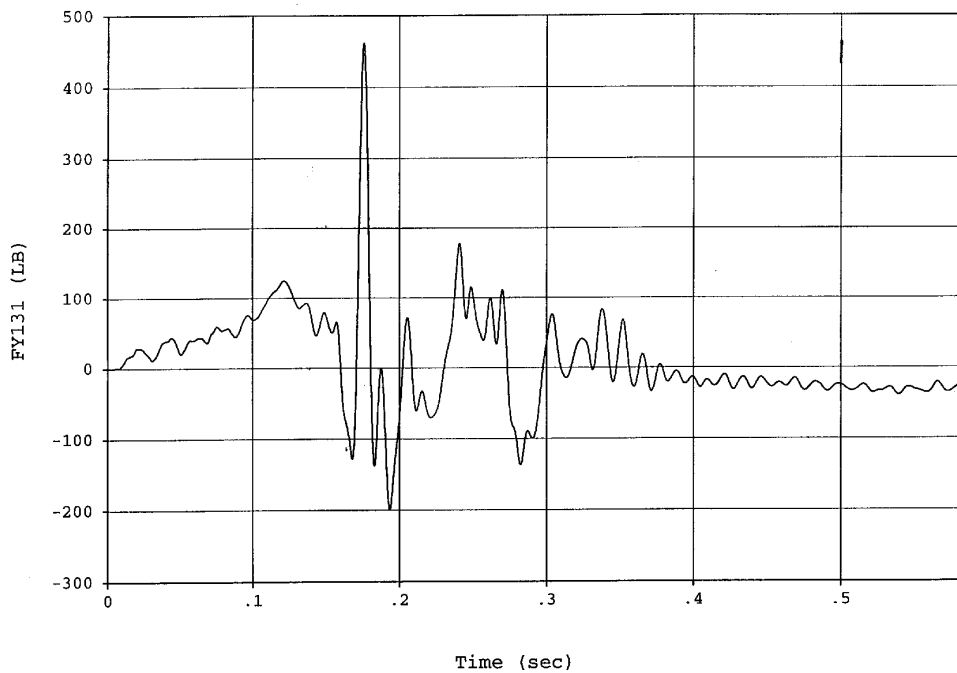


**Figure F39.  Test No. 3 Fore Floor Seat Attachment, y-Direction**
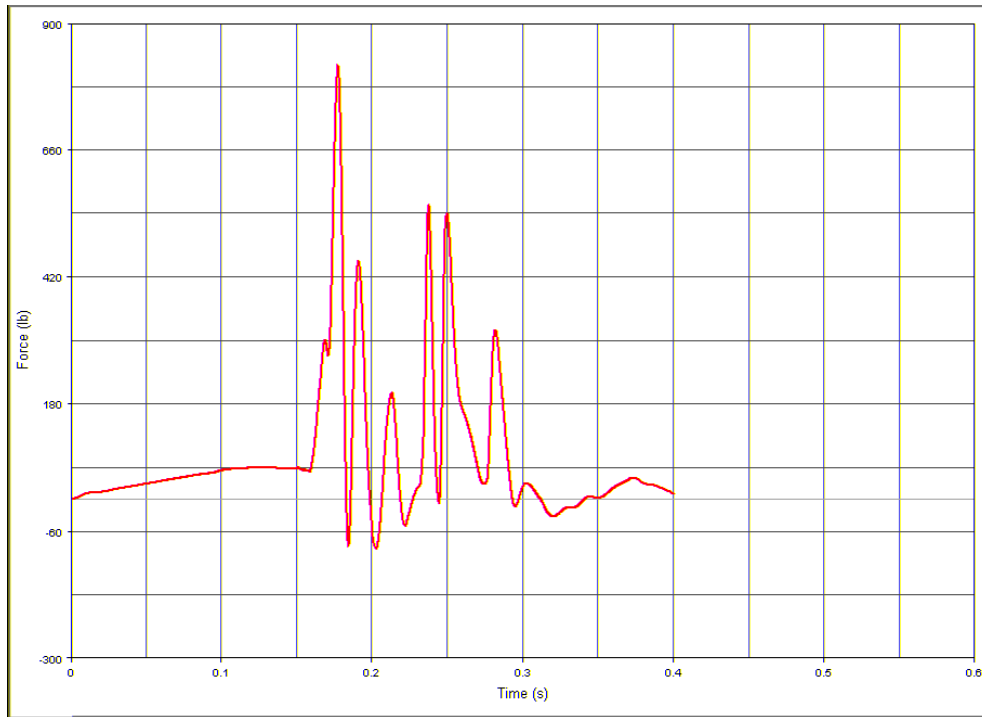
**Figure F40.  Model 2 Fore Floor Seat Attachment, y-Direction**
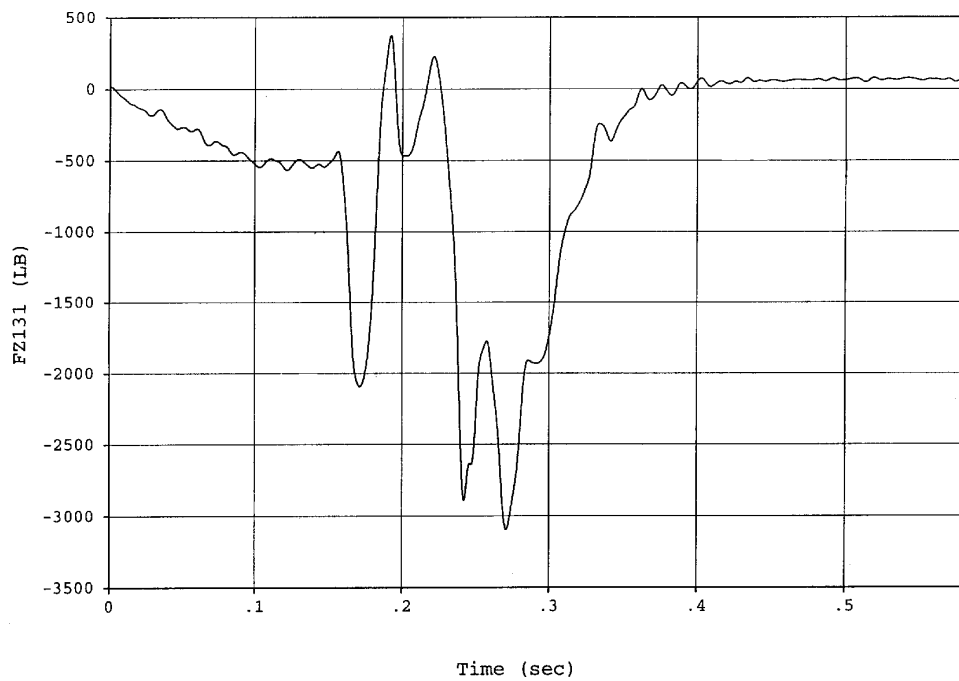


**Figure F41.  Test No. 3 Fore Floor Seat Attachment, z-Direction**
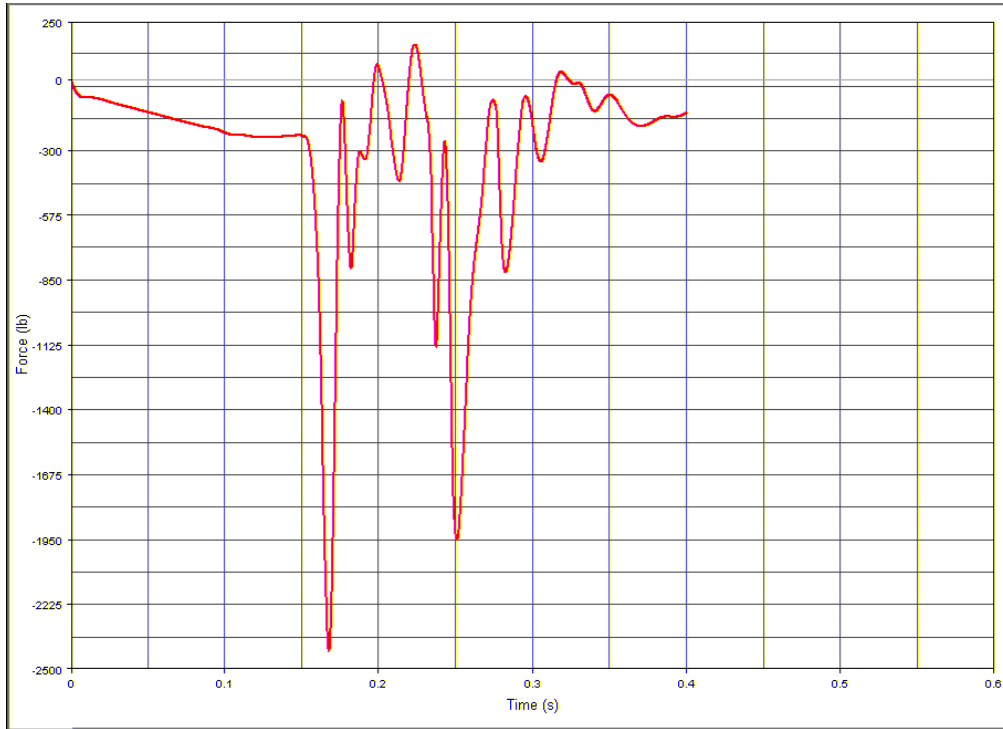
**Figure F42.  Model 2 Fore Floor Seat Attachment, z-Direction**
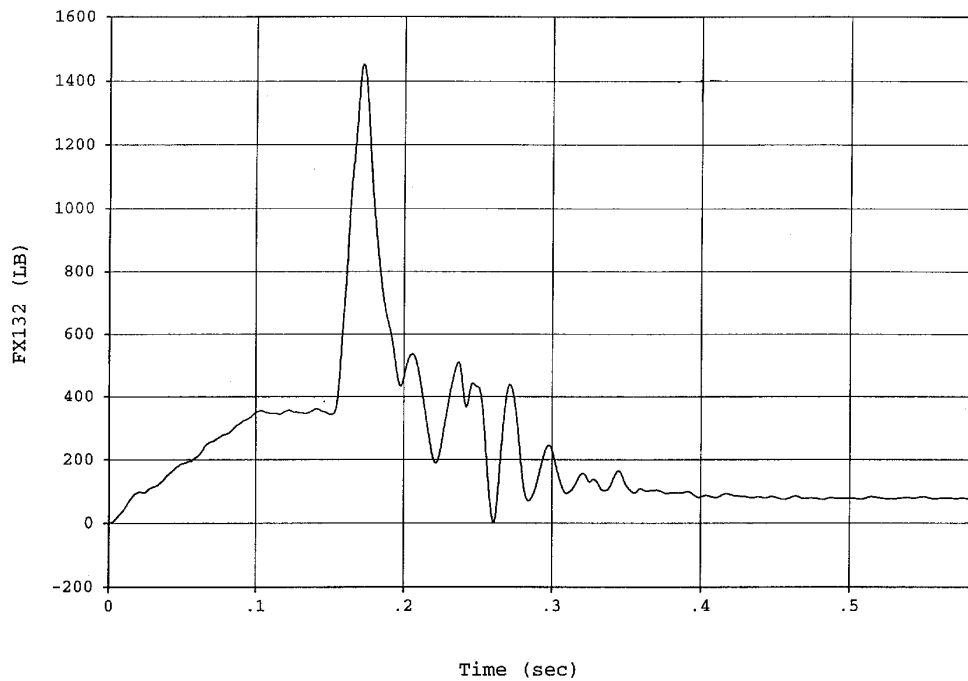


**Figure F43.  Test No. 3 Aft Floor Seat Attachment, x-Direction**

**Figure F44.  Model 2 Aft Floor Seat Attachment, x-Direction**
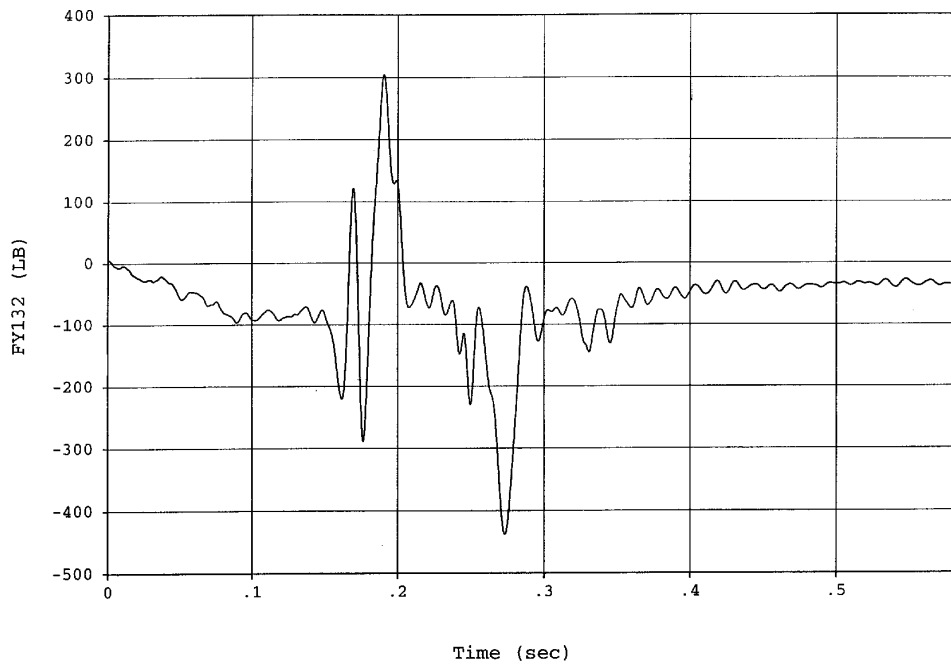


**Figure F45.  Test No. 3 Aft Floor Seat Attachment, y-Direction**

**Figure F46.  Model 2 Aft Floor Seat Attachment, y-Direction**
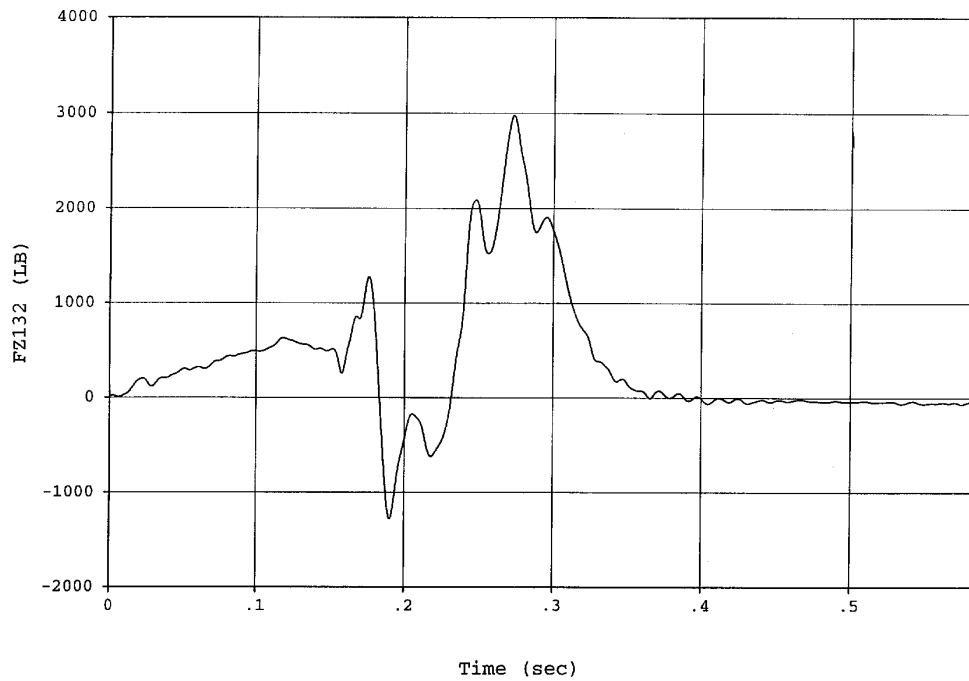


**Figure F47.  Test No. 3 Aft Floor Seat Attachment, z-Direction**

**Figure F48.  Model 2 Aft Floor Seat Attachment, z-Direction**
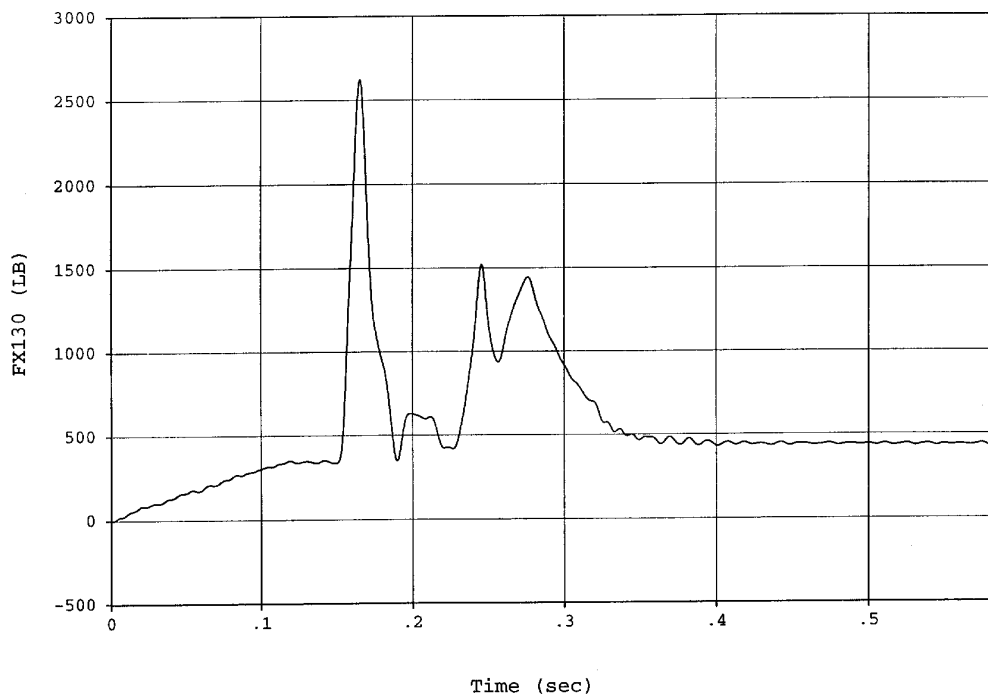


**Figure F49.  Test No. 3 Fore Wall Seat Attachment, x-Direction**

**Figure F50.  Model 2 Fore Wall Seat Attachment, x-Direction**
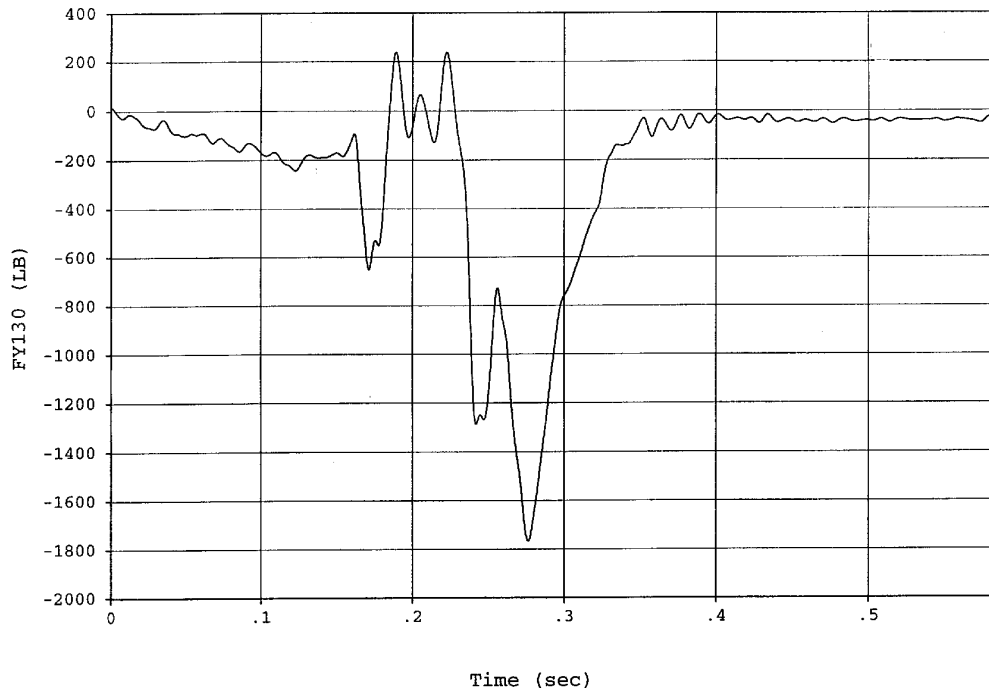


**Figure F51.  Test No. 3 Fore Wall Seat Attachment, y-Direction**

**Figure F52.  Model 2 Fore Wall Seat Attachment, y-Direction**
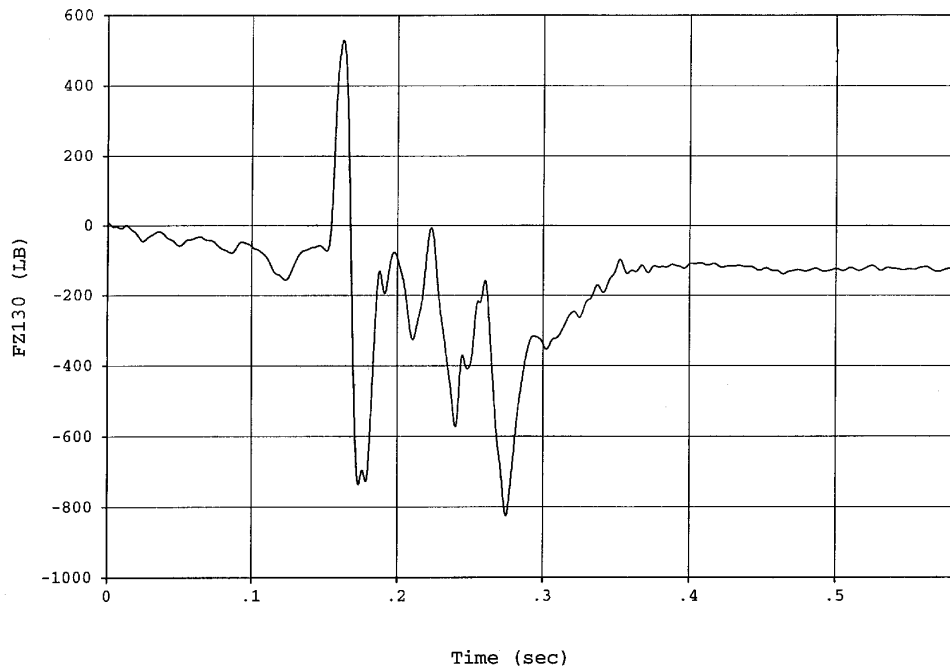


**Figure F53.  Test No. 3 Fore Wall Seat Attachment, z-Direction**

**Figure F54.  Model 2 Fore Wall Seat Attachment, z-Direction**
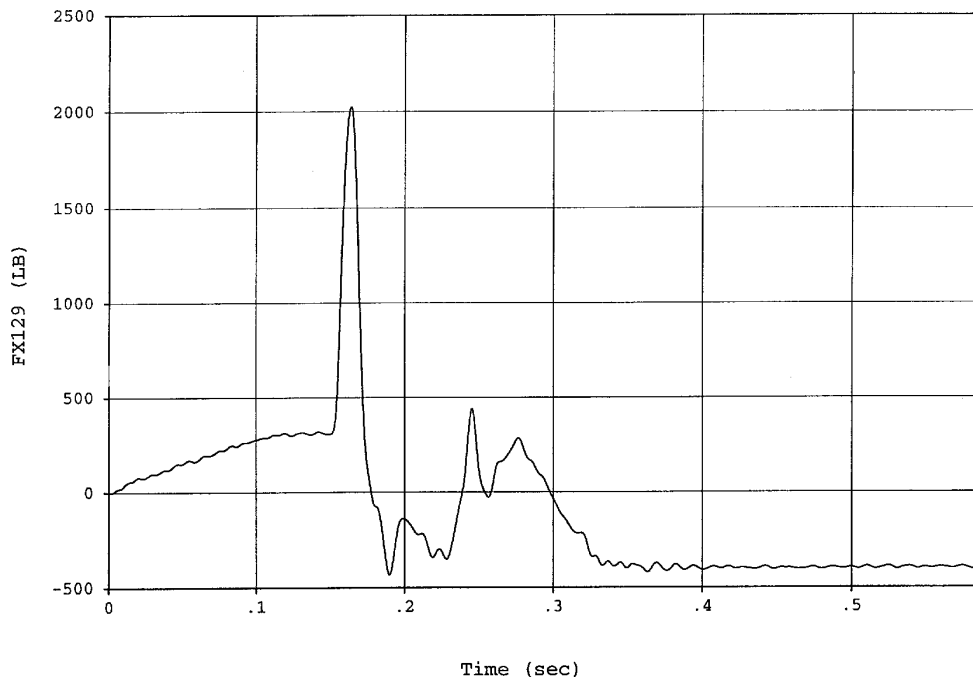


**Figure F55.  Test No. 3 Aft Wall Seat Attachment, x-Direction**

**Figure F56.  Model 2 Aft Wall Seat Attachment, x-Direction**
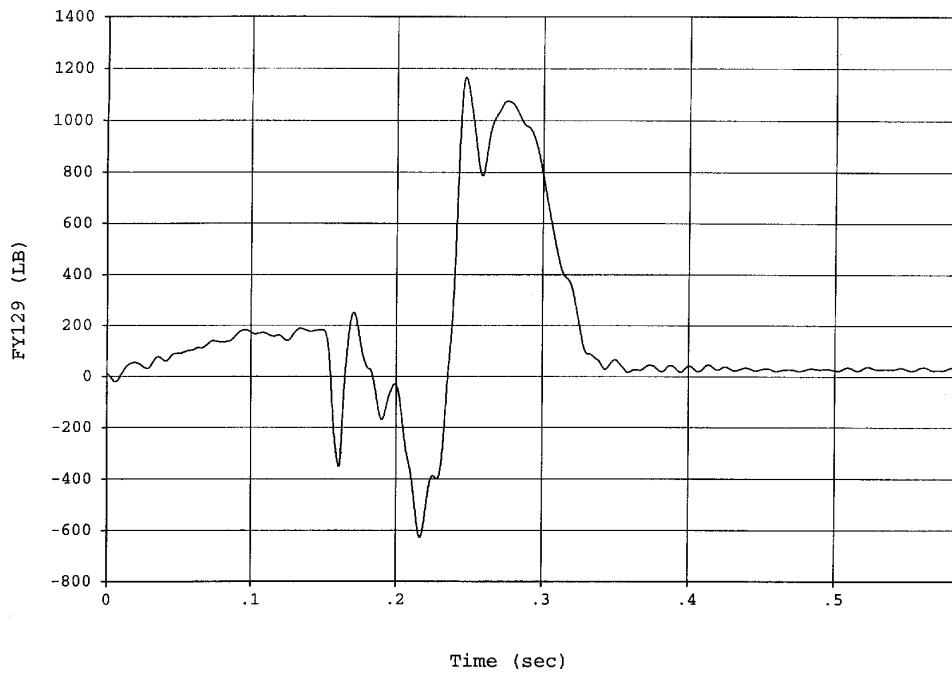


**Figure F57.  Test No. 3 Aft Wall Seat Attachment, y-Direction**

**Figure F58.  Model 2 Aft Wall Seat Attachment, y-Direction**
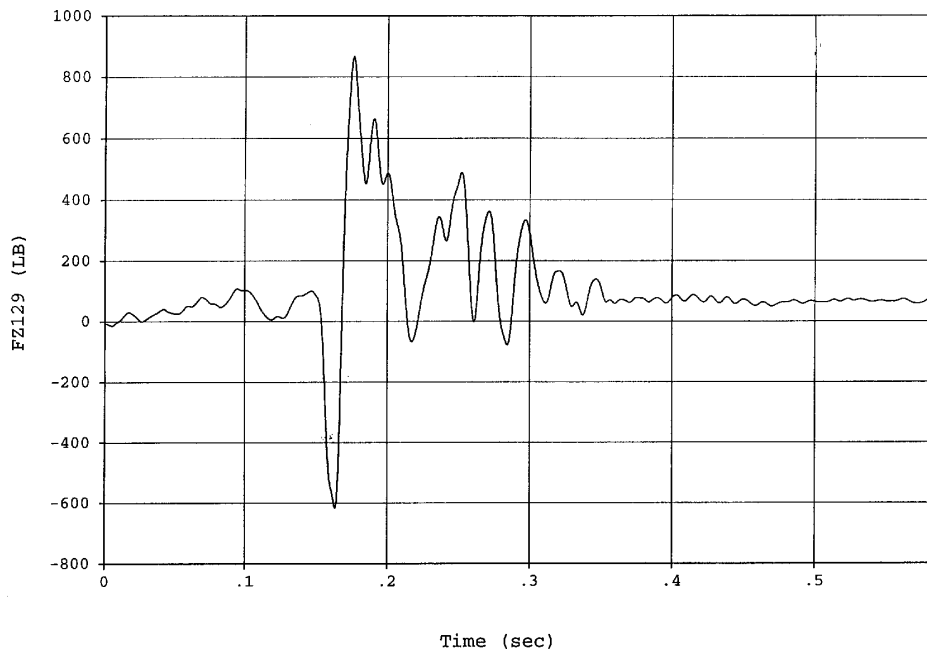


**Figure F59.  Test No. 3 Aft Wall Seat Attachment, z-Direction**

**Figure F60.  Model 2 Aft Wall Seat Attachment, z-Direction**

**TEST NO. 4 AND MODEL 3 SEAT ATTACHMENT LOADS**
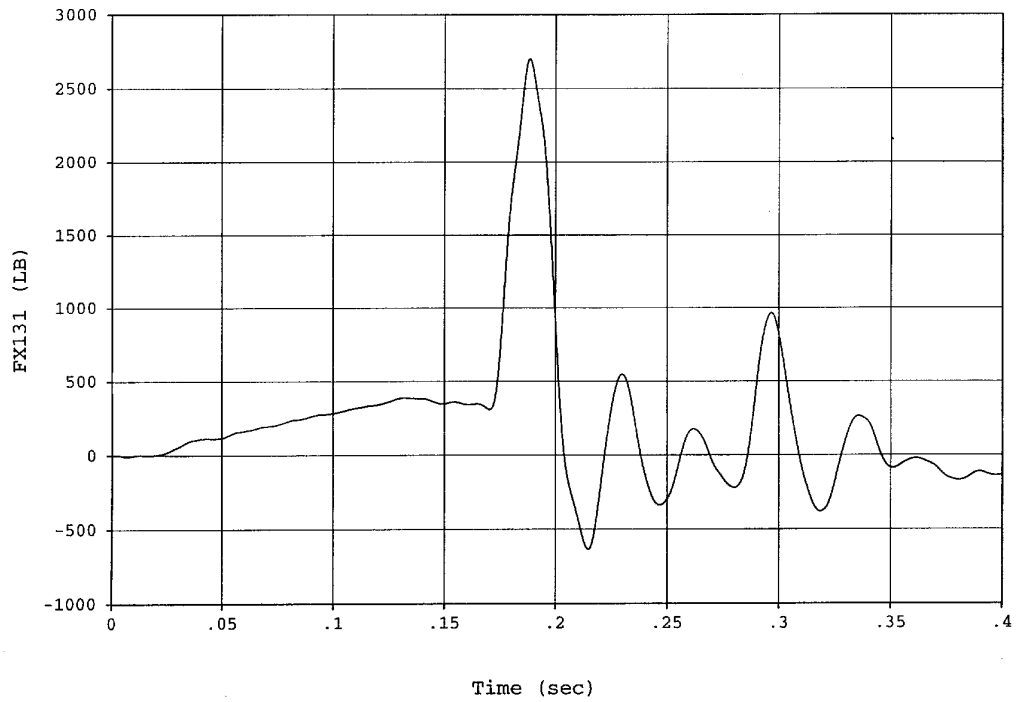


**Figure F61.  Test No. 4 Fore Floor Seat Attachment, x-Direction**

**TEST NO. 4 AND MODEL 3 SEAT ATTACHMENT LOADS (cont.)**
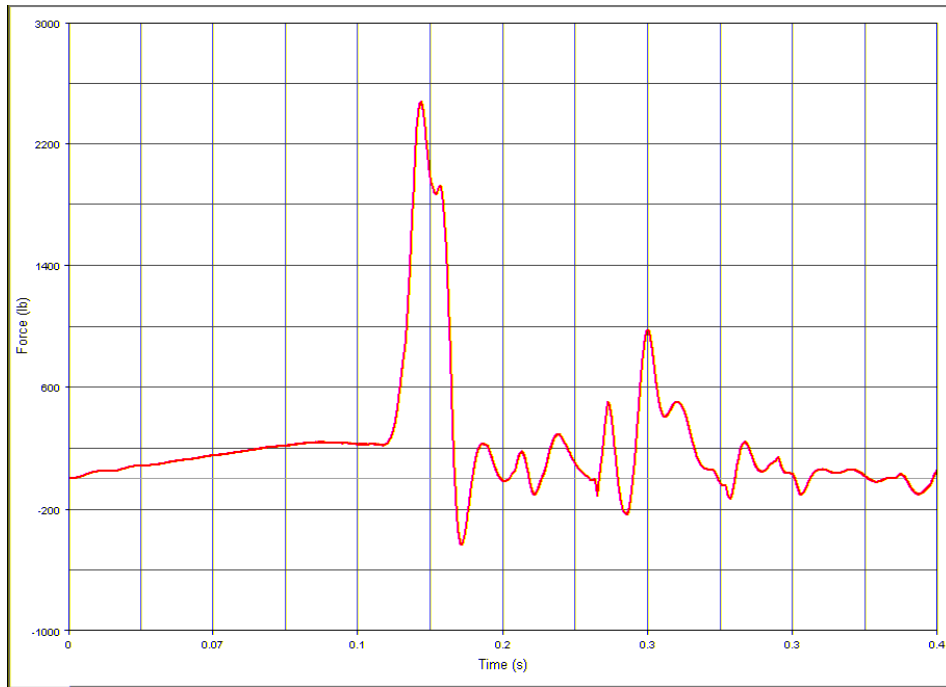


**Figure F62.  Model 3 Fore Floor Seat Attachment, x-Direction**
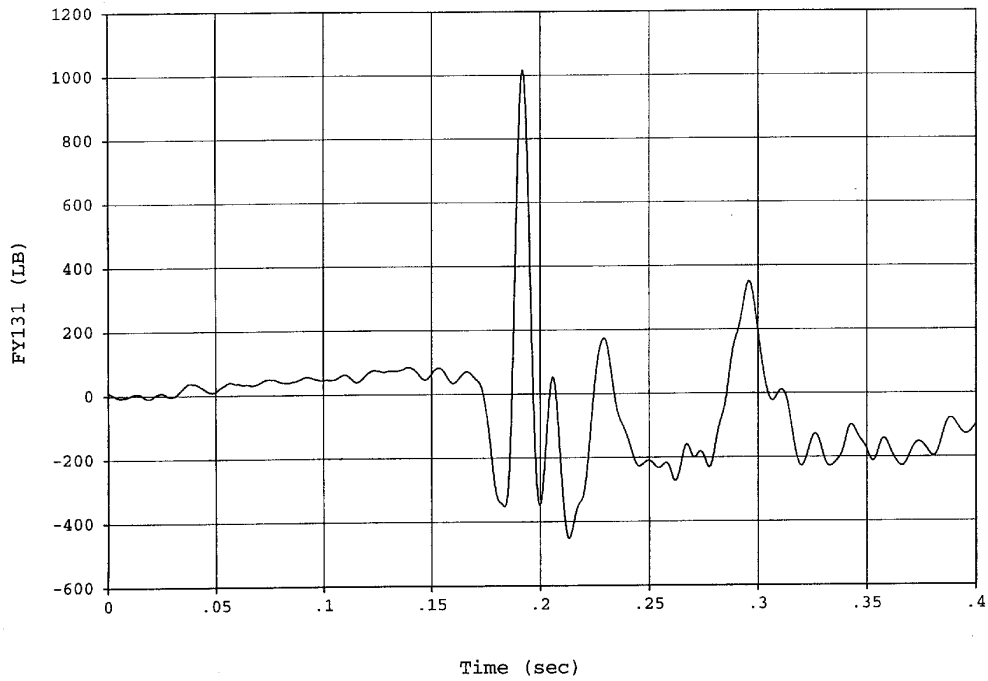


**Figure F63.  Test No. 4 Fore Floor Seat Attachment, y-Direction**
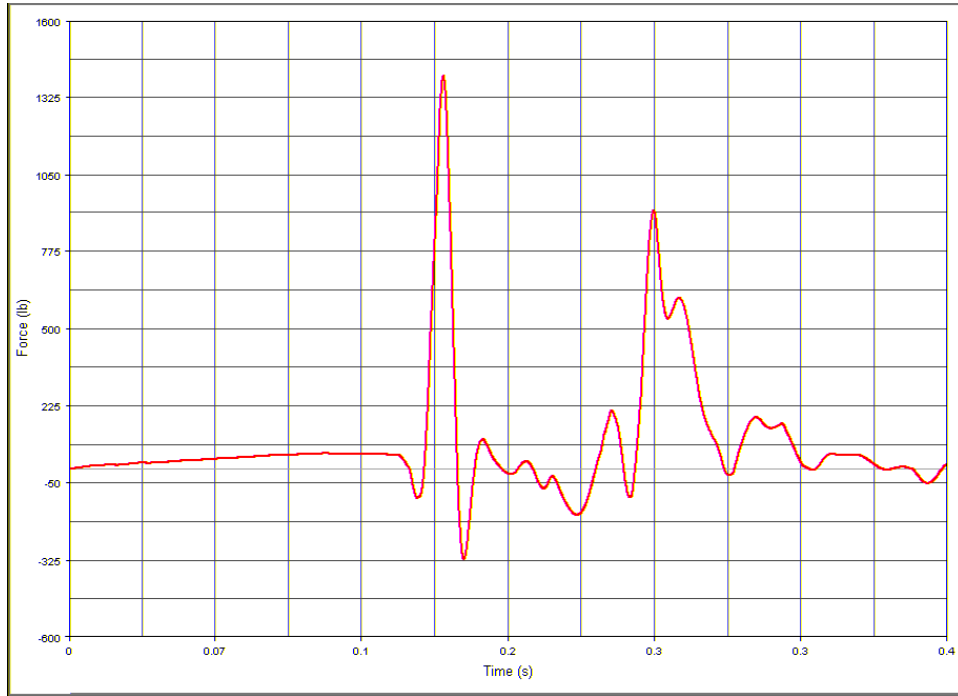
**Figure F64.  Model 3 Fore Floor Seat Attachment, y-Direction**
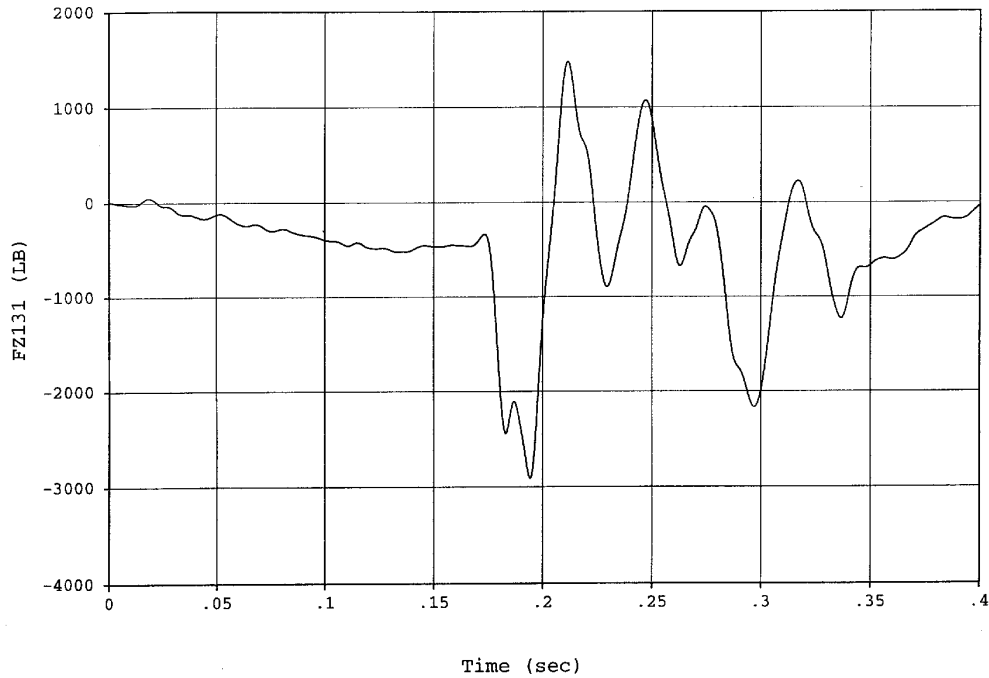


**Figure F65.  Test No. 4 Fore Floor Seat Attachment, z-Direction**
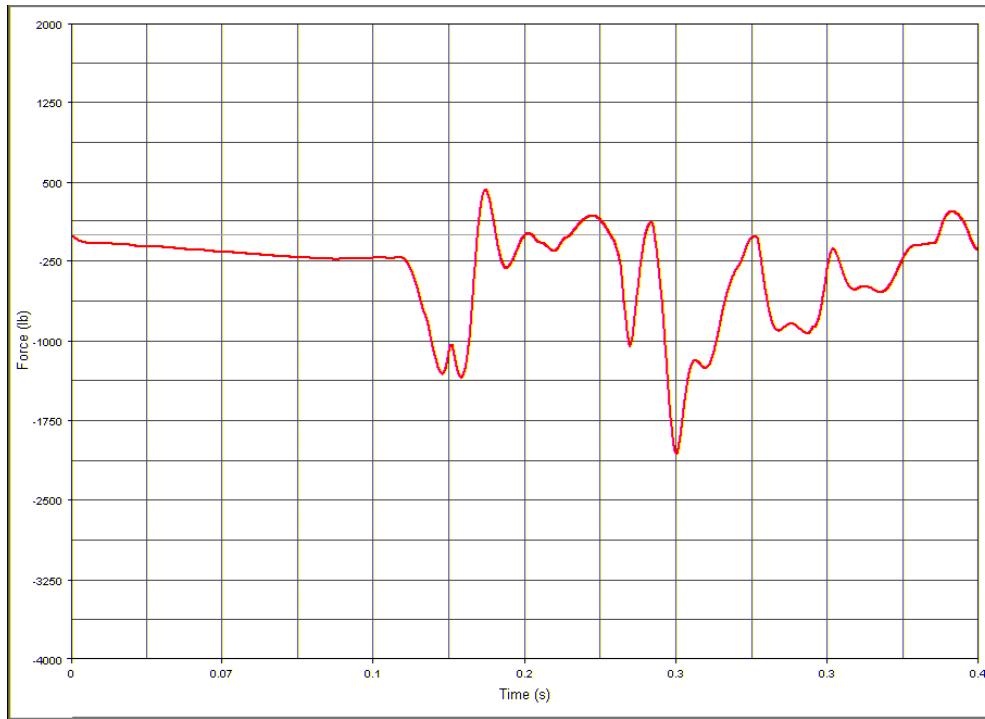
**Figure F66.  Model 3 Fore Floor Seat Attachment, z-Direction**
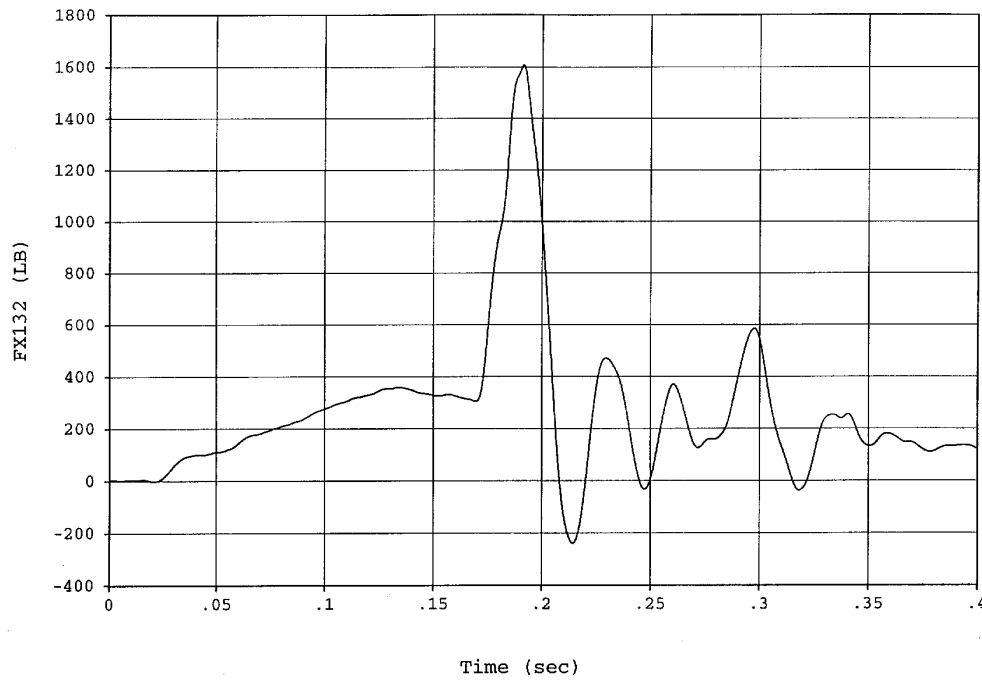


**Figure F67.  Test No. 4 Aft Floor Seat Attachment, x-Direction**

**TEST NO. 4 AND MODEL 3 SEAT ATTACHMENT LOADS (cont.)**
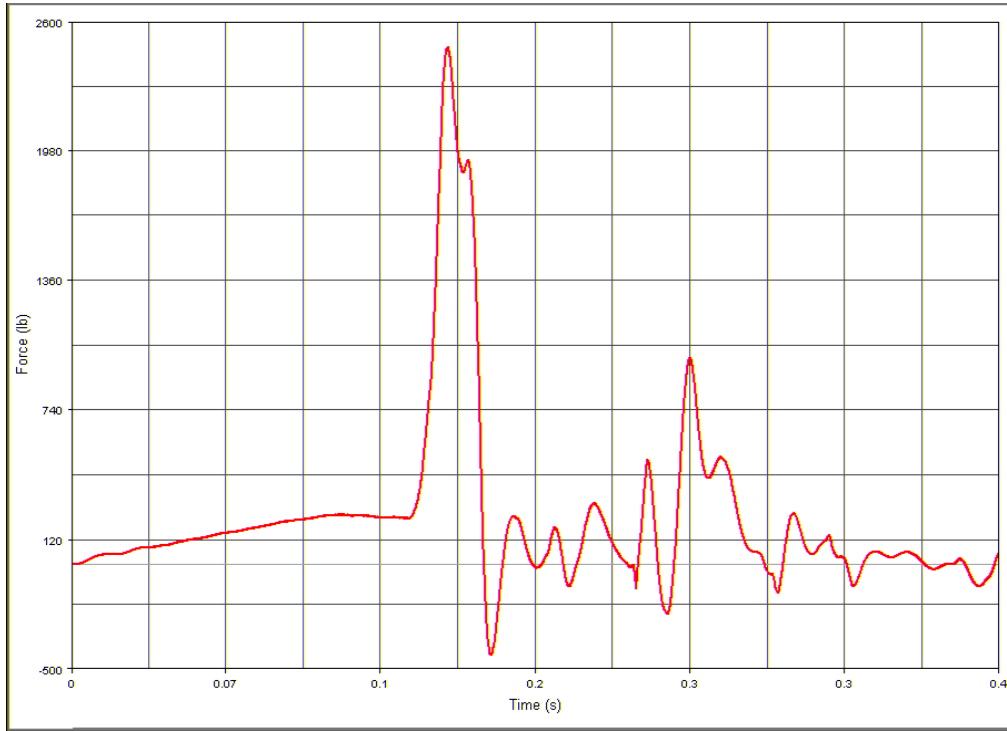


**Figure F68.  Model 3 Aft Floor Seat Attachment, x-Direction**
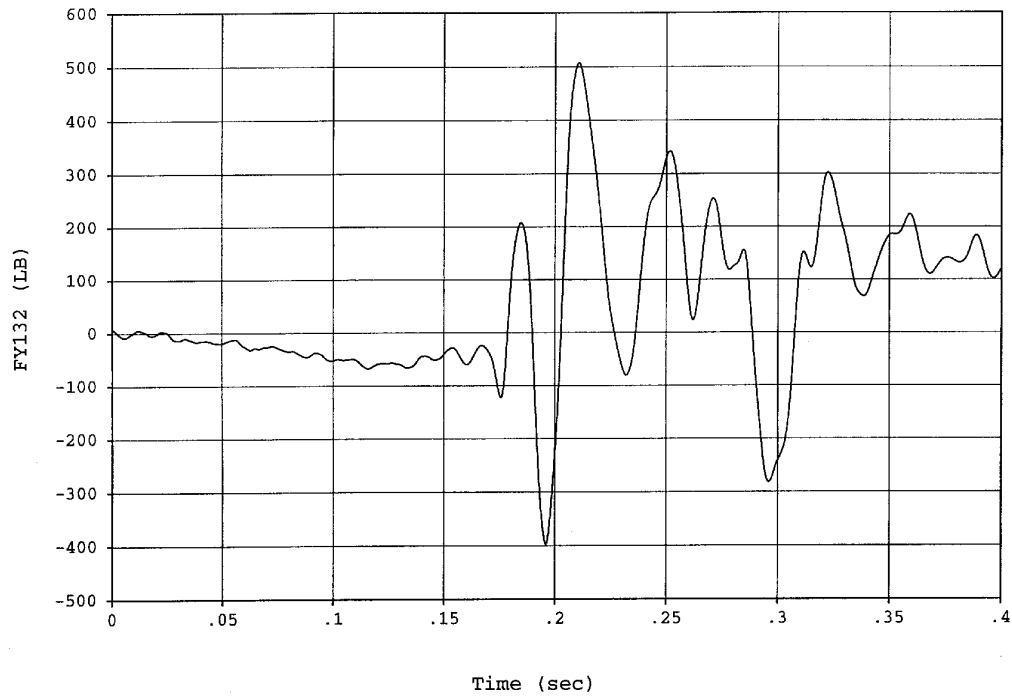


**Figure F69.  Test No. 4 Aft Floor Seat Attachment, y-Direction**
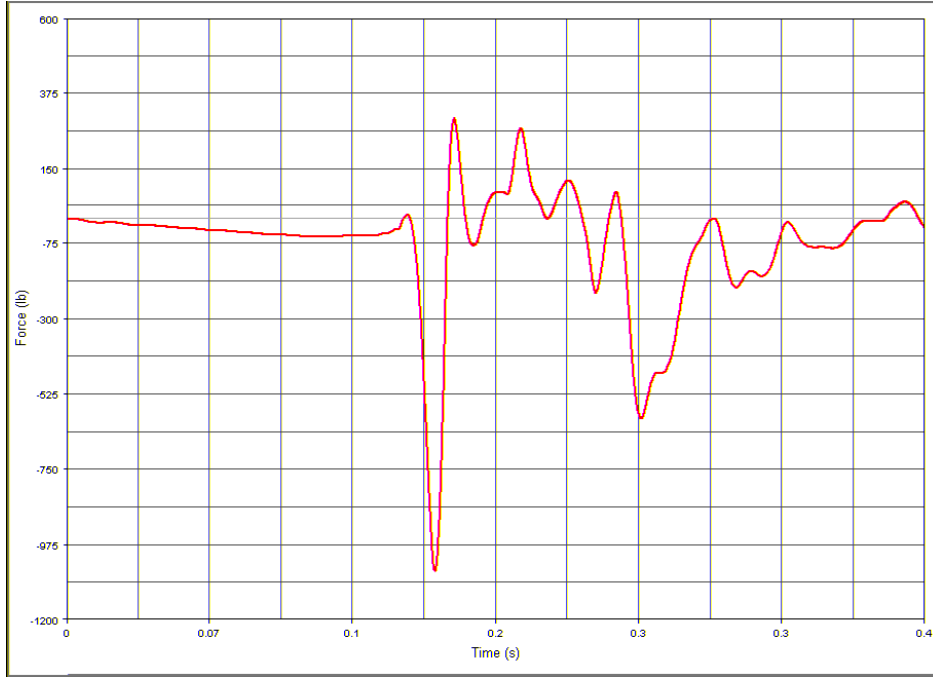
**Figure F70.  Model 3 Aft Floor Seat Attachment, y-Direction**
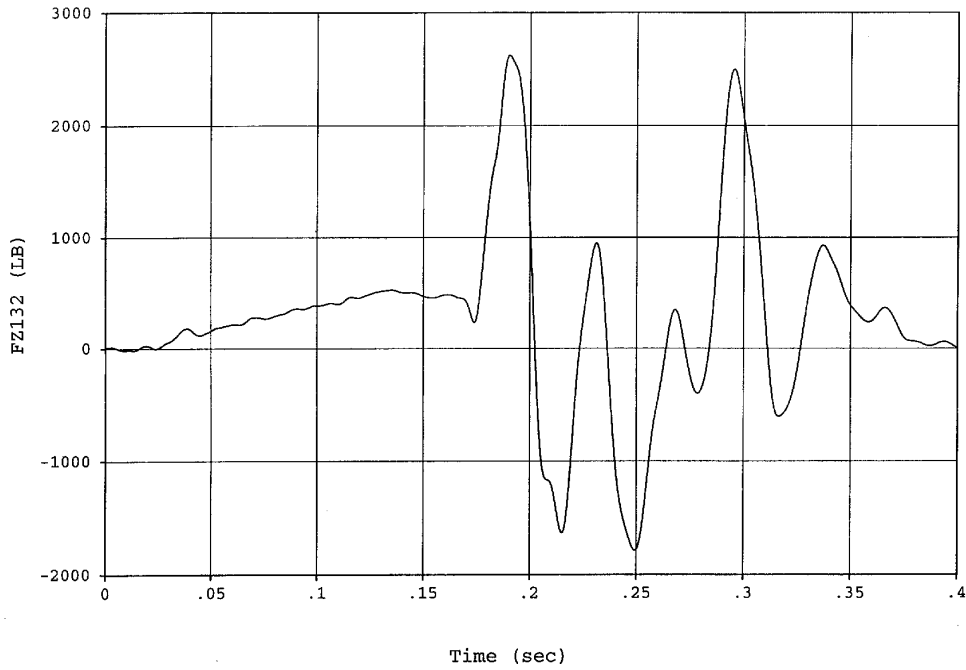


**Figure F71.  Test No. 4 Aft Floor Seat Attachment, z-Direction**
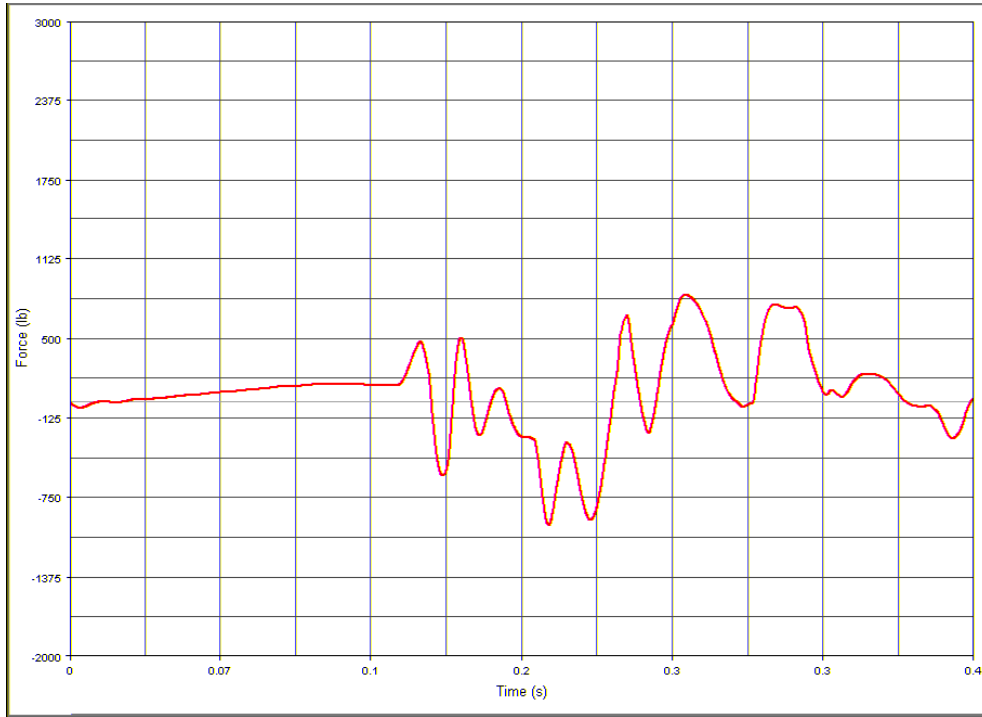
**Figure F72. Model 3 Aft Floor Seat Attachment, z-Direction**
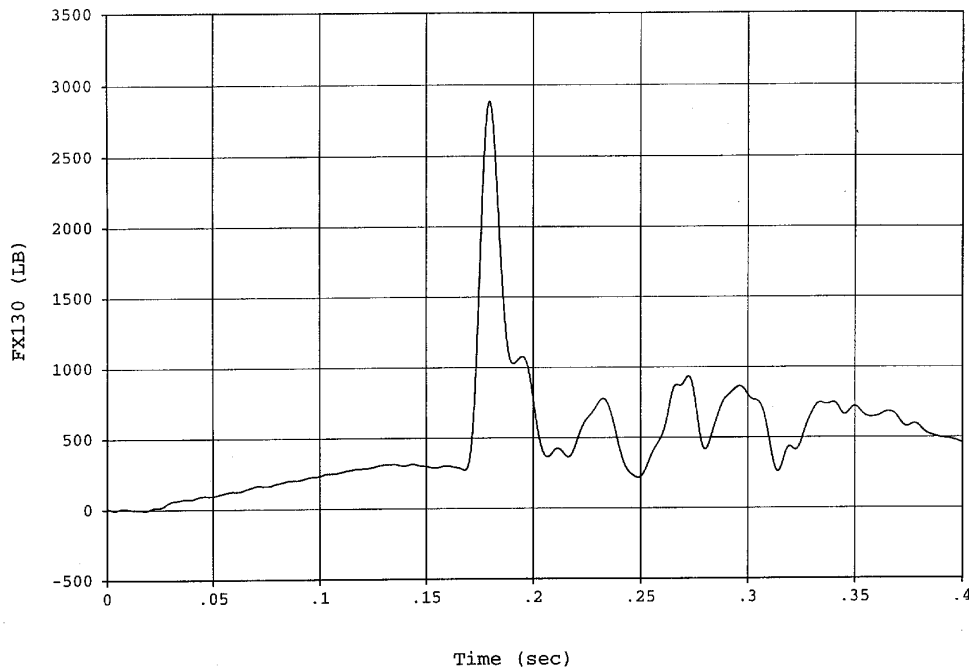


**Figure F73. Test No. 4 Fore Wall Seat Attachment, x-Direction**

**TEST NO. 4 AND MODEL 3 SEAT ATTACHMENT LOADS (cont.)**
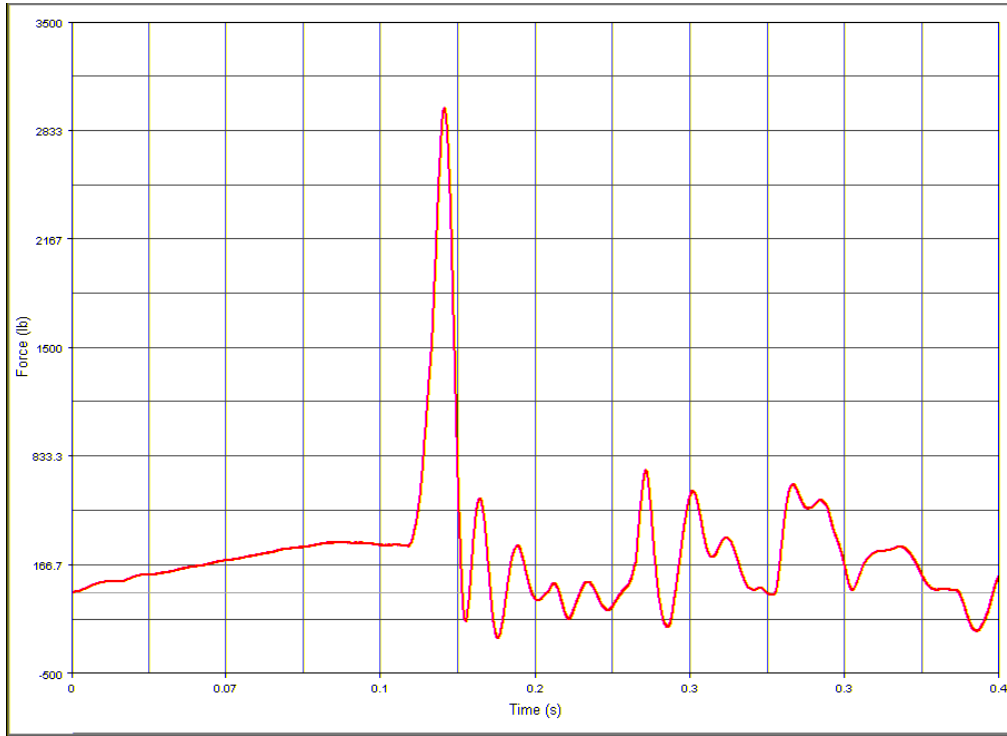


**Figure F74.  Model 3 Fore Wall Seat Attachment, x-Direction**
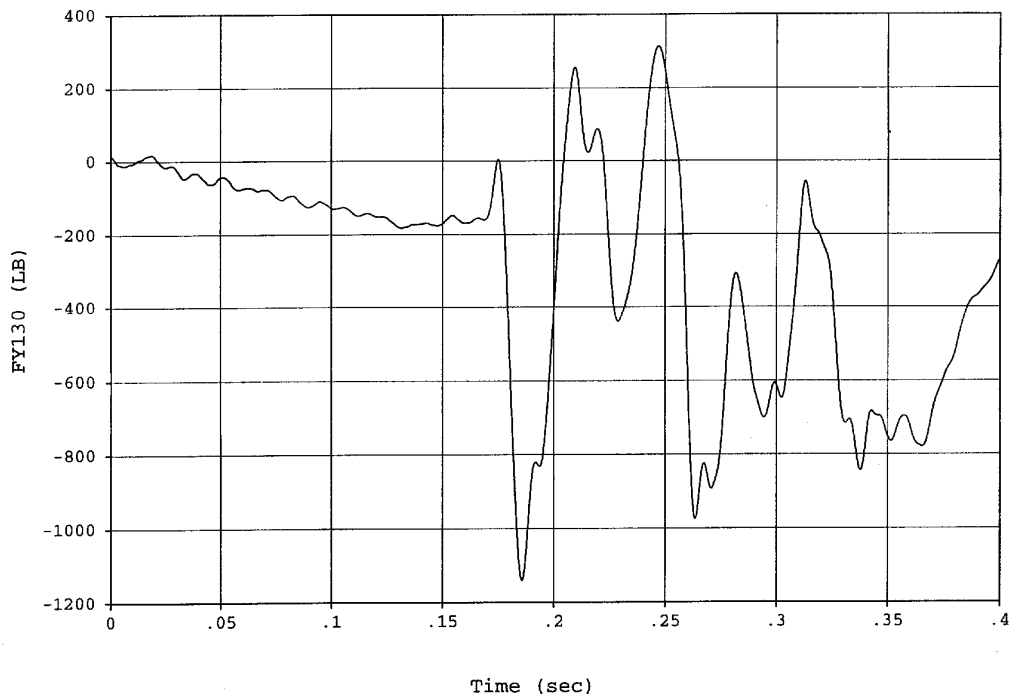


**Figure F75.  Test No. 4 Fore Wall Seat Attachment, y-Direction**

112
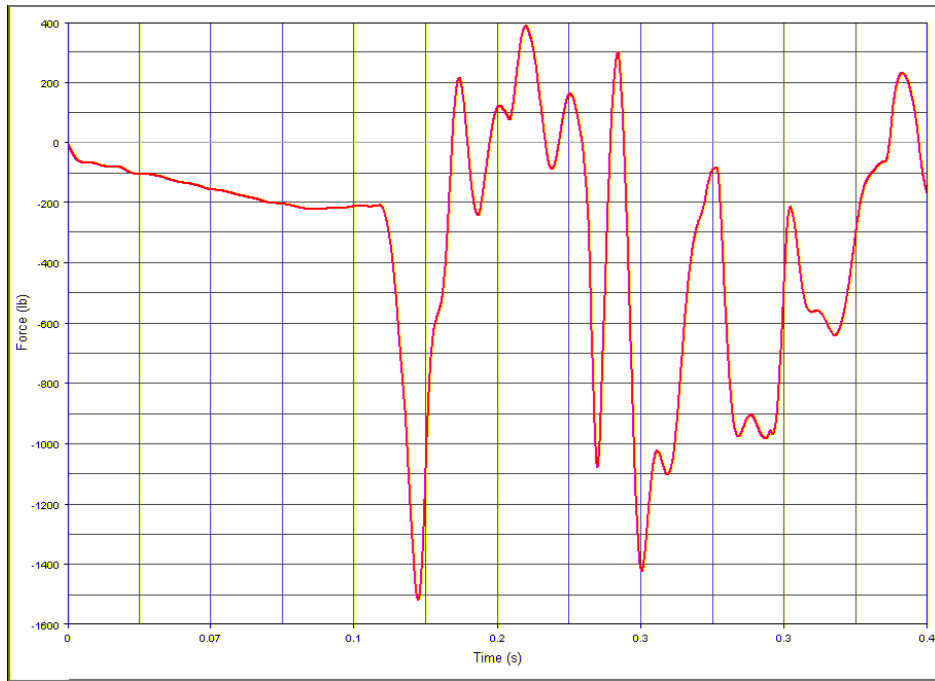
**Figure F76.  Model 3 Fore Wall Seat Attachment, y-Direction**
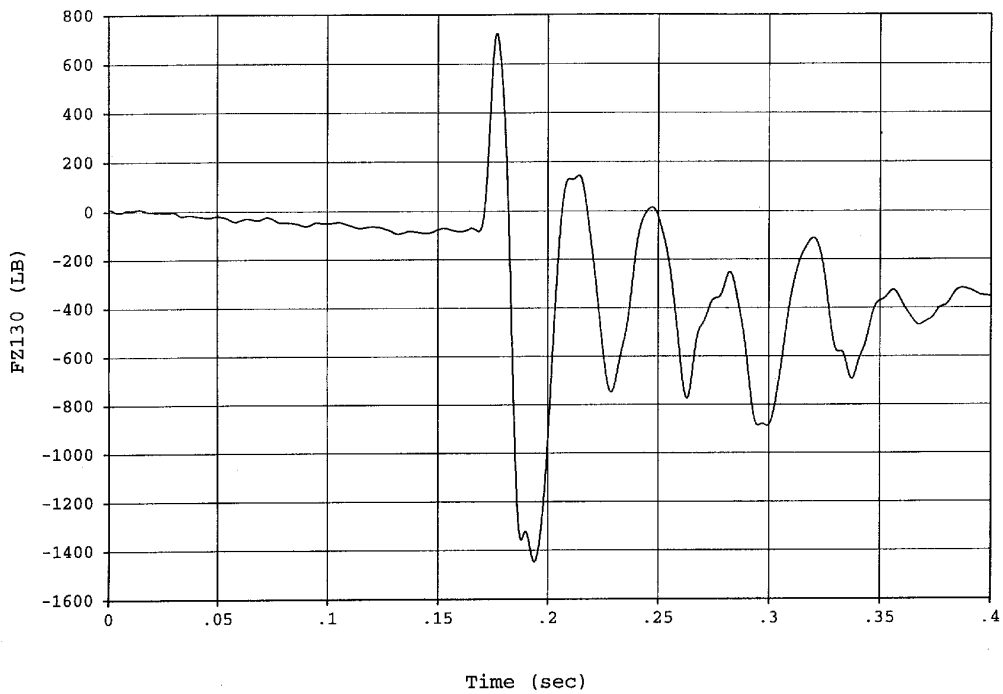


**Figure F77.  Test No. 4 Fore Wall Seat Attachment, z-Direction**

113
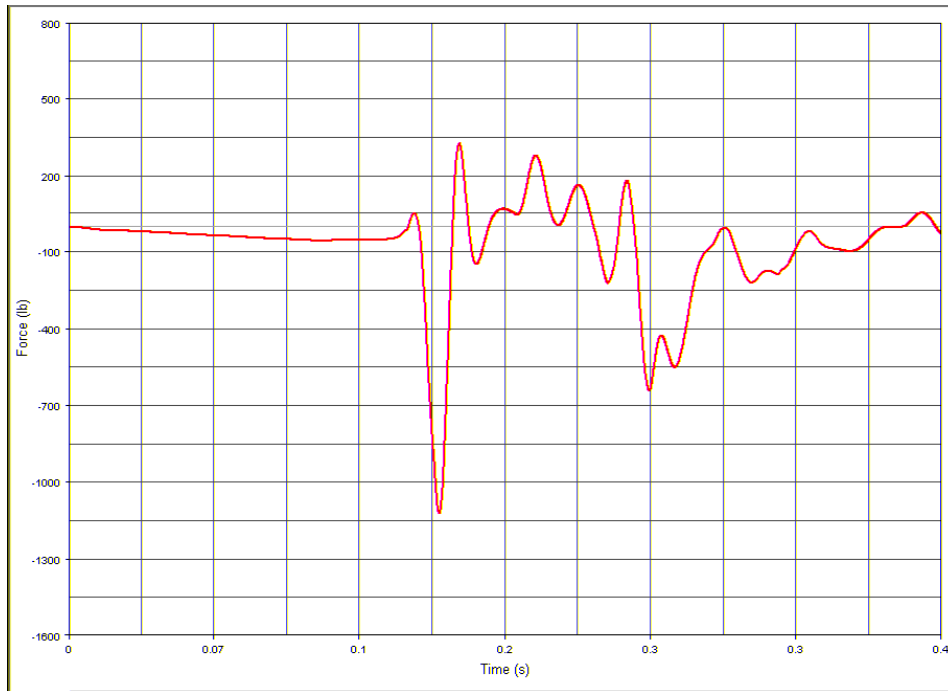
**Figure F78. Model 3 Fore Wall Seat Attachment, z-Direction**
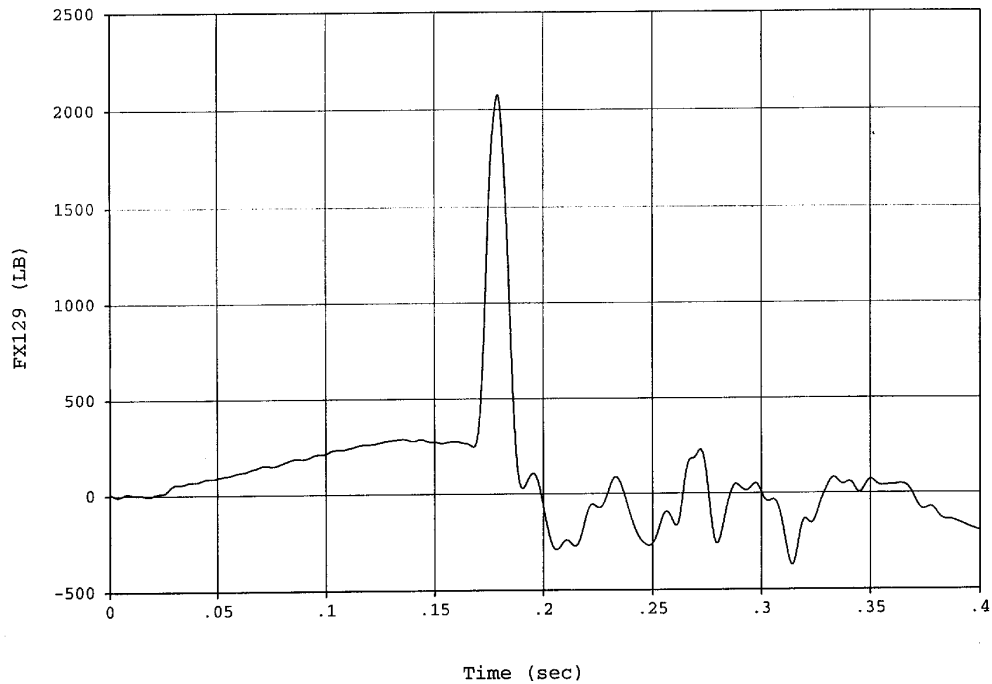


**Figure F79. Test No. 4 Aft Wall Seat Attachment, x-Direction**

114

**TEST NO. 4 AND MODEL 3 SEAT ATTACHMENT LOADS (cont.)**
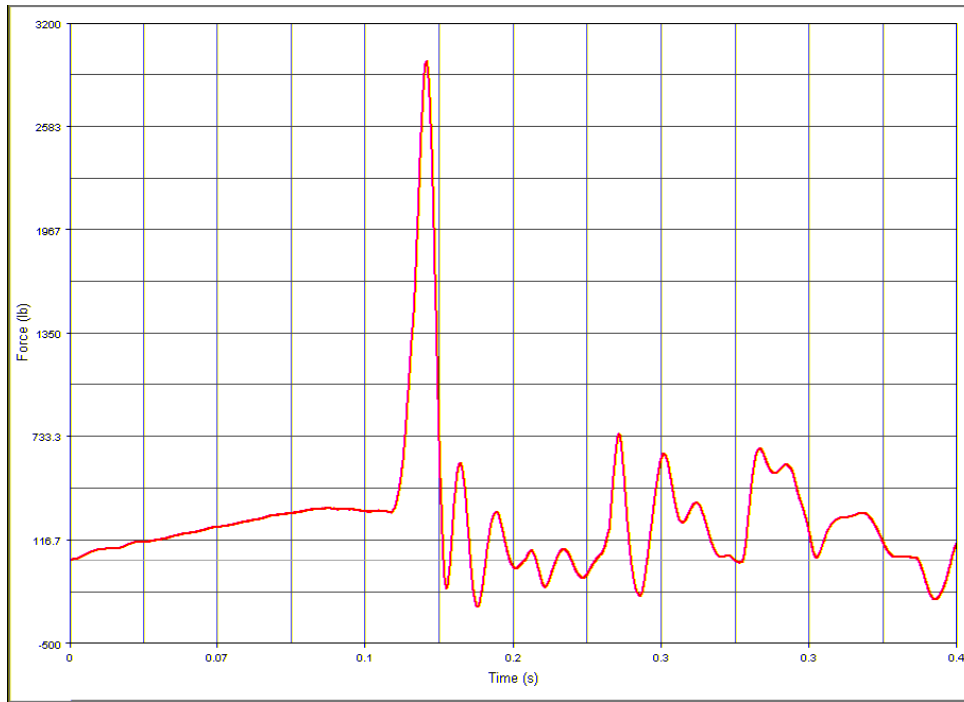


**Figure F80.  Test Model 3 Aft Wall Seat Attachment, x-Direction**
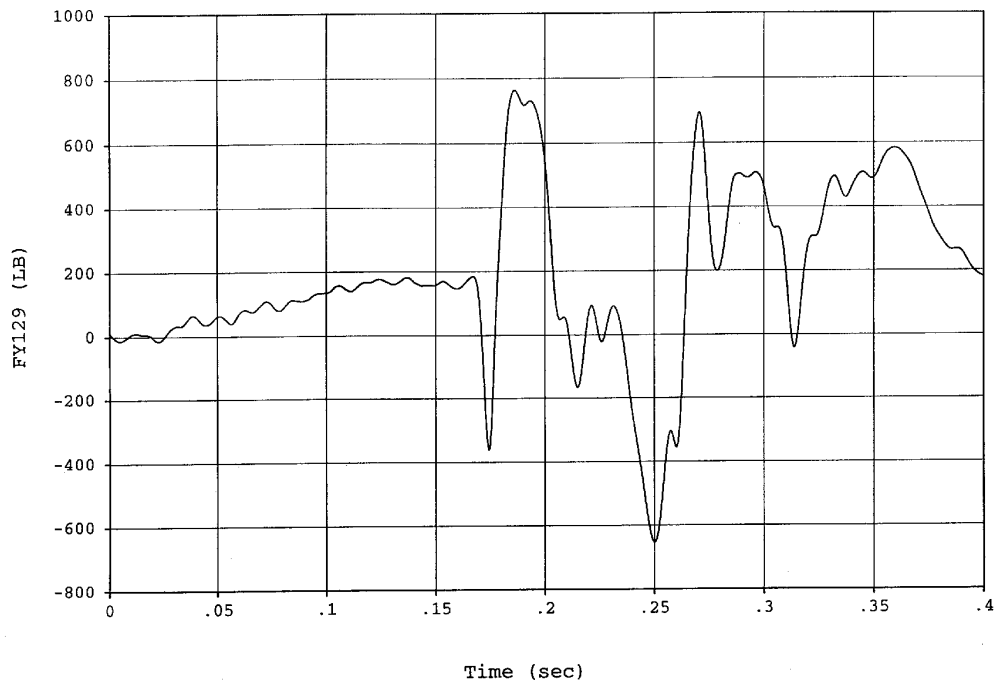


**Figure F81.  Test No. 4 Aft Wall Seat Attachment, y-Direction**

**TEST NO. 4 AND MODEL 3 SEAT ATTACHMENT LOADS (cont.)**
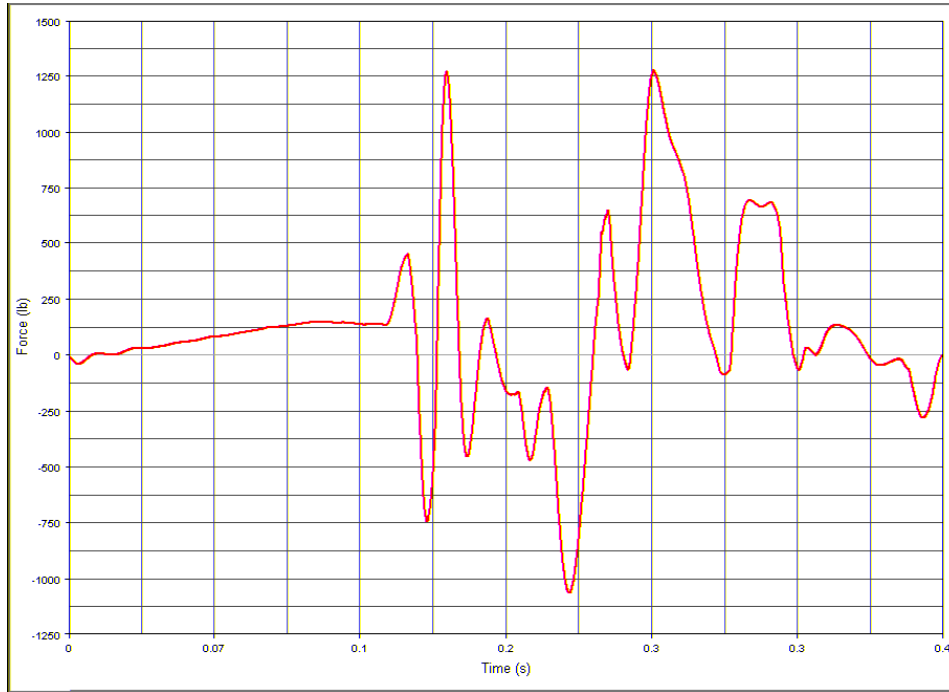


**Figure F82.  Test Model 3 Aft Wall Seat Attachment, y-Direction**
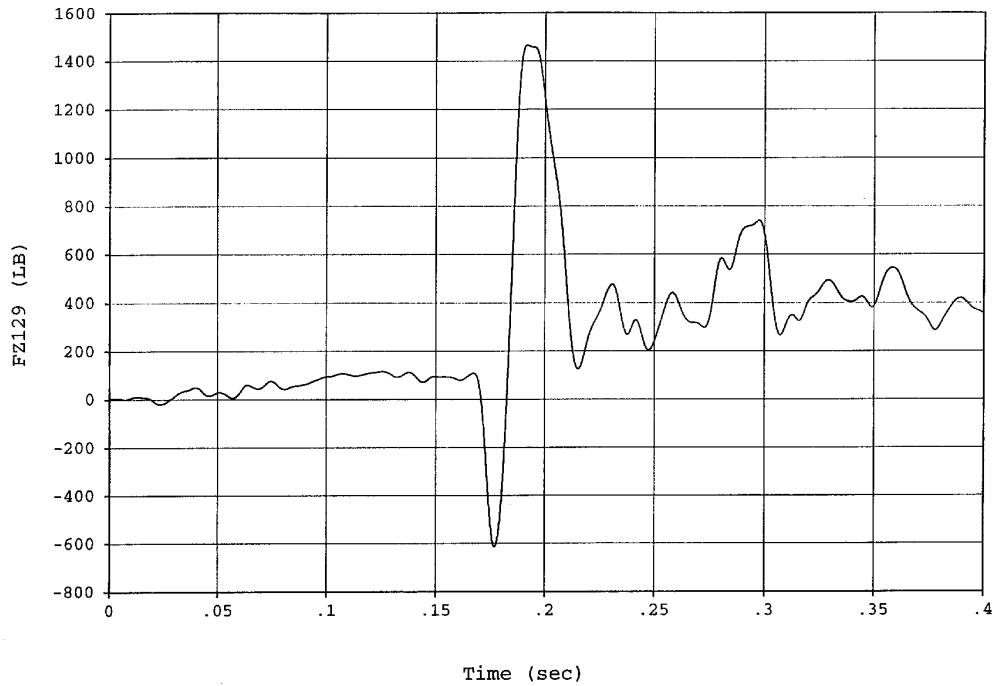


**Figure F83.  Test No. 4 Aft Wall Seat Attachment, z-Direction**

**TEST NO. 4 AND MODEL 3 SEAT ATTACHMENT LOADS (cont.)**
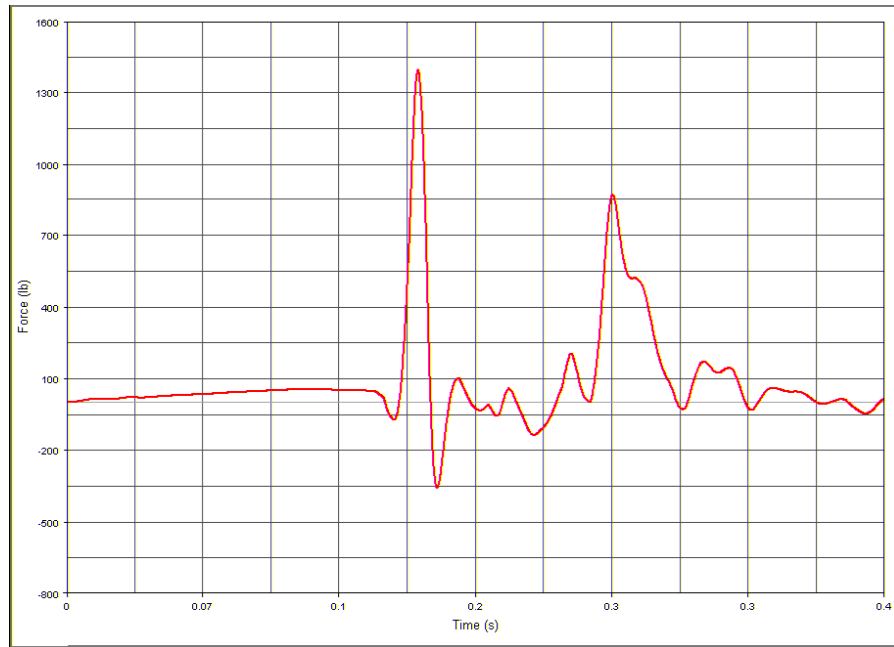


**Figure F84.  Test Model 3 Aft Wall Seat Attachment, z-Direction**

# APPENDIX G

## OCCUPANT INJURY DATA PLOTS
## FROM TESTING AND MODELING RESULTS

### NOTE FOR INJURY DATA PLOTS

**Solid Line = Test**
**Dashed Line = Model**

### TEST NO. 1/MODEL 1, 50TH-PERCENTILE HYBRID III ATD, AISLE SEAT
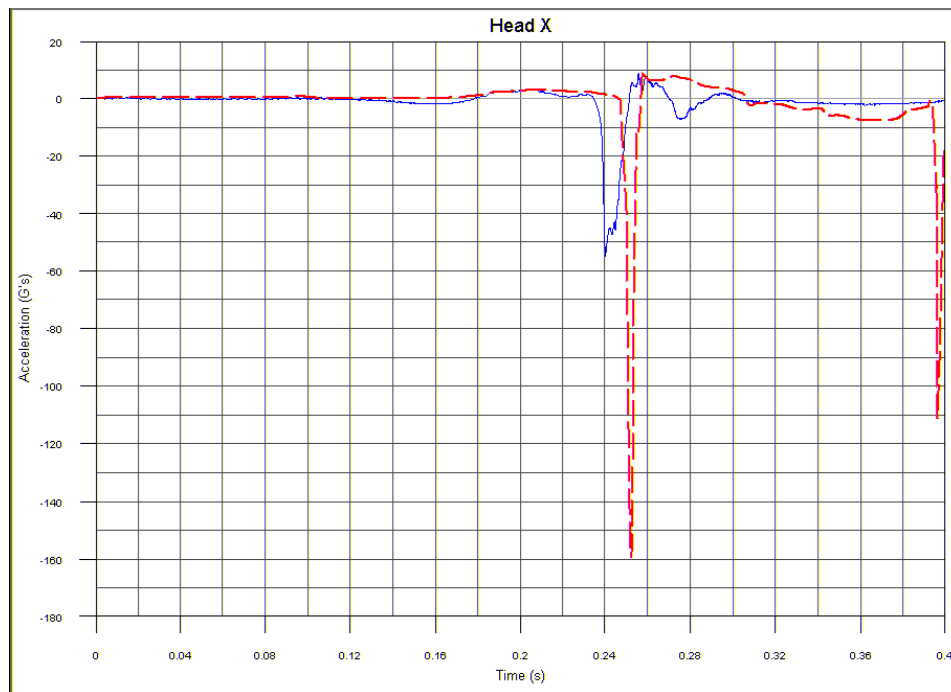


**Figure G1.  Head Acceleration, x-Direction**
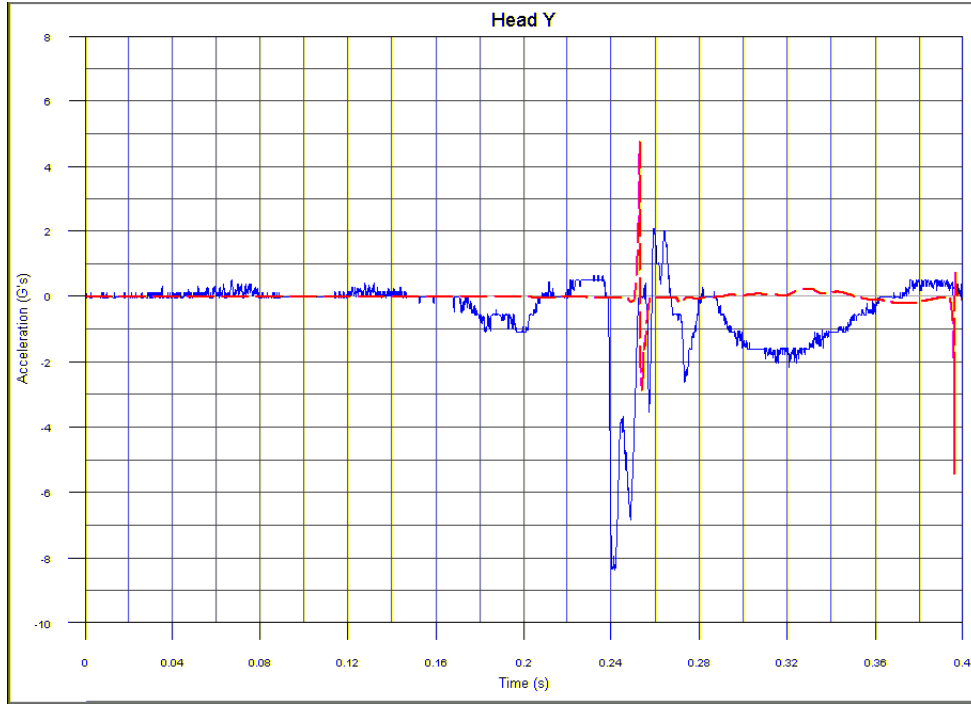
**Figure G2.  Head Acceleration, y-Direction**
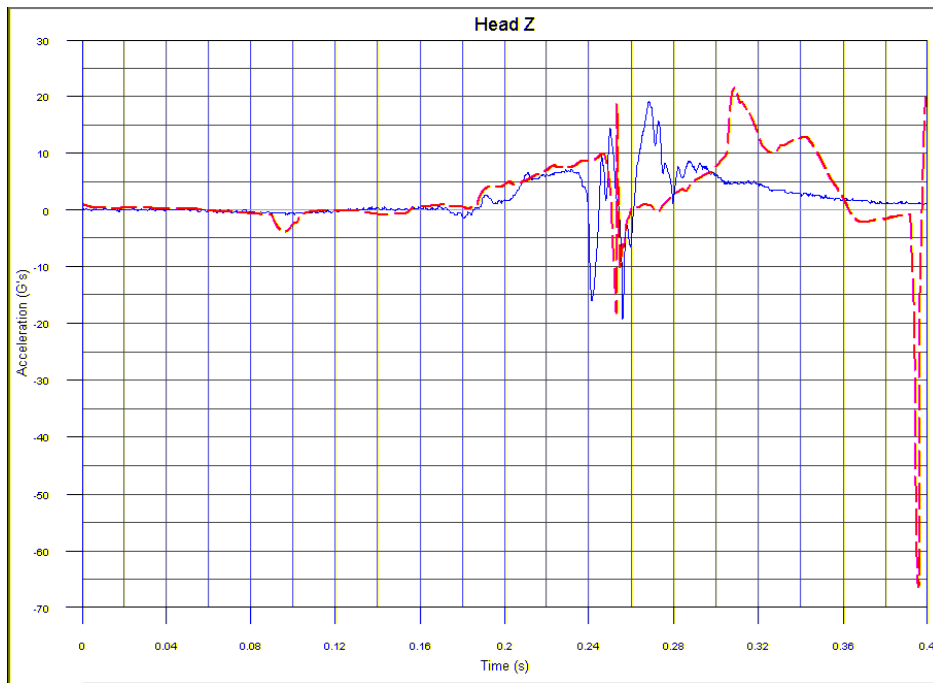


**Figure G3.  Head Acceleration, z-Direction**
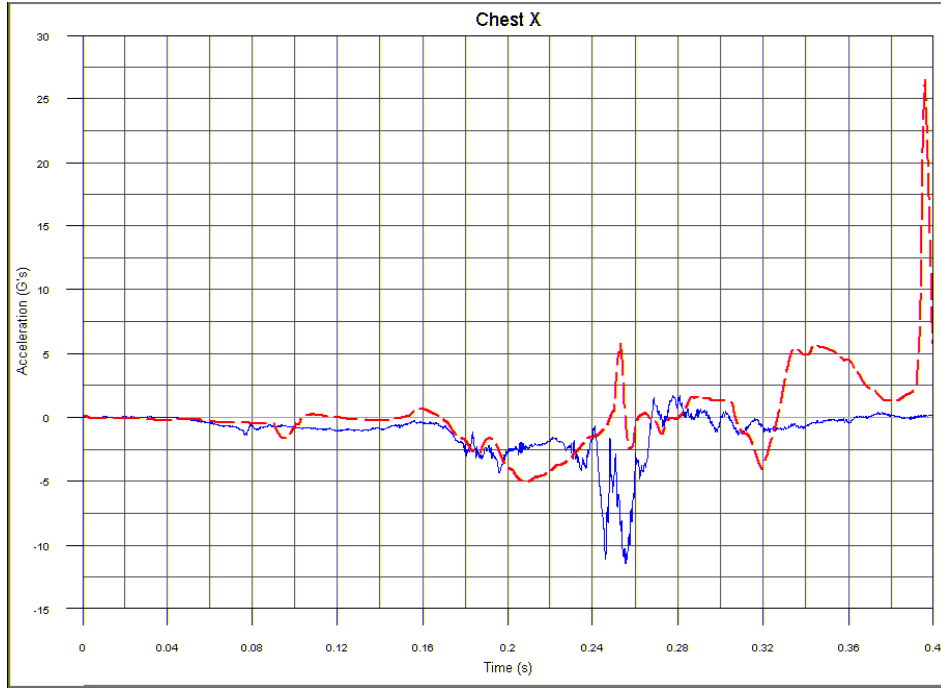
**Figure G4.  Chest Acceleration, x-Direction**
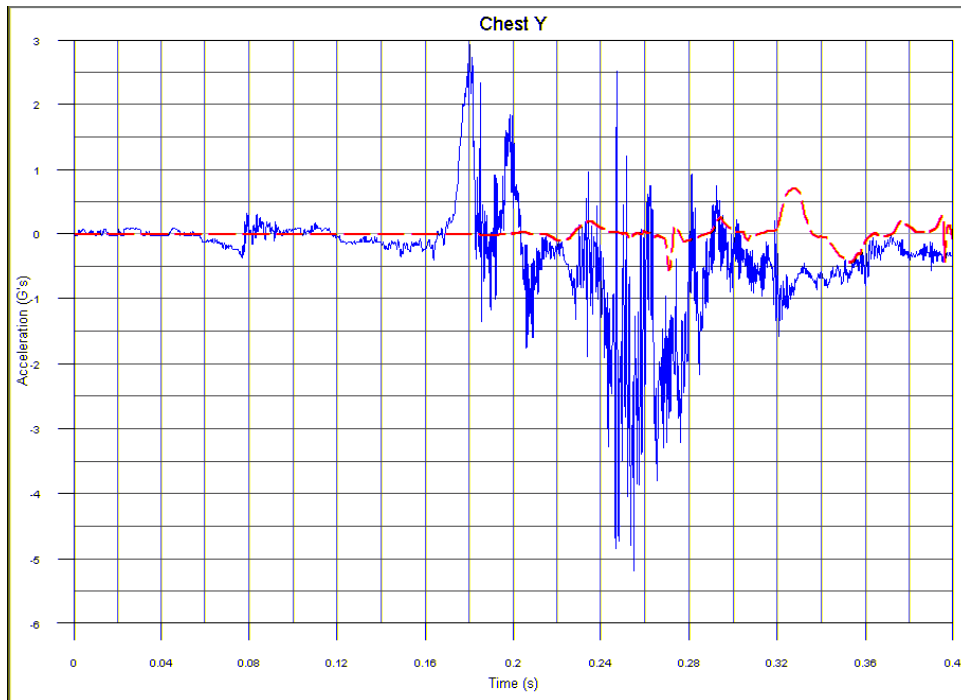


**Figure G5.  Chest Acceleration, y-Direction**
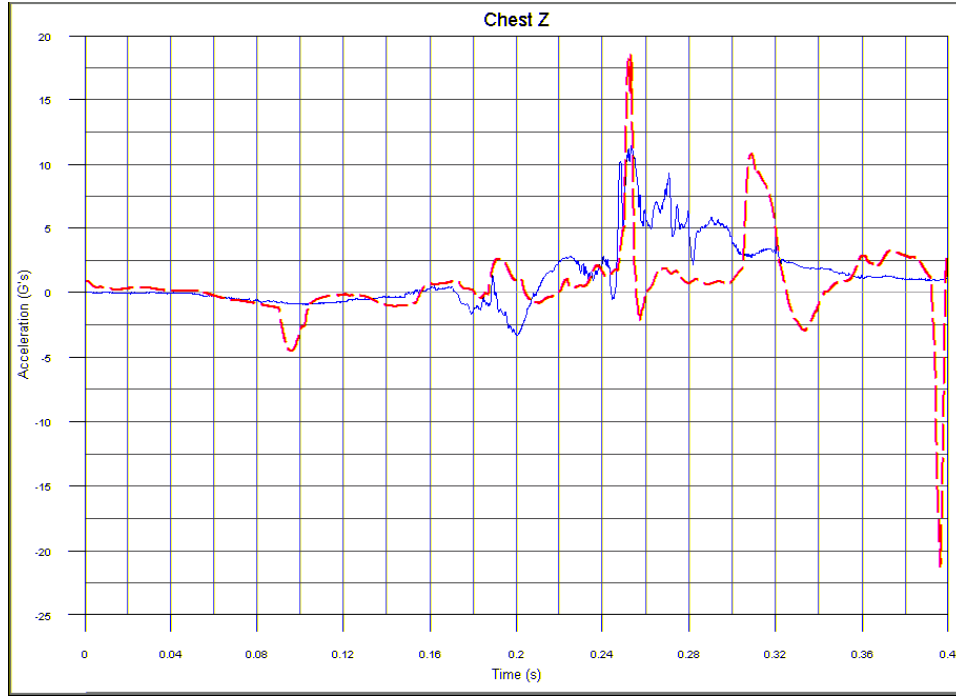
**Figure G6.  Chest Acceleration, z-Direction**
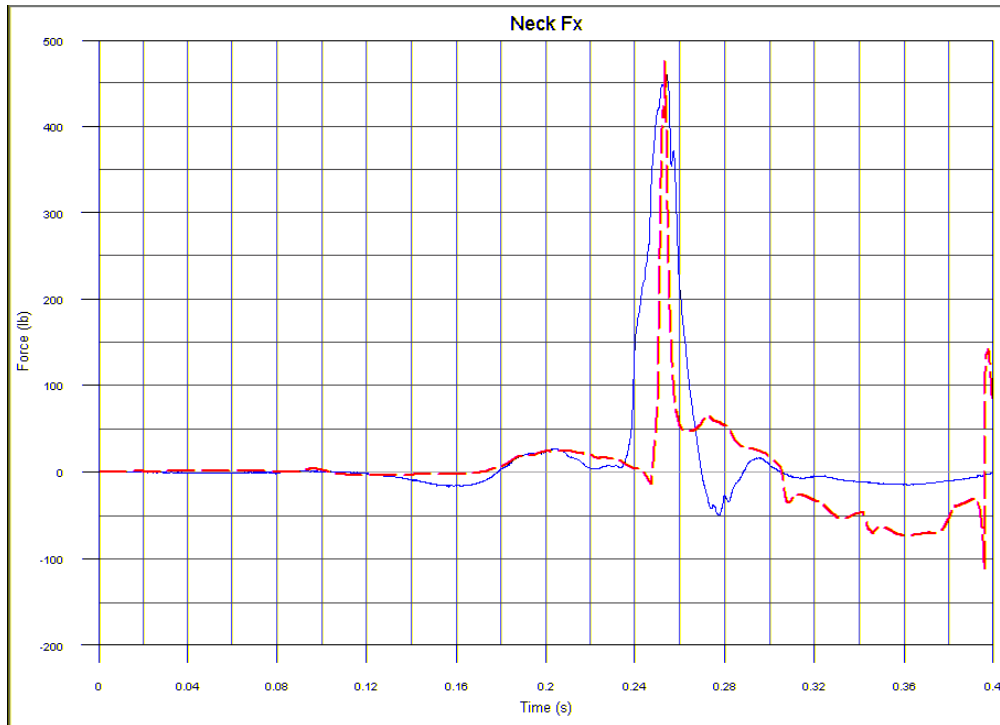


**Figure G7.  Shear Neck Load, x-Direction**
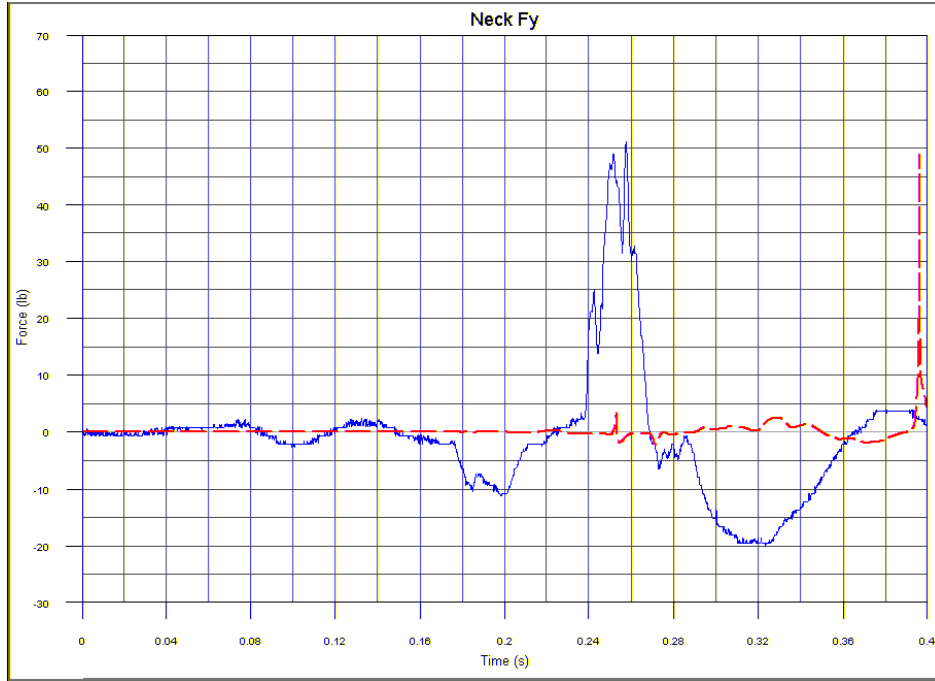
**Figure G8.  Lateral Neck Load, y-Direction**
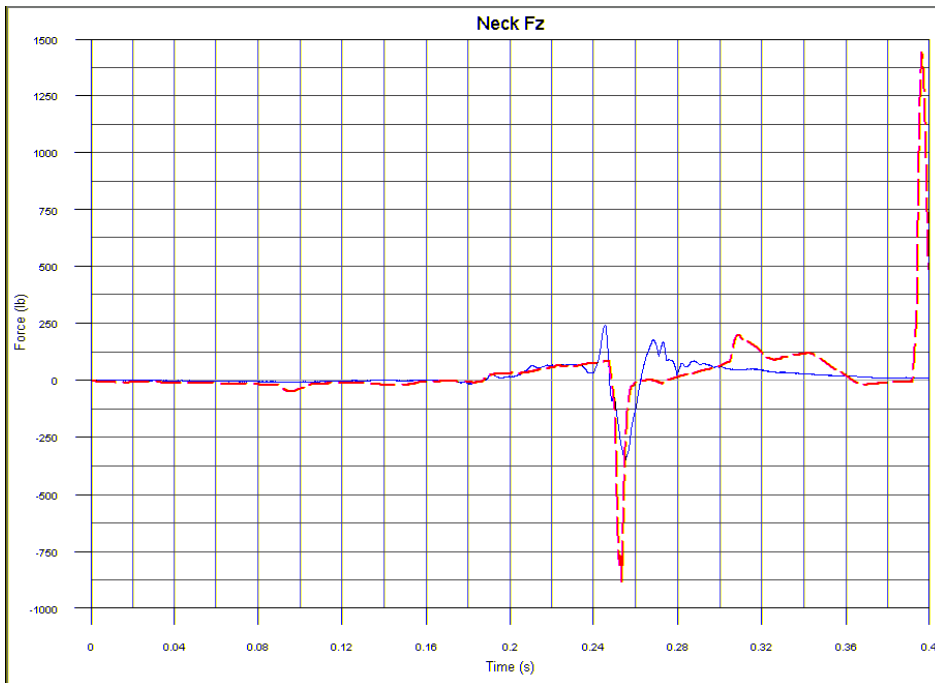


**Figure G9.  Axial Neck Load, z-Direction**

**TEST NO. 1/MODEL 1, 50TH-PERCENTILE HYBRID III ATD, AISLE SEAT (CONT.)**
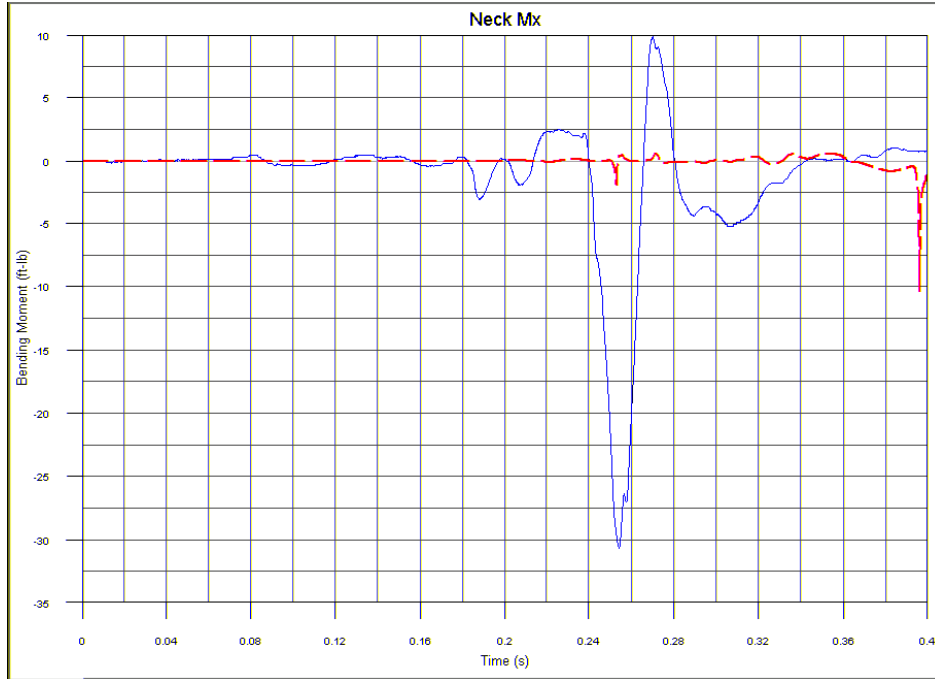


**Figure G10. Lateral Neck Bending Moment, x-axis**
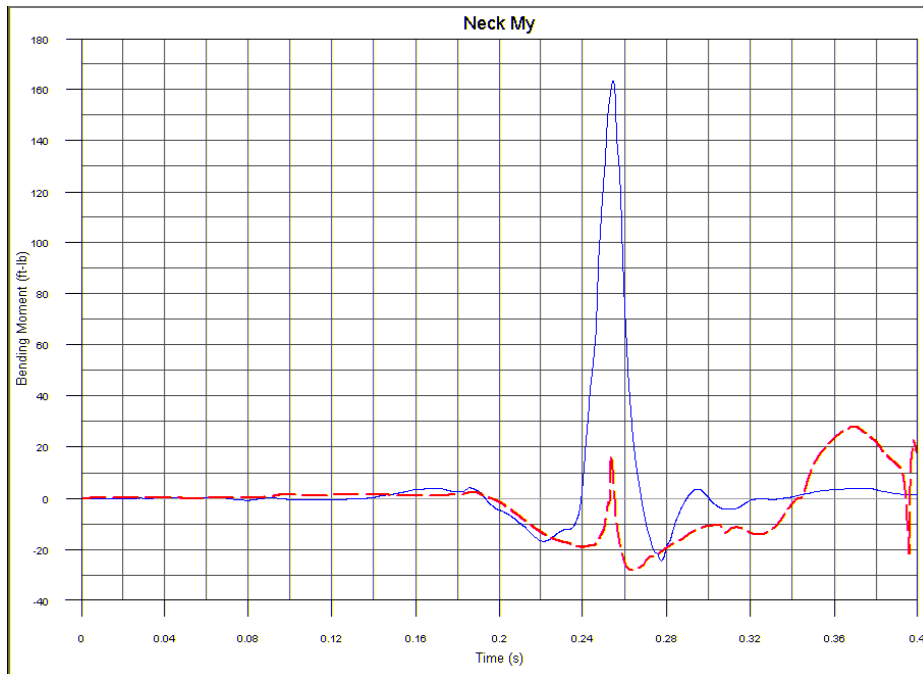


**Figure G11. Fore/Aft Neck Bending Moment, y-Axis**
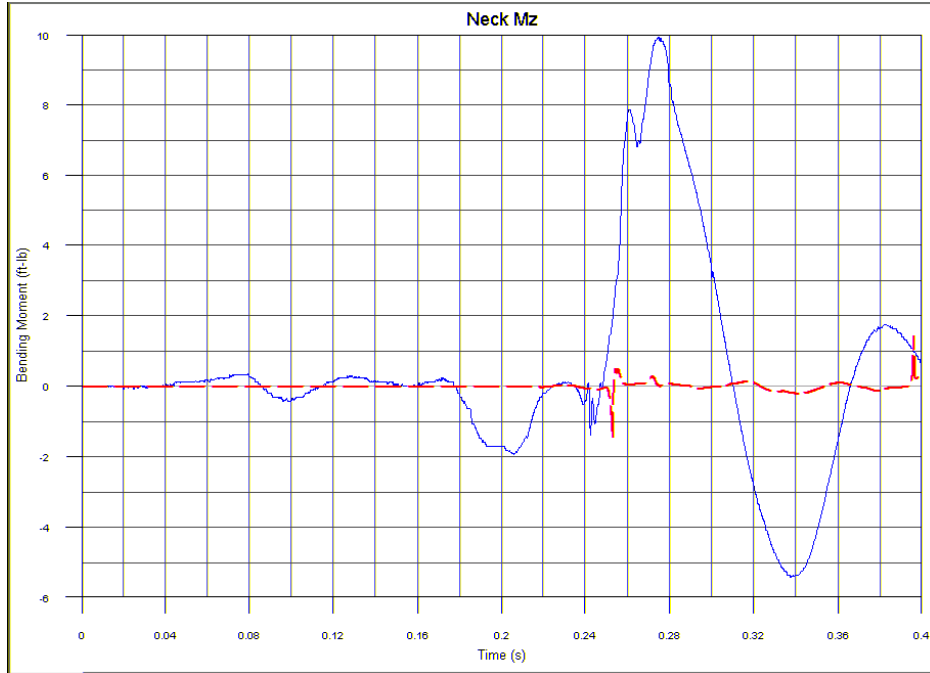
**Figure G12.  Rotational Neck Moment, z-Axis**
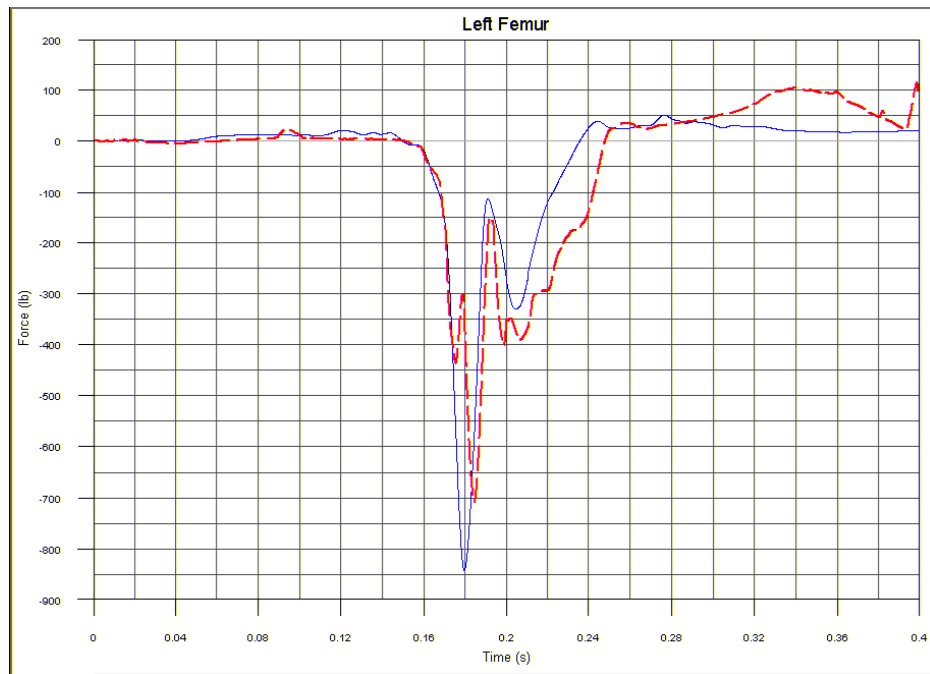


**Figure G13.  Left Femur Load**

**TEST NO. 1/MODEL 1, 50TH-PERCENTILE HYBRID III ATD, AISLE SEAT (CONT.)**
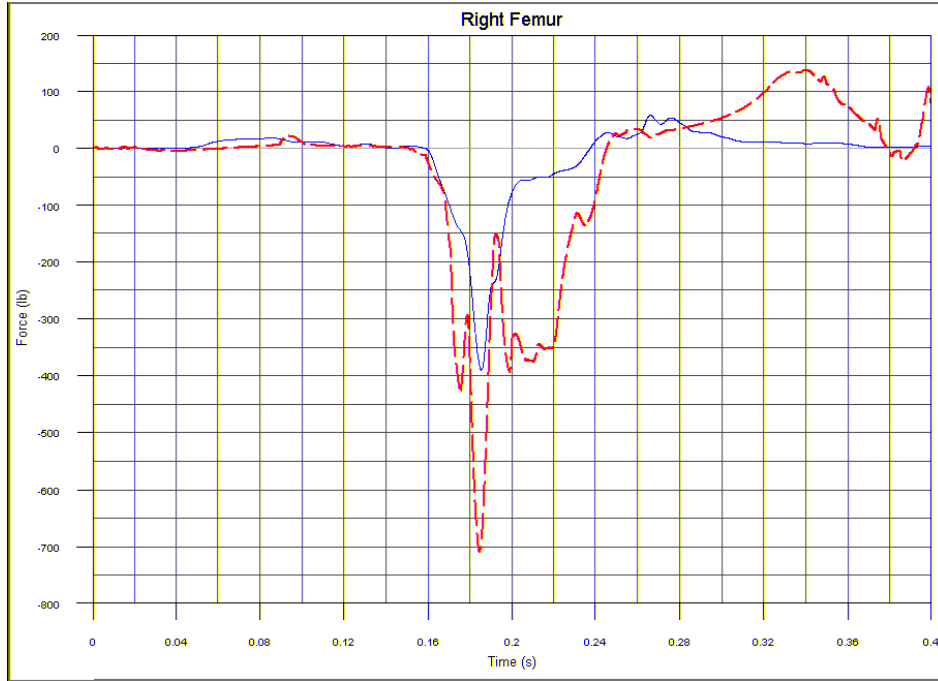


**Figure G14.  Right Femur Load**

**TEST NO. 1/MODEL 1, 50TH-PERCENTILE HYBRID III ATD, WINDOW SEAT**
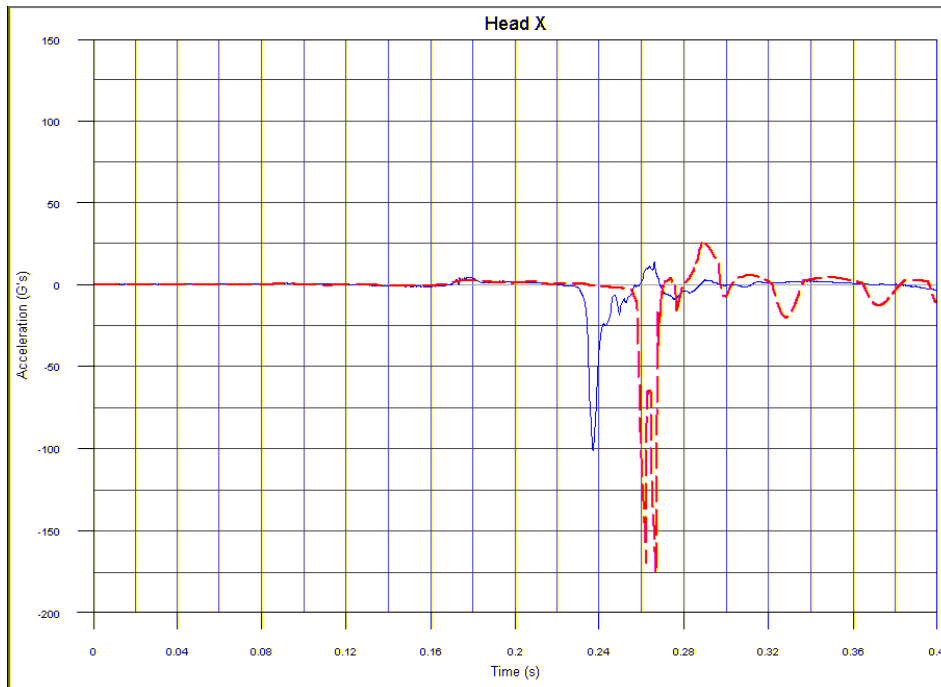


**Figure G15.  Head Acceleration, x-Direction**
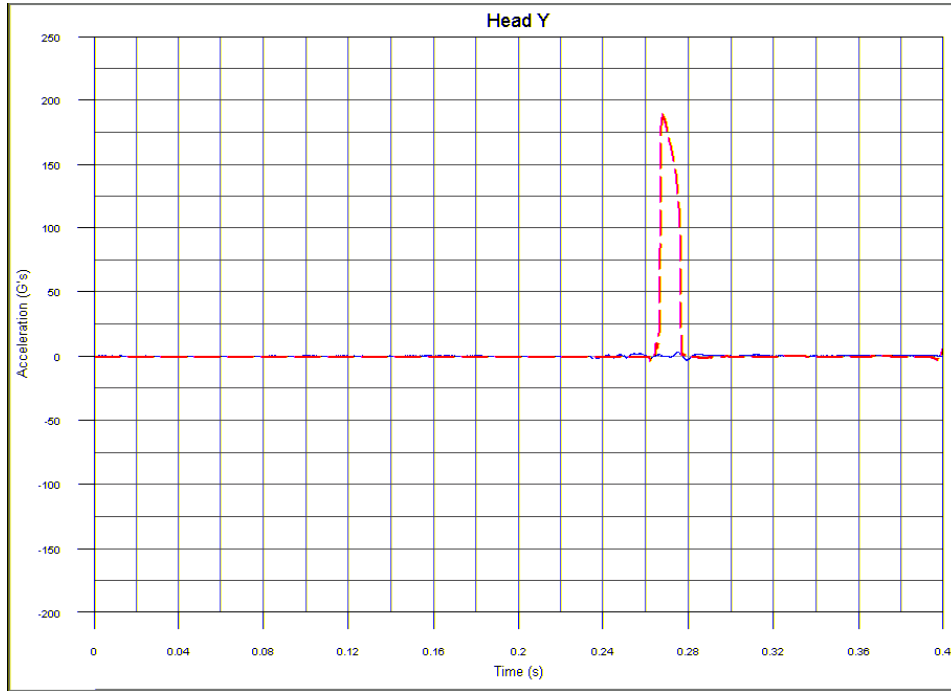
**Figure G16.  Head Acceleration, y-Direction**
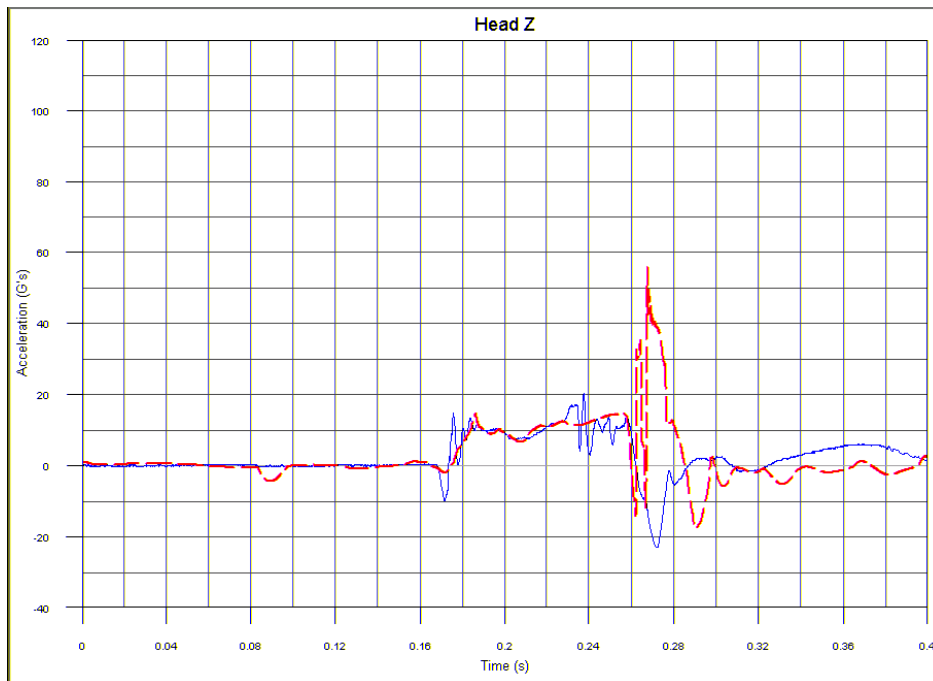


**Figure G17.  Head Acceleration, z-Direction**
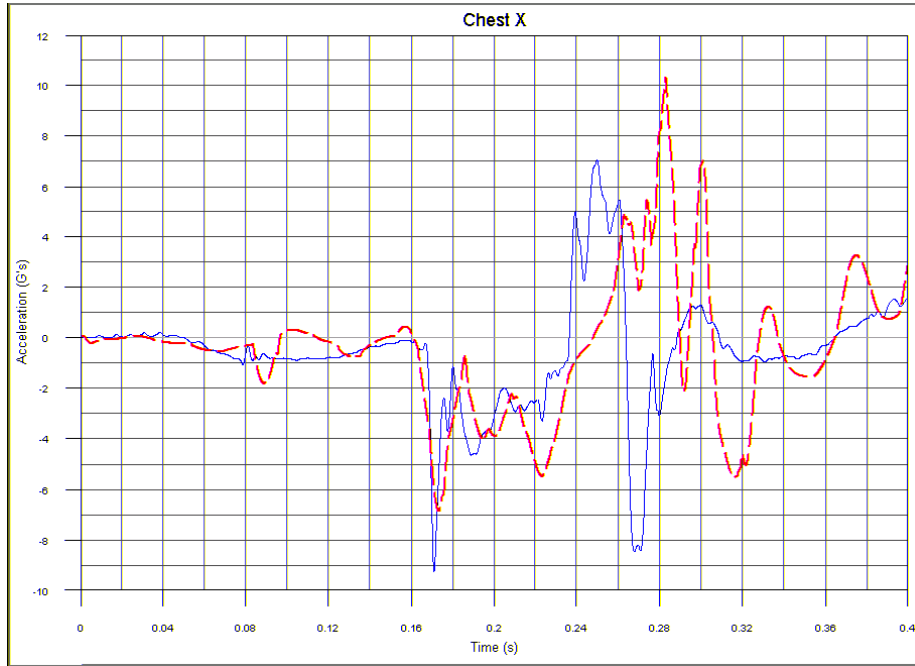
**Figure G18.  Chest Acceleration, x-Direction**
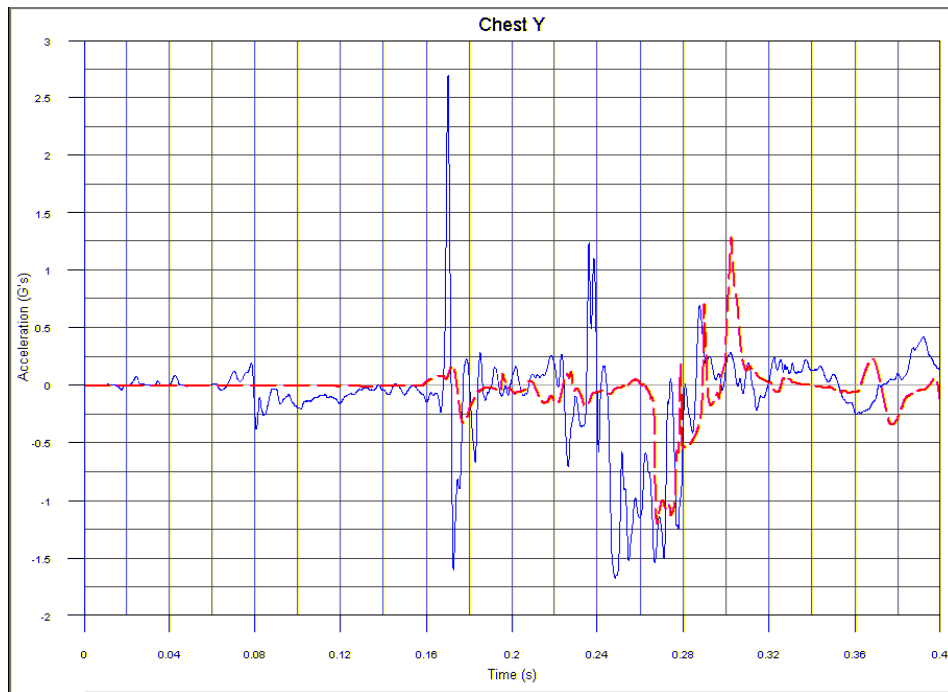


**Figure G19.  Chest Acceleration, y-Direction**
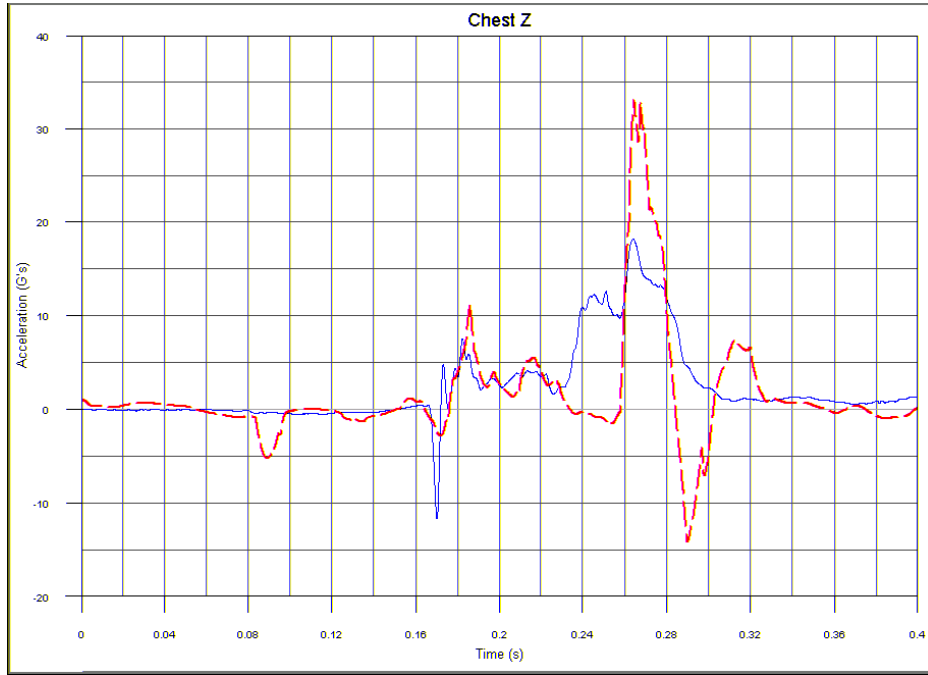
**Figure G20.  Chest Acceleration, z-Direction**
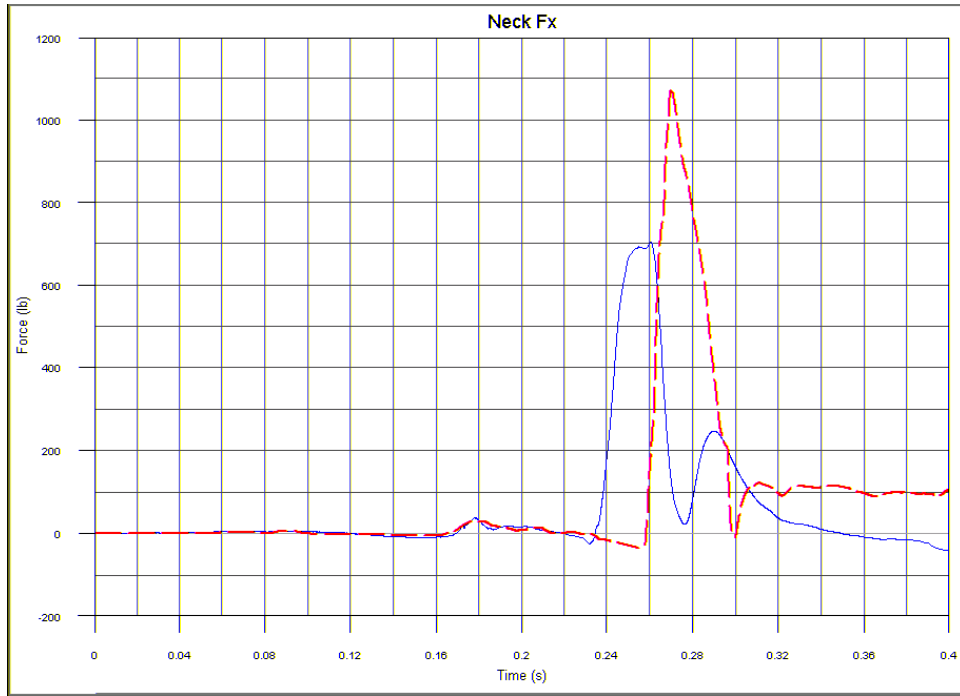


**Figure G21.  Shear Neck Load, x-Direction**
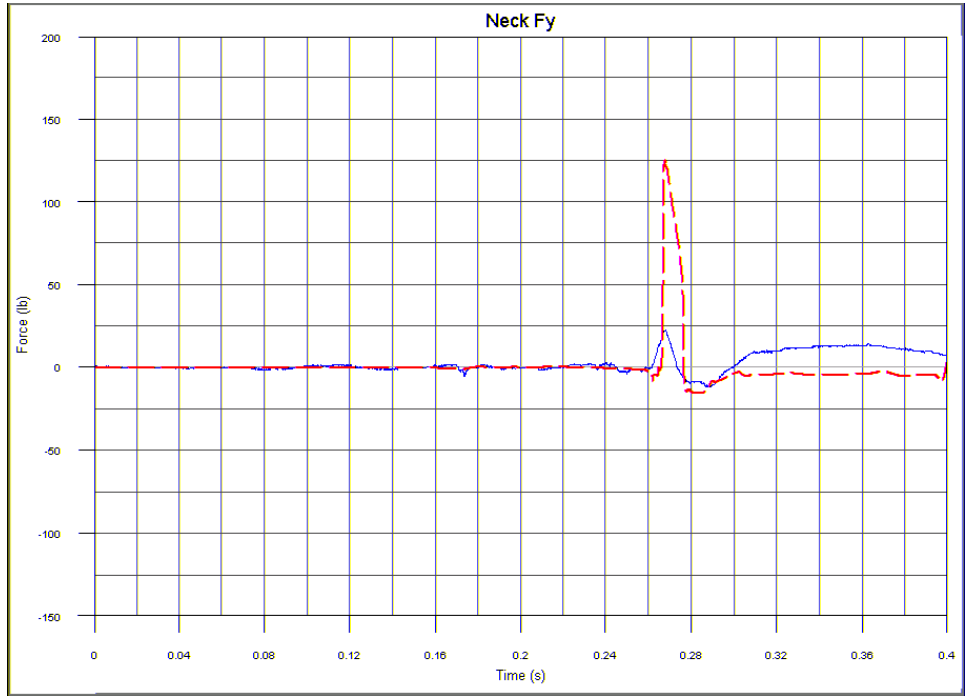
**Figure G22.  Lateral Neck Load, y-Direction**
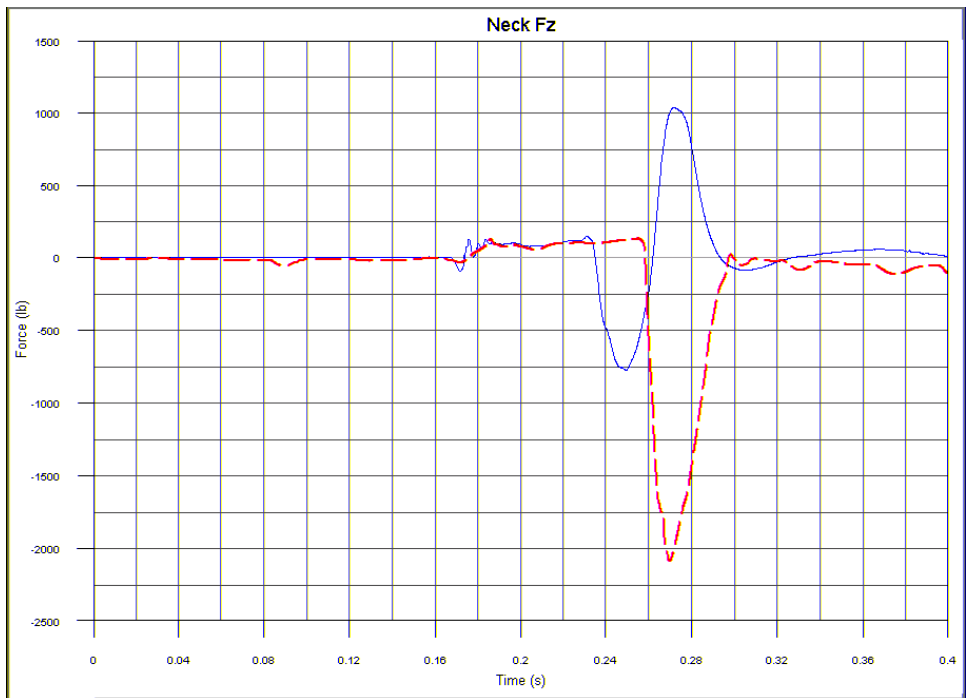


**Figure G23.  Axial Neck Load, z-Direction**

**TEST NO. 1/MODEL 1, 50TH-PERCENTILE HYBRID III ATD, WINDOW SEAT (CONT.)**
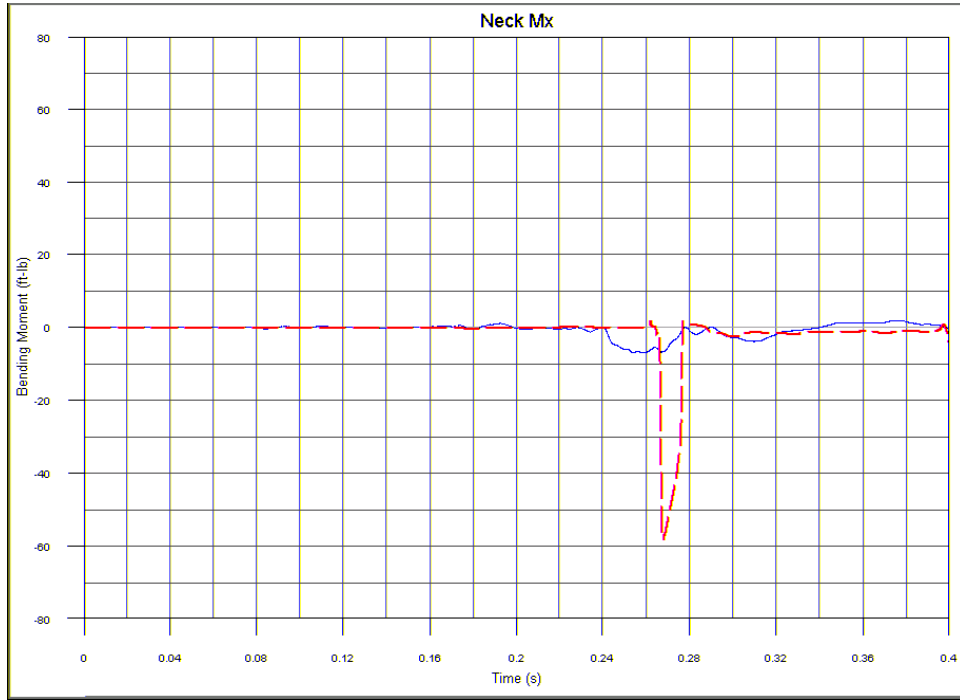


**Figure G24.  Lateral Neck Bending Moment, x-Axis**
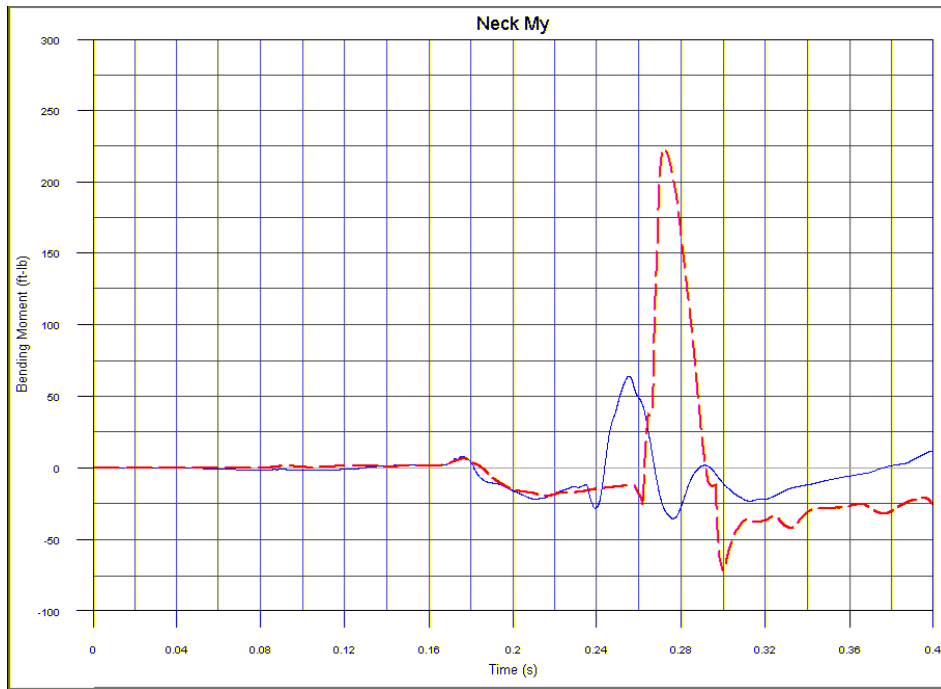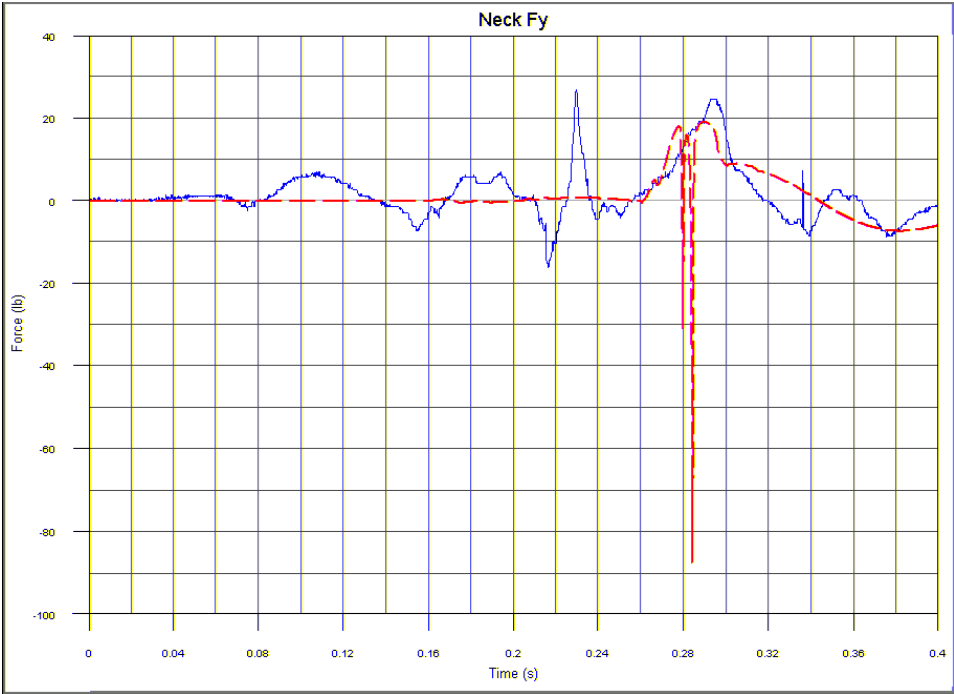


**Figure G25.  Fore/Aft Neck Bending Moment, y-Axis**
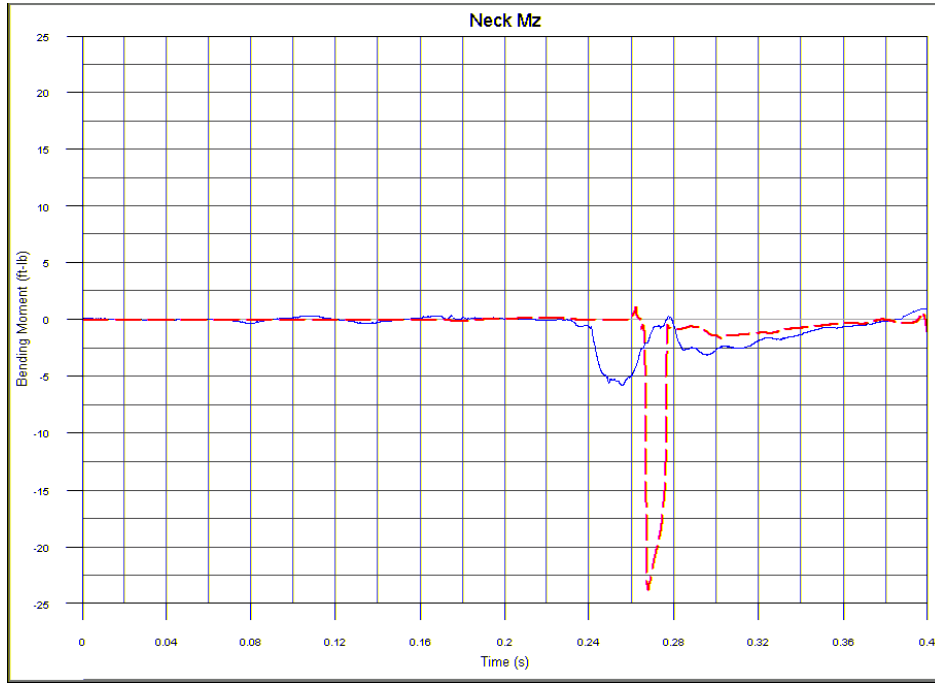
**Figure G26.  Rotational Neck Moment, z-Axis**
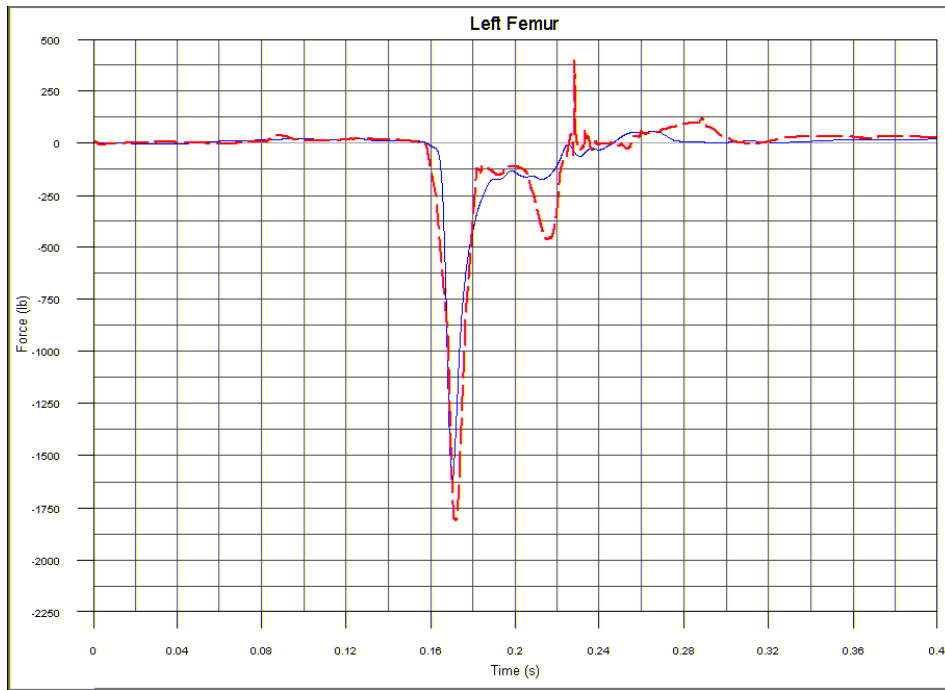


**Figure G27.  Left Femur Load**

## TEST NO. 1/MODEL 1, 50TH-PERCENTILE HYBRID III ATD, WINDOW SEAT (CONT.)
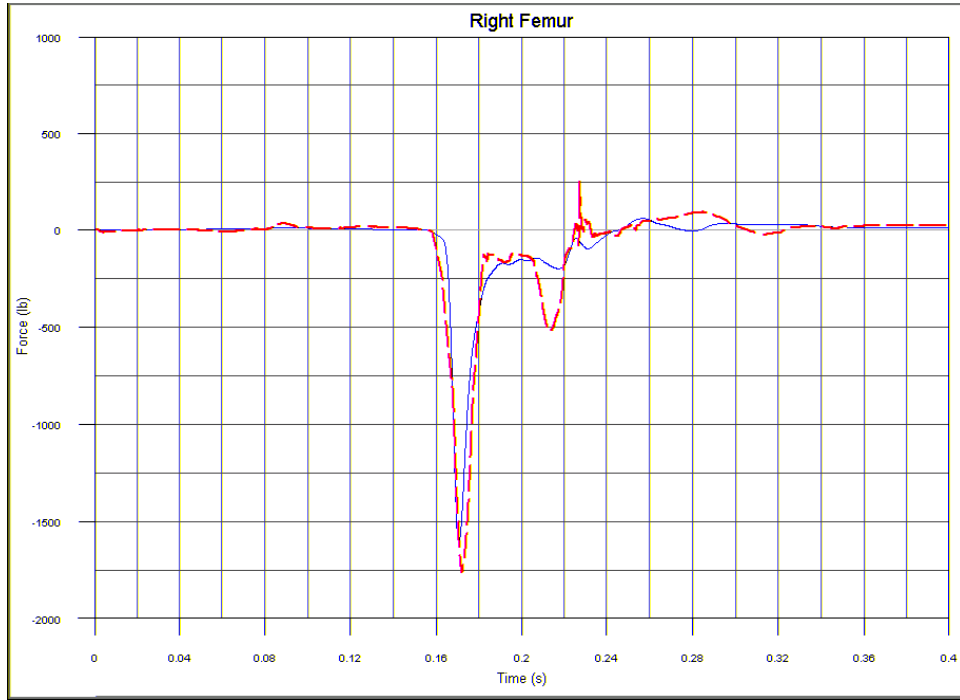


**Figure G28.  Right Femur Load**

## TEST NO. 2, 50TH-PERCENTILE HYBRID III ATD, AISLE SEAT
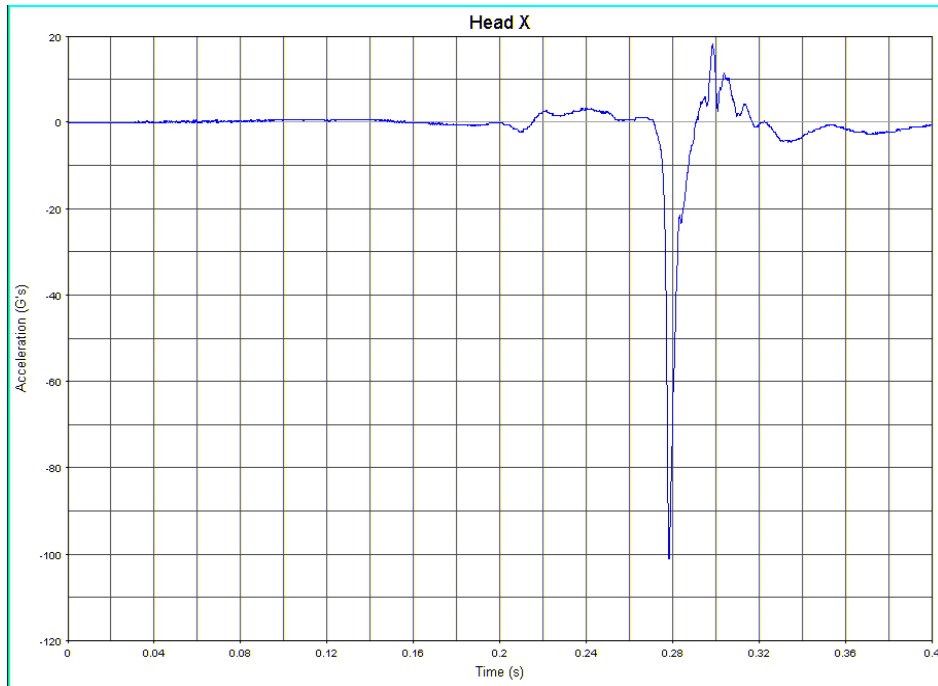


**Figure G29.  Head Acceleration, x-Direction**
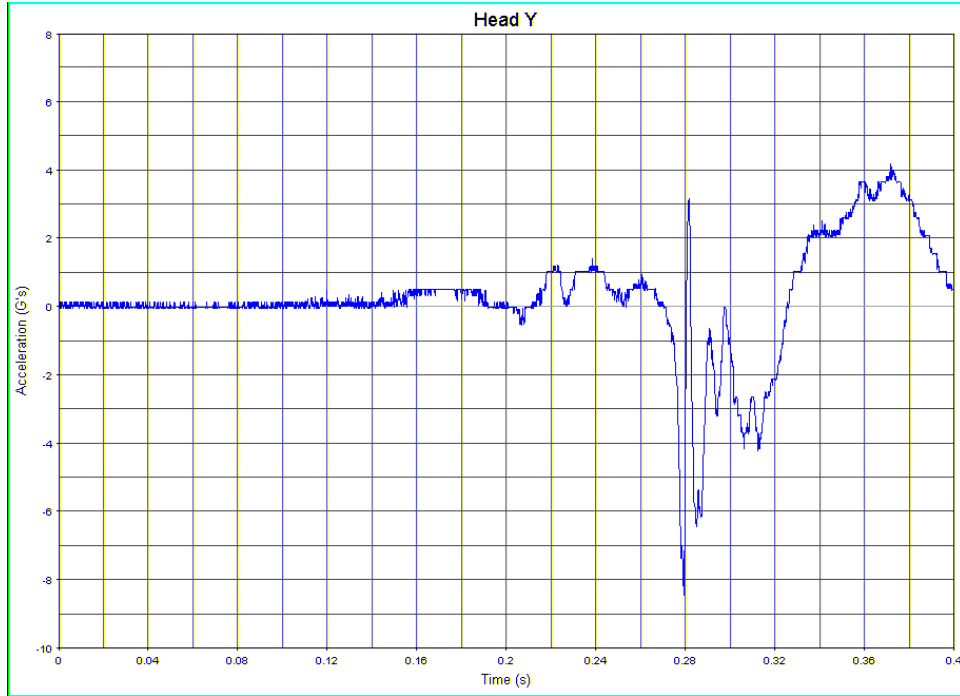
**Figure G30. Head Acceleration, y-Direction**
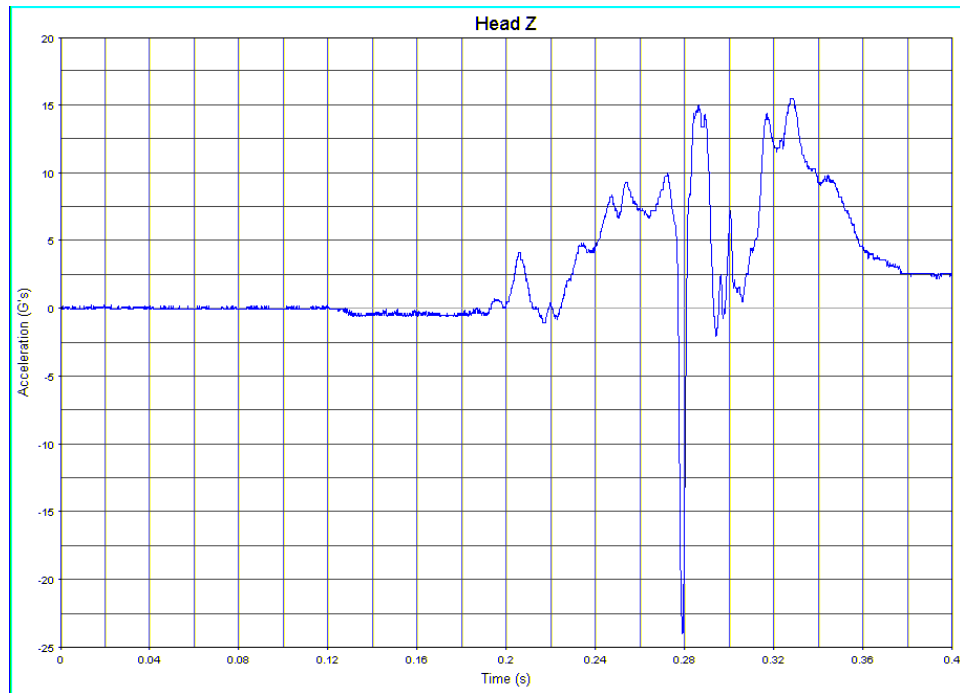


**Figure G31. Head Acceleration, z-Direction**

**TEST NO. 2, 50TH-PERCENTILE HYBRID III ATD, AISLE SEAT (CONT.)**
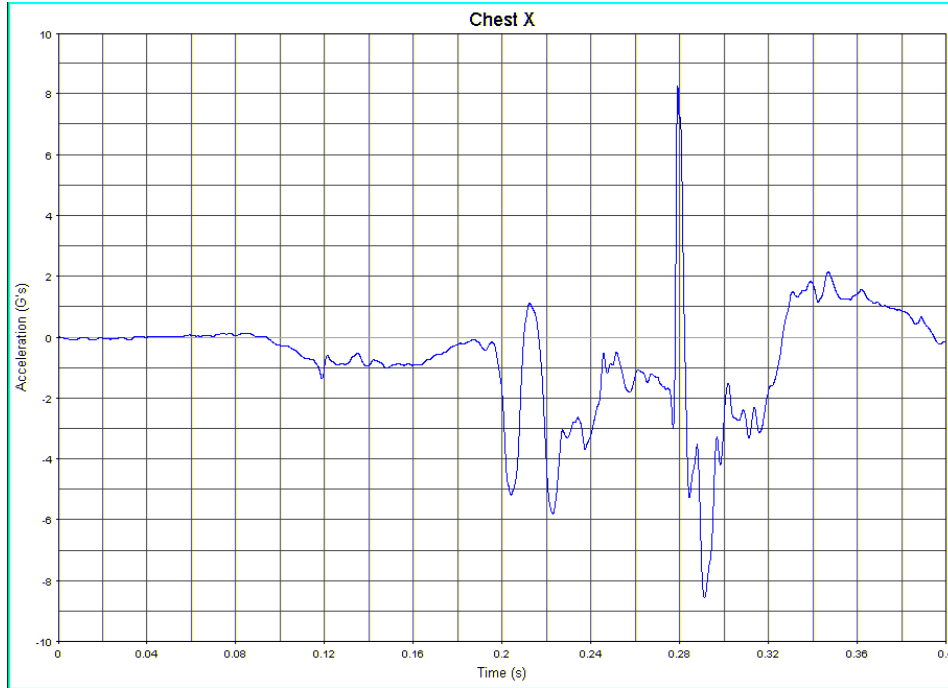


**Figure G32.  Chest Acceleration, x-Direction**
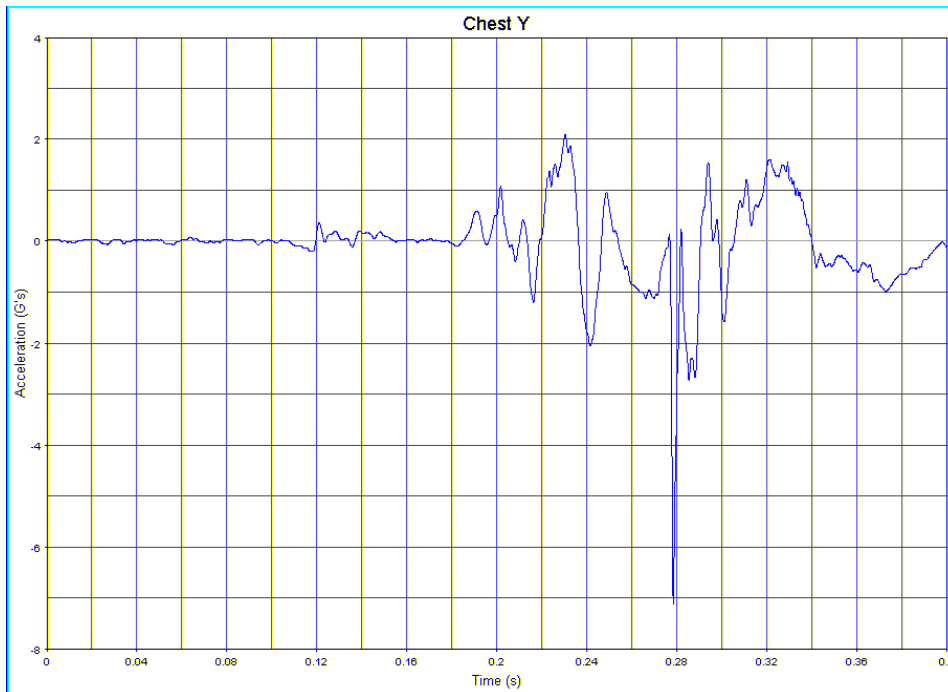


**Figure G33.  Chest Acceleration, y-Direction**
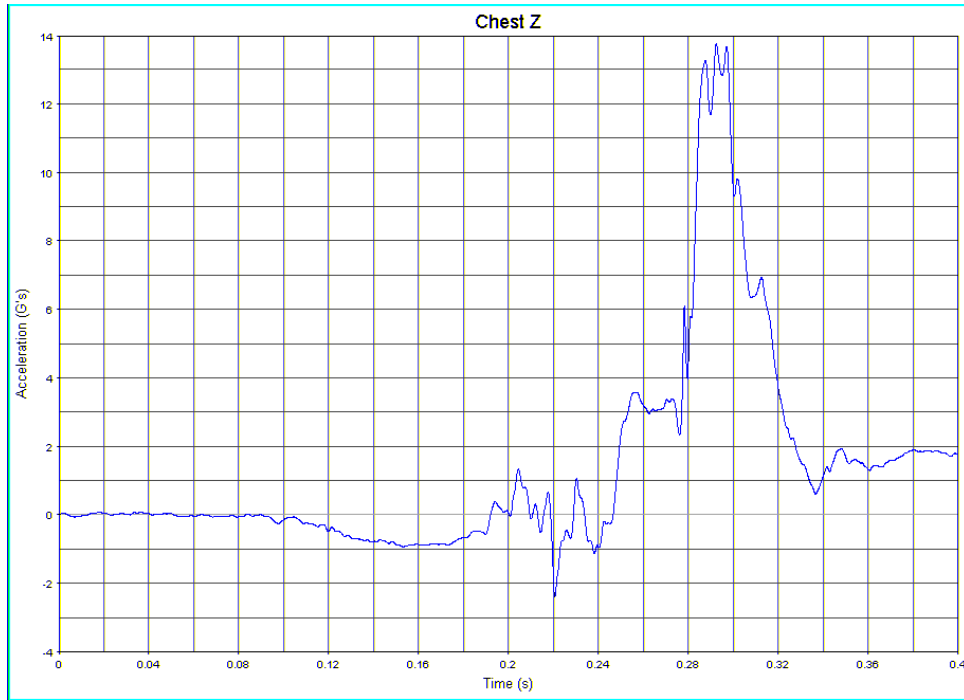
**Figure G34.  Chest Acceleration, z-Direction**
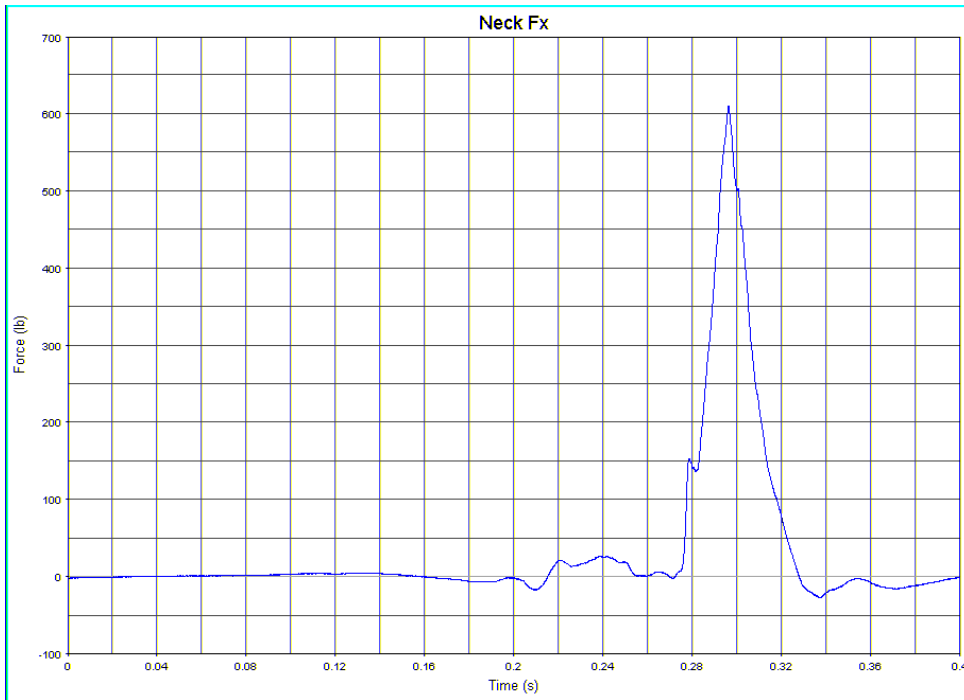


**Figure G35.  Shear Neck Load, x-Direction**
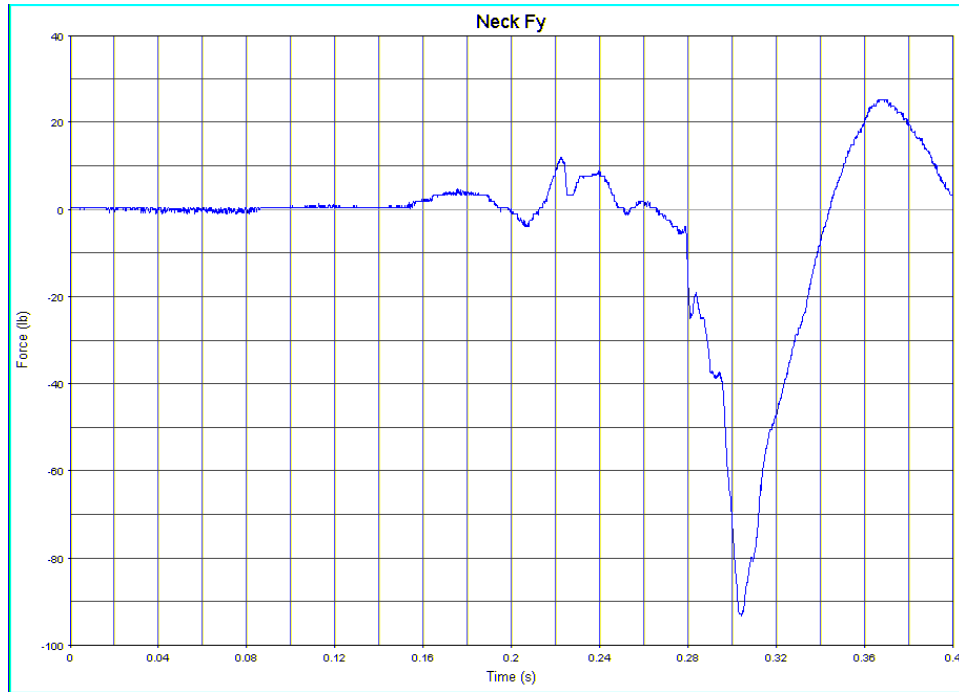
**Figure G36.  Lateral Neck Load, y-Direction**
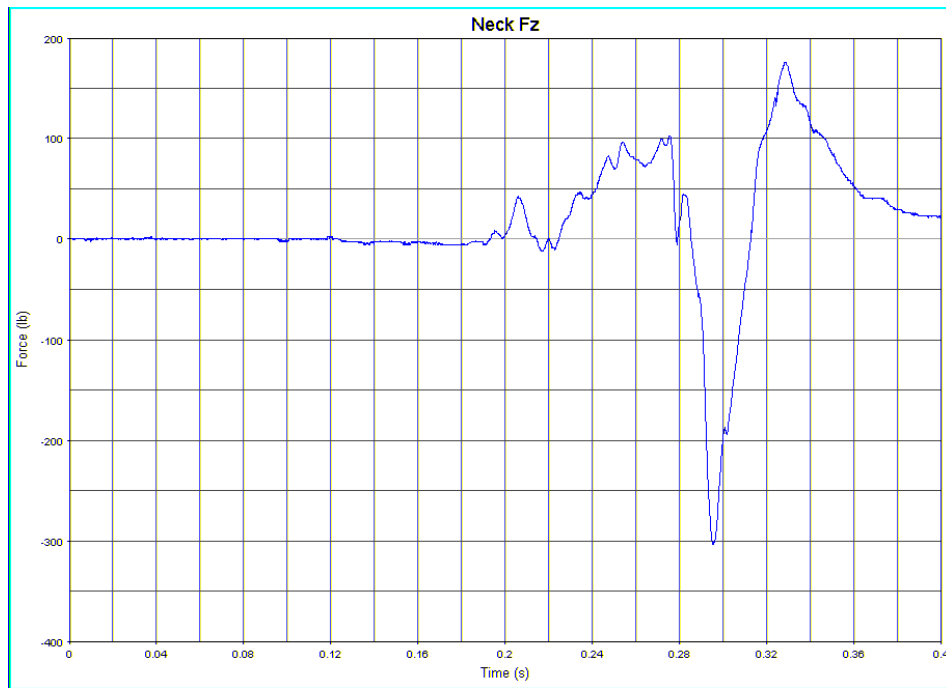


**Figure G37.  Axial Neck Load, z-Direction**

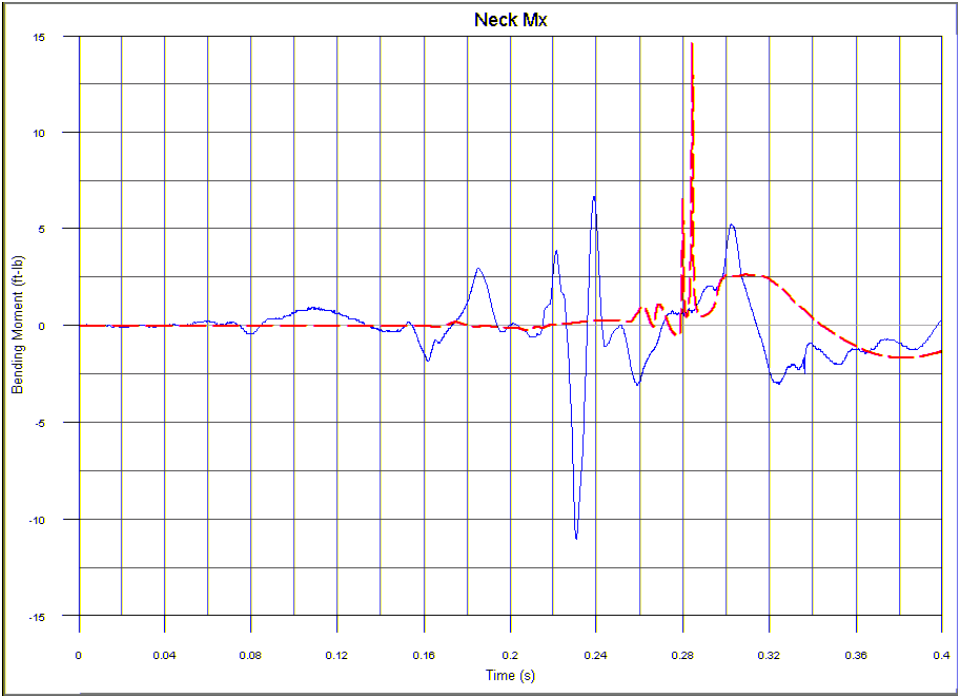# TEST NO. 2, 50TH-PERCENTILE HYBRID III ATD, AISLE SEAT (CONT.)
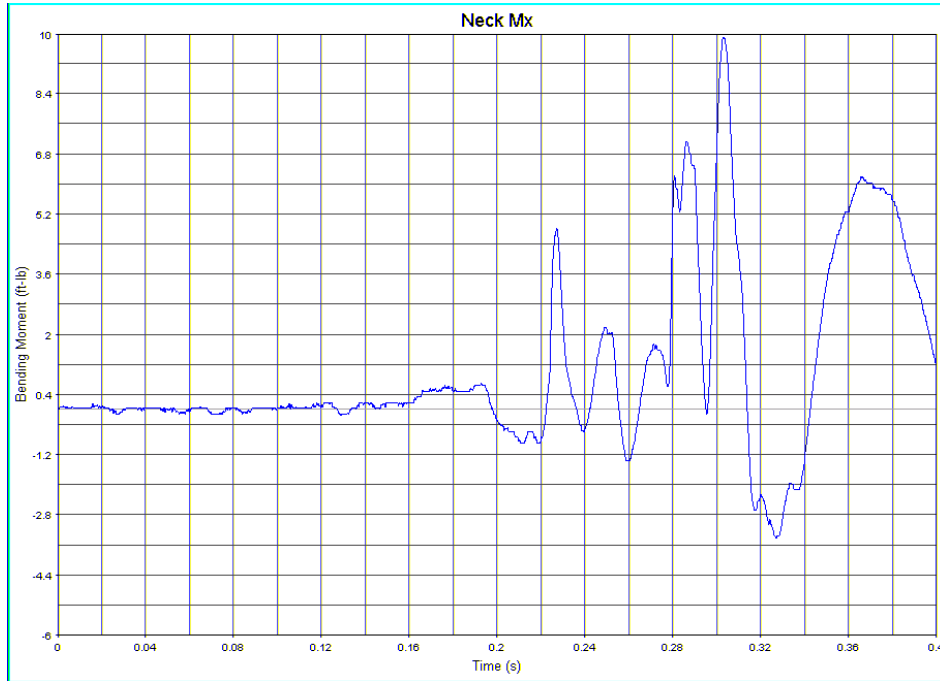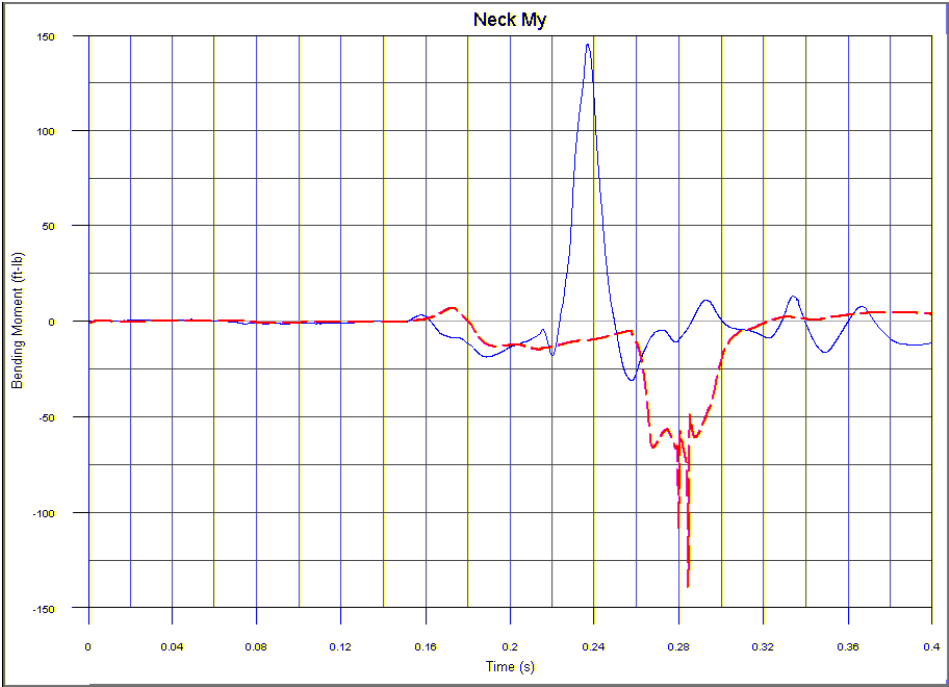


**Figure G38.  Lateral Neck Bending Moment, x-Axis**
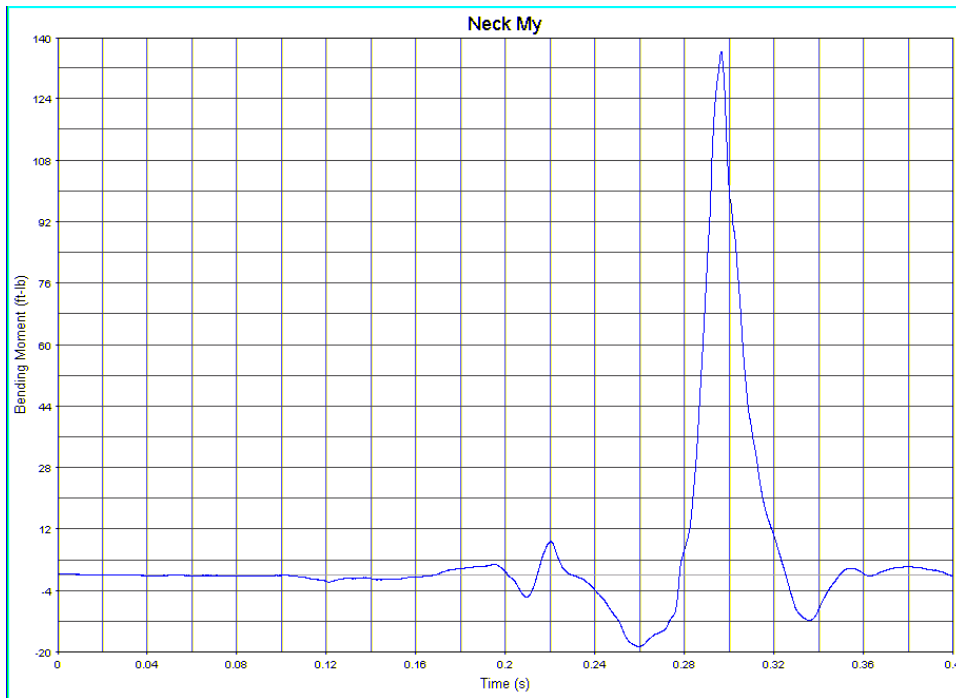


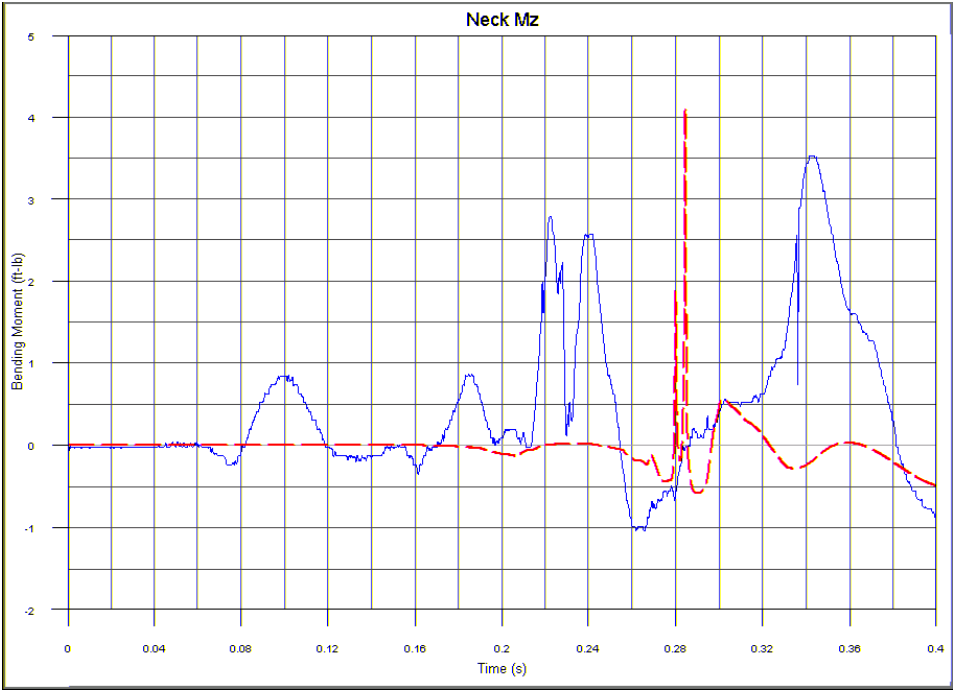**Figure G39.  Fore/Aft Neck Bending Moment, y-Axis**
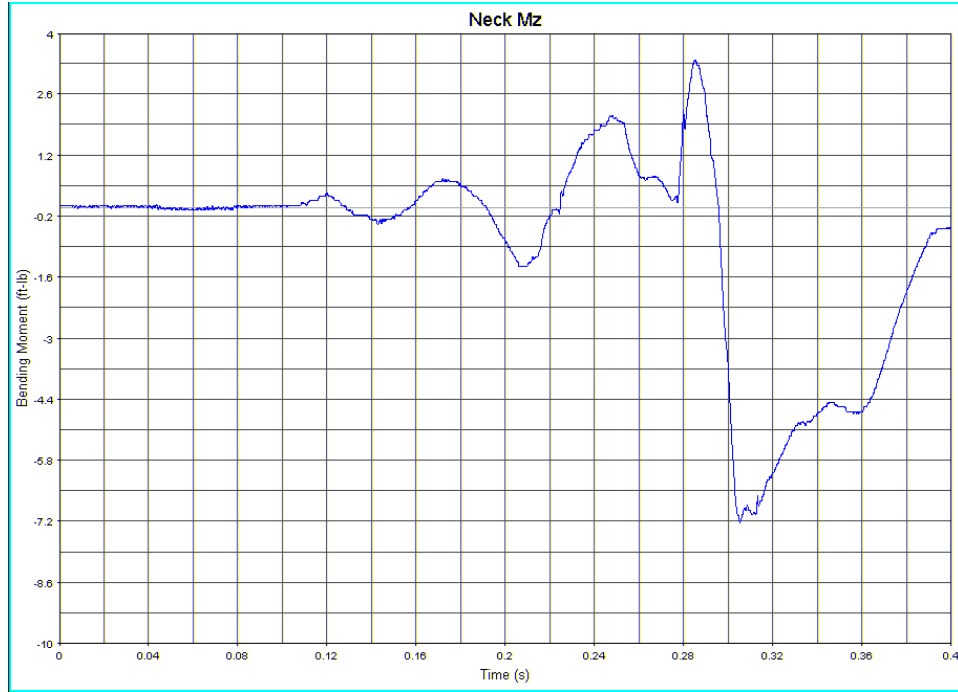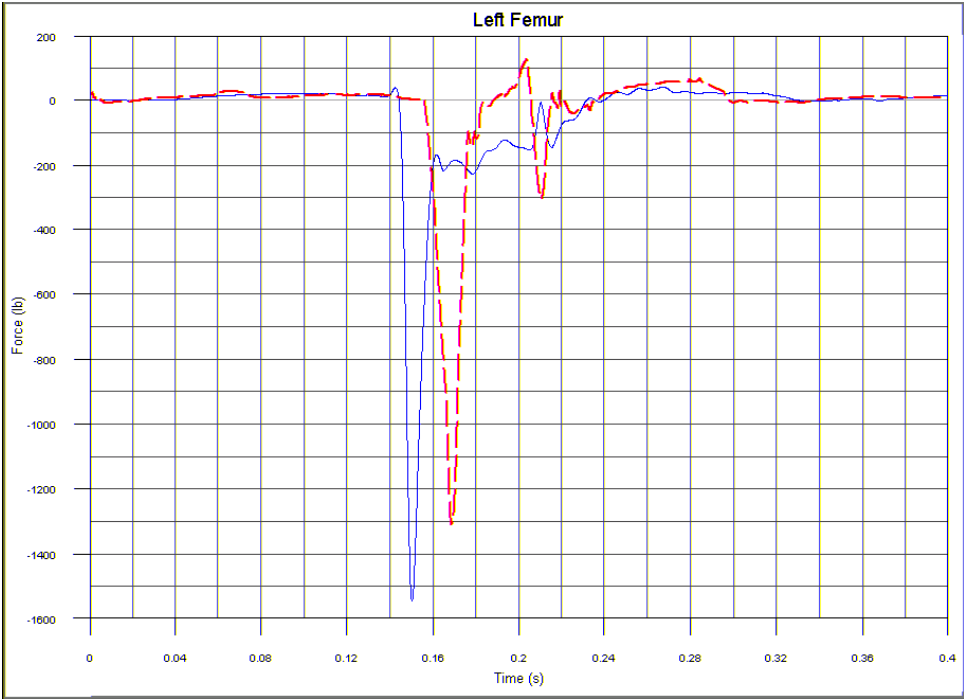
**Figure G40.  Rotational Neck Moment, z-Axis**
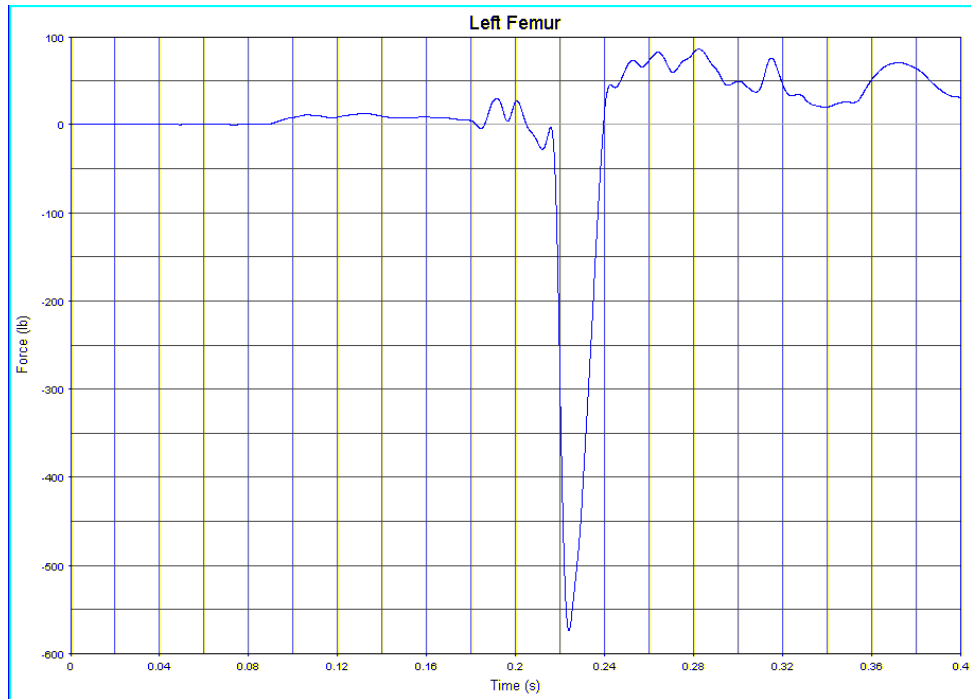


**Figure G41.  Left Femur Load**

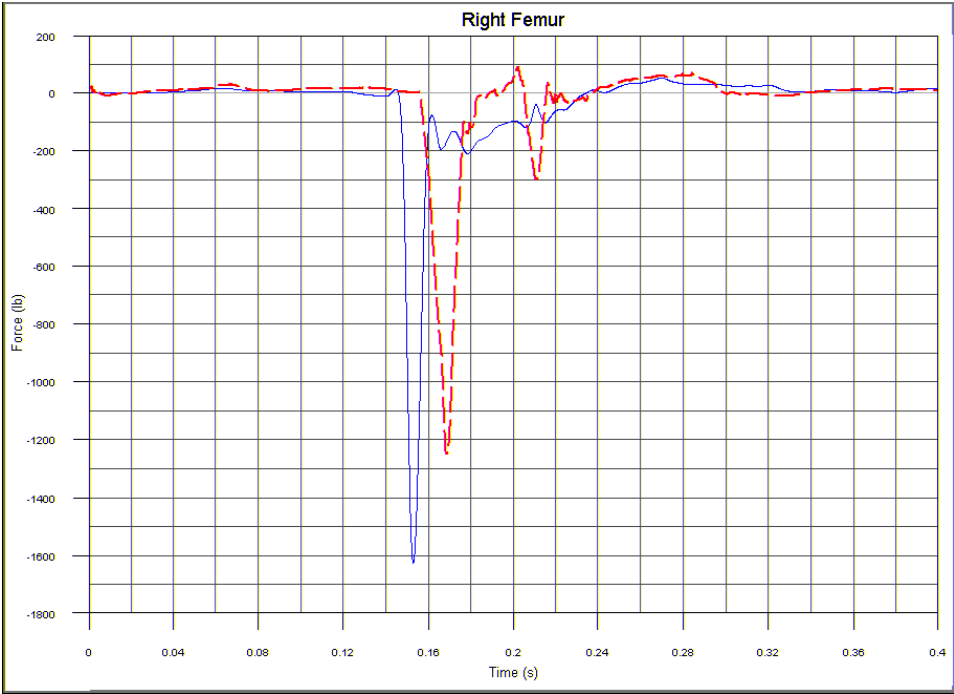# TEST NO. 2, 50TH-PERCENTILE HYBRID III ATD, AISLE SEAT (CONT.)
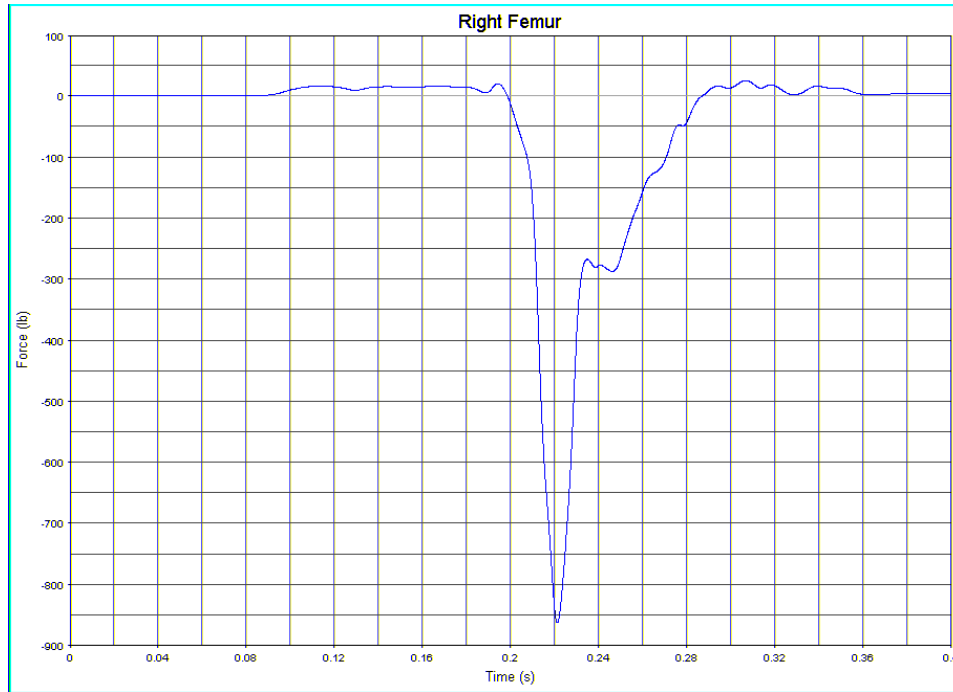


**Figure G42.  Right Femur Load**

# TEST NO. 2, 50TH-PERCENTILE HYBRID III ATD, WINDOW SEAT
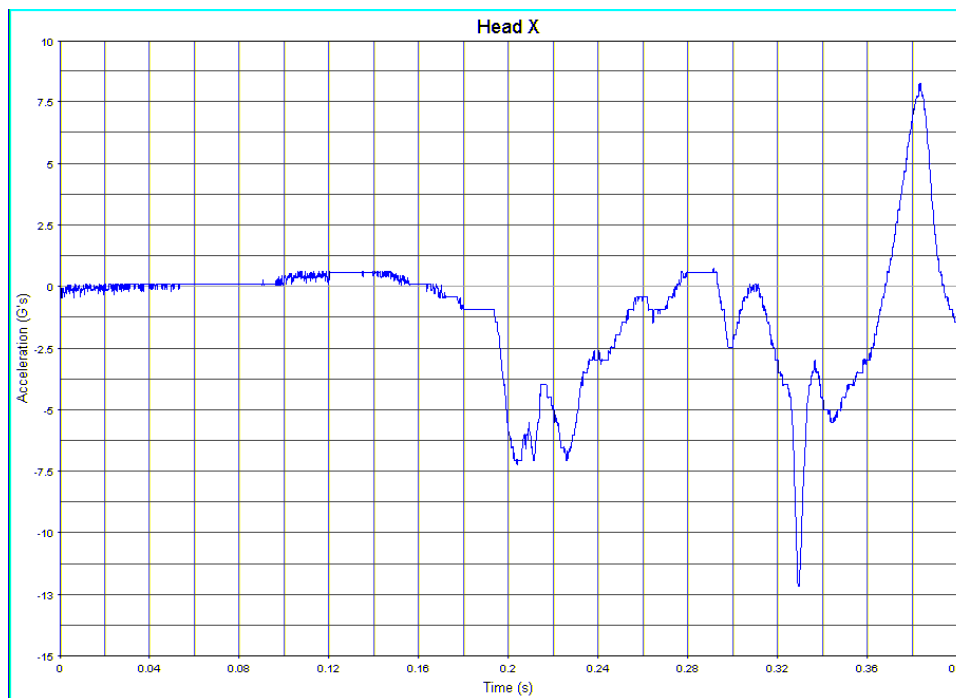


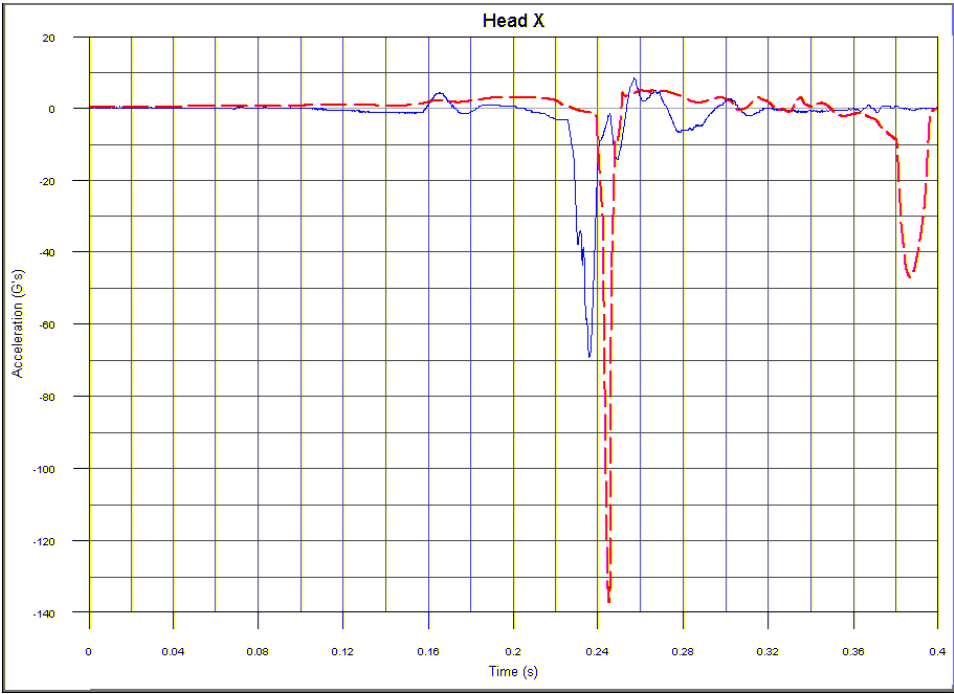**Figure G43.  Head Acceleration, x-Direction**
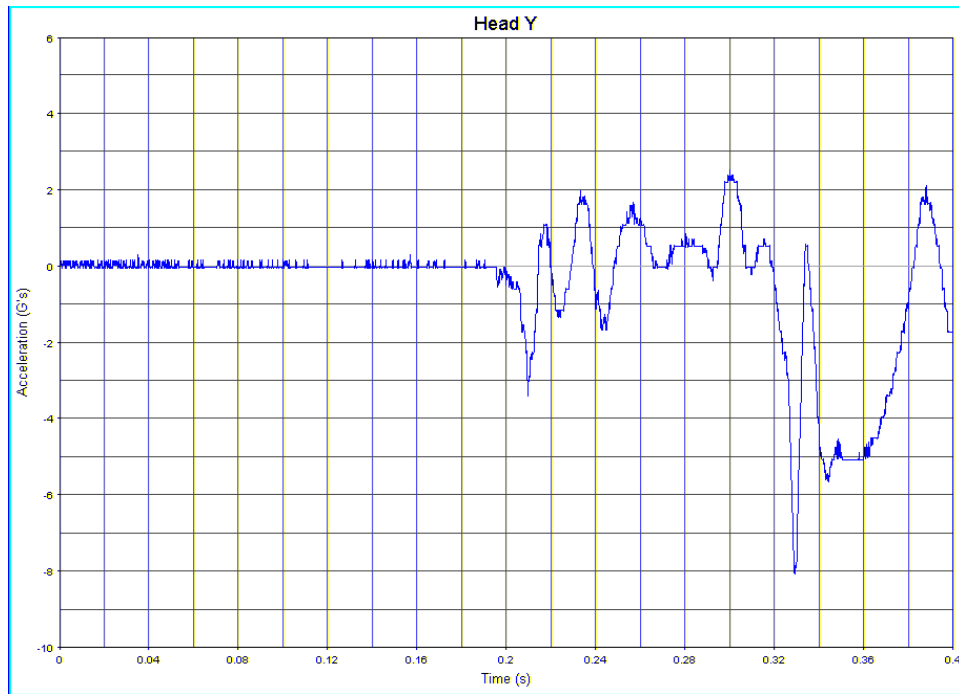
**Figure G44.  Head Acceleration, y-Direction**
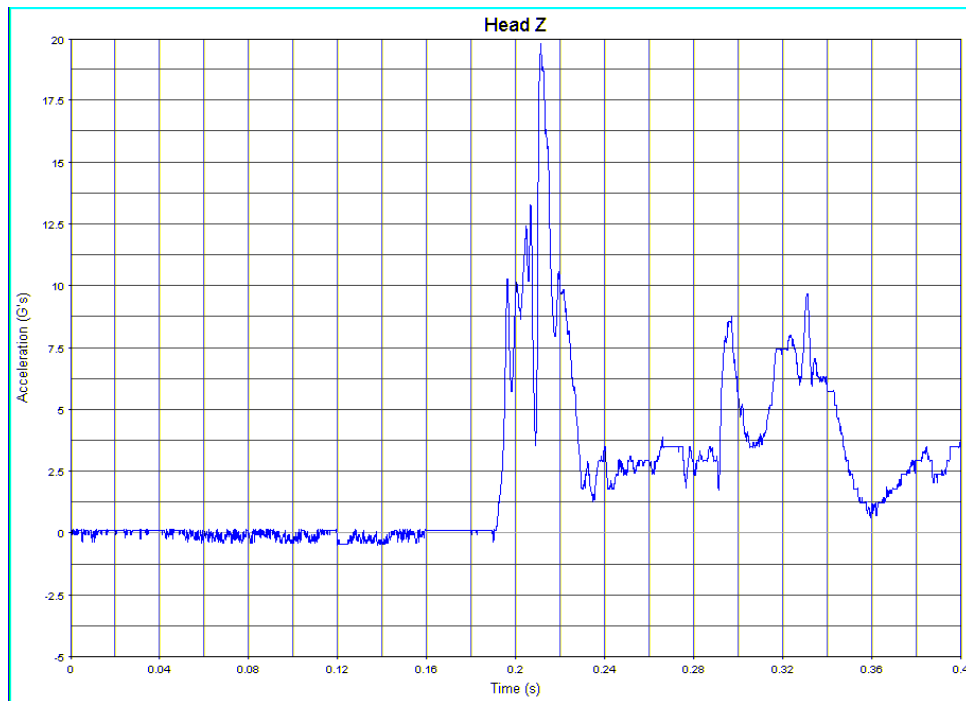


**Figure G45.  Head Acceleration, z-Direction**
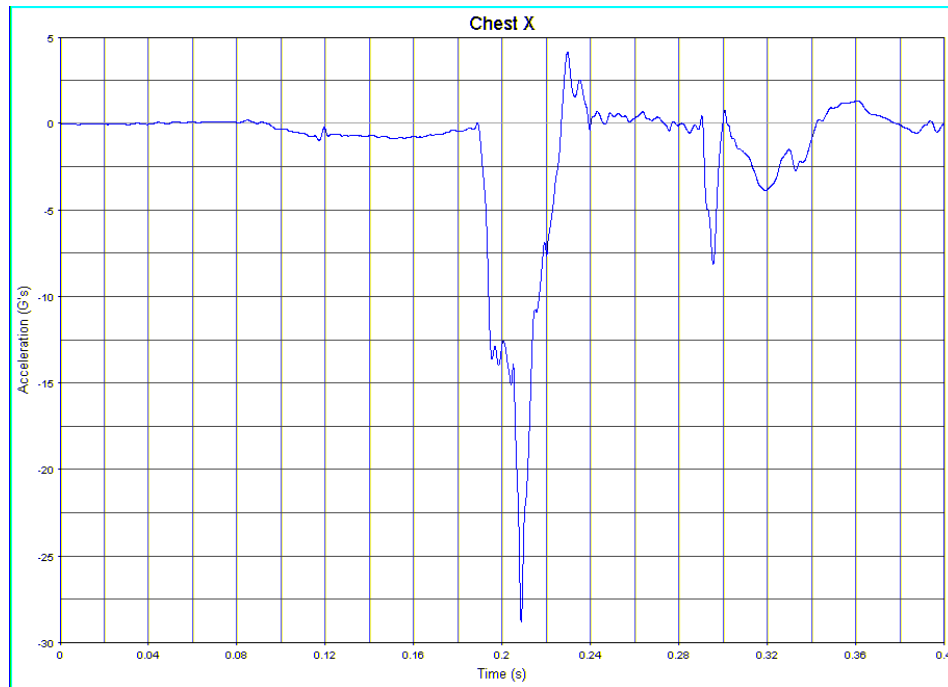
**Figure G46.  Chest Acceleration, x-Direction**
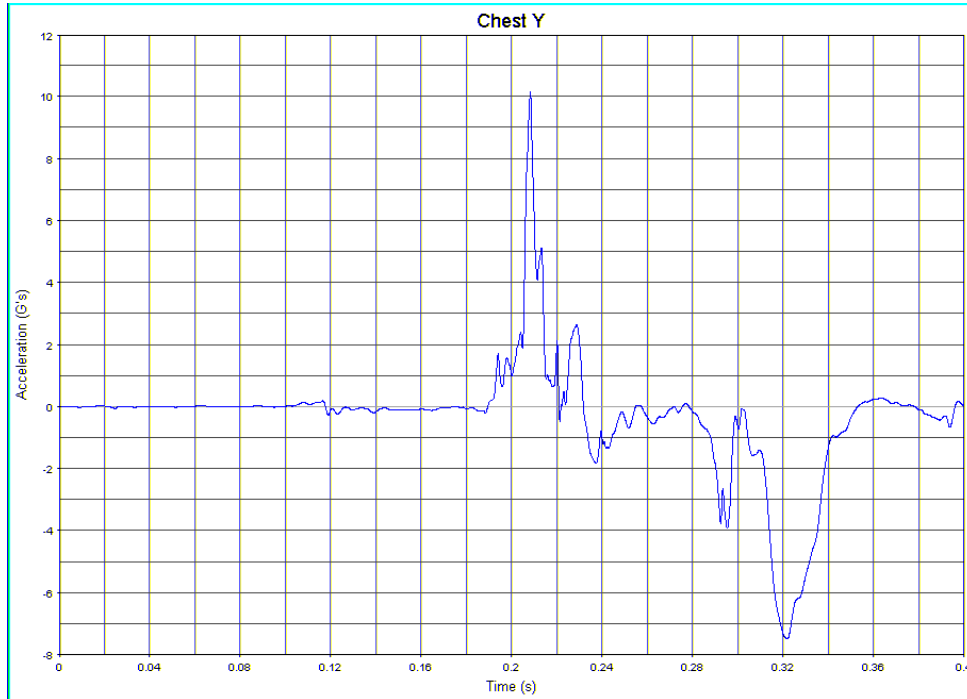


**Figure G47.  Chest Acceleration, y-Direction**
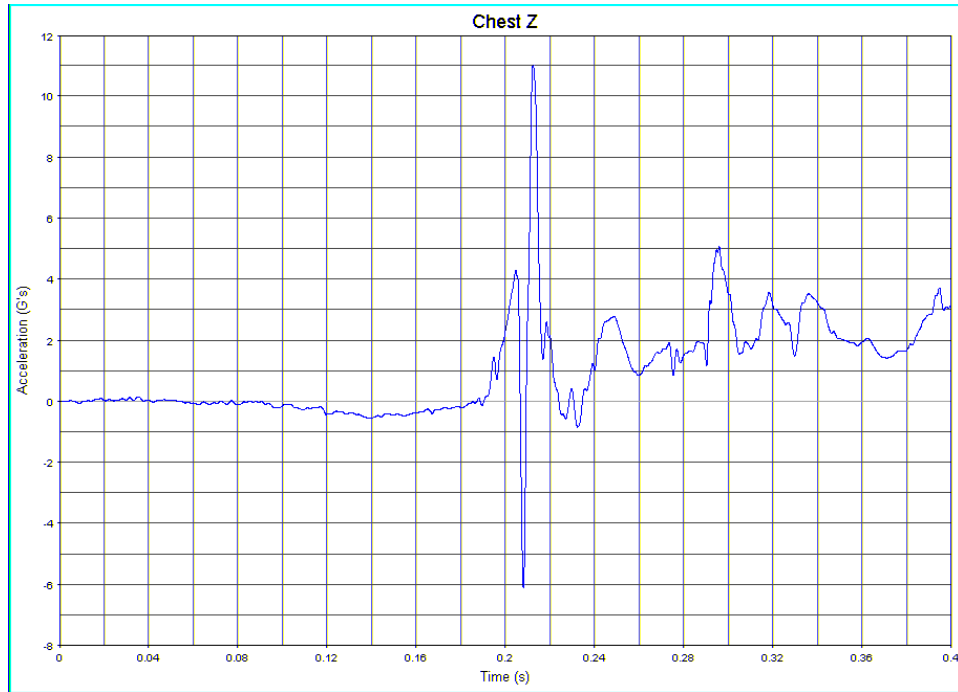
**Figure G48.  Chest Acceleration, z-Direction**
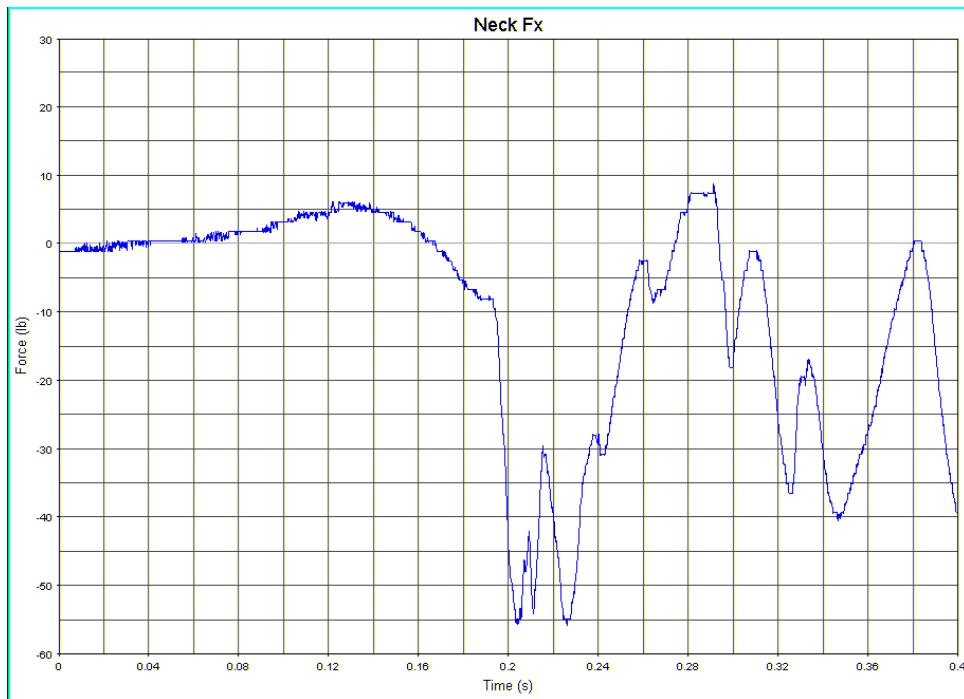


**Figure G49.  Shear Neck Load, x-Direction**
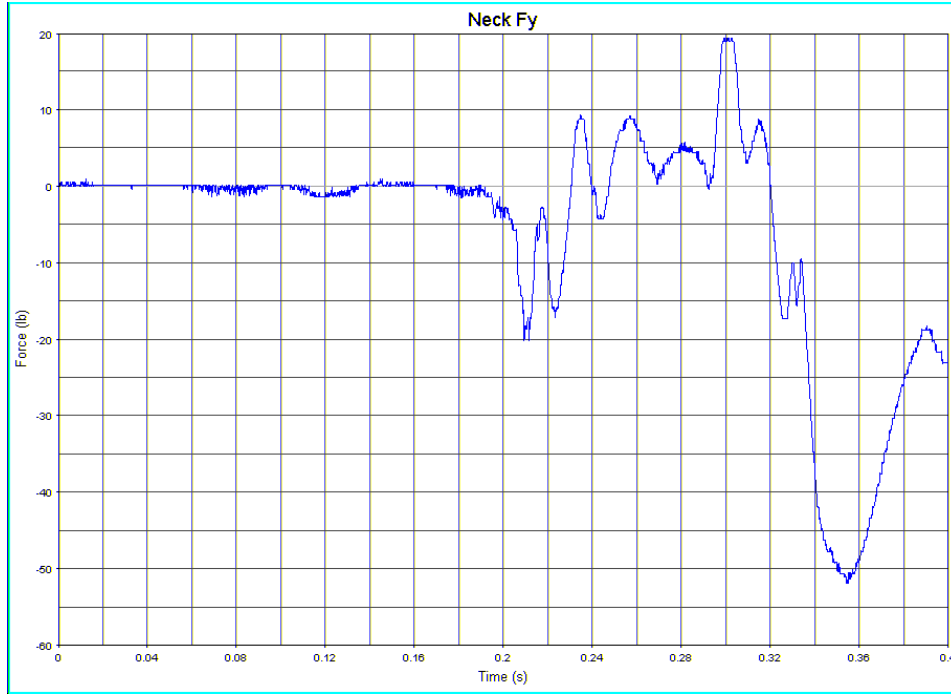
**Figure G50.  Lateral Neck Load, y-Direction**
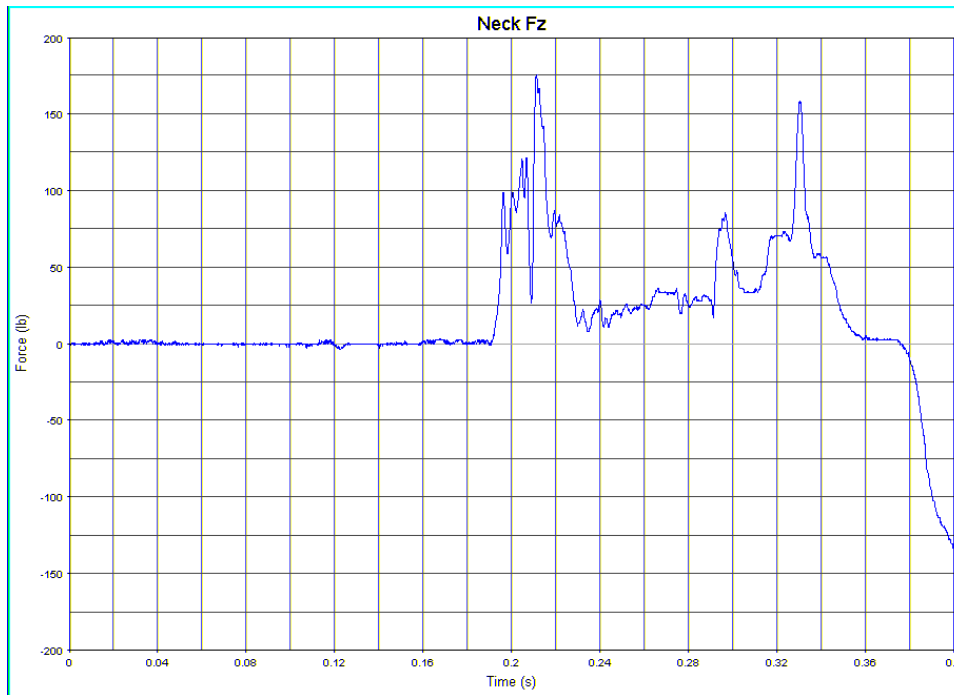


**Figure G51.  Axial Neck Load, z-Direction**
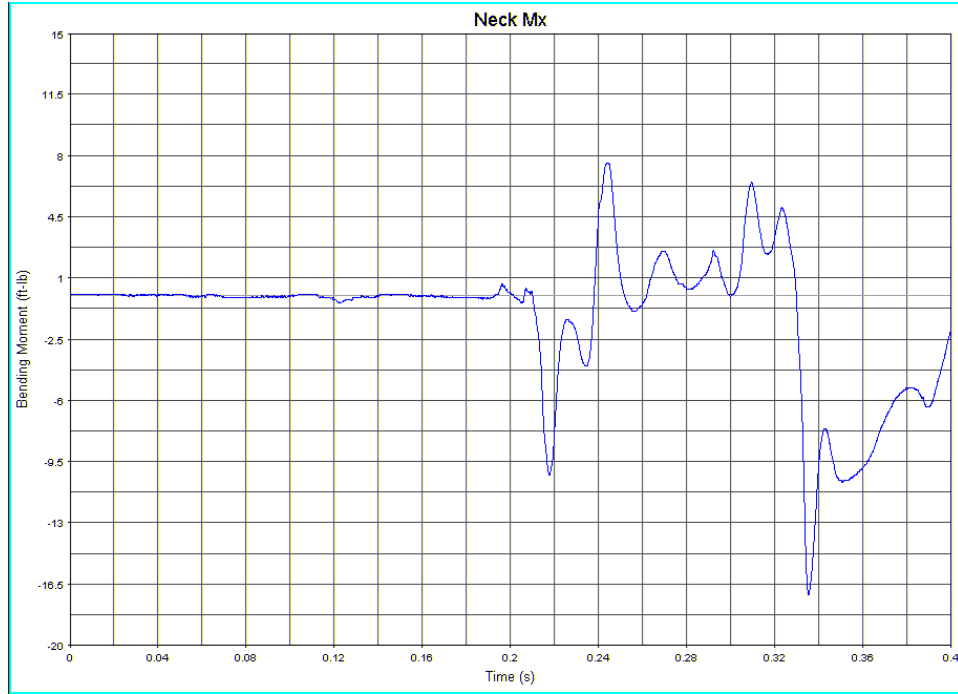
**Figure G52.  Lateral Neck Bending Moment, x-Axis**
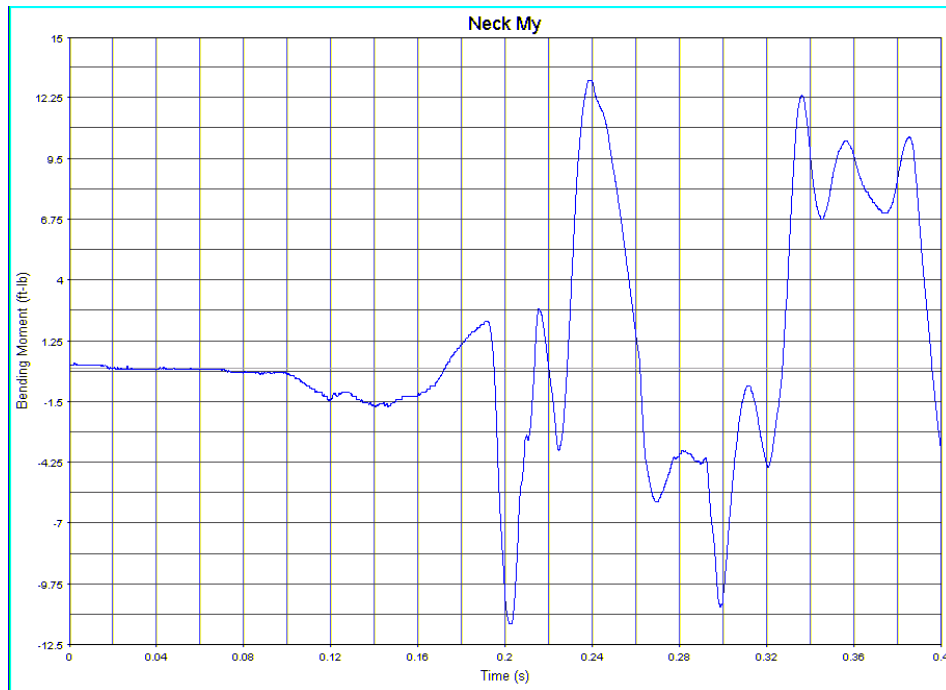


**Figure G53.  Fore/Aft Neck Bending Moment, y-Axis**
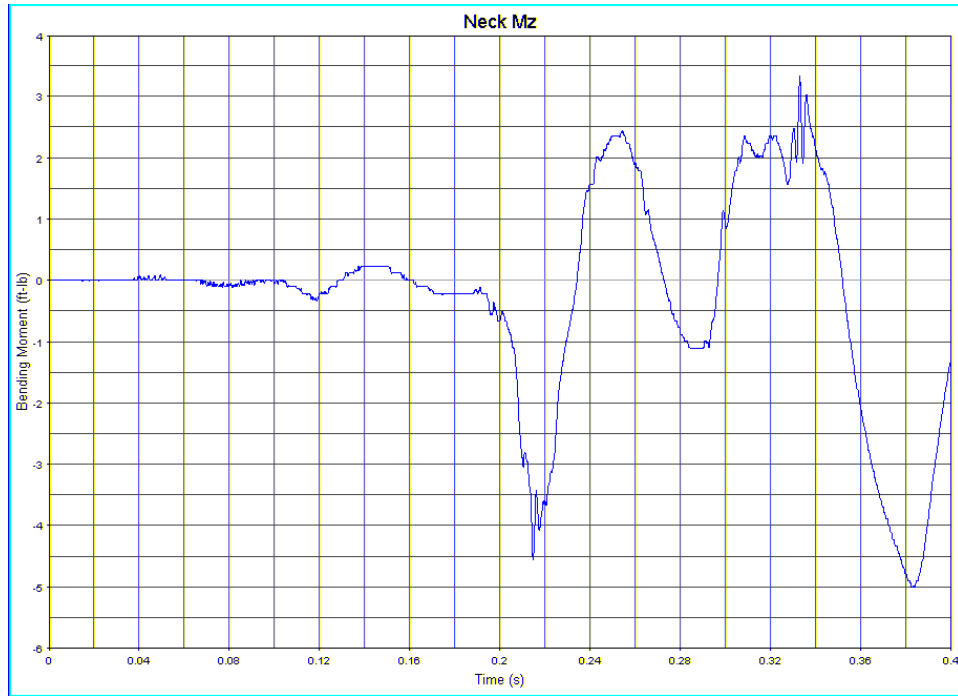
**Figure G54.  Rotational Neck Moment, z-Axis**
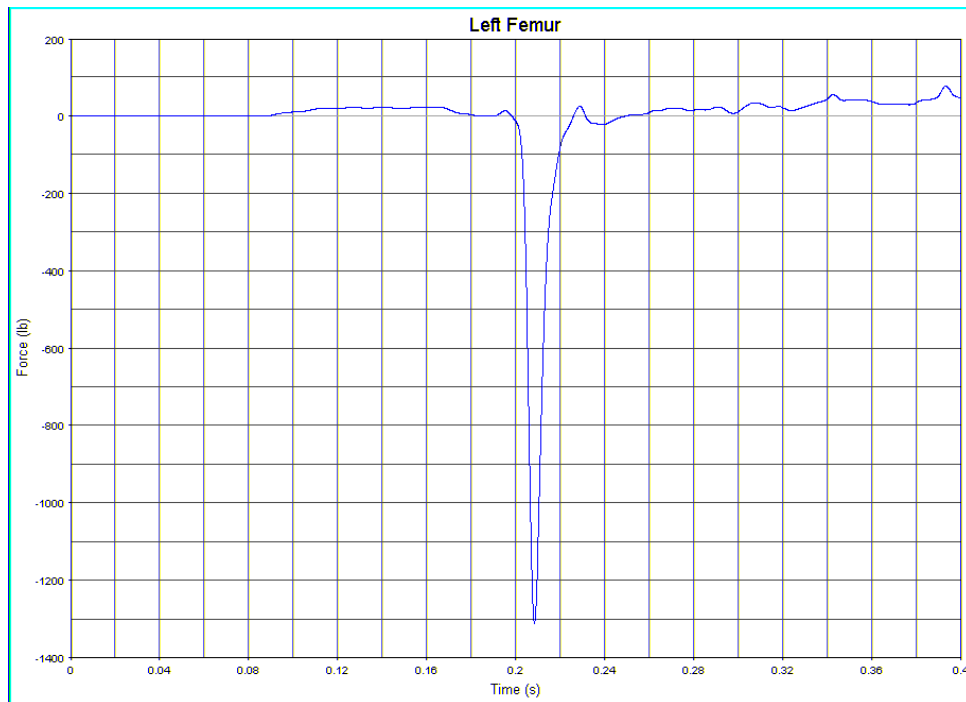


**Figure G55.  Left Femur Load**

**TEST NO. 2, 50TH-PERCENTILE HYBRID III ATD, WINDOW SEAT (CONT.)**
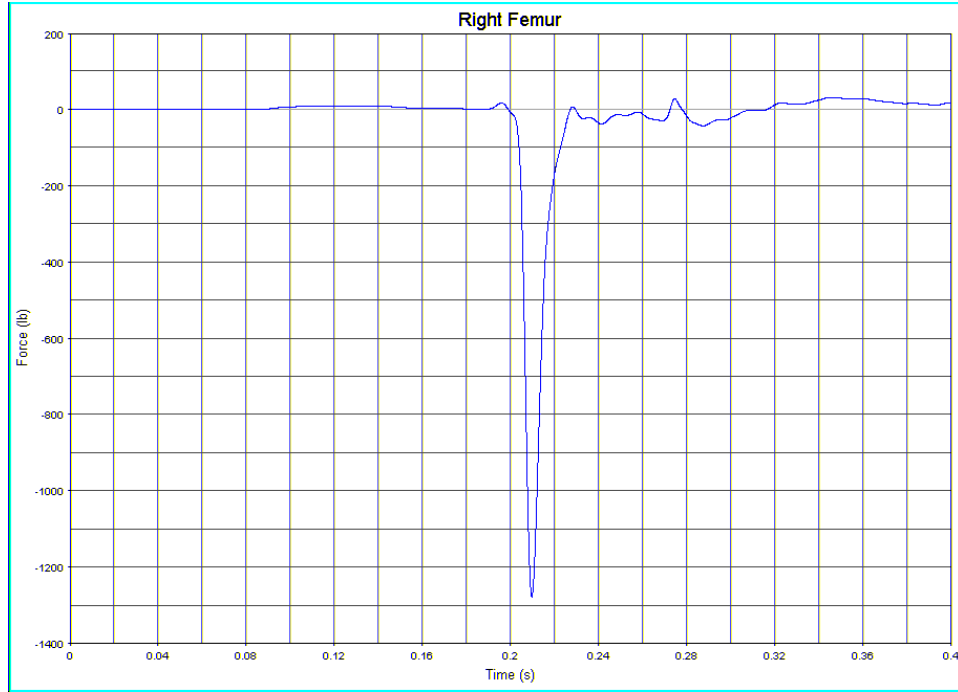


**Figure G56.  Right Femur Load**

**TEST NO. 3/MODEL 2, 50TH-PERCENTILE HYBRID III ATD, AISLE SEAT**
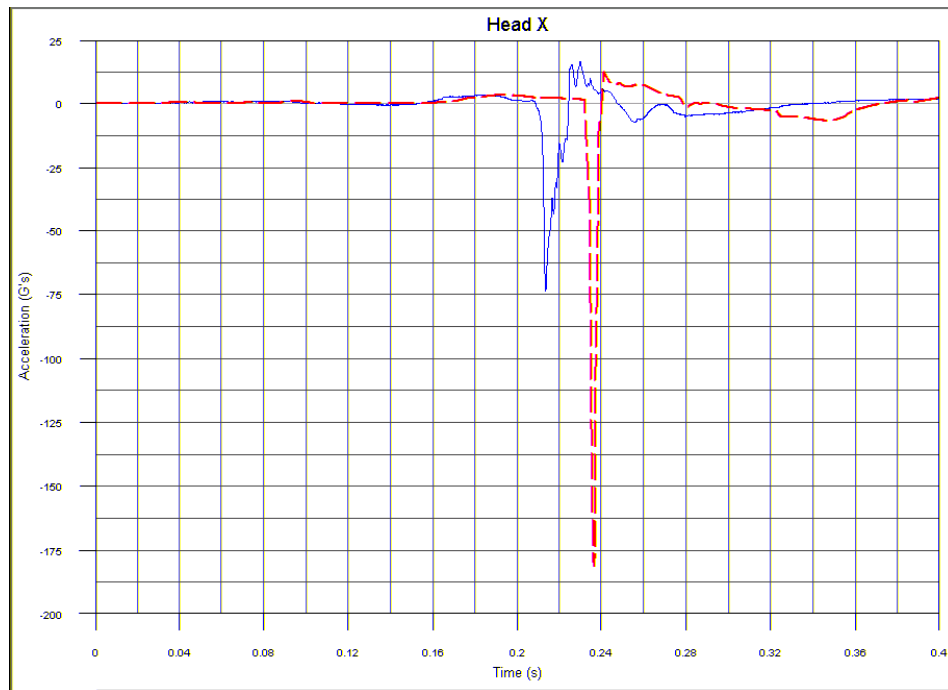


**Figure G57.  Head Acceleration, x-Direction**
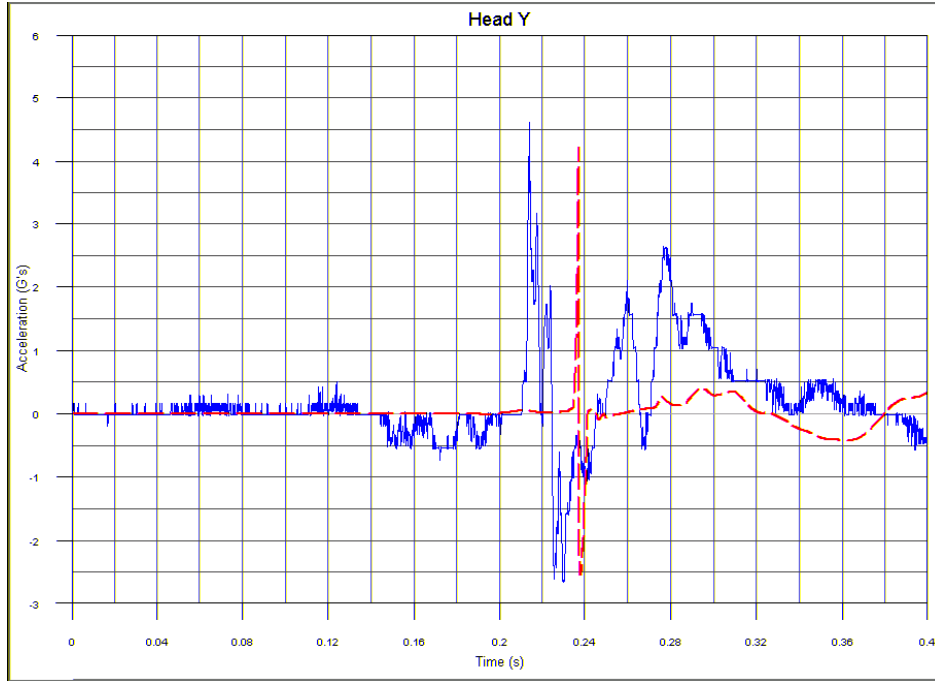
**Figure G58.  Head Acceleration, y-Direction**
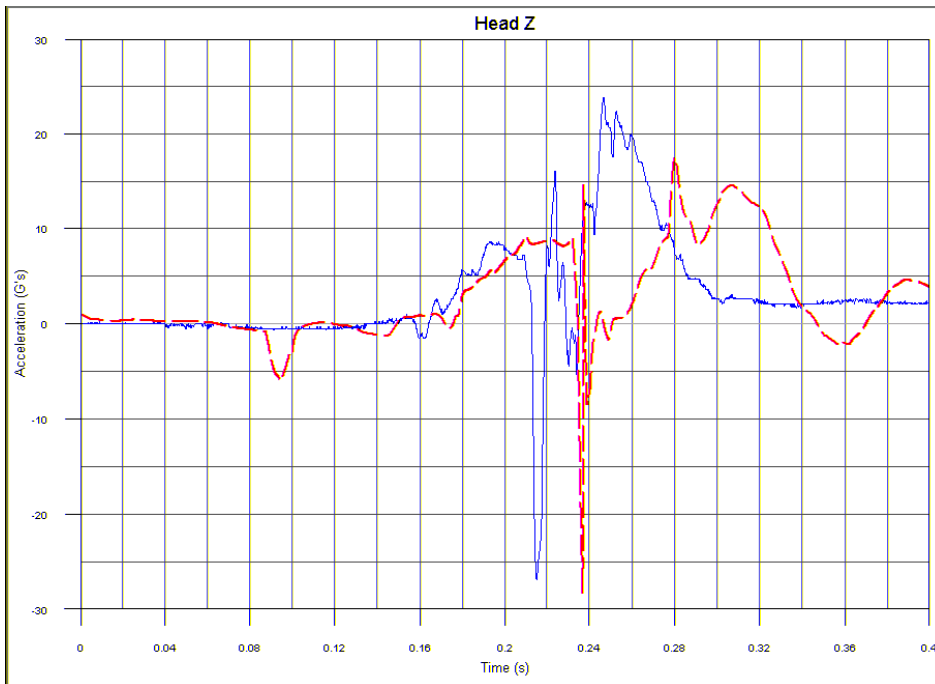


**Figure G59.  Head Acceleration, z-Direction**
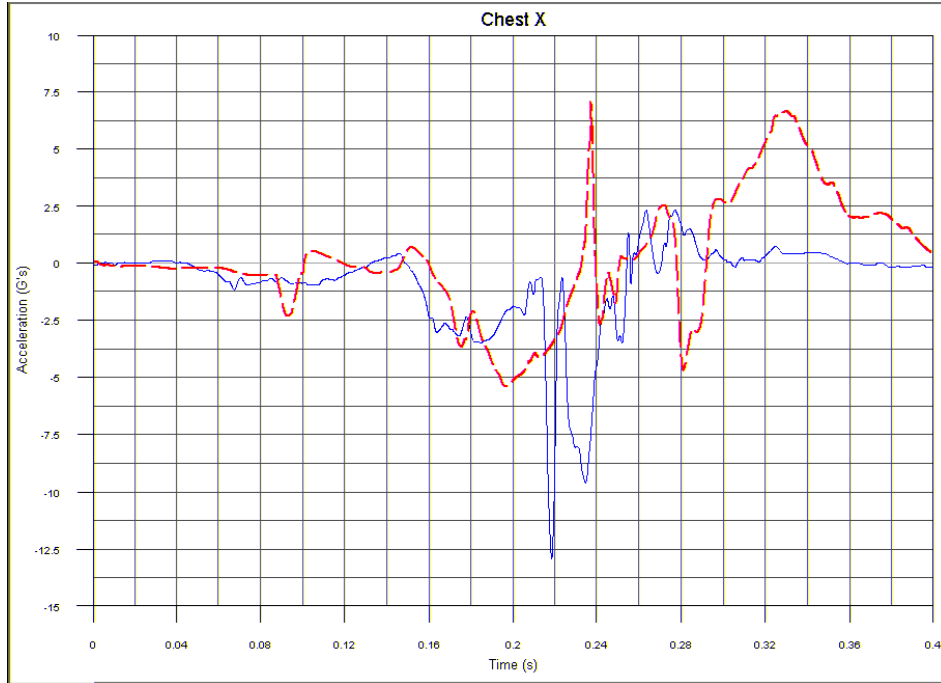
**Figure G60. Chest Acceleration, x-Direction**
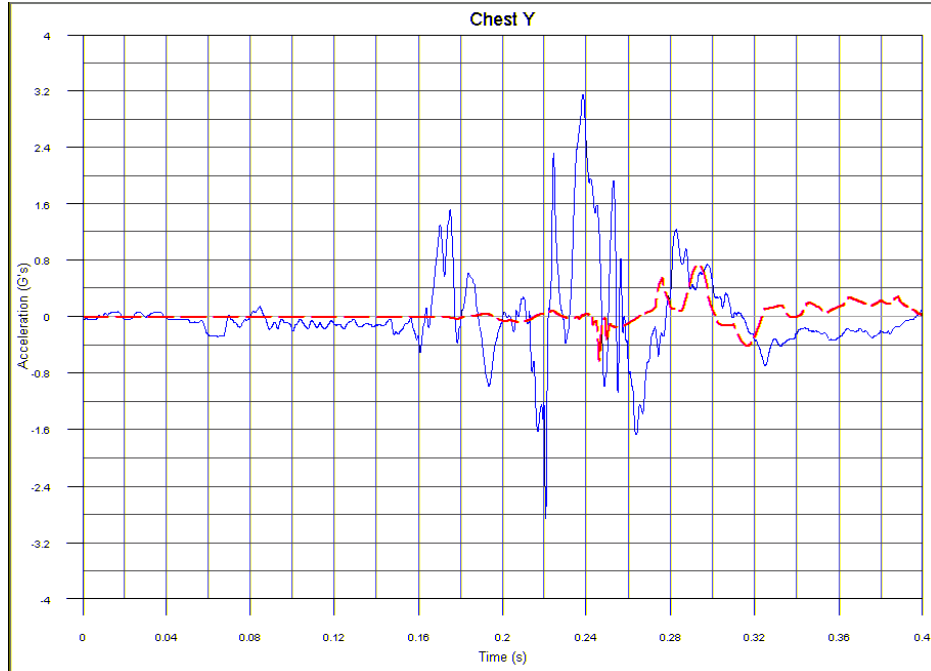


**Figure G61. Chest Acceleration, y-Direction**
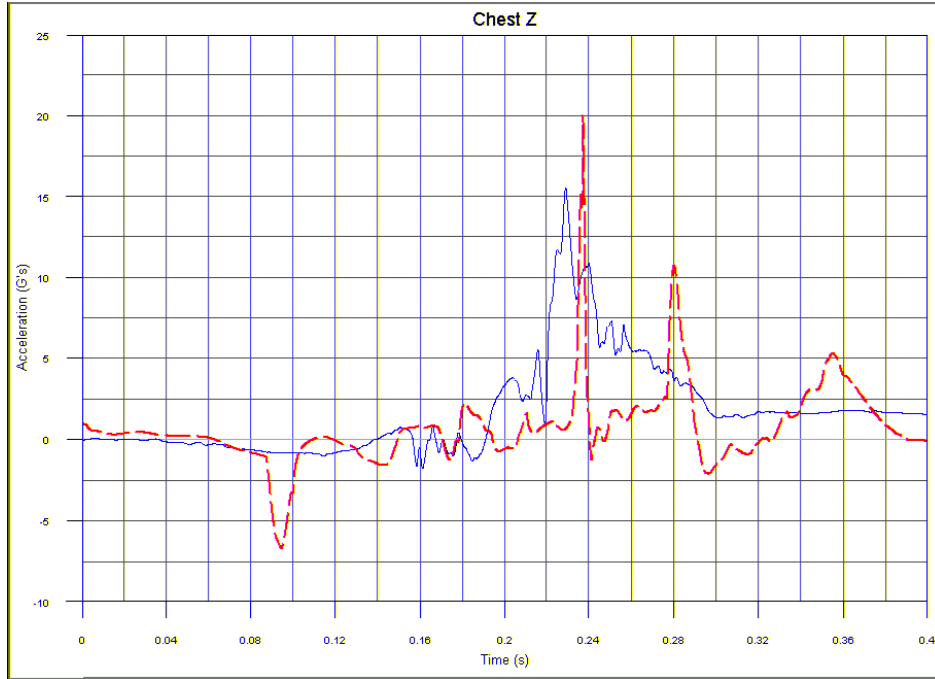
**Figure G62.  Chest Acceleration, z-Direction**
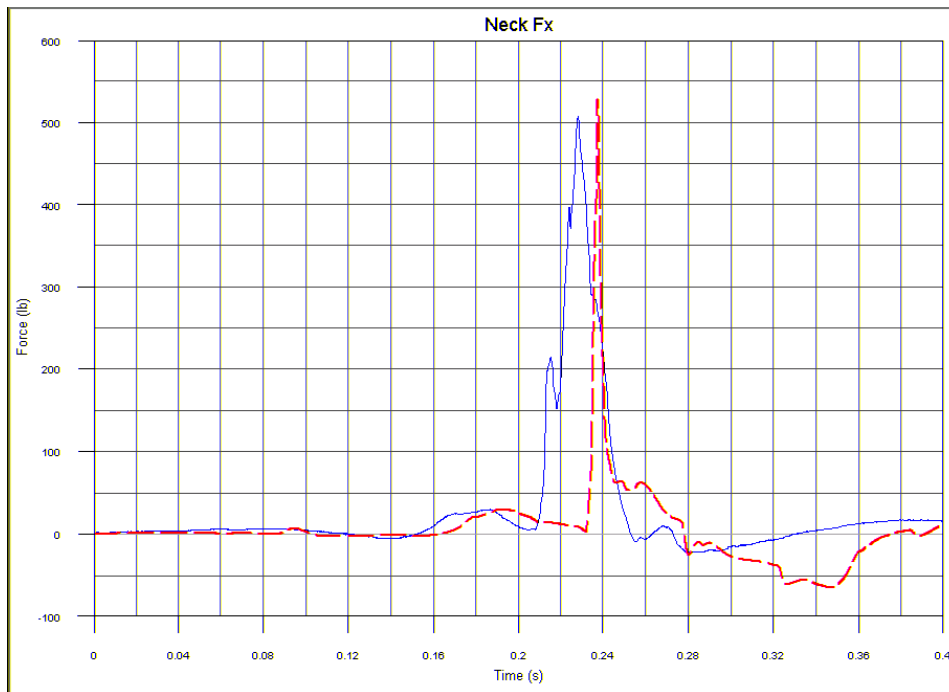


**Figure G63.  Shear Neck Load, x-Direction**
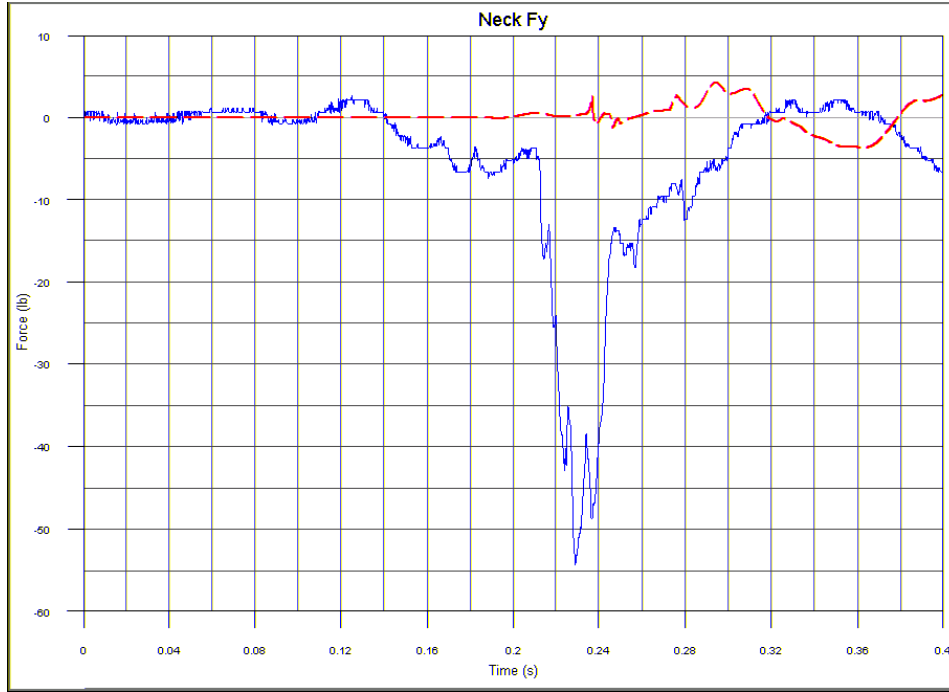
**Figure G64.  Lateral Neck Load, y-Direction**
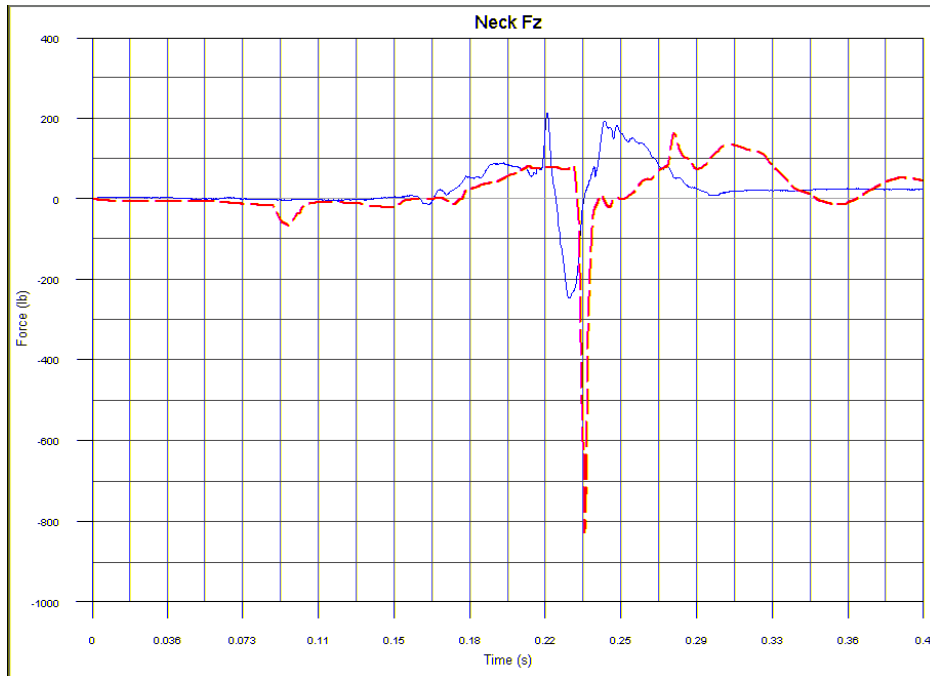


**Figure G65.  Axial Neck Load, z-Direction**

151
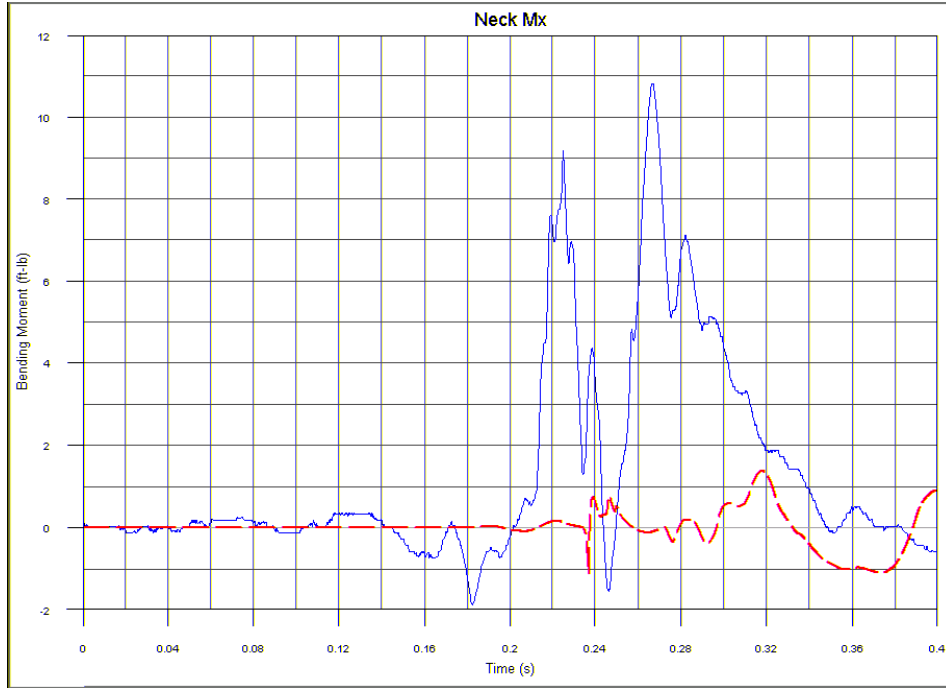
**Figure G66.  Lateral Neck Bending Moment, x-Axis**
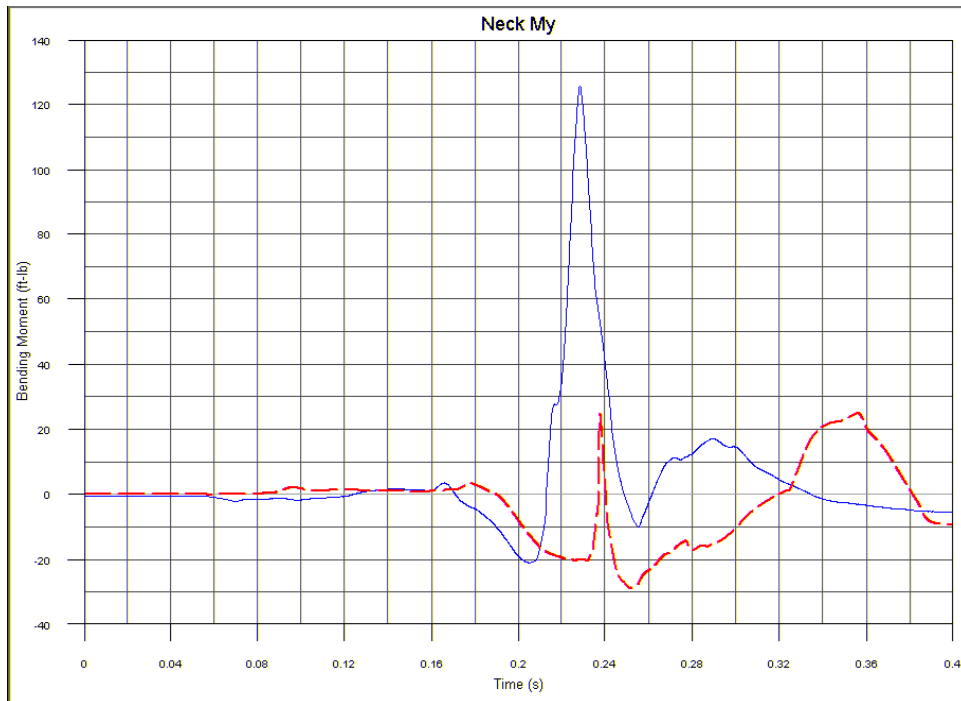


**Figure G67.  Fore/Aft Neck Bending Moment, y-Axis**
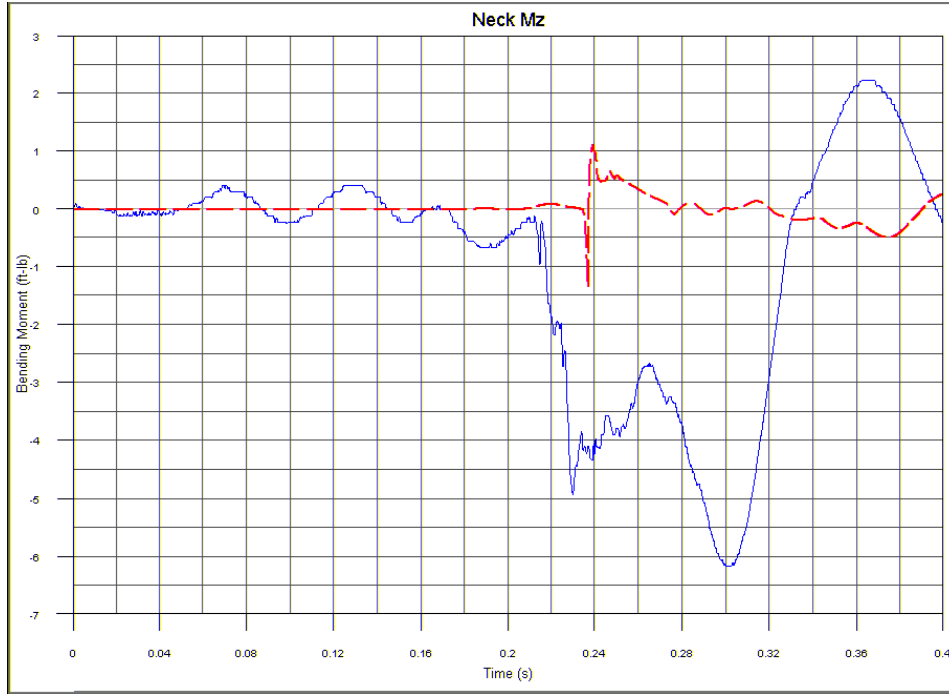
**Figure G68.  Rotational Neck Moment, z-Axis**
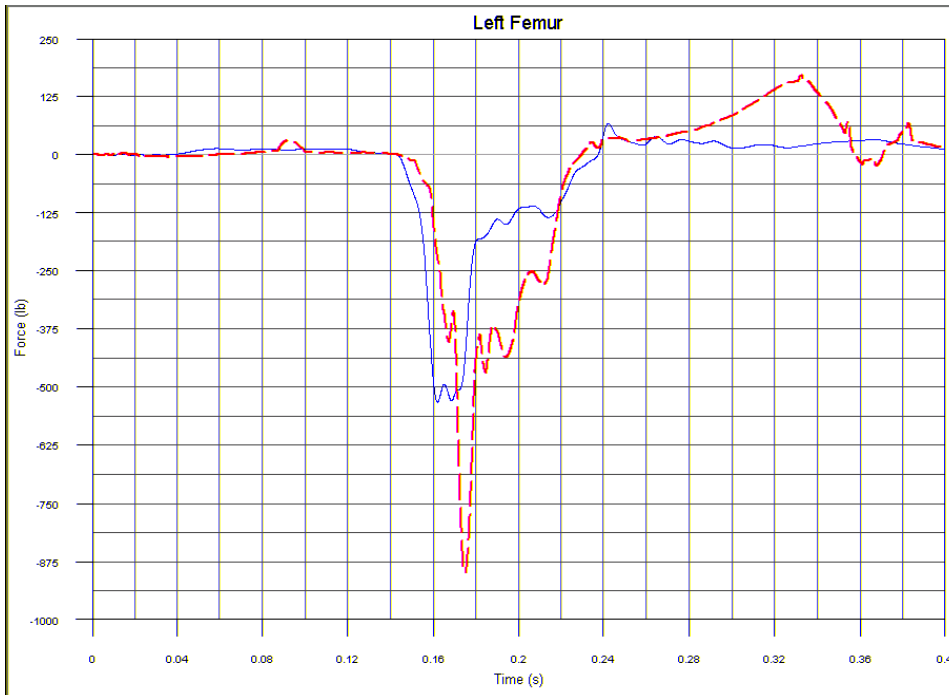


**Figure G69.  Left Femur Load**

**TEST NO. 3/MODEL 2, 50TH-PERCENTILE HYBRID III ATD, AISLE SEAT (CONT.)**
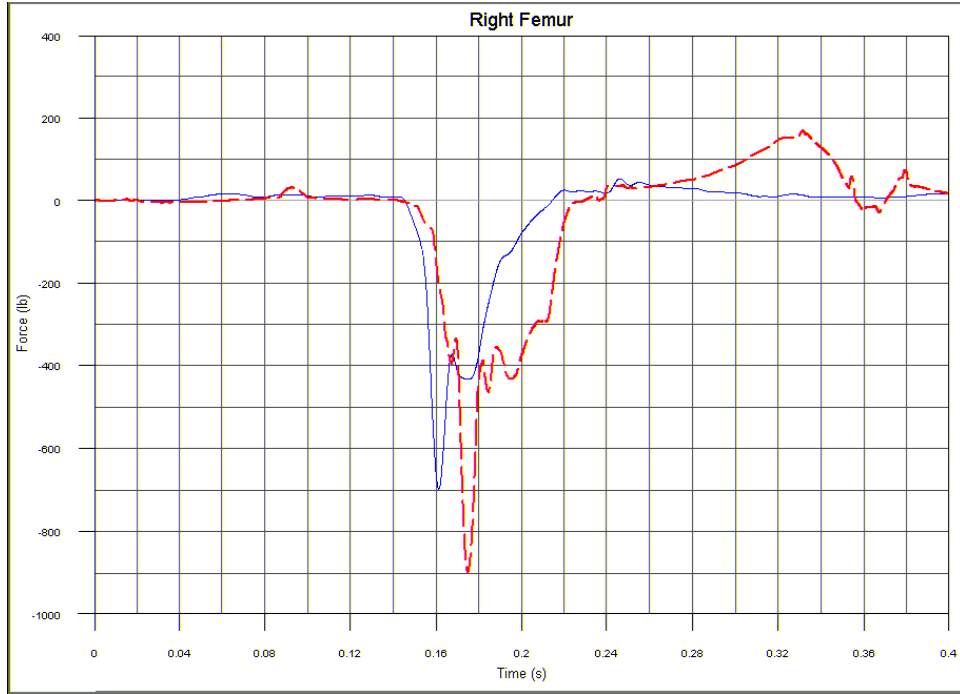


**Figure G70.  Right Femur Load**

**TEST NO. 3/MODEL 2, 50TH-PERCENTILE HYBRID III ATD, WINDOW SEAT**
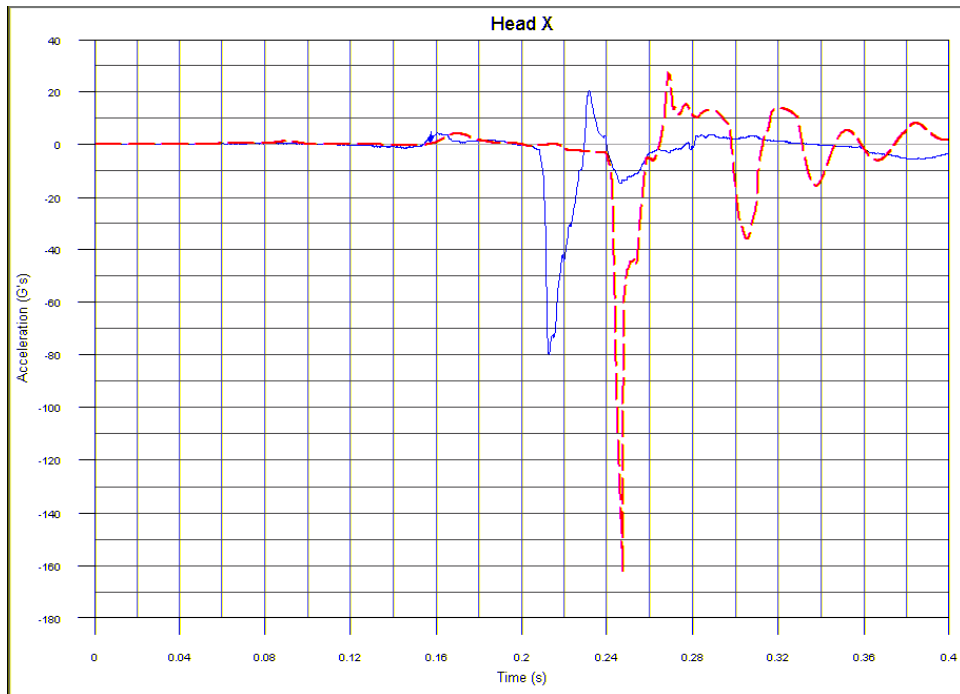


**Figure G71.  Head Acceleration, x-Direction**
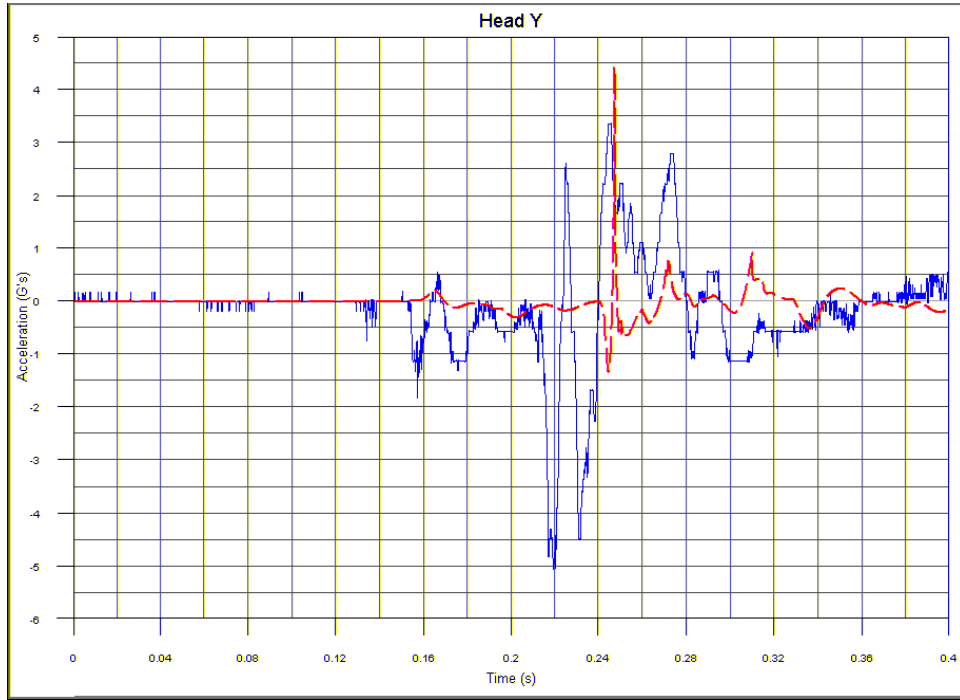
**Figure G72.  Head Acceleration, y-Direction**
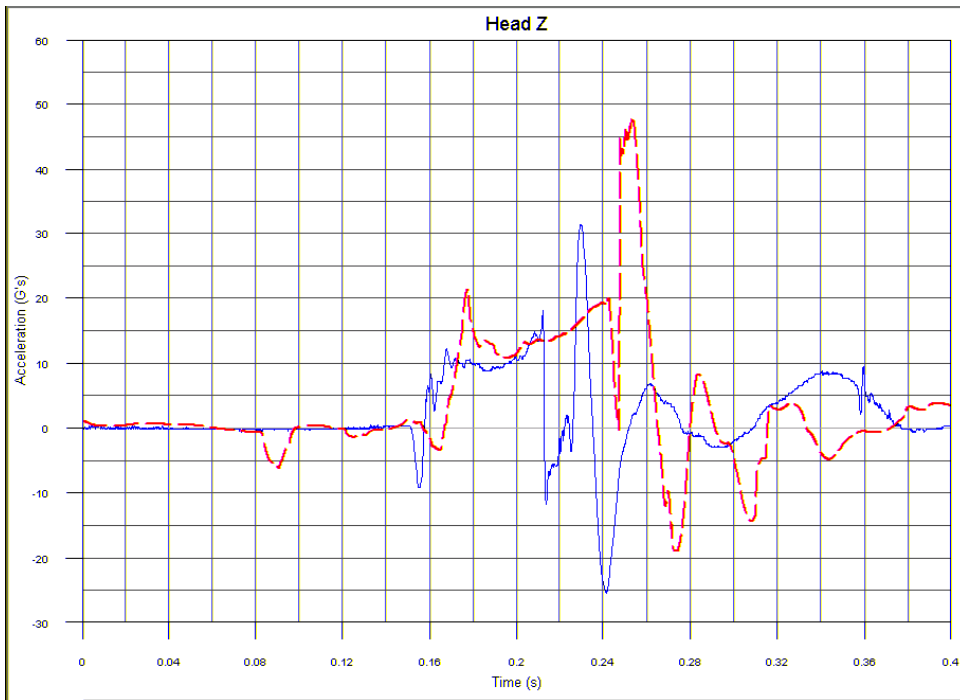


**Figure G73.  Head Acceleration, z-Direction**
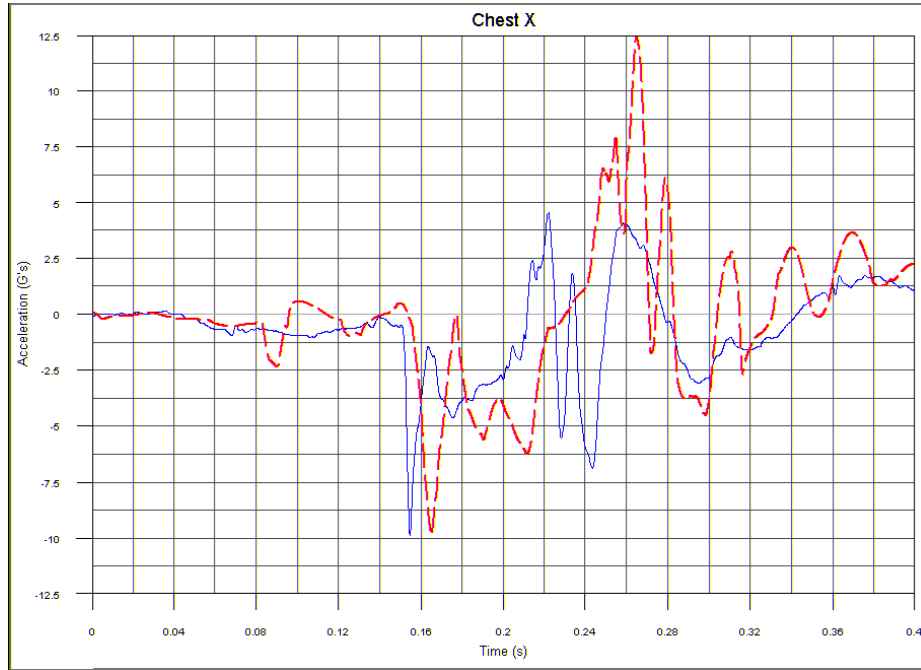
**Figure G74.  Chest Acceleration, x-Direction**
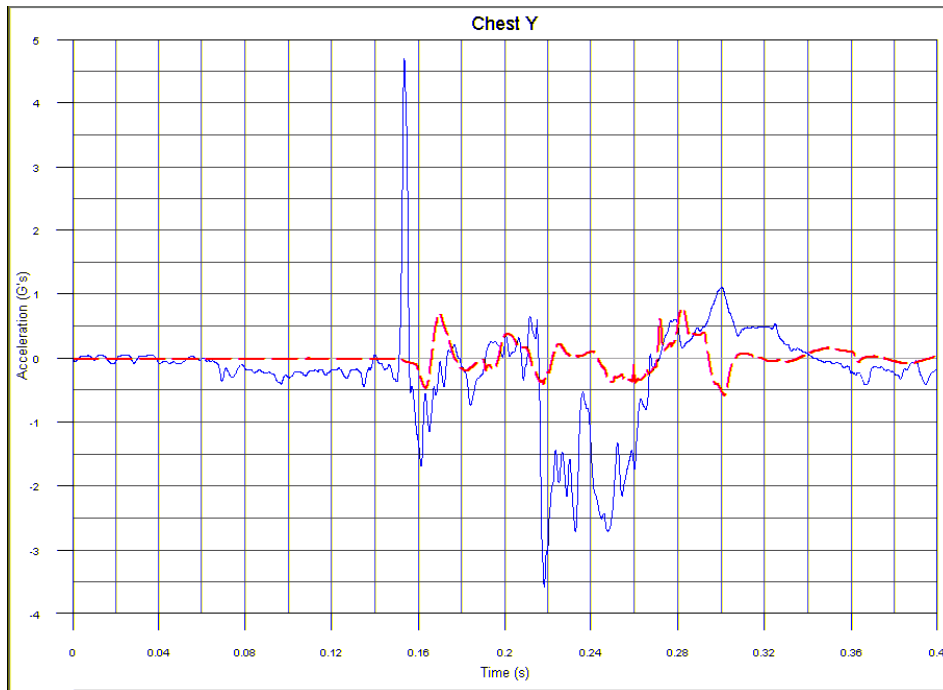


**Figure G75.  Chest Acceleration, y-Direction**
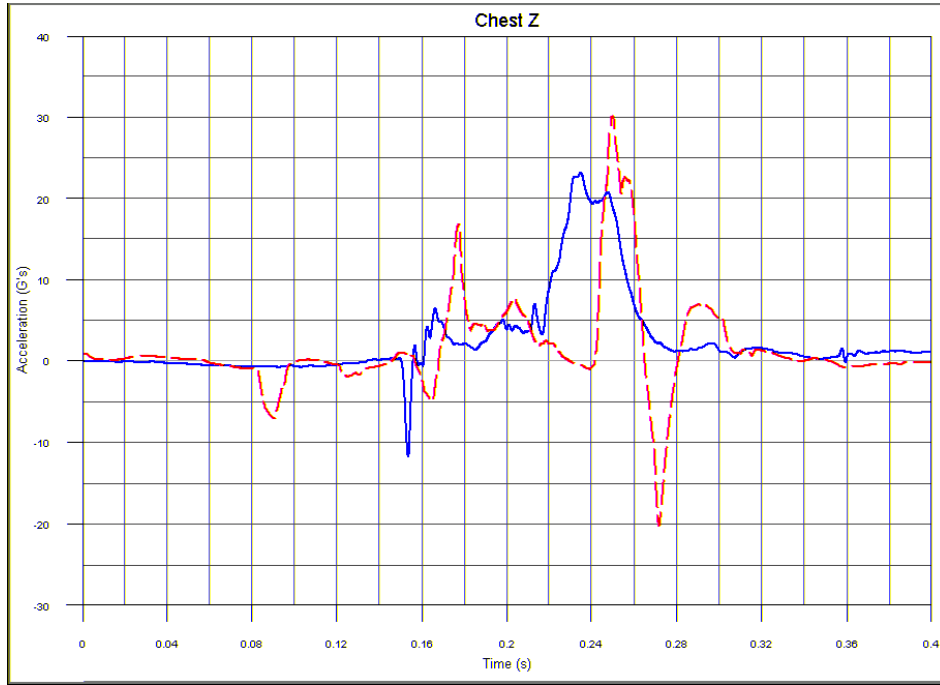
**Figure G76.  Chest Acceleration, z-Direction**
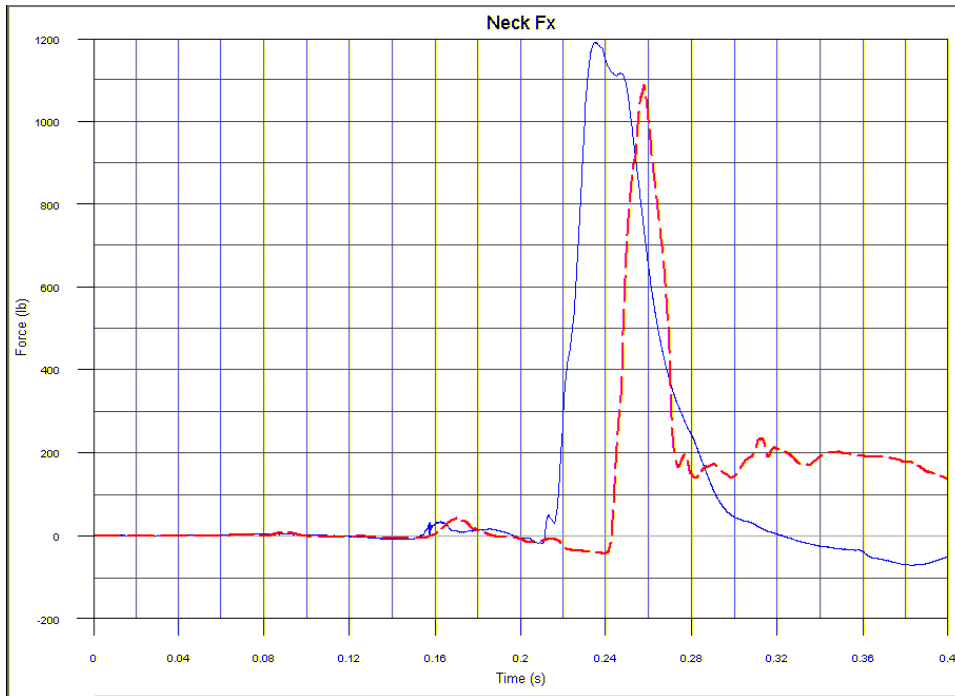


**Figure G77.  Shear Neck Load, x-Direction**
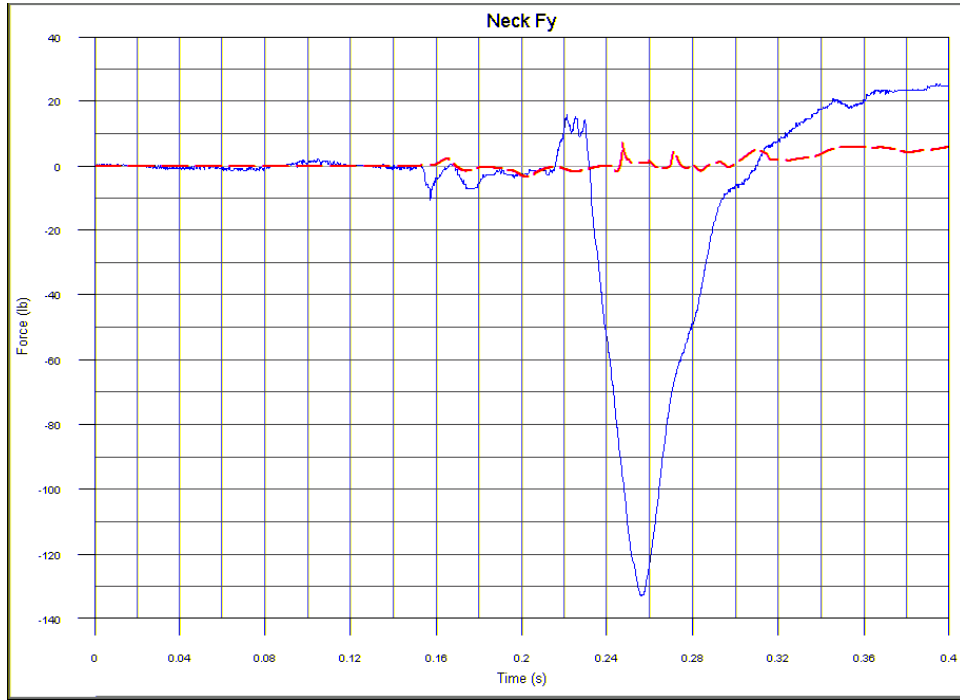
**Figure G78.  Lateral Neck Load, y-Direction**
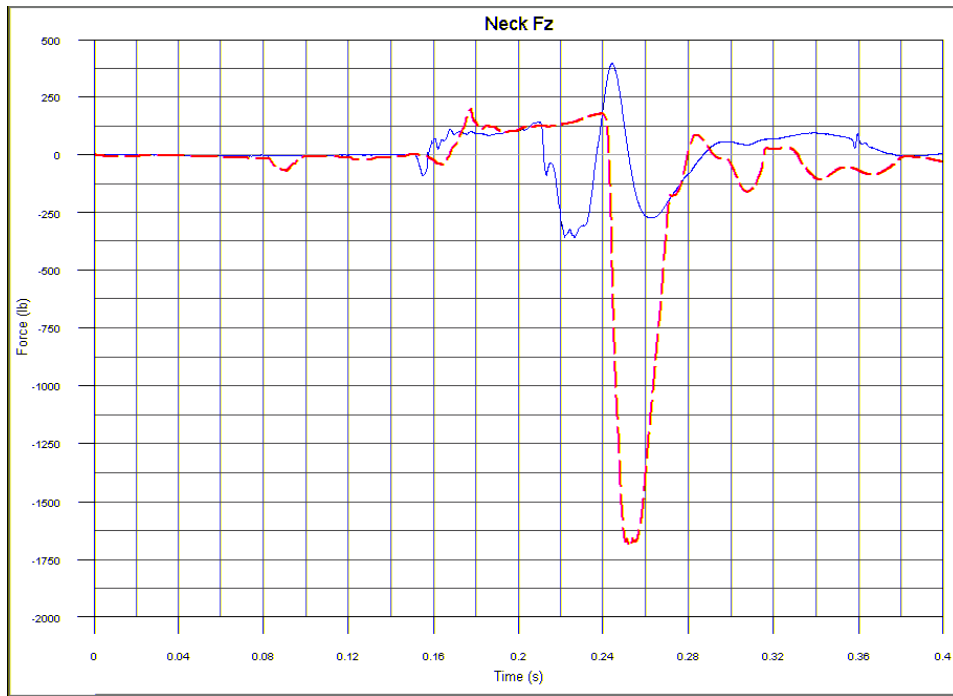


**Figure G79.  Axial Neck Load, z-Direction**
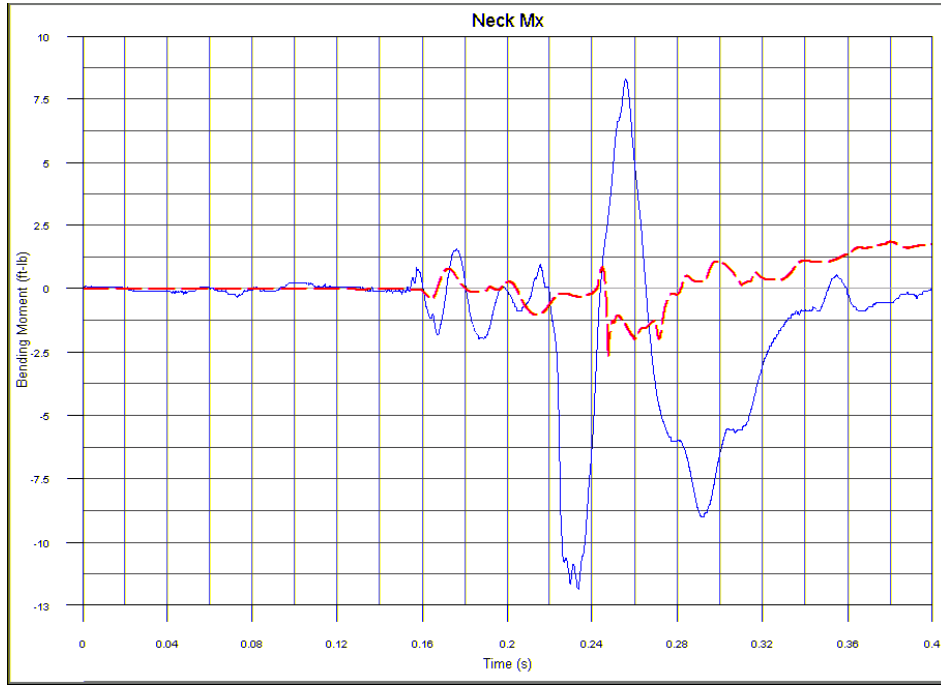
**Figure G80. Lateral Neck Bending Moment, x-Axis**
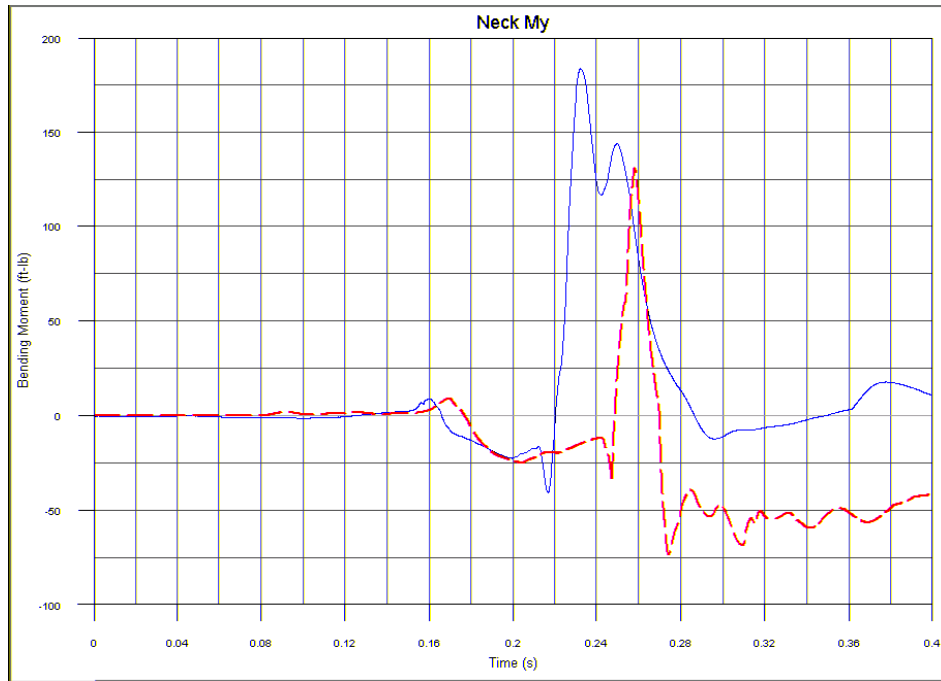


**Figure G81. Fore/Aft Neck Bending Moment, y-Axis**
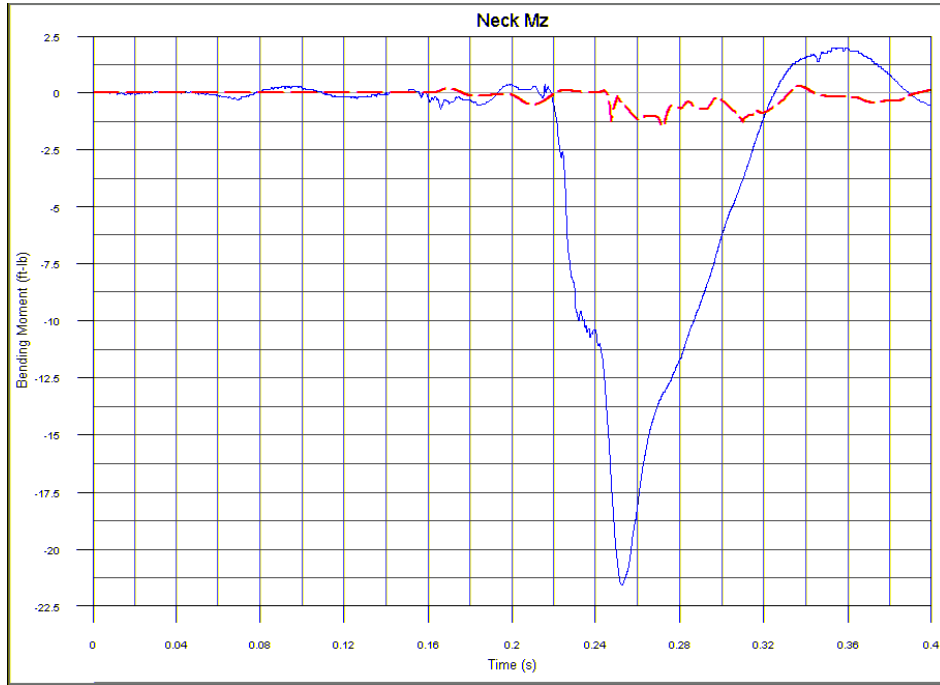
**Figure G82.  Rotational Neck Moment, z-Axis**
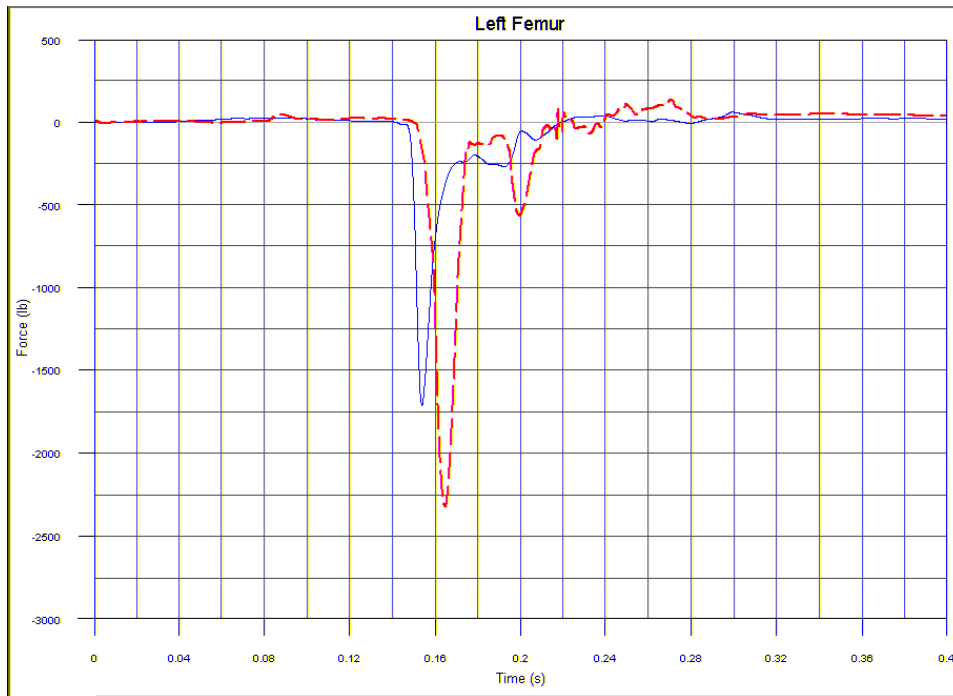


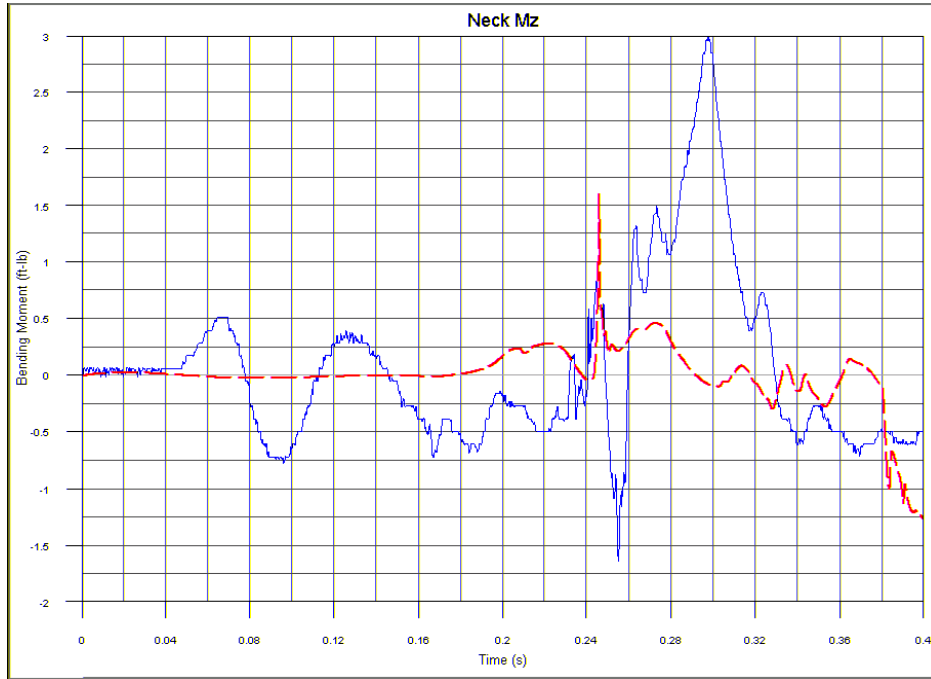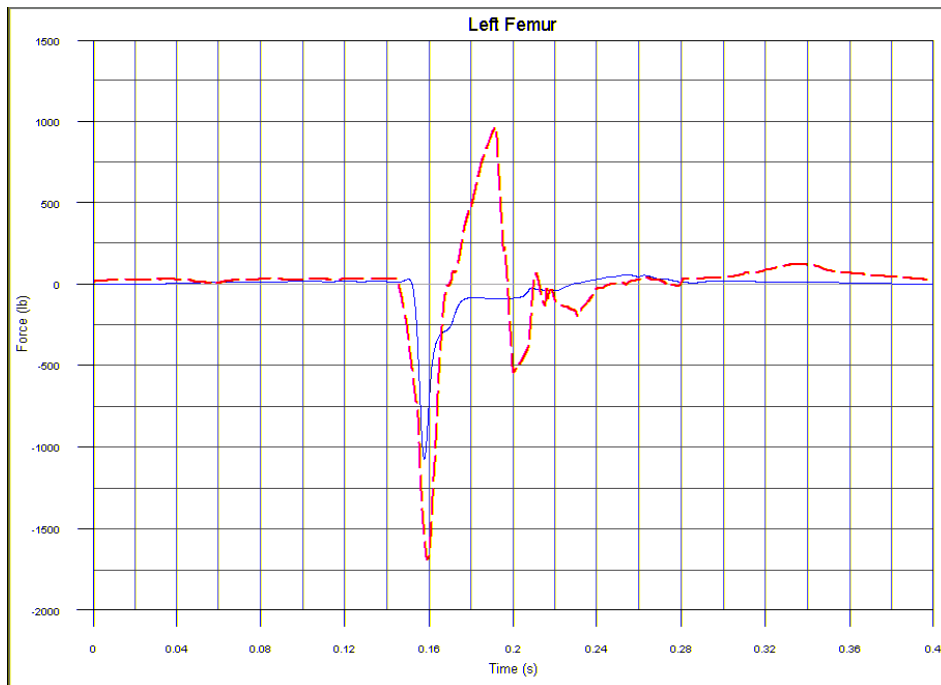**Figure G83.  Left Femur Load**

## TEST NO. 3/MODEL 2, 50TH-PERCENTILE HYBRID III ATD, WINDOW SEAT (CONT.)
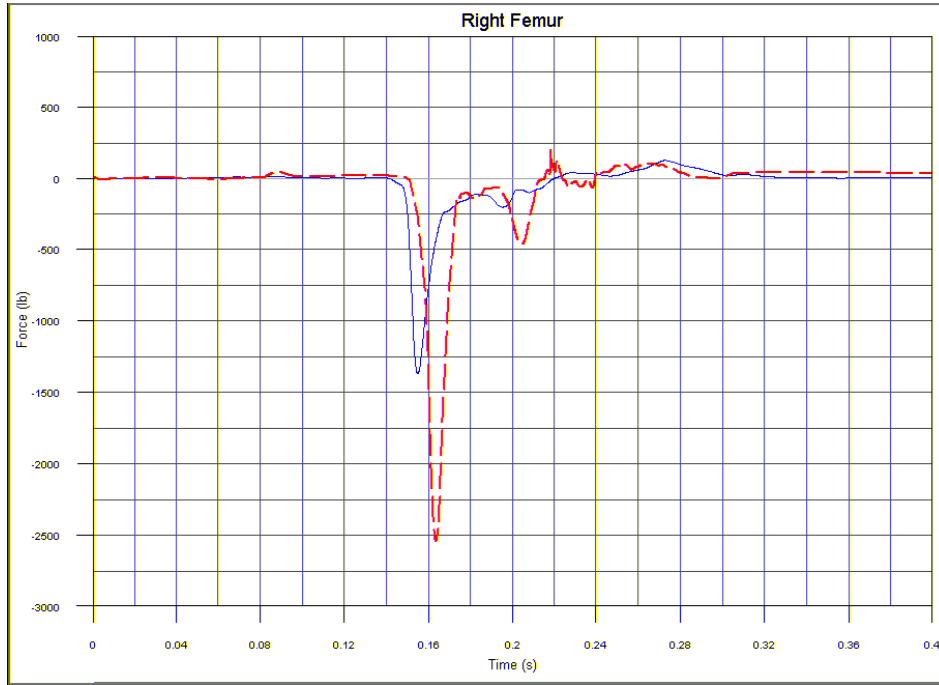


**Figure G84. Right Femur Load**

## TEST NO. 4/MODEL 3, 5TH-PERCENTILE HYBRID III ATD, AISLE SEAT
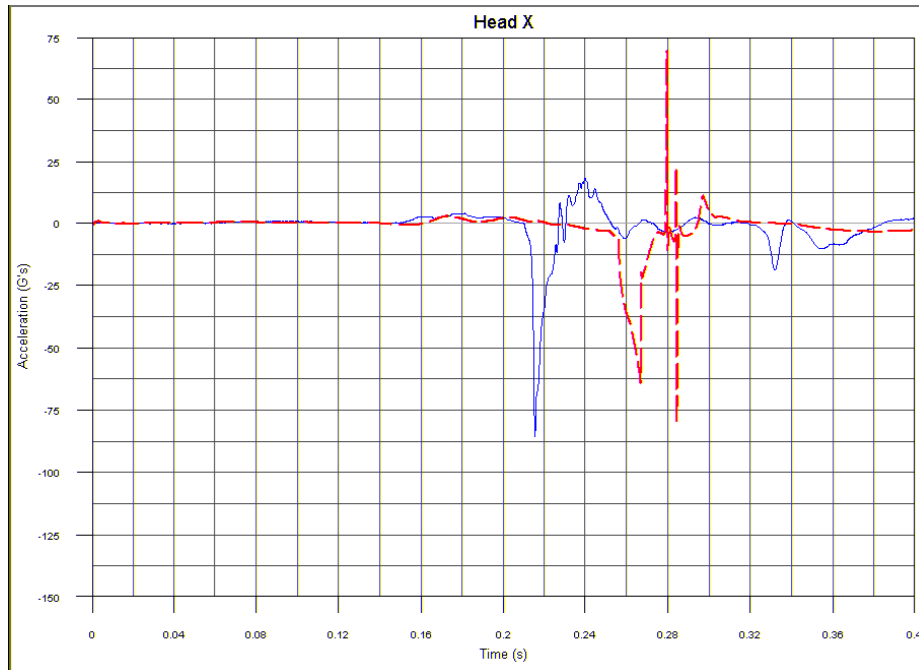


**Figure G85. Head Acceleration, x-Direction**

161
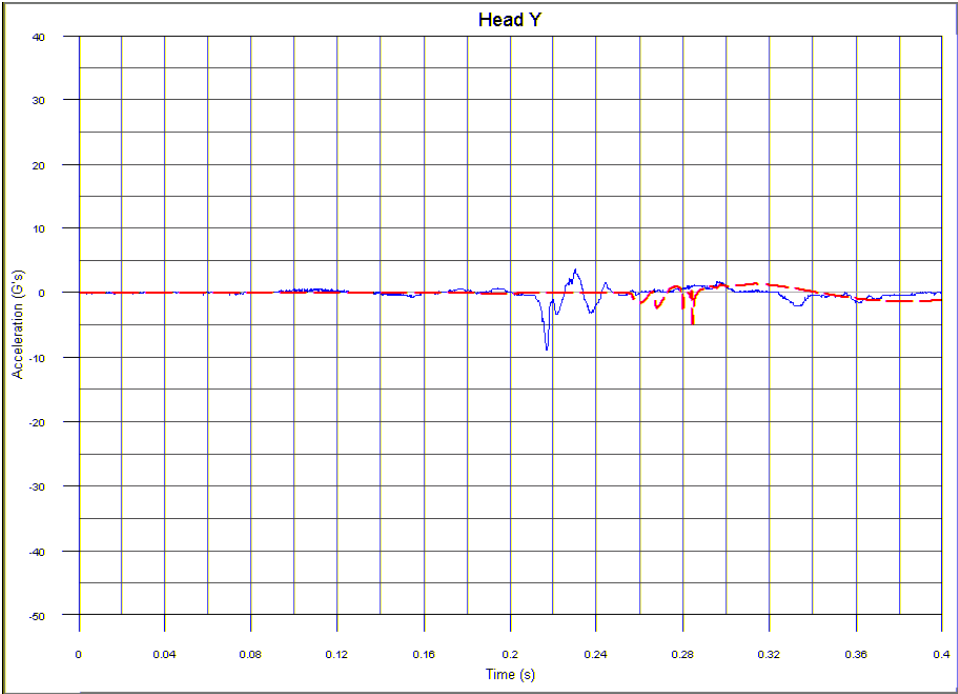
**Figure G86. Head Acceleration, y-Direction**
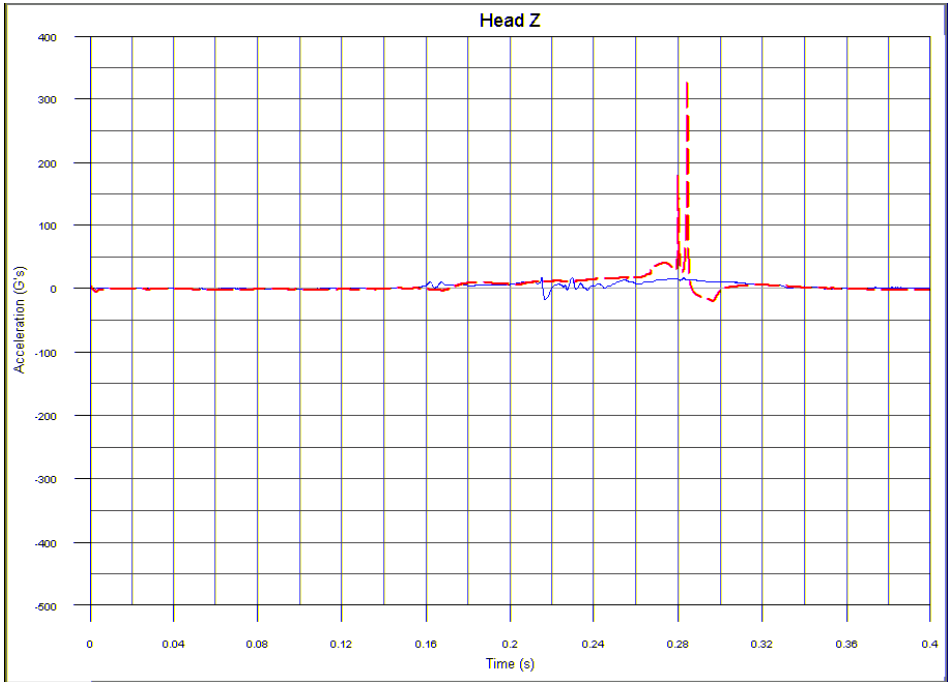


**Figure G87. Head Acceleration, z-Direction**
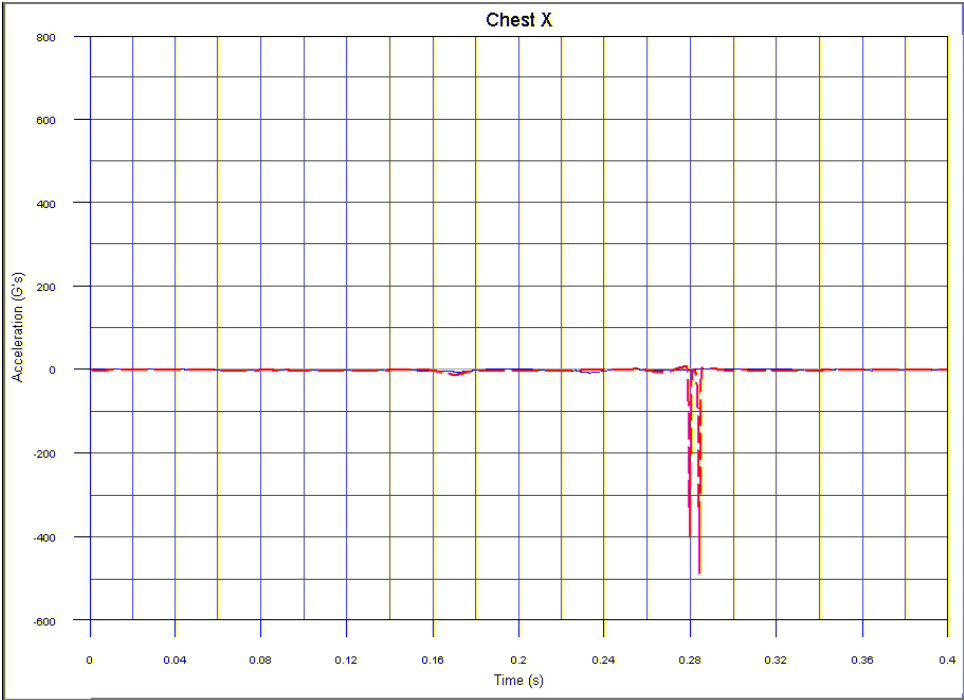
**Figure G88.  Chest Acceleration, x-Direction**
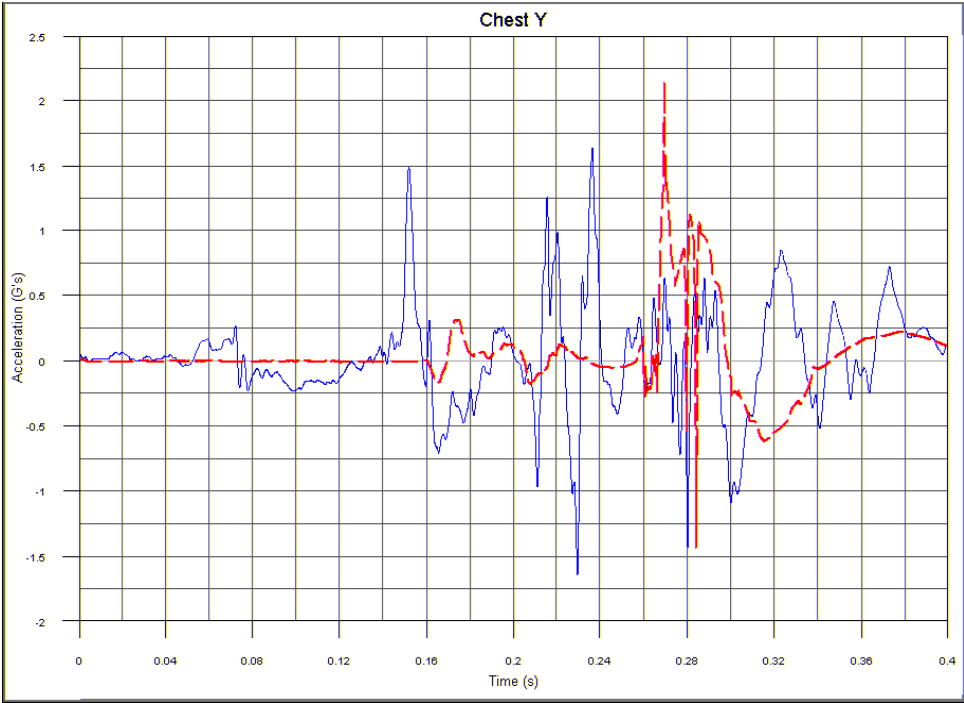


**Figure G89.  Chest Acceleration, y-Direction**
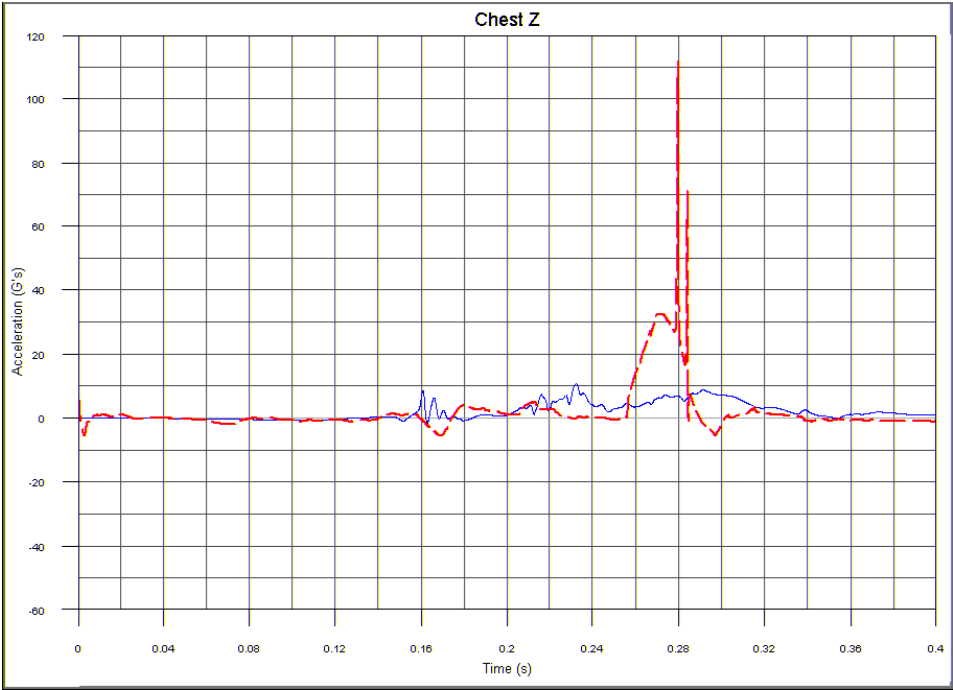
**Figure G90.  Chest Acceleration, z-Direction**
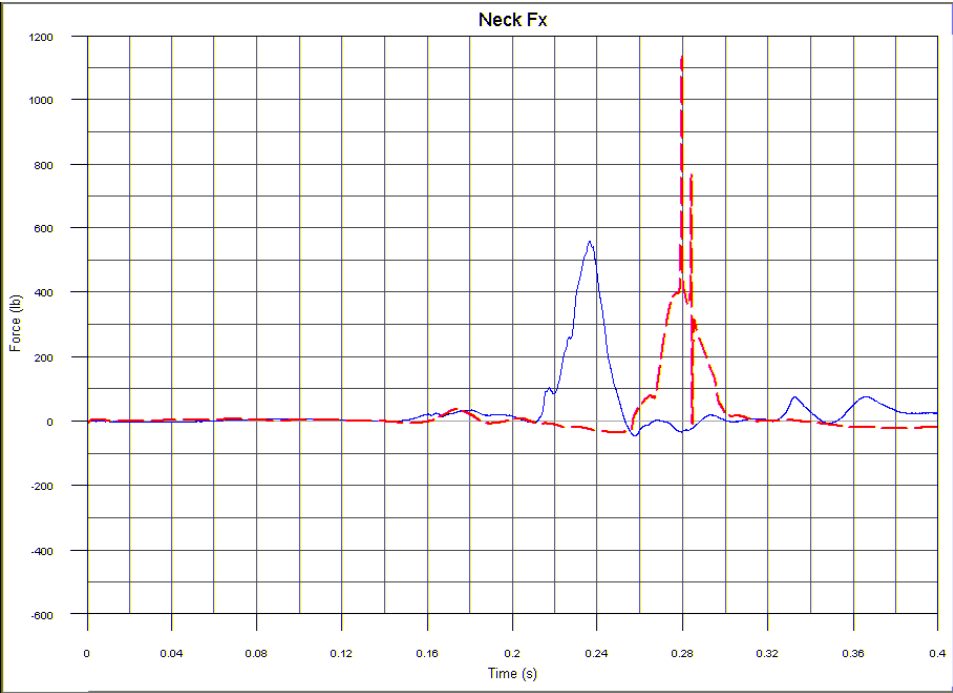


**Figure G91.  Shear Neck Load, x-Direction**

**Figure G92.  Lateral Neck Load, y-Direction**
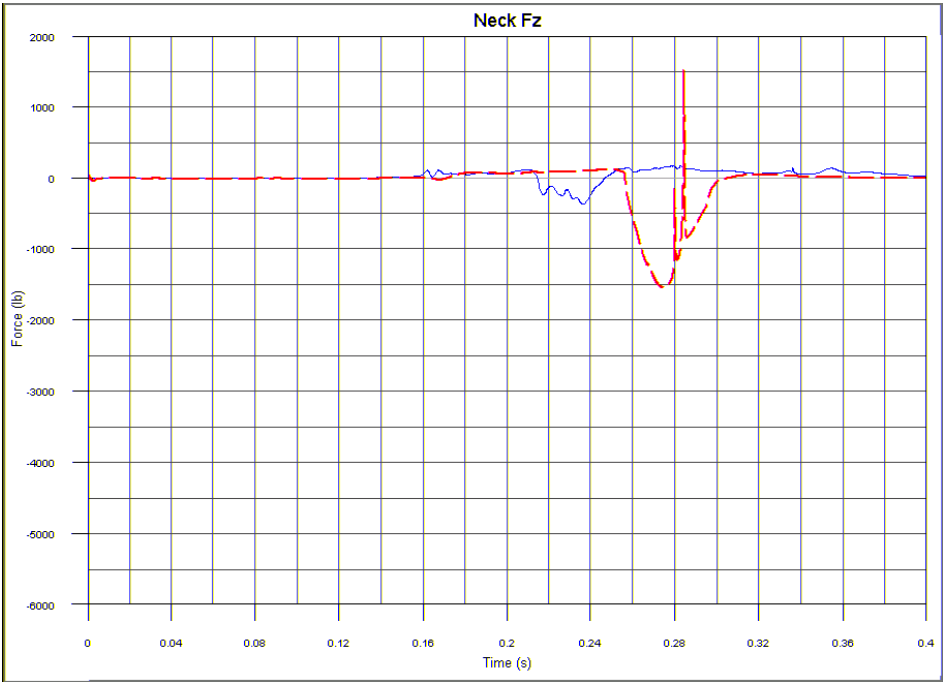


**Figure G93.  Axial Neck Load, z-Direction**

**Figure G94.  Lateral Neck Bending Moment, x-Axis**



**Figure G95.  Fore/Aft Neck Bending Moment, y-Axis**

**Figure G96.  Rotational Neck Moment, z-Axis**



**Figure G97.  Left Femur Load**

**Figure G98.  Right Femur Load**

**TEST NO. 4/MODEL 3, 95TH-PERCENTILE HYBRID III ATD, WINDOW SEAT**



**Figure G99.  Head Acceleration, x-Direction**
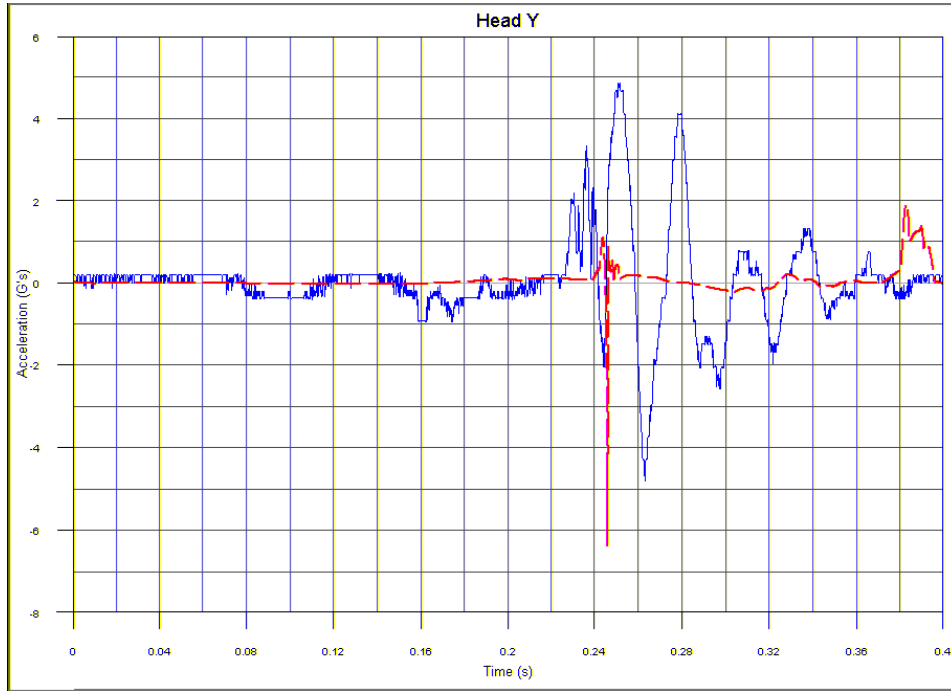
**Figure G100.  Head Acceleration, y-Direction**
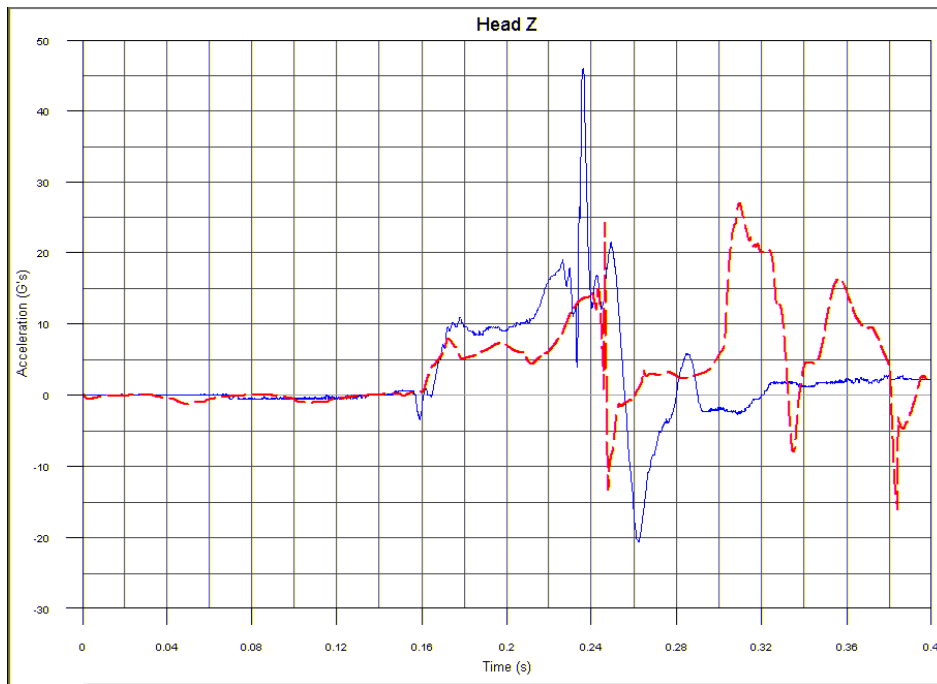


**Figure G101.  Head Acceleration, z-Direction**
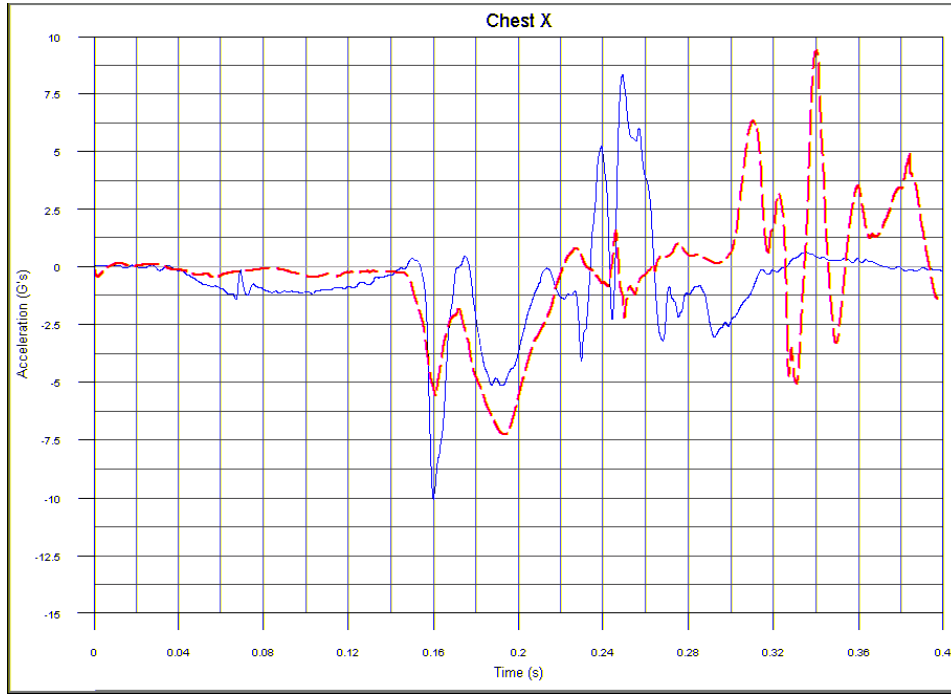
**Figure G102.  Chest Acceleration, x-Direction**
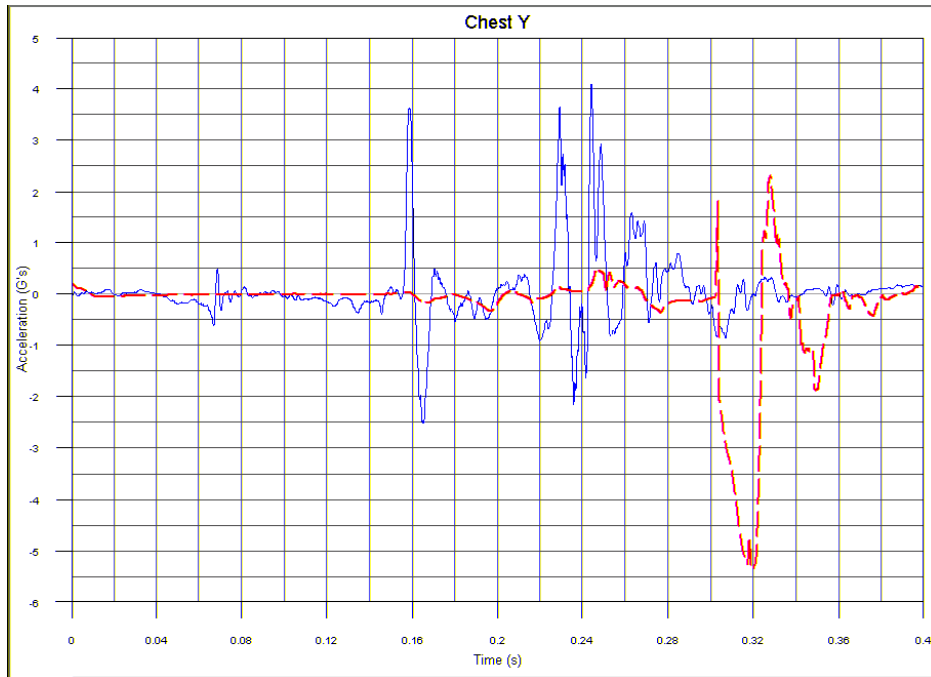


**Figure G103.  Chest Acceleration, y-Direction**
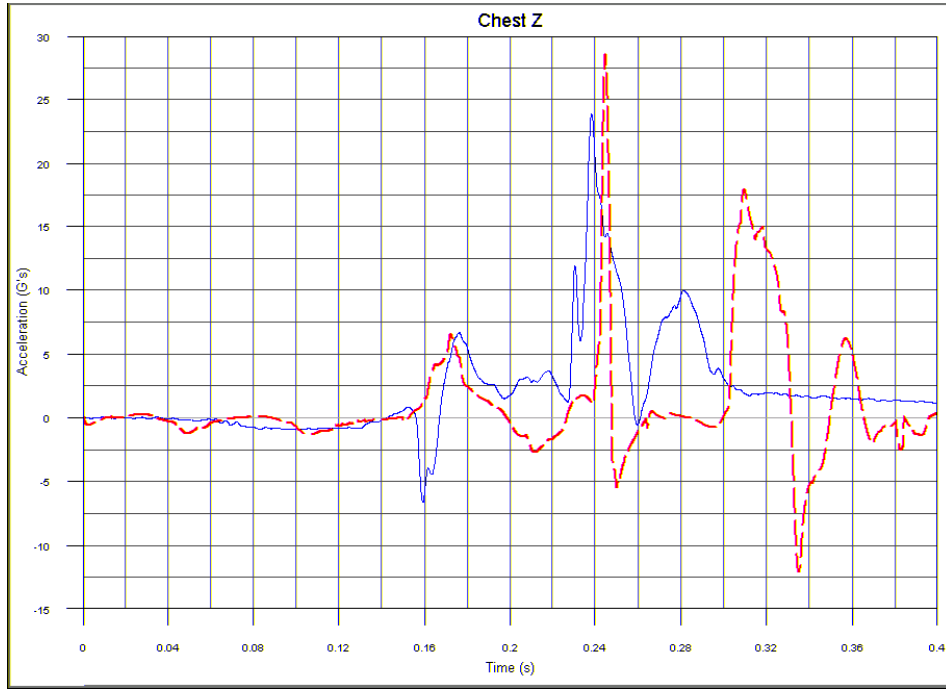
**Figure G104.  Chest Acceleration, z-Direction**
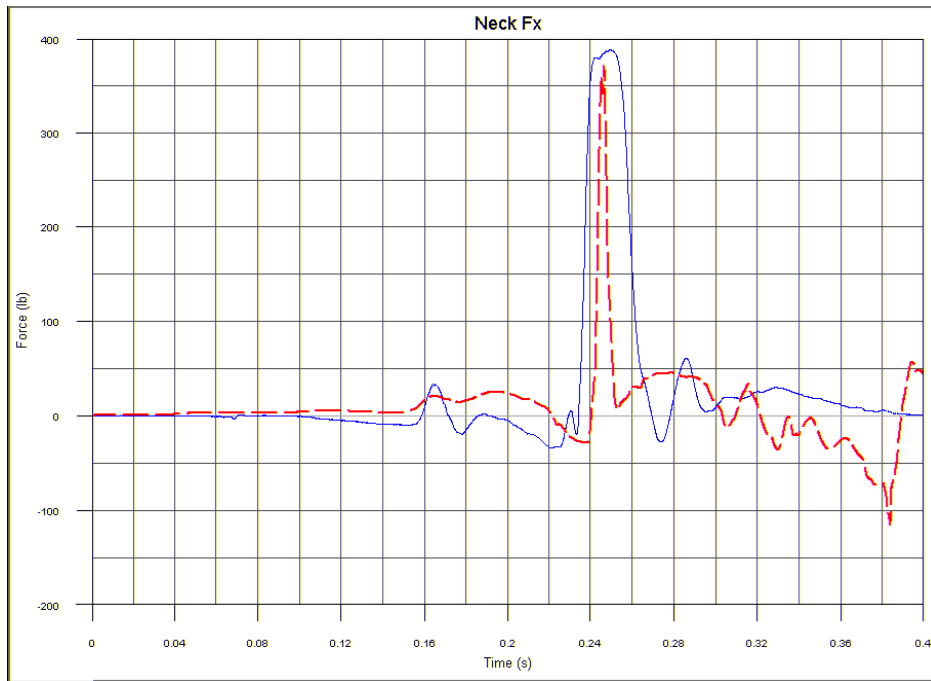


**Figure G105.  Shear Neck Load, x-Direction**
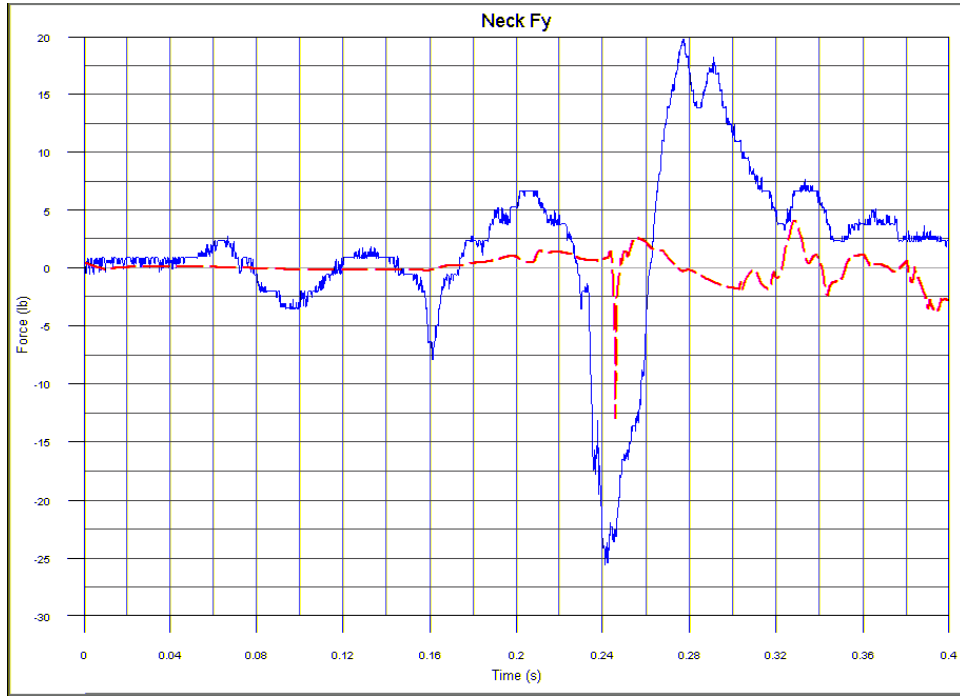
**Figure G106.  Lateral Neck Load, y-Direction**
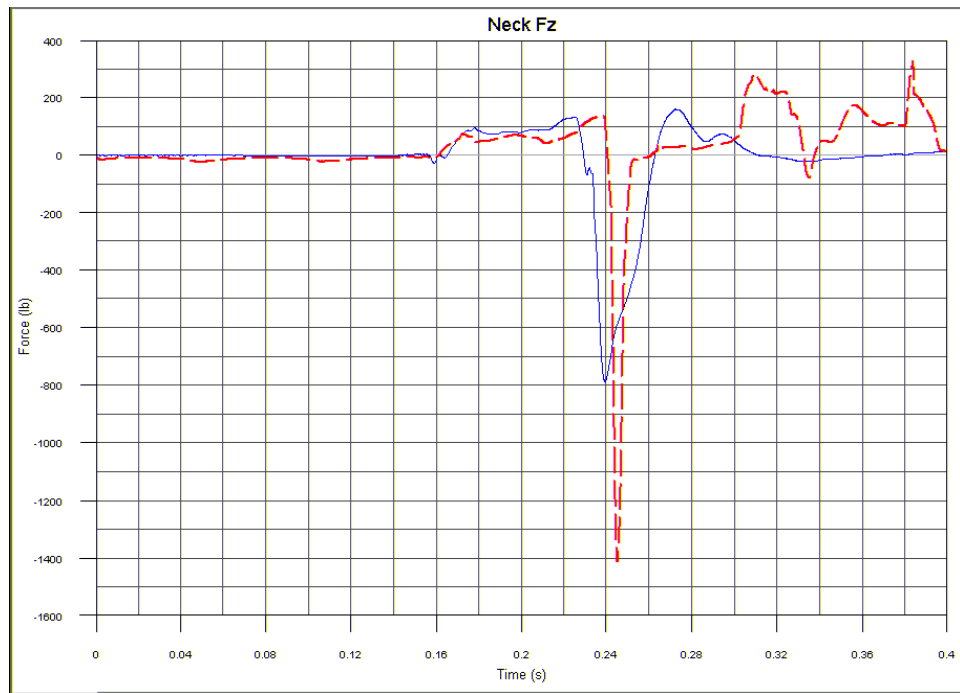


**Figure G107.  Axial Neck Load, z-Direction**
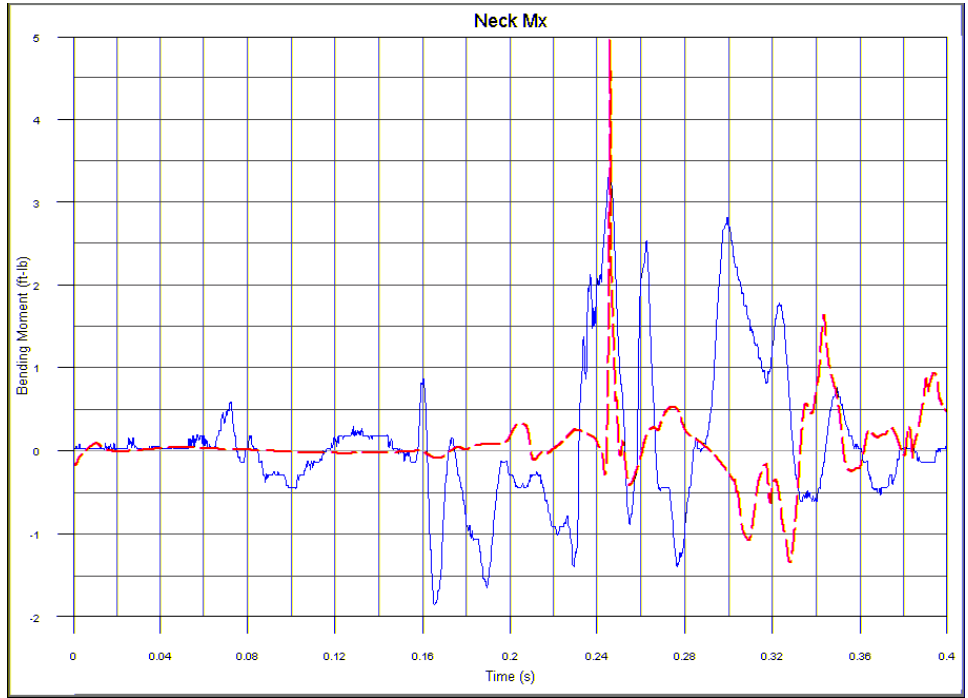
**Figure G108.  Lateral Neck Bending Moment, x-Axis**
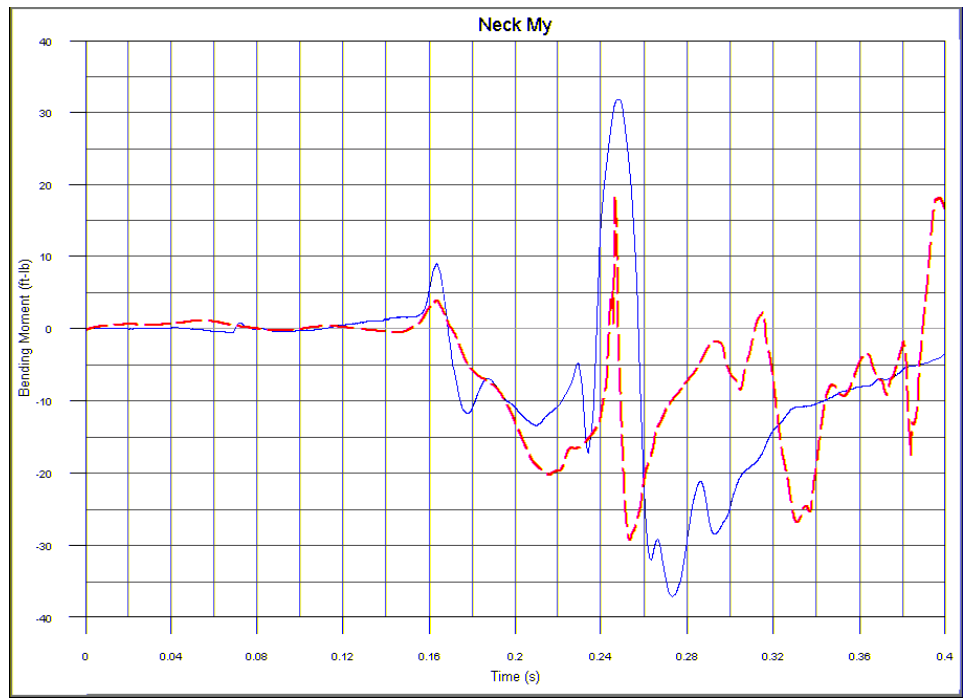


**Figure G109.  Fore/Aft Neck Bending Moment, y-Axis**

**Figure G110.  Rotational Neck Moment, z-Axis**



**Figure G111.  Left Femur Load**

**Figure G112.  Right Femur Load.**

# APPENDIX H

## "SNAP-SHOT" COMPARISONS BETWEEN TESTING AND MODELING OUTPUTS
## FOR  THREE VALIDATED MODELS AND CORRESPONDING TESTS

**Test 00346 - Baseline Test, Model 1**
**Test 00348 - Baseline Test with 9 G crash pulse, Model 2**
**Test 00349 - Baseline Test with 5th- and 95th-Percentile ATDs, Model 3**

**Model View**                                    **Test View**
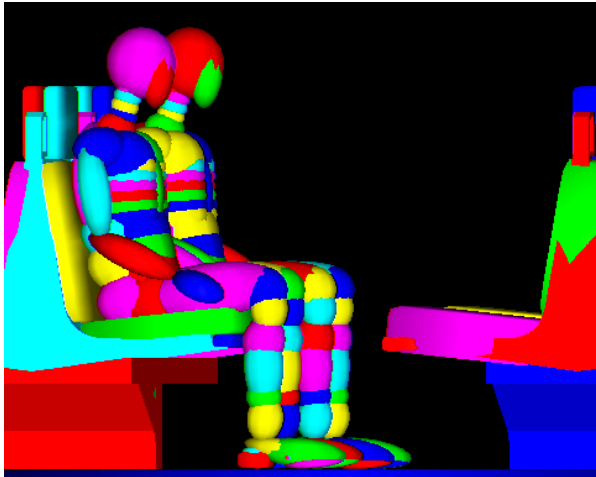
**Initial Position**



**First Contact Between Knee and Seat**
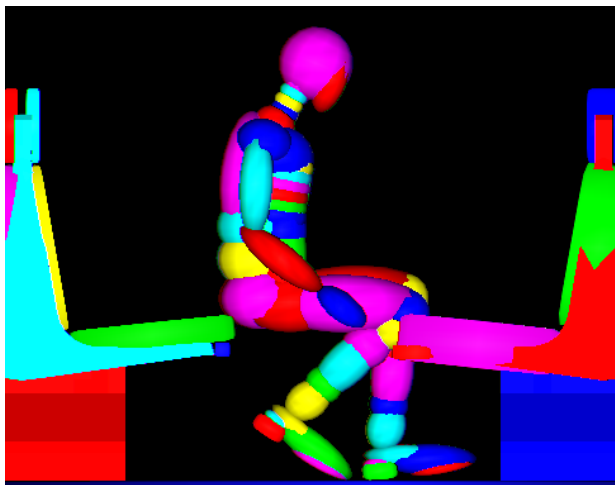


**Head Contact with Seat**
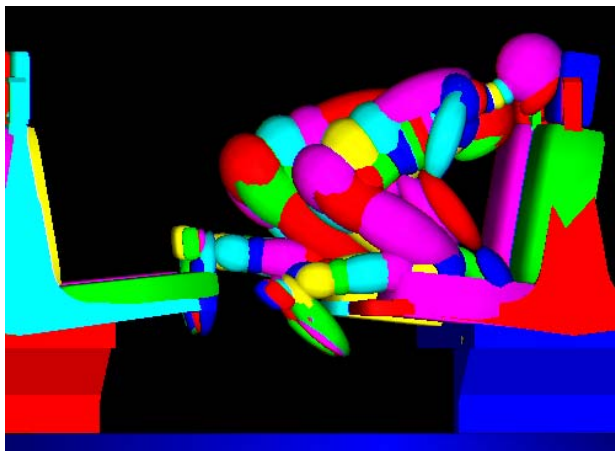


**Figure H1.  Test 00346 and Model 1 – Baseline Test**
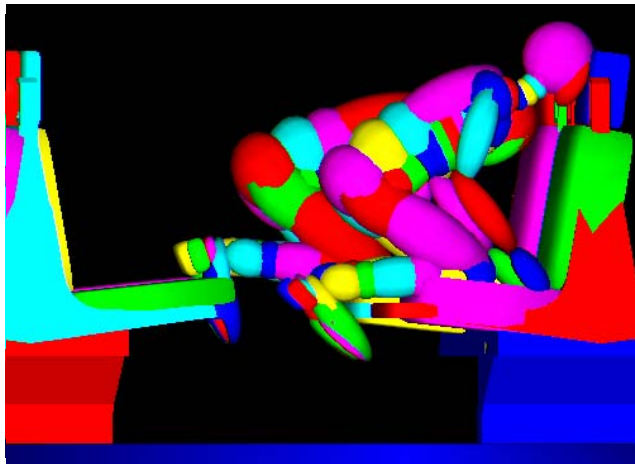
**Model View**

**Test View**
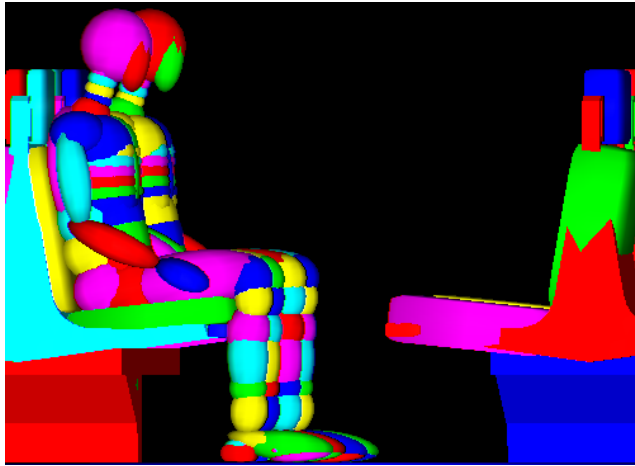
**Initial Position**



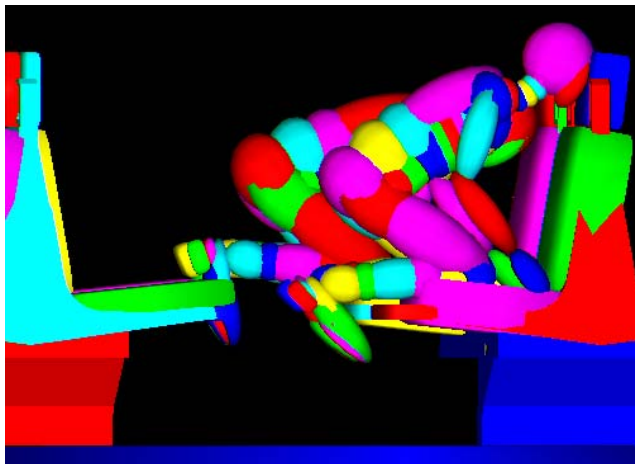**First Contact Between Knee and Seat**



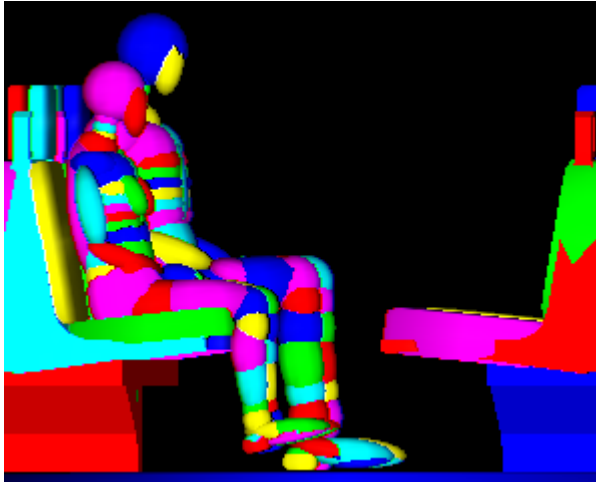**Head Contact with Seat**



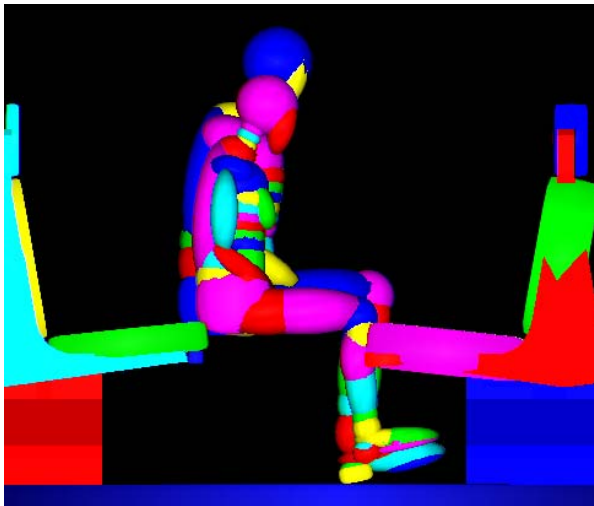**Figure H2.  Test 00348 and Model 2 - Baseline Test with 9 G Crash Pulse**

**Model View** **Test View**

**Initial Position**



**First Contact Between Knee and Seat**
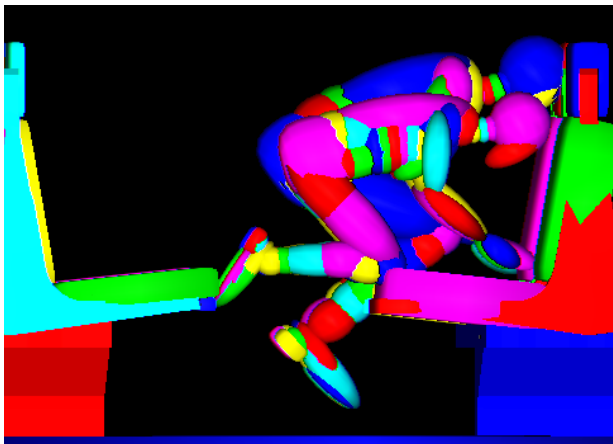


**Head Contact with Seat**



**Figure H3.  Test 00349 and Model 3 – Baseline Test with 5th- and 95th-Percentile ATDs**